Role of Microenvironment in Endometrial Cancer Progression, Metastasis, and Drug Resistance

A Thesis Submitted

In Fulfilment of the Requirements for the Degree of

Doctor of Philosophy

By

SUBHRANSU SEKHAR SAHOO

(M. Sc.)

To

The Faculty of Health and Medicine

School of Biomedical Sciences and Pharmacy

The University of Newcastle, Australia

January 2018

DECLARATIONS PART A

TESTIMONY OF ORIGINALITY

*This thesis contains no material which has been accepted for the award of any other degree or diploma in any university or other tertiary institution and, to the best of my knowledge and belief, contains no material previously published or written by another person, except where due reference has been made in the text. I give consent to the final version of my thesis being made available worldwide when deposited in the University's Digital Repository**, subject to the provisions of the Copyright Act 1968.*

Unless an Embargo has been approved for a determined period.

ACKNOWLEDGEMENT OF COLLABORATION

I hereby certify that the work embodied in this thesis has been done in collaboration with other researchers. I have included as part of the thesis a statement clearly outlining the extent of collaboration, with whom and under what auspices.

ACKNOWLEDGEMENT OF AUTHORSHIP

I hereby certify that the work embodied in this thesis contains published papers of which I am a joint author. I have included as part of the thesis a written statement for each published work, endorsed by my supervisor, attesting to my contribution to the joint publications.

THESIS BY PUBLICATION

I hereby certify that this thesis is in the form of series of published papers of which I am a joint author. I have included as part of the thesis a written statement from each co-author, endorsed by the Faculty Assistant Dean (Research Training), attesting to my contribution to the joint publications.

15-01-2018

Candidate Signature: …….. Date: ……./……./……..

(Subhransu Sekhar Sahoo) (dd/mm/yyyy)

DECLARATIONS PART B

I certify that to the best of my knowledge the work for this thesis entitled **"Role of Microenvironment in Endometrial Cancer Progression, Metastasis, and Drug Resistance"** *has been carried out under my supervision, in the School of Biomedical Sciences and Pharmacy at The University of Newcastle, Australia.*

I the undersigned corresponding author of the following publications:

Sahoo SS, Zhang XD, Hondermarck H, Tanwar PS. **The emerging role of the microenvironment in endometrial cancer.** Submitted to *Cancer and Metastasis Reviews*.

Sahoo SS, Quah MY, Nielsen S, Atkins J, Au GG, Cairns MJ, Nahar P, Lombard JM, Tanwar PS. **Inhibition of extracellular matrix mediated TGF-β signalling suppresses endometrial cancer metastasis**. *Oncotarget,* 2017. 8 (42): p. 71400-71417. (PMID: 29069715)

Sahoo SS, Lombard JM, Lus Y, O'Sullivan R, Wood LG, Nahar P, Jaaback K, Tanwar PS. **Adipose-derived VEGF-mTOR signaling promotes endometrial hyperplasia and cancer: Implications for obese women.** *Mol Cancer Res,* 2017. (PMID: 29133593)

Sahoo SS, Bajwa P, Ko YA, Nahar P, Tanwar PS. **Human placental-like alkaline phosphatase (ALPPL2) as a prognostic biomarker in endometrial cancer.** Submitted to *Proc Natl Acad Sci U S A*.

Bajwa P*, **Sahoo SS***, Tanwar PS. **Age-related mTOR in gynaecological cancers.** *Aging (Albany NY)*, 2017. 9: p. 301-2. (PMID: 28244875) ***Co-first author**

Bajwa P, Nagendra PB, Nielsen S, **Sahoo SS**, Bielanowicz A, Lombard JM, Wilkinson JE, Miller RA, Tanwar PS. **Age related increase in mTOR activity contributes to the pathological changes in ovarian surface epithelium.** *Oncotarget***,** 2016. 7: p. 19214-27. (PMID: 27036037)

Authorise the inclusion of these works and declare that Research Higher Degree candidate ***Subhransu Sekhar Sahoo*** *contributed to these publications. Outlined below are the items that the candidate has contributed towards the fulfilment of the papers:*

- Contributed to conception and design of the studies

- Conducted and designed most of the experiments

- Critically analyzed and interpreted the results

- Prepared and organized the figures

- Contributed in drafting and revision of the manuscripts

- Contributed to formatting initial and revised versions of the manuscripts

15-01-2018

Supervisor Signature: …….. Date: ……/……/……..

(Pradeep S. Tanwar) (dd/mm/yyyy)

ACKNOWLEDGEMENTS

The completion of this thesis would not have been possible without the support of many people.

Firstly, I would like to express my gratitude to my principal supervisor Dr. Pradeep Tanwar for giving me an opportunity to work on this exciting and innovative project. He provided me an outstanding atmosphere for doing research, allowed me to follow my own ideas and has always been there through my ups and downs of the experiments. As well, I would like to thank my co-supervisor Dr. Janet Holt for her continuous support and encouragement. Thank you, both for your guidance across the long course of my studies.

Many thanks to my Ph.D. advisory committee members, Dr. Susan Hua and Prof. Tamas Zakar for their thoughtful advice and suggestions during different milestones of my Ph.D. candidature.

I would like to acknowledge the members of gynaecology oncology group for their help, encouragement, and co-operation.

I would also like to extend my gratitude to members of Department of Medical Biochemistry for their assistance throughout the journey.

Thanks to The University of Newcastle International Postgraduate Research Scholarship (UNIPRS) for financially supporting my tuition fee. My Ph.D. research was also supported by funding from National Health and Medical Research Council (NHMRC), the Australian Research Council, and the Cancer Institute NSW.

Lastly, I am grateful to my parents for their support and motivation that made this thesis possible.

LIST OF PUBLICATIONS INCLUDED AS PART OF THE THESIS

Chapter 1

Sahoo SS, Zhang XD, Hondermarck H, Tanwar PS. **The emerging role of the microenvironment in endometrial cancer.** Submitted to *Cancer and Metastasis Reviews*.

Chapter 2

Sahoo SS, Quah MY, Nielsen S, Atkins J, Au GG, Cairns MJ, Nahar P, Lombard JM, Tanwar PS. **Inhibition of extracellular matrix mediated TGF-β signalling suppresses endometrial cancer metastasis**. *Oncotarget,* 2017. 8 (42): p. 71400-71417. (PMID: 29069715)

Chapter 3

Sahoo SS, Lombard JM, Lus Y, O'Sullivan R, Wood LG, Nahar P, Jaaback K, Tanwar PS. **Adipose-derived VEGF-mTOR signaling promotes endometrial hyperplasia and cancer: Implications for obese women.** *Mol Cancer Res,* 2017. (PMID: 29133593)

Chapter 4

Sahoo SS, Bajwa P, Ko YA, Nahar P, Tanwar PS. **Human placental-like alkaline phosphatase (ALPPL2) as a prognostic biomarker in endometrial cancer.** Submitted to *Proc Natl Acad Sci U S A*.

Addendum

A1:

Bajwa P*, **Sahoo SS***, Tanwar PS. **Age-related mTOR in gynaecological cancers.** *Aging (Albany NY)*, 2017. 9: p. 301-2. (PMID: 28244875) ***Co-first author**

A2:

Bajwa P, Nagendra PB, Nielsen S, **Sahoo SS**, Bielanowicz A, Lombard JM, Wilkinson JE, Miller RA, Tanwar PS. **Age related increase in mTOR activity contributes to the pathological changes in ovarian surface epithelium.** *Oncotarget***,** 2016. 7: p. 19214-27. (PMID: 27036037)

LIST OF ABBREVIATIONS

2D	Two-dimension
3D	Three-dimension
ACM	Adipocyte-conditioned medium
ALPPL2	Placental-like alkaline phosphatase 2
ANGPT1	Angiopoietin-1
AT	Adipose tissue
AUC	Area under the ROC curve
BMI	Body mass index
CA-125	Cancer antigen 125
CCL2	C-C motif chemokine ligand 2
cDNA	Complementary deoxyribonucleic acid
CDX	Cell line derived xenograft
CI	Confidence interval
CM	Conditioned media
DAB	Diaminobenzidine
E2	Estrogen
EC	Endometrial cancer
ECM	Extracellular matrix
EH	Endometrial hyperplasia
EHS	Engelbreth-holm-swarm
ELISA	Enzyme-linked immunosorbent assay
EMT	Epithelial-mesenchymal transition
FDR	False discovery rate
FFPE	Formalin-fixed paraffin-embedded
FN1	Fibronectin
FOXA2	Forkhead box A2
GFOLD	Generalized log2 fold change
GFP	Green fluorescent protein
H&E	Hematoxylin and eosin
HGF	Hepatocyte growth factor
IF	Immunofluorescence
IHC	Immunohistochemistry
IL	Interleukin
IPA	Ingenuity pathway analysis
IVIS	In vivo imaging system
MET	Mesenchymal-epithelial transition
mTOR	Mammalian target of rapamycin
MUC16	Mucin 16
OSE	Ovarian surface epithelium
P4	Progesterone
PACM	Preadipocyte-conditioned medium
PCV	Packed cell volume

PI3K	Phosphoinositide-3-kinase
PIK3CA	Phosphatidylinositol-4,5-bisphosphate 3-kinase catalytic subunit alpha
poly-HEMA	Polyhydroxyethylmethacrylate
qRT PCR	Quantitative reverse transcription polymerase chain reaction
RFP	Red fluorescent protein
RGF-BME	Reduced growth factor-basement membrane extract
RIPA	Radioimmunoprecipitation assay buffer
RNA	Ribonucleic acid
ROC	Receiver operative characteristic
SAT	Subcutaneous adipose tissue
SD	Standard deviation
SEM	Standard error mean
SFM	Serum-free medium
STR	Short tandem repeat
TCGA	The cancer genome atlas
TGF-β	Transforming growth factor beta
TME	Tumor microenvironment
VAT	Visceral adipose tissue
VEGF	Vascular endothelial growth factor
VEGFR2	Vascular endothelial growth factor receptor 2

TABLE OF CONTENTS

Abstract

Endometrial cancer is the most frequently diagnosed cancer of the female reproductive tract. Obesity is an independent risk factor for this disease and approximately 50% of cases are associated with high body mass index (BMI). Like many cancers, the progression of high-grade or metastatic endometrial cancer is mediated through a supportive tumor microenvironment (TME). Currently, the precise role of TME towards endometrial cancer progression is unclear. To manifest the tumor-stroma interaction, we investigated both non-cellular (extracellular matrix, ECM) and cellular (adipocyte) components of the endometrial cancer microenvironment. 1) In the first part, we found that conversion of glandular epithelium of endometrial cells to non-glandular epithelium is a hallmark of cancer, and this transition is facilitated by TGF-β signaling through ECM. Mechanistically our results revealed that fibronectin of ECM facilitates activation of TGF-β pathway and promotes metastasis. Moreover, interruption of TGF-β signaling significantly suppresses endometrial cancer metastasis. 2) In the second part, we demonstrated the interaction between adipocytes and endometrial cancer cells using human biopsies and a hyperphagic obese mouse model. We found that hypertrophied adipocytes secrete VEGF, which stimulates angiogenesis in the uterus as well as endometrial cell proliferation through active mTOR signaling. Taken together these findings provide new understanding on TME during endometrial carcinogenesis and render novel ideas of co-targeting tumor cells as well as stromal signals to suppress metastatic progression. 3) Furthermore, inhibiting microenvironment-derived signals, early diagnosis of the disease is necessary to suppress the spread of cancer. Therefore, we examined differential expression of soluble and secreted proteins in healthy and cancer patients and found placental-like alkaline phosphatase (ALPPL2) as a potential secreted protein in endometrial cancer patients. Interestingly with the existing knowledge of hyperestrogenic state is a major risk factor for endometrial cancer, our results ascertained that estrogen stimulates expression of this protein. Thus, ALPPL2 can be used as a prognostic biomarker for endometrial cancer. Collectively our research provides new insights towards endometrial cancer microenvironment as well as its early diagnosis.

Thesis Overview

Introduction

The tissue microenvironment comprises the extracellular matrix, fibroblasts, adipocytes, immune and inflammatory cells, which altogether maintains the integrity of normal tissue architecture. Disruption of normal tissue homeostasis between epithelial cells and the surrounding stroma leads to tumor development. These early neoplastic changes are highly reflected by the ability of tumor cell to corrupt the surrounding stroma and turn it from restrictive to a supportive environment. Defects in tissue microenvironment have been well established in many human cancers including endometrial cancer. However, the altered stromal signaling in the tumor microenvironment (TME) which promotes differentiated to malignant endometrial cancer cell behavior is not well investigated. TME consists of both non-cellular and cellular component. To understand the role of TME in endometrial cancer progression and metastasis, we investigated extracellular matrix (ECM) of TME as a non-cellular component. Furthermore, we analyzed the contribution of adipocytes (a cellular component of TME) towards endometrial carcinogenesis as epidemiological studies suggest that obesity impose a significant risk factor for endometrial cancer and approximately 50% of the cases are related to obesity. In addition to exploring mechanisms of endometrial cancer progression and metastasis in the microenvironment, we also emphasized to find out a novel biomarker for early detection and diagnosis of the disease, which may suppress endometrial cancer-associated death.

Aims

1. To define the role of extracellular matrix in endometrial cancer metastasis.
2. To examine the effect of adipocytes in endometrial cancer initiation and progression.
3. To find out a novel biomarker which can predict endometrial cancer at an early stage.

Organization of Thesis

This thesis comprises six different chapters followed by discussion and conclusion. The outcomes of hypothesis and aims of this thesis are demonstrated in first four chapters. The last two chapters (5 and 6) are additional publications during my Ph.D. where I have contributed significantly to the study and is a co-first author in one publication.

Chapter 1

This chapter contains a review manuscript on **"The emerging role of the microenvironment in endometrial cancer"** which is submitted for publication in ***Cancer and Metastasis Reviews*** journal. This review summarises the literature behind the research described in this thesis. It also highlights the current understanding of endometrial cancer microenvironment as well as novel outcomes of this thesis, which may aid further research in this field.

Chapter 2

This chapter contains a research paper entitled as **"Inhibition of extracellular matrix mediated TGF-β signalling suppresses endometrial cancer metastasis"** which is published in the journal ***Oncotarget***. This paper address the first aim of this thesis. In this study, we investigated how endometrial cancer cells change their shape, organization, and behavior in three-dimensional (3D) ECM substratum. Using RNA seq and bioinformatics tool, we found that TGF-β signaling was upregulated in endometrial cancer colonies forming a non-glandular shape in the 3D matrix. We further proved that fibronectin activates TGF-β signaling in endometrial cancer colonies and promotes metastasis in *in vitro* assays as well as in human patient samples. Moreover, using a metastatic endometrial cancer CDX mouse model, we showed that inhibition of TGF-β pathway significantly suppresses endometrial cancer metastasis. Collectively this study emphasizes the role of ECM proteins in endometrial cancer metastasis.

*****This study is featured in few media reports highlighting the significance of the project.

****Please refer to appendices.***

Chapter 3

To achieve the second aim of the thesis, we investigated the function of one major cellular component of endometrial cancer microenvironment that is adipocyte. The outcome of this study is published in the journal ***Molecular Cancer Research*** that is entitled as **"Adipose-derived VEGF-mTOR Signaling Promotes Endometrial Hyperplasia and Cancer: Implications for Obese Women"**. This study involves the use of human female adipose tissue from patients undergoing bariatric surgery and a hyperphagic obese mouse model. Using human biopsy samples in different *in vitro* and *in vivo* assays, we demonstrated that hypertrophied adipocytes in visceral adipose tissue secrete VEGF, which in a paracrine manner activates mTOR signaling in endometrial glands. Activation of mTOR pathway promotes endometrial hyperplasia and cancer initiating lesions. The positive correlation of VEGF and mTOR signaling is also ascertained in obese endometrial cancer patient samples. This study for the first time provides a plausible mechanism of adipocyte and endometrial cancer cell interaction.

*This study is also featured in University of Newcastle's news as well as in many media reports emphasizing the importance of the result.

Please refer to appendices.

Chapter 4

The focus of this chapter is to identify a prognostic biomarker, so that diagnosis of endometrial cancer can be done at an early stage, which may increase patient outcomes. The manuscript entitled as **"Human placental-like alkaline phosphatase (ALPPL2) as a prognostic biomarker in endometrial cancer"** summarises the results and findings of the study and is submitted to ***Proceedings of the National Academy of Sciences of the United States of America*** journal for publication. Using transcriptome analysis and other *in vitro* experiments, we found that *ALPPL2* is an estrogen-responsive gene and its expression is upregulated in endometrial cancer organoids. Furthermore, immunohistochemistry, western blot and ELISA analysis of normal and endometrial cancer patient samples demonstrated upregulation of ALPPL2 protein in the patients' group compared to normal individuals. Overall, this study offers an avenue for early diagnosis of endometrial cancer by use of a novel biomarker, ALPPL2.

Addendum A1 and A2

The two papers mentioned in the addendum are additional publications to this thesis. A1 contains an editorial **"Age-related mTOR in gynaecological cancers"** published in the *Aging* journal and A2 contains a paper entitled as **"Age related increase in mTOR activity contributes to the pathological changes in ovarian surface epithelium"** which is published in the journal *Oncotarget.* Both these studies describe the association of increased mTOR signaling and ovarian cancer in the aged population.

Discussion and Conclusion

The discussion and conclusion session of this thesis summarises all the key outcomes of several chapters (especially chapter 2, 3, and 4) that altogether brings novel outcomes in the field of endometrial cancer research and would avail to develop better-targeted therapies to improve clinical outcomes in endometrial cancer patients.

Chapter 1

The Emerging Role of the Microenvironment in Endometrial Cancer

Preface

Personalized treatments for endometrial cancer patients have a modest success rate as most studies have focused on chemotherapy or radiotherapy to suppress cancer cell survival and growth. Although genetic alterations in *PIK3CA*, *PTEN*, and *KRAS* are essential for endometrial tumor development but not sufficient to generate malignant tumors. However, the mutual interactions between tumor and stromal cells in the tumor microenvironment drive high-grade and metastatic cancers. Therefore, disruption of tumor-stroma crosstalk is essential to suppress cancer progression. This idea will lead to new and novel treatment options to target stromal signals along with tumor cells and might improve endometrial cancer patient outcomes. In this chapter, we review the role of various microenvironment-derived signals towards endometrial carcinogenesis and how inhibition of stromal signaling suppresses metastatic endometrial cancer progression.

UON Graduate Research

Co-authorship declaration

THE UNIVERSITY OF NEWCASTLE AUSTRALIA

Statement of Authors' Contributions

This statement summarises the intellectual input by all the authors in the review paper entitled **"The emerging role of the microenvironment in endometrial cancer"**.
This review paper is submitted to the Journal ***Cancer and Metastasis Reviews***.

Authors	Statement of contribution
Subhransu S. Sahoo (First and lead author)	Wrote the initial draft Made figures and tables for the review manuscript Edited and revised the manuscript
Xu Dong Zhang (Co-author)	Revised the manuscript
Hubert Hondermarck (Co-author)	Edited and revised the manuscript
Pradeep S. Tanwar (Corresponding author)	Edited the manuscript Provided intellectual inputs

Subhransu S. Sahoo

Xu Dong Zhang

Hubert Hondermarck

Pradeep S. Tanwar

Robert Callister - Faculty Assistant Dean Research Training

Publication

This review manuscript has submitted to the journal ***Cancer and Metastasis Reviews***.

The emerging role of the microenvironment in endometrial cancer

Subhransu S. Sahoo[1,2,3], Xu Dong Zhang[2,3], Hubert Hondermarck[2,3], Pradeep S. Tanwar[1,2,3*]

[1]Gynaecology Oncology Group; [2]School of Biomedical Sciences and Pharmacy**,** University of Newcastle, Callaghan 2308, New South Wales, Australia

[3]Hunter Medical Research Institute, New Lambton Heights 2305, New South Wales, Australia

*Address correspondence to:

Dr. Pradeep Tanwar
Australian Research Council Future Fellow
Cancer Institute NSW CD Fellow
Group Leader, Gynaecology Oncology Group
LS236, University Drive
University of Newcastle
Callaghan NSW 2308 Australia
Email: pradeep.tanwar@newcastle.edu.au
Phone: +61-2-49215148

Disclosure statement: The authors have nothing to disclose

Abstract

Endometrial cancer (EC) is one of the most frequently diagnosed cancer in women and despite recent therapeutic advances, in many cases, treatment failure results in cancer recurrence, metastasis, and death. Current research demonstrates that the interactive crosstalk between two discrete cell types (tumor and stroma) promotes tumor growth and investigations have uncovered the dual role of stromal cells in the normal and cancerous state. In contrast to tumor cells, stromal cells within the tumor microenvironment (TME) are genetically stable. However, tumor cells modify adjacent stromal cells in the TME. The alteration in signaling cascades of TME from anti-tumorigenic to pro-tumorigenic enhances metastatic potential and/or confer therapeutic resistance. Therefore, the TME is a fertile ground for the development of novel therapies. Furthermore, disrupting cancer-promoting signals from the TME or re-educating stromal cells may be an effective strategy to impair metastatic progression. We review here the paradoxical role of different non-neoplastic stromal cells during specific stages of EC progression. We also suggest that specific inhibition of microenvironment-derived signals may suppress metastatic EC progression and offer novel potential therapeutic interventions.

Keywords

Endometrial cancer, TME, Stromal cells, Metastasis, Chemoprevention

1. Introduction

Worldwide, endometrial cancer (EC) is the most prevalent invasive gynecologic malignancy (Siegel et al., 2016). Although early diagnosis, surgery, and chemotherapy have reduced EC mortality, still in many cases these patients eventually succumb to their malignancy. The mechanisms involved with the aggressive transformation of tumor cells are poorly understood. The molecular signals derived from stromal cells and/or extracellular matrix (ECM) most likely play an important role in the progression of an indolent tumor to a malignant state (Bonnans et al., 2014; Lu et al., 2012). The interaction between tumor cells and the tumor microenvironment (TME) regulates cancer progression of almost all types of cancer (Hanahan and Coussens, 2012; Hanahan and Weinberg, 2011). This concept was proposed early, in 1889 by Stephen Paget in his "seed and soil" hypothesis, which suggests that a seed (the tumor cells) can only grow in a fertile soil (the microenvironment) (Paget, 1989). Similarly, tumor cells (seed) can thrive only where microenvironment (soil) is somewhat favorable.

Dynamic reciprocity between cells and their microenvironment is crucial for both normal tissue homeostasis and tumor growth (Ungefroren et al., 2011). The tissue microenvironment consists of both cellular (fibroblasts, myofibroblasts, blood vessels, pericytes, adipocytes, smooth muscle cells, immune and inflammatory cells) and non-cellular (ECM) components (Bhowmick and Moses, 2005). In the normal state, cells exchange information with other cell types by direct cell-cell contact or through ECM (Bissell and Radisky, 2001). The ECM is a repository of growth factors, cytokines, and structural proteins, which are produced by the crosstalk between epithelial cells and surrounding stromal cells (Miles and Sikes, 2014). The basal surface of epithelial cells forms the basement membrane, which separates epithelial and stromal compartment. In this manner, a normal well-differentiated epithelium is separated by a well-delineated basement membrane from the dermal or stromal compartment (Mueller and Fusenig, 2004). However, during the transition to pre-malignant state or progression to carcinoma, the normal tissue homeostasis gets disturbed, which results in proliferation of epithelial cells and invasion of these tumor cells to the stromal compartment through the degraded basement membrane (Mueller and Fusenig, 2004). Furthermore, the crosstalk of soluble factors or proteins between tumor cells and non-cancerous stromal cells supports tumor development and progression (Fang and Declerck, 2013; Quail and Joyce, 2013). Consequently, tumor cells misdirect the surrounding stroma and turn it from restrictive to the supportive environment. Eventually, the supportive microenvironment sustains the tumor cells to disseminate.

Thus, tissue microenvironment has reciprocal functions in the healthy and diseased state. In the healthy state, normal microenvironment provide antitumorigenic signals to maintain epithelial tissue homeostasis (Bissell and Hines, 2011). However, during the progression of cancer, the reactive stromal components promote tumor cell proliferation through diverse signaling cascades. Moreover, oncogenic mutations in the tumor cells are not sufficient to drive high-grade cancerous state unless the molecular signaling cascades have been perturbed by the microenvironment (Figure 1). Thus, TME has a significant contribution towards driving tumor progression. In this review, we discuss the current understanding of endometrial carcinoma from a microenvironment vantage point, highlighting the stromal cell-derived signaling cascades involved in the progression of high-grade EC.

2. Endometrial cancer microenvironment

Carcinogenesis is a multistep process, starting from the initial carcinogenic stimulus to the final manifestation of cancer. Although uncontrolled growth is a fundamental characteristic of cancer cells, these cells also require a proper microenvironment to survive and develop (Bissell and Hines, 2011). Like in most cancers, TME also contributes a pivotal role in EC progression (Felix et al., 2010). Indeed, mutations in *PTEN*, *KRAS*, *p53* and microsatellite instability initiates EC lesions, but this does not lead to high-grade cancer or metastasis unless supported by the microenvironment (Lax et al., 2000). The microenvironment of EC cells is populated by diverse cell types including fibroblasts, myofibroblasts, adipocytes, endothelial cells, macrophages and inflammatory cells (Table 1) (Felix et al., 2010). These cells communicate with EC cells through cytokines, growth factor or express receptors for ligand binding secreted from EC cells. Thus, the reciprocal interactions between EC cells and various stromal cells generate a favorable environment conducive to invasion and metastasis. Invasion and metastasis of tumor cells are the major reasons for treatment failure and poor prognosis in EC patients. The identification of microenvironment-derived signals or stromal cell-derived proteins can potentially serve as biomarkers for high-grade metastatic EC. Thus, in order to study how the expression of these proteins enhances EC progression and metastasis, these proteins need to be explored and investigated thoroughly. In this review, we address the role of various stromal proteins and pathways, which contribute to endometrial carcinogenesis.

2.1 The role of stromal myofibroblasts in EC microenvironment

Out of several other stromal cells, myofibroblasts have a dominant contribution in cancer progression (Kalluri, 2016; Kalluri and Zeisberg, 2006). Stromal myofibroblasts secrete diverse

milieu of cytokines and growth factors to boost EC growth, motility, angiogenesis, and metastasis. Out of several growth factors, hepatocyte growth factor (HGF), secreted by myofibroblasts is a potent growth-promoter that plays an important role in EC microenvironment (Choi et al., 2009; Steffan et al., 2011). Studies have demonstrated the interaction between endometrial stromal cells and EC cells through HGF/Met pathway (Li et al., 2015a). Endometrial myofibroblasts secrete HGF, which interacts with its receptor Met on EC cells and induce invasion of EC cells (Li et al., 2015a; Li et al., 2015b). Furthermore, in a recent study, both *ex vivo* and *in vivo* experiments show the activation of HGF/c-Met/Akt signaling pathway in EC (Li et al., 2015b). Phosphorylation of Met receptor by HGF further phosphorylates downstream Akt protein, which promotes the proliferation of epithelial cells via the modulation of cyclin D1 transcription (Li et al., 2015b) (Figure 2a). This also explains why *in vitro* assays that show highly significant results with AKT/PI3K inhibitors in endometrial epithelial cell culture have failed to translate into the clinic because stromal inputs are missing in *in vitro* conditions.

Furthermore, increasing evidence suggests that myofibroblasts stimulate tumor progression through CXCL12 secretion (Sun et al., 2010). The chemokine CXCL12 (also known as stromal-derived factor-1, SDF-1) plays a critical role of chemoattractant in the tumor niche. It primarily binds to its cognate receptor CXCR4 to regulate trafficking of normal and malignant cells. Thus in a paracrine manner, CXCL12 attracts CXCR4 expressing tumor cells to new tumor niche resulting in the invasion and metastasis of tumor cells (Figure 2b) (Gelmini et al., 2009; Kodama et al., 2007). In addition, Immunohistochemistry and real-time quantitative PCR studies have also shown an elevated level of CXCR4 mRNA in human EC patient tissue samples (Gelmini et al., 2009; Kodama et al., 2007). These data suggest that interaction between CXCL12 and CXCR4 on endometrial tumor cell triggers tumor cell invasion.

Besides myofibroblasts, several studies have demonstrated the significant contribution of cancer-associated fibroblasts (CAF) in EC. Tumor-derived growth factors such as transforming growth factor-beta (TGF-β) differentiates stromal fibroblasts into myofibroblasts. Myofibroblasts acquire a higher level of the alpha smooth muscle actin (αSMA) protein and turn into cancer-associated fibroblasts (CAF) (Hanahan and Weinberg, 2011; Paunescu et al., 2011). In case of EC, the number of CAF increases with pro-malignant features. CAF in active stroma secretes higher levels of collagen I and III than those of normal tissue, which facilitates desmoplasia by deposition of the dense collagen matrix. In addition, CAF contribute significantly to the progression of EC by chronic secretion of cytokines such as IL-6, IL-8, monocyte chemotactic protein-1 (MCP-1 or CCL2),

chemokine ligand 5 (CCL5 or RANTES) and vascular endothelial growth factor (VEGF) than normal endometrial fibroblast cells (Subramaniam et al., 2016; Subramaniam et al., 2013) (Figure 2c). VEGF is a potent growth factor that stimulates more vasculature around the tumor and supports angiogenesis. The secreted cytokines also act as a chemoattractant for migration and invasion of EC cells from primary sites to secondary sites.

In summary, stromal myofibroblasts and CAF enhance EC growth and metastasis, which suggests a significant contribution of the microenvironment in EC progression.

2.2 Macrophages in EC microenvironment

Macrophages are one of the major stromal components and release several growth factors, cytokines, and chemokines, which facilitates tumor growth and invasion. Depending upon phenotypic diversity, macrophages have the dual role in cancer and can either promote or inhibit cancer progression. Typically macrophages exist in two basic phenotypes, M1 macrophages with their cytotoxic potential are considered as anti-tumor phenotype and M2 macrophages associated with wound healing and tissue repair function are regarded as the pro-tumor phenotype (Noy and Pollard, 2014). A growing body of evidence suggests the vital role of tumor-associated macrophages (TAM) in neoplastic transformation and progression of EC (Dun et al., 2013; Espinosa et al., 2010; Kelly et al., 2015; Kubler et al., 2014). Endometrial carcinomas have a higher macrophage density than benign endometrium (Dun et al., 2013). Comparatively high-grade endometrioid carcinomas or type II EC with myometrial invasion have more stromal M2 TAMs than type I endometrioid adenocarcinomas without myometrial invasion (Espinosa et al., 2010). EC cell-derived chemoattractants, such as colony stimulating factor-1 (CSF-1) and the CC chemokines help in the oncogenic recruitment of macrophages through blood vessels (Espinosa et al., 2014) (Figure 2d). Moreover, immunohistochemistry and tissue microarray studies have shown the presence of three macrophage response markers (CD163, FCGR2A, and FGCR3A) in endometrioid EC cells (Espinosa et al., 2014). Investigations have also demonstrated that expression of CSF-1 on EC cells facilitate infiltration of mononuclear macrophages. Besides the recruited macrophages, the *in situ* macrophages in the uterus significantly contribute to EC progression. Macrophages reside in the peri-necrotic and perivascular areas of the uterus and promote endometrial carcinogenesis by the production of pro-inflammatory cytokines such as tumor necrosis factor-α (TNF-α), IL-1β, IL-6 and oxygen free radicals (Friedenreich et al., 2013). IL-1β signals through IL-1R on EC cell surface (Figure 2e). Accumulation of TAMs in necrotic regions is characterized by low oxygen tension or hypoxic TME which further drives angiogenesis (Friedenreich et al., 2013). Thus, TAMs have a potential contribution towards endometrial

carcinogenesis via production of cytokines, reactive oxygen species and the establishment of a hypoxic environment, which altogether triggers the process of angiogenesis (Kelly et al., 2015). This concludes in addition to uncontrolled tumor cell division, macrophage-derived cytokines promotes tumor cell growth and spread to secondary sites.

2.3 Stromal signaling in EC microenvironment

2.3.1 ECM-derived TGF-β signaling

Besides cellular components of the microenvironment, non-cellular components such as ECM plays an important role in fibrosis and EC metastasis. Our recent investigations show that ECM-derived TGF-β signaling promotes EC metastasis (Sahoo et al., 2017b). Out of several ECM proteins, fibronectin (FN1) activates TGF-β pathway in EC cells (Figure 2f). Our study also highlights surplus deposition of fibronectin protein at metastatic sites of human EC patients compared to the primary origin of the tumor (Uterus) and suppression of TGF-β pathway significantly impairs EC cell invasion and metastasis (Sahoo et al., 2017b). Thus, inhibition of microenvironment-derived signals can reduce EC metastasis.

2.3.2 Stromal APC signaling

Apart from genetic alterations in tumor cells, mutations in the stromal component promote the progression of benign endometrial polyps to an advanced metastatic stage. Our study has shown the crucial role of stromal adenomatous polyposis coli (APC) in controlling the proliferative potential of the endometrial epithelium (Tanwar et al., 2011). APC is a multi-domain protein that regulates Wnt signaling by controlling the availability of β-catenin. In addition, APC interacts with several other proteins to regulate various cellular processes including cell proliferation, differentiation, and migration. However, stromal deletion of APC contributes to the development of EC. Histologic analyses of APC^{cKO} mutant mouse model has shown the progressive development of endometrial hyperplasia, increase in stromal myofibroblast population, diminished expression of estrogen receptor α (ERα), progesterone receptor (PR) and higher levels of VEGF and SDF-1, which collectively indicates an advanced stage of human EC (Tanwar et al., 2011).

2.3.3 Stromal LKB1 signaling

LKB1 (liver kinase B1) is a negative regulator of mTOR pathway. Stromal LKB1 signaling plays a major role in EC progression (Tanwar et al., 2012). The stromal cell-specific loss of *Lkb1* induces high-grade EC in uterine epithelium by activating mammalian target of rapamycin complex 1 (mTORC1) (Tanwar et al., 2012). LKB1 inactivation also results in an abnormal cell autonomous

production of the inflammatory cytokine-chemokine (C-C motif) ligand 2 (CCL2) which facilitates recruitment of macrophages to promote tumor growth (Pena et al., 2015).

2.3.4 Stromal HAND2 signaling

Hypermethylation of *HAND2* gene in endometrial stroma significantly contributes to the development of EC. Epigenome-wide analysis of human EC patients' tissue samples shows hypermethylation of *HAND2* gene in the endometrial stroma (Jones et al., 2013). Interestingly, transgenic mouse model harboring *Hand2* knockout has shown to develop precancerous endometrial lesions (Jones et al., 2013). This study shows the importance of endometrial stroma in EC development and progression.

2.3.5 Stromal VEGF signaling

Majority of the EC cells express epithelial membrane protein-2 (EMP2) on their cell surface. EMP2 is a novel oncogene which promotes tumor angiogenesis and endothelial cell tube formation through increased vascular endothelial growth factor (VEGF) expression (Gordon et al., 2013). EMP2 activates hypoxia-induced transcription factor-1α (HIF-1α) in a hypoxic microenvironment through FAK-Src signaling axis and upregulates VEGF expression (Gordon et al., 2013) (Figure 2g). Upregulated VEGF in stroma binds to VEGF receptor (VEGFR) on tumor cell to stimulate growth and proliferation. Moreover, increased level of VEGF expression in patients with endometrioid EC is a predictor of poor prognosis (Kamat et al., 2007).

2.3.6 Stromal estrogen signaling

Steroid signals in the stroma also contribute to EC progression. Stromal estrogen receptor (ERα) mediates mitogenic effects of estrogen on endometrial cell proliferation (Chung et al., 2015). Existing evidence clearly demonstrates the contribution of unopposed estrogen towards tumorigenesis and progression of endometrial carcinoma (Hecht and Mutter, 2006). In postmenopausal women, in spite of low levels of circulating plasma estrogen, the crosstalk of tumor and stromal cells contribute to the increase in aromatase activity and estrogen biosynthesis (Takahashi-Shiga et al., 2009). The positive feedback loop between IL-6, aromatase and *in situ* estrogen maintains elevated estrogen signaling in EC microenvironment (Che et al., 2014). *In situ* estrogen binds to ERα and induces upregulation of IL-6 in EC cell via activation of the NF-κB pathway (He et al., 2009). IL-6 further stimulates aromatase expression in the endometrial stromal cell through the IL-6 receptor. Increased aromatase expression synthesizes more estrogen, which promotes cancer progression (Che et al., 2014) (Figure 2h).

These findings all together highlight the importance of various TME-derived signaling in EC progression.

2.4 Adipocytes: A key cell type in EC microenvironment

Adipocytes are the predominant cell type in adipose tissue, which maintains energy homeostasis in the body (Cristancho and Lazar, 2011). Alternatively, in obese individuals, the hypertrophied adipocytes induce tumorigenesis (Nieman et al., 2013). Increased adiposity or obesity is not only a major risk factor for cardiovascular disease and type-2 diabetes but also an important cause for multiple types of cancers including EC (Calle and Kaaks, 2004; Reeves et al., 2007). Approximately 57% of EC cases in the United States are related to obesity, which supports the notion that obesity is a major risk factor for EC (Onstad et al., 2016). In fact, high BMI (Body Mass Index) is strongly associated with the development of EC (Calle et al., 2003). In a recent meta-analysis study, Renehan *et al* show that each increase in BMI of 5 kg/m^2 significantly increases a woman's risk of developing EC with a relative risk of 1.59 (Renehan et al., 2008). Besides, the epidemiologic studies revealed that the risk of EC is higher in western countries as well as in women who live a sedentary lifestyle (Fader et al., 2009; Morice et al., 2016). However, the mechanism by which obesity promotes tumorigenesis vary by cancer site. In case of EC, the potential players involved in the interaction of adipocytes and EC cells are elevated estrogen levels, insulin, insulin growth factor-1 (IGF-1), adipokines (leptin, resistin), cytokines (IL-6, TNFα) and VEGF-mTOR signaling (Calle and Kaaks, 2004; Hlavna et al., 2011; Lumeng et al., 2007; Sahoo et al., 2017a).

Mechanism relating obesity or adiposity to EC risk

2.4.1 Leptin resistance

Leptin, a pleiotropic cytokine has significant contribution in EC progression (Carino et al., 2008). Leptin is a small non-glycosylated protein coded by obese (*OB*) gene and secreted by adipocytes. As a primary function, it regulates energy intake and expenditure. Upon leptin resistance, obese individuals exhibit higher levels of circulating leptin (Guo et al., 2012). Leptin signals through binding to its receptor (OB-R) and triggers several canonical and non-canonical signaling pathways (Daley-Brown et al., 2015). Reported Studies have shown overexpression of OB-R in EC cells as compared to normal endometrial cells (Carino et al., 2008; Wincewicz et al., 2008). In malignant EC cells, leptin signaling is also associated with the recruitment of several pro-angiogenic factors such as VEGF, IL-1β, LIF (leukemia inhibitory factor) to their respective receptors, VEGFR, IL-1R and LIFR (Carino et al., 2008) (Figure 3a). These signals collectively contribute to endometrial carcinogenesis.

2.4.2 Insulin resistance

In obesity, due to excess visceral adiposity, the level of circulating free fatty acids (FFA) increases along with peptide hormones such as leptin, resistin, TNFα and the level of adiponectin decreases. The altered secretion of adipokines leads to insulin resistance (reduced metabolic response of muscle, liver and adipose tissues to insulin). Insulin resistance results in hyperinsulinemia, which reduces the levels of IGF-1 binding proteins (IGFBP1, IGFBP2) and thereby increases IGF-1 availability (Baxter, 2014). Increased levels of bioavailable insulin and IGF-1 signal through the insulin receptor (IR) and IGF-1 receptor (IGF-1R), respectively to promote EC cell proliferation (Mu et al., 2012). Ligand binding to IR and IGF-1R phosphorylates insulin receptor substrate 1 (IRS-1) which further results in activation of PI3K/AKT/mTOR pathway and promotes EC cell survival and proliferation (Schmandt et al., 2011) (Figure 3b).

2.4.3 EC cell-adipocyte interactions

In high BMI patients, the hypertrophied adipocytes secrete increasing amounts of pro-inflammatory cytokines such as MCP-1, TNFα, IL-6, and IL-8 (Ouchi et al., 2011). The increased level of inflammatory cytokines results in the infiltration of lymphocytes, macrophages and endothelial cells, which alters adipose tissue microenvironment. In a paracrine manner, the secreted cytokines also promote EC cell proliferation (Nieman et al., 2013). Moreover, adipocytes in contact with cancer cells differentiate and reprogrammed into cancer-associated adipocytes (CAA) (Dirat et al., 2010). CAA secretes adipokines to simulate adhesion, migration, and invasion of tumor cells.

In addition to secretion of cytokines and adipokines, our recent findings suggest that in obese individuals, visceral adipose tissue (VAT) secrete surplus VEGF. Using EC tissue biopsies and an obese mouse model, our results ascertain that high VEGF in visceral adipocytes promotes vasculature in the uterus and upregulates mTOR signaling in the endometrial glands (Figure 3c) (Sahoo et al., 2017a). Thus, in a paracrine manner, the hypertrophied adipocytes in EC microenvironment of obese women stimulate endometrial hyperplasia and/or cancer through VEGF-mTOR signaling axis (Sahoo et al., 2017a).

2.4.4 Adipocyte-derived estrogen signaling

Obesity or adiposity influences the synthesis of endogenous sex steroids, such as estrogen in postmenopausal women (Nieman et al., 2013). In adipocytes, 17β-hydroxysteroid dehydrogenase converts androstenedione to testosterone and estrone to estradiol (Nieman et al., 2013). Besides adipose tissue is a predominant source of enzyme aromatase which converts androstenedione to

estrone and testosterone to estradiol (Zhao et al., 2016). Thus, obese individuals have high circulating levels of estrone and estradiol, which leads to excess estrogen production. Besides, obesity leads to hyperinsulinemia and increases IGF1 bioactivity, which in turn results in the reduced hepatic synthesis of sex hormone binding globulin (SHBG) (Simo et al., 2014). SHBG has a high binding affinity for testosterone and estradiol and maintains normal hormone level. Whereas, the adiposity induced decrease in SHBG leads to increase in bioavailable estradiol and subsequently elevated estrogen level (Simo et al., 2014). Endometrial cells express estrogen receptor and are sensitive to estrogen stimulus, which induces endometrial hyperplasia (Saloniemi et al., 2010). Thus, in obesity, the phenomenon of estrogen generation by adipocytes is an important risk factor for EC development.

3. Targeting EC microenvironment for chemoprevention

Like in most cancers, genetic mutations in oncogenes and/or tumor suppressor genes result in deregulated cell division in the endometrium, which leads to the development of EC. Current targeted approaches aim to eliminate tumor cell by disrupting the activated cancer-signaling pathway such as PI3K/Akt/mTOR signaling which is a well-known upregulated pathway in EC (Bajwa et al., 2017; Rudd et al., 2011). Although most tumor cells show good initial response towards chemotherapy, EC cells eventually develop chemoresistance and disease relapse. Besides, most of the targeted therapies in EC are used against a single dominant driver mutation or to block essential biochemical pathways and mutant proteins that are required for tumor cell growth and survival. However, most EC patients exhibit genetic heterogeneity (Cancer Genome Atlas Research et al., 2013), which leads to a limited therapeutic response of targeted agents.

The complex and heterogeneous TME mediates resistance of the solid tumor to drugs. Increasing evidence suggests that disruption of the TME that facilitates tumor cell infiltration may provide an additional level of therapeutic intervention as well as serve as a novel paradigm to treat cancers (Fang and Declerck, 2013; Ramos and Bentires-Alj, 2015). Such as modulation of progesterone receptor signaling in the EC microenvironment by progesterone therapy results in resolution of endometrial tumor cells (Carlson et al., 2012; Decruze and Green, 2007; Janzen et al., 2013; Kokka et al., 2010). Besides, investigations also show the effectiveness of immunotherapy such as therapeutic cancer vaccines against EC (Longoria and Eskander, 2016; Vanderstraeten et al., 2014; Vanderstraeten et al., 2015). Moreover as already described in this review, inhibition of the ECM-derived TGF-β signaling by small molecule inhibitors significantly suppresses EC metastasis beyond the uterus (Sahoo et al., 2017b). Given the cytotoxic effect of

chemotherapy, despite killing tumor cells, perturbation of microenvironment-derived signals may provide a broad roadmap to convert these challenges into opportunities. This strategy may render the idea of chemoprevention (such as hormonal therapy, immunotherapy) and may deteriorate the side effects of chemo drugs on other cell types. Thus, targeting stromal component of TME and molecular characterization of the sub-population of *de novo* resistant cells in the genetically stable microenvironment can more effectively eradicate tumor cells from EC patients and improve quality of life.

4. Conclusions

High grade or metastatic EC has long been associated with substantial changes in the extracellular environment. Moreover, it is increasingly evident that a single insult (genetic mutations) is not sufficient to initiate the disease, and that a second hit (microenvironment-derived signals) may be required to drive tumor-progression. The neoplastic and non-neoplastic cells in the microenvironment communicate in concert to produce a stromal microenvironment that is conducive to endometrial carcinogenesis. Although it is well demonstrated that the TME can foster a pro-tumor milieu the precise mechanism by which tumor and stromal cells communicate for the formation of a favorable environment remains elusive. Interestingly, recent evidence in other cancers has shown that nerves present in the TME also promotes tumor progression and that the nerve-cancer cell crosstalk is essential for cancer growth and metastasis (Boilly et al., 2017; Jobling et al., 2015) and whether the neural compartment is involved in EC should be investigated. Thereby, further *in vivo* and clinical study of the therapeutic targeting of EC microenvironment is warranted. Looking forward, we believe that this rapidly moving field will guide rational design of combinational therapies to target both tumor cell and its microenvironment.

Figures

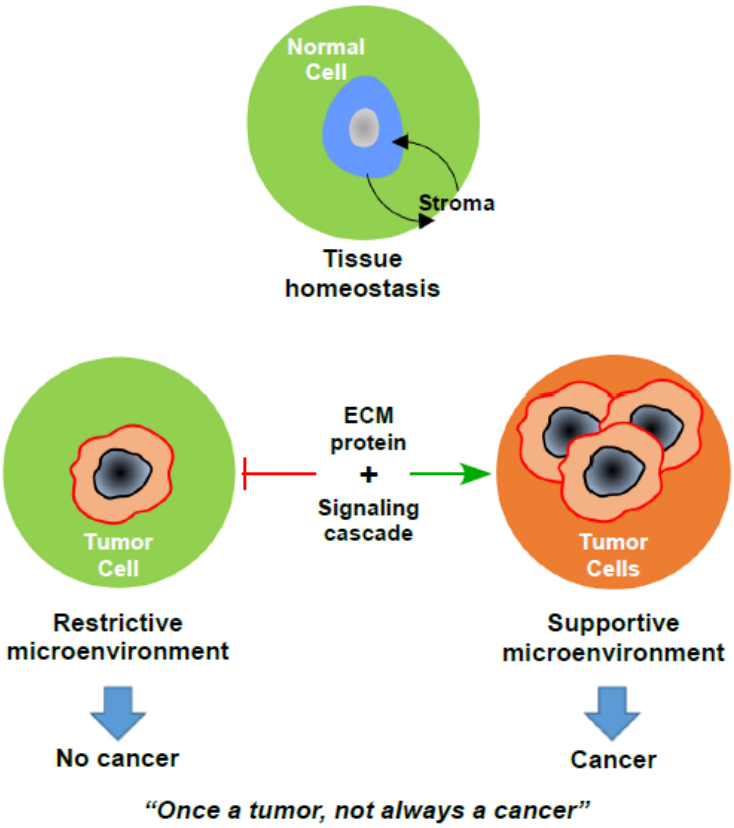

Figure 1. The Paradox of cancer development. Upon loss of tissue homeostasis, the progression of an occult tumor to frank carcinoma requires significant changes in the microenvironment.

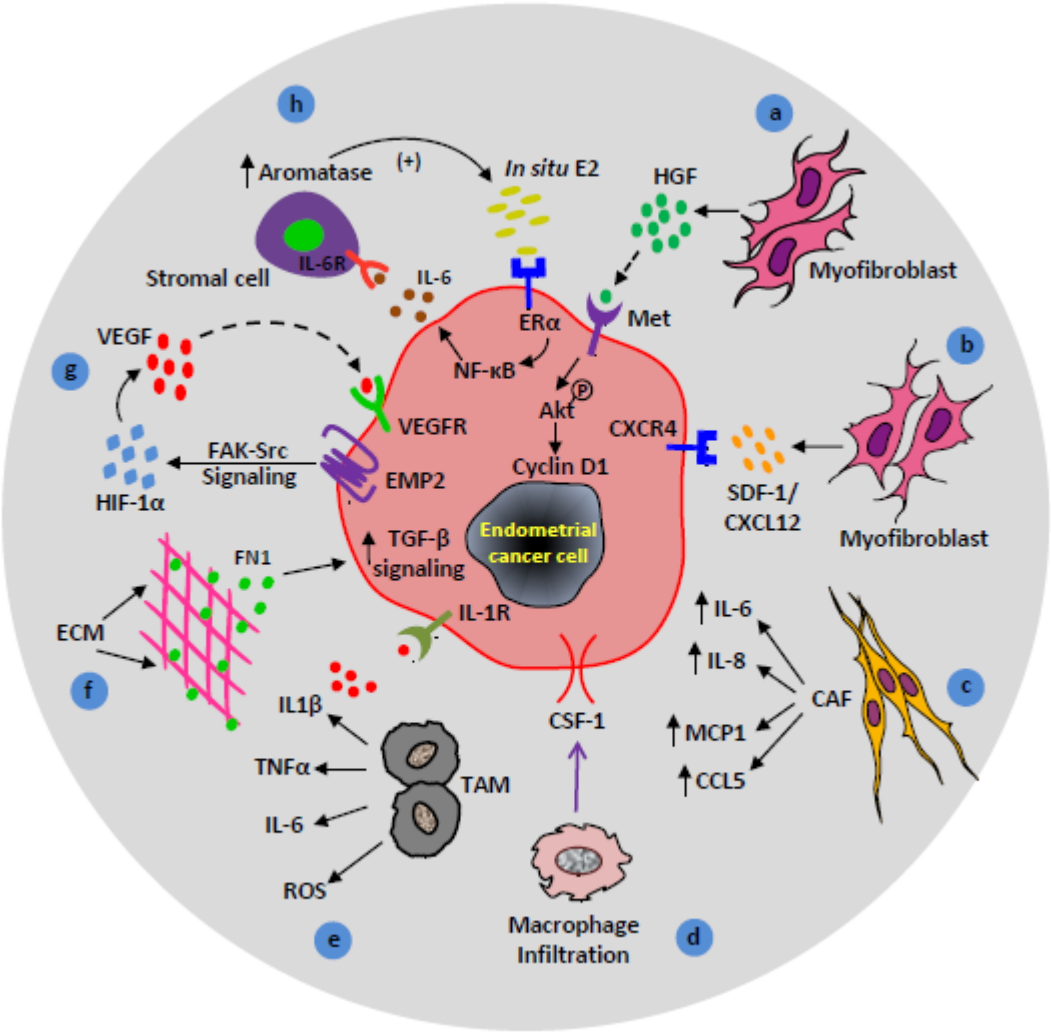

Figure 2. Multifactorial contributions of activated/recruited stromal cells in EC progression. (a) HGF stimulates proliferation of EC cells via HGF/c-Met/Akt signaling pathway. (b) Myofibroblasts promote tumor growth via CXCR4/CXCL12 signaling axis. (c) CAF secrete cytokines (IL-6, IL-8, and MCP-1) and chemokines (CCL5/RANTES) to promote cancer progression. (d) Macrophage response, colony-stimulating factor 1 (CSF1) signals macrophage infiltration to the endometrial reactive stroma. (e) Tumor-associated macrophages contribute to endometrial carcinogenesis via the production of cytokines (IL1β, TNFα, IL-6) and reactive oxygen species (ROS). (f) ECM protein, fibronectin upregulates TGF-β signaling in EC cells which facilitates EC metastasis. (g) Under hypoxic conditions, EMP2 enhances angiogenesis through FAK-Src and HIF-1α signaling pathway. (h) A positive feedback loop between *in situ* estrogen (E_2), IL-6, and aromatase upregulate EC cell proliferation.

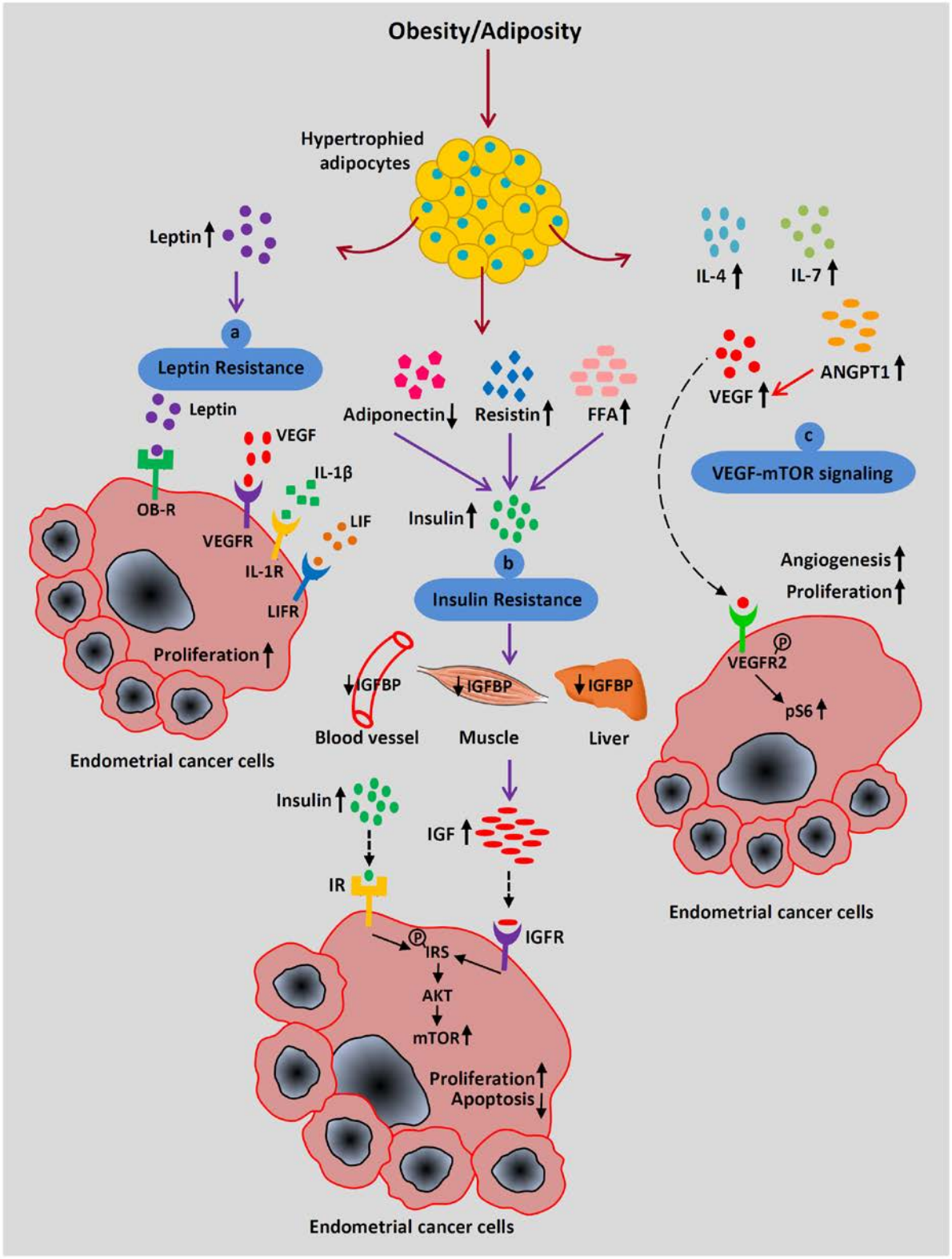
Obesity/Adiposity
Hypertrophied adipocytes
Leptin
a
Leptin Resistance
Leptin
OB-R
VEGF
VEGFR
IL-1β
IL-1R
LIF
LIFR
Proliferation
Endometrial cancer cells
Adiponectin
Resistin
FFA
Insulin
b
Insulin Resistance
IGFBP
IGFBP
IGFBP
Blood vessel
Muscle
Liver
Insulin
IR
IGF
IGFR
IRS
AKT
mTOR
Proliferation
Apoptosis
Endometrial cancer cells
IL-4
IL-7
ANGPT1
VEGF
c
VEGF-mTOR signaling
Angiogenesis
Proliferation
VEGFR2
pS6
Endometrial cancer cells

Figure 3. Systemic effects of increased adiposity on EC progression (a) High level of circulating leptin binds to its receptor OB-R to trigger signaling pathway as well as recruits pro-angiogenic factors such as VEGF, IL-1β, LIF to induce cancer progression and metastasis. (b) Increased FFA, resistin and decreased adiponectin secretion, contributes to insulin resistance, which leads to increase insulin synthesis. Hyperinsulinemia is associated with decreased bioavailability of IGFBP and the simultaneous increase in IGF-1 production. Insulin and IGF-1 signal through IR and IGFR respectively to promote EC progression via mTOR activation. (c) Hypertrophied adipocytes secrete increasing amount of pro-inflammatory cytokines (IL-4, IL-7), ANGPT1 and VEGF to infiltrate endothelial cells, which facilitates angiogenesis. VEGF acts as a key mediator of EC cell-adipocyte interaction and binds to its receptor, VEGFR2 on EC cell surface. Phosphorylation of VEGFR2 activates downstream targets and upregulates mTOR pathway through a high pS6 level.

Table 1. The stromal cell population in the EC microenvironment has distinct functions during tumorigenesis.

Cell type	Roles in endometrial cancer		References
	Anti-tumorigenic	**Pro-tumorigenic**	
Fibroblasts	Release growth factors and maintain tissue integrity	Limited	46, 47
Myofibroblasts	Facilitate deposition of collagen fibers in ECM and involve in wound healing	Chronic secretion of HGF and CXCL12 promote EC cell proliferation and angiogenesis	17, 34, 50, 55, 56, 93, 96
Cancer-associated fibroblasts (CAF)	Limited	ECM remodeling Provide oncogenic signals and secrete cytokines for infiltration of tumor cells and macrophages	77, 94, 95
Macrophages (M1)	Provide pro-inflammatory response and secrete TH1 cytokines	Limited	71
Tumor-associated macrophages (M2)	Limited	Provide anti-inflammatory response and secrete TH2 cytokines Support angiogenesis and invasion	26, 28, 49, 52
Uterine stroma	Provides structural support to endometrium	Expression of aromatase synthesizes *in situ* E2 to induce endometrial hyperplasia	16, 18, 39, 97
Adipocytes	Function as an endocrine organ, accumulate lipids and store as energy	Limited	20
Cancer-associated adipocytes (CAA)	Limited	Chronic adipokine and cytokine secretion leads to leptin and insulin resistance Aromatase synthesis results in excess estrogen production	4, 13, 41, 105, 107

Acknowledgements

This work was in part supported by funding from the National Health and Medical Research Council, the Australian Research Council, and the Cancer Institute NSW. S.S.S. is a recipient of the University of Newcastle Postgraduate Research Fellowship.

Chapter 2

Inhibition of Extracellular Matrix Mediated TGF-β Signalling Suppresses Endometrial Cancer Metastasis

Preface

Endometrial cancer being the most prevalent invasive gynecological malignancy has inadequate knowledge of its metastatic progression. Although the preliminary diagnosis of patients with chemotherapy has reduced EC-specific mortality, in many cases most of these patients eventually succumb to their malignancy. Thus, metastatic disease is responsible for poor patient outcomes with limited treatment options and necessitates exploring the mechanisms of onset of metastasis. In many cancers, the progression of indolent tumors to frank carcinomas is mediated through a supportive tumor microenvironment (TME). However, the precise role of the microenvironment in endometrial cancer metastasis is poorly investigated. In this chapter, we demonstrated how extracellular matrix (ECM) of TME promotes endometrial cancer metastasis. This chapter comprises an article entitled as **"Inhibition of extracellular matrix mediated TGF-β signalling suppresses endometrial cancer metastasis"** which is published in the journal *Oncotarget*.

UON Graduate Research

Co-authorship declaration

THE UNIVERSITY OF NEWCASTLE AUSTRALIA

Statement of Authors' Contributions

This statement summarises the intellectual input by all the authors in the paper entitled **"Inhibition of extracellular matrix mediated TGF-β signalling suppresses endometrial cancer metastasis"** in the Journal ***Oncotarget***, 2017.

Authors	Statement of contribution
Subhransu S. Sahoo (First and lead author)	Designed the study Performed all the *in vitro* and *in vivo* experiments including bioluminescent imaging Performed statistical analysis of the data including Ingenuity Pathway Analysis Made figures and tables for the paper Wrote and edited the manuscript
Min Yuan Quah (Co-author)	Helped with bioluminescent imaging
Sarah Nielsen (Co-author)	Provided endometrial cancer patient tissue sections
Joshua Atkins (Co-author)	Analysed the RNA seq data
Gough G. Au (Co-author)	Helped with bioluminescent imaging
Murray J. Cairns (Co-author)	Analysed the RNA seq data
Pravin Nahar (Co-author)	Helped with collection of clinical samples
Janine M. Lombard (Co-author)	Revised the manuscript
Pradeep S. Tanwar (Corresponding author)	Supervised the study Edited the manuscript Provided financial support

Subhransu S. Sahoo

Min Yuan Quah

Sarah Nielsen

Joshua Atkins

Gough G. Au

Murray J. Cairns

Pravin Nahar

Janine M. Lombard

Pradeep S. Tanwar

Robert Callister - Faculty Assistant Dean Research Training

UON Graduate Research

Co-authorship declaration

THE UNIVERSITY OF NEWCASTLE AUSTRALIA

Statement of Authors' Contributions

This statement summarises the intellectual input by all the authors in the paper entitled **"Inhibition of extracellular matrix mediated TGF-β signalling suppresses endometrial cancer metastasis"** in the Journal ***Oncotarget***, 2017.

Authors	Statement of contribution
Subhransu S. Sahoo (First and lead author)	Designed the study Performed all the *in vitro* and *in vivo* experiments including bioluminescent imaging Performed statistical analysis of the data including Ingenuity Pathway Analysis Made figures and tables for the paper Wrote and edited the manuscript
Min Yuan Quah (Co-author)	Helped with bioluminescent imaging
Sarah Nielsen (Co-author)	Provided endometrial cancer patient tissue sections
Joshua Atkins (Co-author)	Analysed the RNA seq data
Gough G. Au (Co-author)	Helped with bioluminescent imaging
Murray J. Cairns (Co-author)	Analysed the RNA seq data
Pravin Nahar (Co-author)	Helped with collection of clinical samples
Janine M. Lombard (Co-author)	Revised the manuscript
Pradeep S. Tanwar (Corresponding author)	Supervised the study Edited the manuscript Provided financial support

Subhransu S. Sahoo

Min Yuan Quah

Sarah Nielsen

Joshua Atkins

Gough G. Au

Murray J. Cairns

Pravin Nahar

Janine M. Lombard

Pradeep S. Tanwar

Faculty Assistant Dean Research Training

UON Graduate Research

Co-authorship declaration

THE UNIVERSITY OF NEWCASTLE AUSTRALIA

Statement of Authors' Contributions

This statement summarises the intellectual input by all the authors in the paper entitled **"Inhibition of extracellular matrix mediated TGF-β signalling suppresses endometrial cancer metastasis"** in the Journal ***Oncotarget***, 2017.

Authors	Statement of contribution
Subhransu S. Sahoo (First and lead author)	Designed the study Performed all the *in vitro* and *in vivo* experiments including bioluminescent imaging Performed statistical analysis of the data including Ingenuity Pathway Analysis Made figures and tables for the paper Wrote and edited the manuscript
Min Yuan Quah (Co-author)	Helped with bioluminescent imaging
Sarah Nielsen (Co-author)	Provided endometrial cancer patient tissue sections
Joshua Atkins (Co-author)	Analysed the RNA seq data
Gough G. Au (Co-author)	Helped with bioluminescent imaging
Murray J. Cairns (Co-author)	Analysed the RNA seq data
Pravin Nahar (Co-author)	Helped with collection of clinical samples
Janine M. Lombard (Co-author)	Revised the manuscript
Pradeep S. Tanwar (Corresponding author)	Supervised the study Edited the manuscript Provided financial support

Subhransu S. Sahoo

Min Yuan Quah

Sarah Nielsen

Joshua Atkins

Gough G. Au

Murray J. Cairns

Pravin Nahar

Janine M. Lombard

Pradeep S. Tanwar

Faculty Assistant Dean Research Training

Publication

www.impactjournals.com/oncotarget/ Oncotarget, Advance Publications 2017

Inhibition of extracellular matrix mediated TGF-β signalling suppresses endometrial cancer metastasis

Subhransu S. Sahoo[1], Min Yuan Quah[2], Sarah Nielsen[3], Joshua Atkins[4], Gough G. Au[2], Murray J. Cairns[4], Pravin Nahar[5], Janine M. Lombard[6] and Pradeep S. Tanwar[1]

[1] Gynaecology Oncology Group, School of Biomedical Sciences and Pharmacy, University of Newcastle, Callaghan, New South Wales, Australia

[2] The Picornaviral Research Unit, School of Biomedical Sciences and Pharmacy, University of Newcastle, Callaghan, New South Wales, Australia

[3] Hunter Cancer Biobank, University of Newcastle, Callaghan, New South Wales, Australia

[4] Discipline of Pharmacy and Experimental Pharmacology, School of Biomedical Sciences and Pharmacy, University of Newcastle, Callaghan, New South Wales, Australia

[5] Department of Maternity and Gynaecology, John Hunter Hospital, New Lambton Heights, New South Wales, Australia

[6] Department of Medical Oncology, Calvary Mater Newcastle, Waratah, New South Wales, Australia

Correspondence to: *Pradeep S. Tanwar,* ***email:*** *pradeep.tanwar@newcastle.edu.au*

Keywords: microenvironment, ECM, endometrial cancer, TGF-β signalling, metastasis

Received: *May 05 2017* ***Accepted:*** *May 07, 2017* ***Published:*** *May 22, 2017*

ABSTRACT

Although aggressive invasion and distant metastases are an important cause of morbidity and mortality in patients with endometrial cancer (EC), the requisite events determining this propensity are currently unknown. Using organotypic three-dimensional culture of endometrial cancer cell lines, we demonstrated anti-correlated TGF-β signalling gene expression patterns that arise among extracellular matrix (ECM)-attached cells. TGF-β pathway seemed to be active in EC cells forming non-glandular colonies in 3D-matrix but weaker in glandular colonies. Functionally we found that out of several ECM proteins, fibronectin relatively promotes Smad phosphorylation suggesting a potential role in regulating TGF-β signalling in non-glandular colonies. Importantly, alteration of TGF-β pathway induced EMT and MET in both type of colonies through slug protein. The results exemplify a crucial role of TGF-β pathway during EC metastasis in human patients and inhibition of the pathway in a murine model impaired tumour cell invasion and metastasis depicting an attractive target for therapeutic intervention of malignant tumour progression. These findings provide key insights into the role of ECM-derived TGF-β signalling to promote endometrial cancer metastasis and offer an avenue for therapeutic targeting of microenvironment derived signals along with tumour cells.

INTRODUCTION

The extracellular matrix (ECM) is a major component of the cellular microenvironment and regulates normal tissue development and homoeostasis. Stromal-epithelial communication in early development and steroid signalling is important for normal uterine functions. ECM of female reproductive tract undergoes extensive structural remodelling for decidualization, implantation and endometrial regeneration [1]. In contrast, abnormal ECM dynamics contributes to the pathological processes such as endometriosis, infertility, cancer and metastasis. The signalling alteration in uterine stroma or ECM that regulates remodelling of the differentiated endometrium to a disease or metastatic cancerous state is currently unclear. Studies have shown the crucial role of stromal signals in controlling the proliferative potential of endometrial epithelium [2-4]. Epi-genome wide methylation analysis revealed hypermethylation of Hand2 gene in endometrial stroma significantly contributes to endometrial cancer

[5]. Adipocytes in the microenvironment of higher body mass index (BMI) patients also promote endometrial cancer development [6, 7]. Given that stromal components probably significantly contribute to growth and development of endometrial cancer, relatively limited work has been carried out to address the role of the ECM in uterine biology and cancer.

The tissue microenvironment comprises of fibroblasts, adipocytes, immune cells as cellular and ECM as a non-cellular component and is known for its role in maintaining the integrity of normal tissue architecture. Disruption of the normal balance between epithelial cells and the surrounding stroma leads to tumour progression [8, 9]. These early neoplastic changes are highly reflected by the ability of tumour cells to misdirect the surrounding stroma and turn it from restrictive to the supportive environment. Once the tug of war is won by tumour cells, the restrictive microenvironment itself sustains the tumour cells to disseminate. This suggests that progression of occult tumours to frank carcinomas require significant changes in the microenvironment [10]. Thus, within the mature tissue, cell autonomous heterogeneity due to the mutations in oncogene or tumour suppressor gene is not sufficient to cause cancer unless the molecular signalling cascade has been perturbed by the microenvironment.

Cellular heterogeneity cannot be exclusively interpreted by random biological noise but there are substantial contributions from a cell's local surrounding environment [11, 12]. As compared to conventional two-dimensional (2D) cell culture, organotypic three-dimensional (3D) basement membrane cultures allow monitoring of cell-to-cell differences by providing an extra dimension to grow and by supporting cells in reconstituted basement membrane matrix or ECM [13]. The more realistic geometry of *in vivo* organisation and ECM context can give rise to non-genetic variations of a cell at its molecular level [14].

3D cell culture models have been widely used in many epithelial cancers to study cellular phenotypic changes and drug resistance mechanism [15-18]. In this study, we have addressed the molecular alterations of a cell by changing its environment and determined correlation of phenotypic divergence to the propensity of cancer progression. Using 3D basement membrane cultures of human uterine epithelium (endometrium) originated cancer cells, we have uncovered a dynamic heterogeneity that develops consecutively from 2D to 3D culture in absence and presence of ECM. ECM attached endometrial cancer cells form distinct glandular and non-glandular architecture. The dynamic molecular cascade regulating this discrete phenotype is controlled by anti-correlated transcriptional programs of the transforming growth factor-β (TGF-β) signalling pathway. The dichotomous role of TGF-β signalling as pro-tumorigenic or tumour suppressive is well known in many human cancers [19]. Cancer cells either avoid the tumour suppressive action of TGF-β through inactivation of membrane receptors or undergo a TGF-β induced epithelial-mesenchymal transition (EMT) that promotes cancer cell invasion and metastasis [20]. Here we show that the TGF-β pathway is upregulated in ECM attached cells not forming glands whereas the same signalling is downregulated in cells forming glands. The cellular heterogeneity adapted due to the matrix is also reversed by either activation or suppression of TGF-β signalling. On the other hand, the cellular phenotypic and molecular changes strongly correlate with the metastatic feature of cancer cells. These observations have very significant implications with respect to examining adaptive cellular heterogeneity due to microenvironment and its impact on cancer metastasis.

RESULTS

EC cells have distinct phenotypic divergence in different microenvironment

To examine the contribution of microenvironment towards tumour heterogeneity, we cultured human endometrial cancer (EC) cell lines, Ishikawa and MFE-296 on plastic substratum (2D) and as 3D spheroids in absence and presence of reconstituted basement membrane matrix or ECM (Figure 1A). In contrast to monolayer culture, where every cell lines adopted loosely non-distinct morphologies, marked differences were acquired when grown on 3D ECM (Figure 1A). In 3D spheroid culture, Ishikawa forms glandular colony whereas MFE-296 forms non-glandular pattern of colonies (Figure 1A). To further investigate the cellular organization of each colony, we analysed confocal z-stack sections of individual colonies. Ishikawa 3D colonies have epithelial morphology (marked by pan-cytokeratin staining) and forms a central hollow lumen on day 7 of culture (marked by F-actin staining and nuclei organization) compared to MFE-296 non-glandular colonies (Figure 1B). Besides, Ishikawa and MFE-296 colonies have similar pattern of growth in 2D culture, but significant differences emerged in proliferation rate (2.4 ± 0.1 fold) and colony size (1.7 ± 0.4 fold) when grown on 3D matrix on day 6 (Figures 1C). This suggested that in 3D, under the influence of ECM derived cues, cells forming glandular structure undergo controlled growth and organize into polarized manner, whereas, cells forming non-glandular morphology proliferate more rapidly to develop disorganized aggregates.

To understand how endometrial stromal cells, a cell type primarily responsible for ECM deposition in the uterus [2, 21], influence the growth of endometrial epithelial cells, we developed a unique method of co-culturing these two cell types. We labelled endometrial epithelial cells and stromal fibroblast cells with RFP and GFP, respectively. Co-culture of epithelial and stromal

cells revealed, non-glandular colony forming cells (MFE-296 RFP$^+$) grow robustly around the stroma (HESC GFP$^+$) but glandular colony forming cells (Ishikawa RFP$^+$) have restricted growth with round morphology (Figure 1D). These results using different culture models provided evidence for substantial contributions of microenvironment or ECM towards cellular phenotypic diversity.

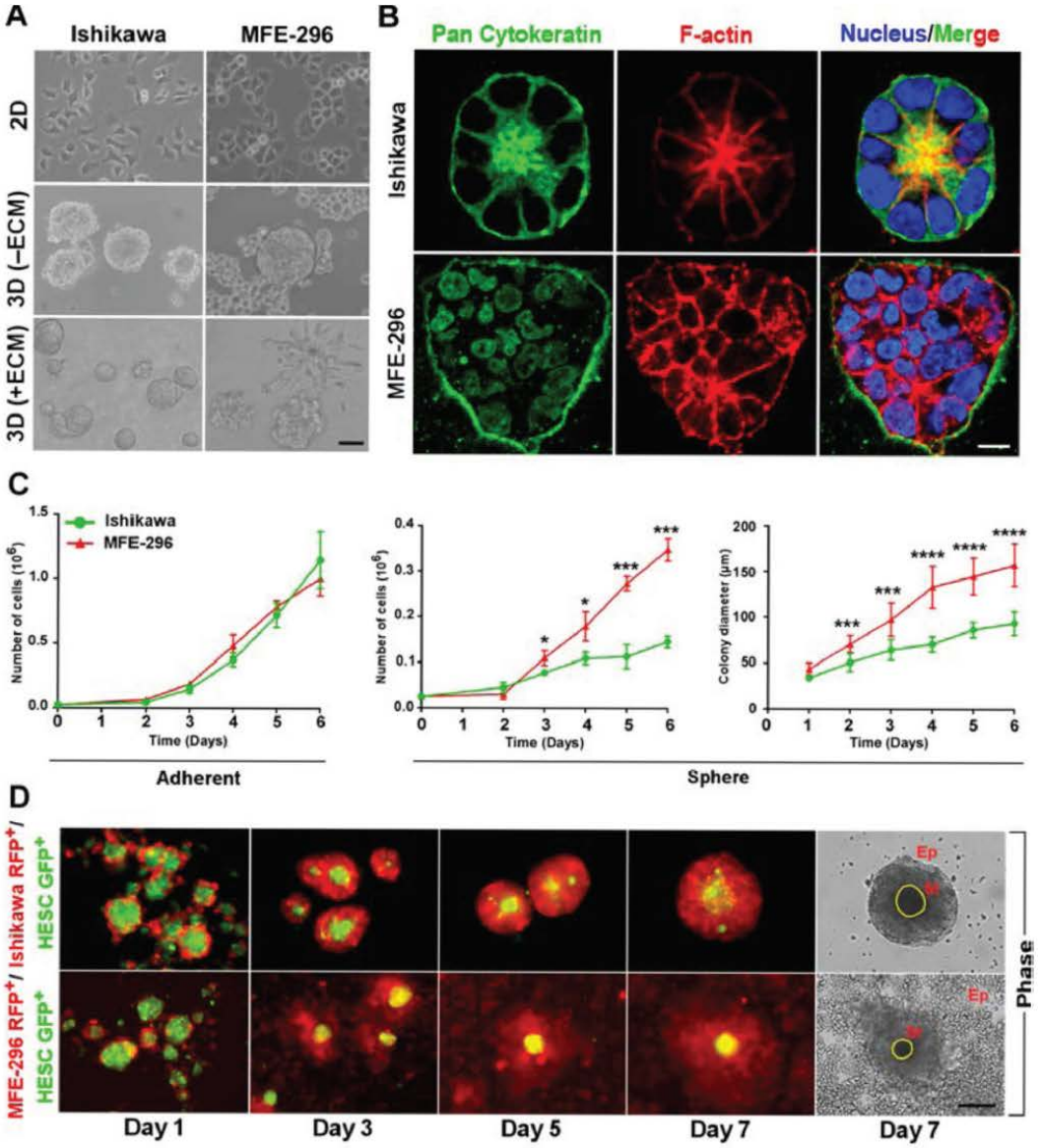

Figure 1: Endometrial cancer cells form distinct glandular and non-glandular pattern in reconstituted basement membrane and with endometrial stromal fibroblast co-culture. A. Ishikawa and MFE-296 cells were grown as monolayers (top row), spheroids without ECM (middle row) and spheroids with ECM (bottom row), Phase contrast scale bar, 50 μm. **B.** Cells were cultured in RGF-BME for 7 days, stained for pan-cytokeratin (green), phalloidin (red), counterstained with Hoechst (blue), and imaged by confocal microscopy. One representative confocal section is shown out of 100 similar colonies. Phase contrast scale bar, 50 μm; confocal scale bar, 10 μm, Phase contrast scale bar, 50 μm. **C.** Comparison of cell proliferation and colony diameter between adherent (left) and spheroid (right) culture ($n = 3$). **D.** Fluorescence and phase contrast images of endometrial epithelial and fibroblast co-culture. Ep: Epithelial cells, St: Stromal cells. Scale bar, 200 μm. Error bars represent mean ± SD; ns = $P > 0.05$, *$P < 0.05$, **$P < 0.01$, ***$P < 0.001$, ****$P < 0.0001$.

TGF-β signalling pathway is upregulated in 3D non-glandular colonies

To gain mechanistic insights into how endometrial cells respond to change in the microenvironment, we performed next generation RNA-Seq analysis on monolayer and 3D cultured spheroids. On day 7, cells completely form 3D structures with the unique cellular organization; therefore, we postulated this could be a critical time-point to see gene expression changes as compared to monolayer culture. RNA-Seq analysis identified 666 and 614 transcripts differentially expressed in Ishikawa (401 upregulated, 265 downregulated) and MFE-296 (426 upregulated, 188 downregulated) spheroids compared to 2D culture (> 2-fold change, $P < 0.05$) respectively (Figure 2A). In addition, we detected 55 and 35 most common genes in glandular (Ishikawa) and non-glandular (MFE-296) colony forming cells from adherent to spheroid culture and defined as ECM signature genes (Figure 2B). Ingenuity pathway analysis (IPA) of these genes revealed up and down regulation of several canonical cancer signalling pathways, such as estrogen-dependent breast cancer signalling, inhibition of angiogenesis by TSP1, Wnt/β-catenin, TGF-β and notch signalling and upstream target genes, such as NUPR1, RABL6, SMARCA4, HIF1A and TGFB1 in 3D glandular and non-glandular colonies (Figure 2C). However, both pathway and upstream regulator analysis displayed a comparable response of TGF-β signalling pathway in glandular and non-glandular 3D structures (Figure 2C). Out of the several pathways identified, TGF-β pathway has been known to be a major pathway in cancer progression and metastasis. This prompted us to further investigate whether ECM attached glandular and non-glandular colonies are regulated by TGF-β pathway with distinct metastatic propensity.

Notably, both TGF-β signalling pathway and upstream regulator TGF-β1 are more upregulated in non-glandular colonies (MFE-296; activation z-score, 4.008; *p*-value, 6.78E-06) compared to glandular colonies (Ishikawa; activation z-score, 2.188; *p*-value, 1.59E-12) (Figure 2C). Specifically, in accordance with the information contained in the IPA Knowledge Base (Ingenuity Systems), 17 TGF-β signalling related transcripts were upregulated (> 2-fold) in MFE-296 colonies vs monolayers, with 15 genes being known positive regulator of the pathway. However, 15 TGF-β signalling related transcripts (12 positive regulators) were downregulated (> 2-fold) in Ishikawa colonies vs monolayers (Figure 2D, Supplementary Table S1 and Supplementary Table S2). Notably, *Angptl4*, *Smad7*, *Twist1*, *Jun*, *Snai2* and *Vegfa* transcripts were upregulated (> 4-fold) in MFE-296 but not in Ishikawa, supporting an enrichment of TGF-β signalling target genes in 3D non-glandular colonies. To further verify the results from RNA-Seq data, quantitative RT-PCRs for the human TGF-β signalling pathway were performed and an overall upregulation of this pathway was detected in 3D colonies compared to monolayer culture (Supplementary Table S3 and Supplementary Table S4). As expected, TGF-β activated Smad-mediated transcriptional regulatory genes *Smad6*, *Smad7*, *Gadd45b*, *Smad3* and *Serpine1* were upregulated (> 2-fold) in non-glandular colonies whereas *Smad6*, *Serpine1* and *Tgfbi* genes were downregulated (> 2-fold) in glandular colonies confirming IPA analysis (Figure 2E). Notably, universal TGF-β responsive genes *Smad6*, *Smad7* and *Serpine1* have opposite expression pattern in 3D glandular and non-glandular colonies. An additional exploratory analysis of comparison of TGF-β signalling target genes between 3D (+ECM) cultured colonies of MFE-296 and Ishikawa demonstrated a hyper-activation of downstream genes in non-glandular vs glandular colonies (Figure 2F). Such observations of the pattern of gene expression correlate with dynamic phenotypic alteration of cells from adherent to spherical architecture.

ECM proteins enhance TGF-β signalling in non-glandular colonies

To find out whether the differences in TGF-β signalling activity encountered by mRNA analysis are reproducible at translational level, we investigated phosphorylation of Smad proteins (downstream molecules of TGF-β signalling pathway) in different culture environment (Figure 3A). Active TGF-β signalling leads to phosphorylation of SMAD proteins (Smad 2 and 3) [22]. We reproducibly detected significant upregulation (1.9 ± 0.3-fold) of p-Smad2 protein expression in 3D (+ECM) cultured MFE-296 cells (non-glandular) compared to monolayers whereas modest difference (0.8 ± 0.1-fold) was observed in case of Ishikawa colonies (glandular) (Figure 3A). We further ascertained expression of p-Smad2 protein in most of the EC cells forming glandular and non-glandular colonies (Supplementary Figure S1A). Reciprocal changes in p-Smad2 expression were observed, which was decreased in case of glandular colonies (ECC-1, HEC-1-B, MFE-280 and KLE) and increased in case of non-glandular colonies (COLO 684 and HEC-1-A) (Figure S1A). However, very low or non-detectable p-Smad2 expression was seen in two endometrial cell lines (RL95-2 and AN3 CA) in both 2D and 3D culture conditions (Supplementary Figure S1A). As ECM contact alters p-Smad2 expression, we addressed whether further activating or blocking TGF-β signalling pathway could alter the adaptive response of the 3D colonies. We treated these colonies with human TGF-β1 cytokine to activate the pathway and inhibited with SB-431542, which blocks TGF-β receptor I phosphorylation followed by downstream SMAD phosphorylation [23,

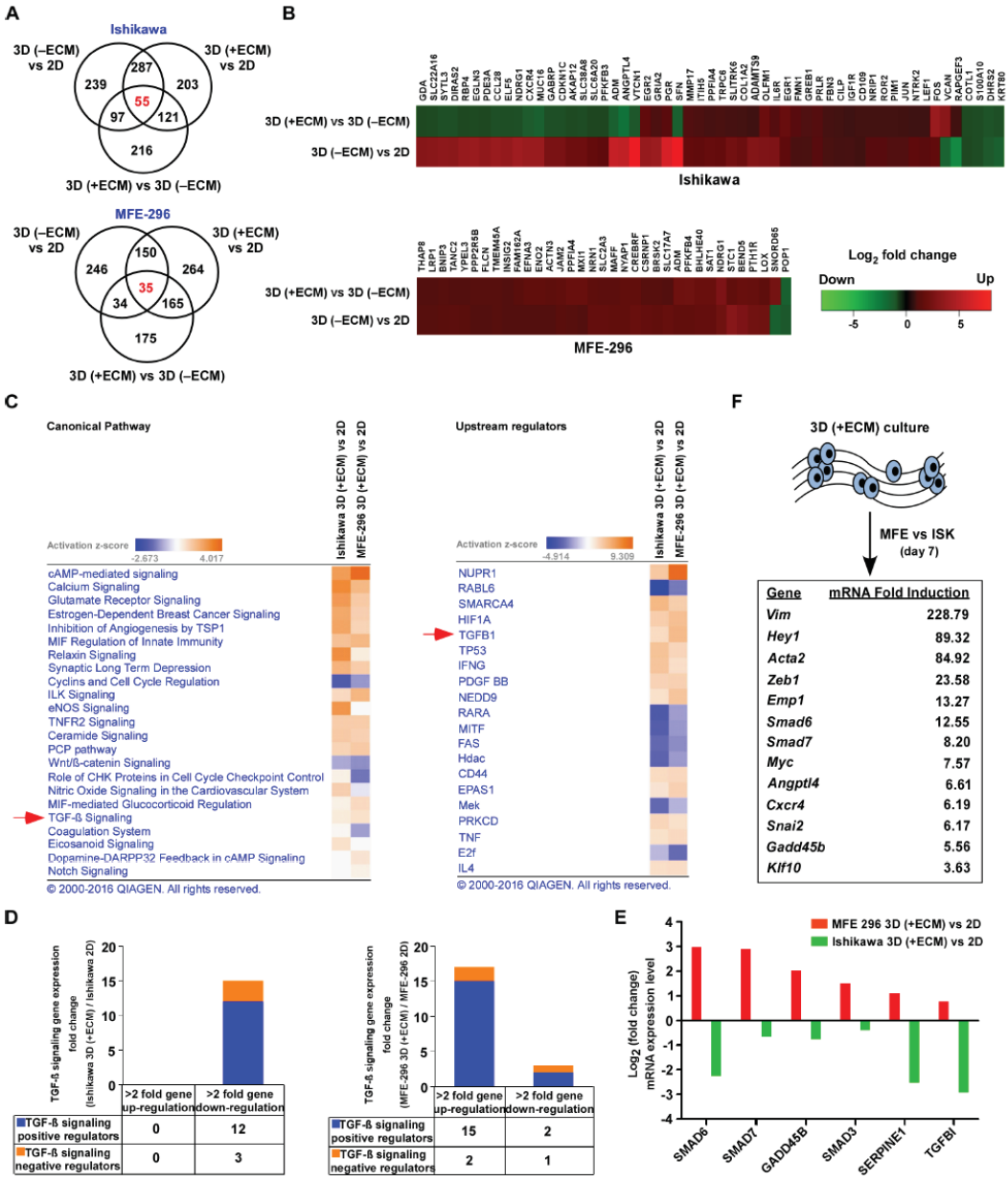

Figure 2: Gene networks and canonical pathways in EC monolayers vs 3D colonies. A. Venn diagram representing genes differentially expressed (> 2-fold, $P < 0.05$) between varying culture conditions in Ishikawa (top) and MFE-296 (bottom) cells. **B.** Heat map showing hierarchical clustering of common differential expression profiles for Ishikawa (55 genes, top) and MFE-296 (35 genes, bottom) cells grown as 3D (-ECM) to monolayer or 3D (+ECM) to 3D (-ECM) culture ($P < 0.05$). Rows represent culture groups and columns represent individual genes. Each cell corresponds to the level of expression of a particular gene. Red represents an up-regulation and green a down-regulation in gene expression. **C.** Network of differentially expressed genes generated using the IPA bioinformatics tool was compared in 2D and 3D for canonical pathway (left) and upstream regulator (right) analysis and ranked by activation z-score. **D.** Stacked diagram represents number of TGF-β signalling genes upregulated (> 2-fold) or downregulated (> 2-fold) in Ishikawa (left) and MFE-296 (right) colonies in contrast to monolayer. **E.** Validation of gene expression profiles in 3D colonies vs monolayer of Ishikawa and MFE-296 cells by human TGF-β signalling pathway RT^2 Profiler PCR Array. **F.** List of most strongly induced TGF-β signalling target genes after 7 days of 3D (+ECM) culture in MFE-296 (MFE) vs Ishikawa (ISK) cells.

24]. In the 3D context, hTGF-β1 treatment increased p-Smad2 expression (2.2 ± 0.4-fold) in MFE-296 cells compared to basal level and co-treatment with SB-431542 abolished the expression (Supplementary Figure S1B). Similarly, increasing doses of hTGF-β1 and SB-431542 increased ($P < 0.001$) or decreased ($P < 0.05$) p-Smad2 expression in Ishikawa and MFE-296 cells, respectively (Supplementary Figure S1C). We confirmed these results

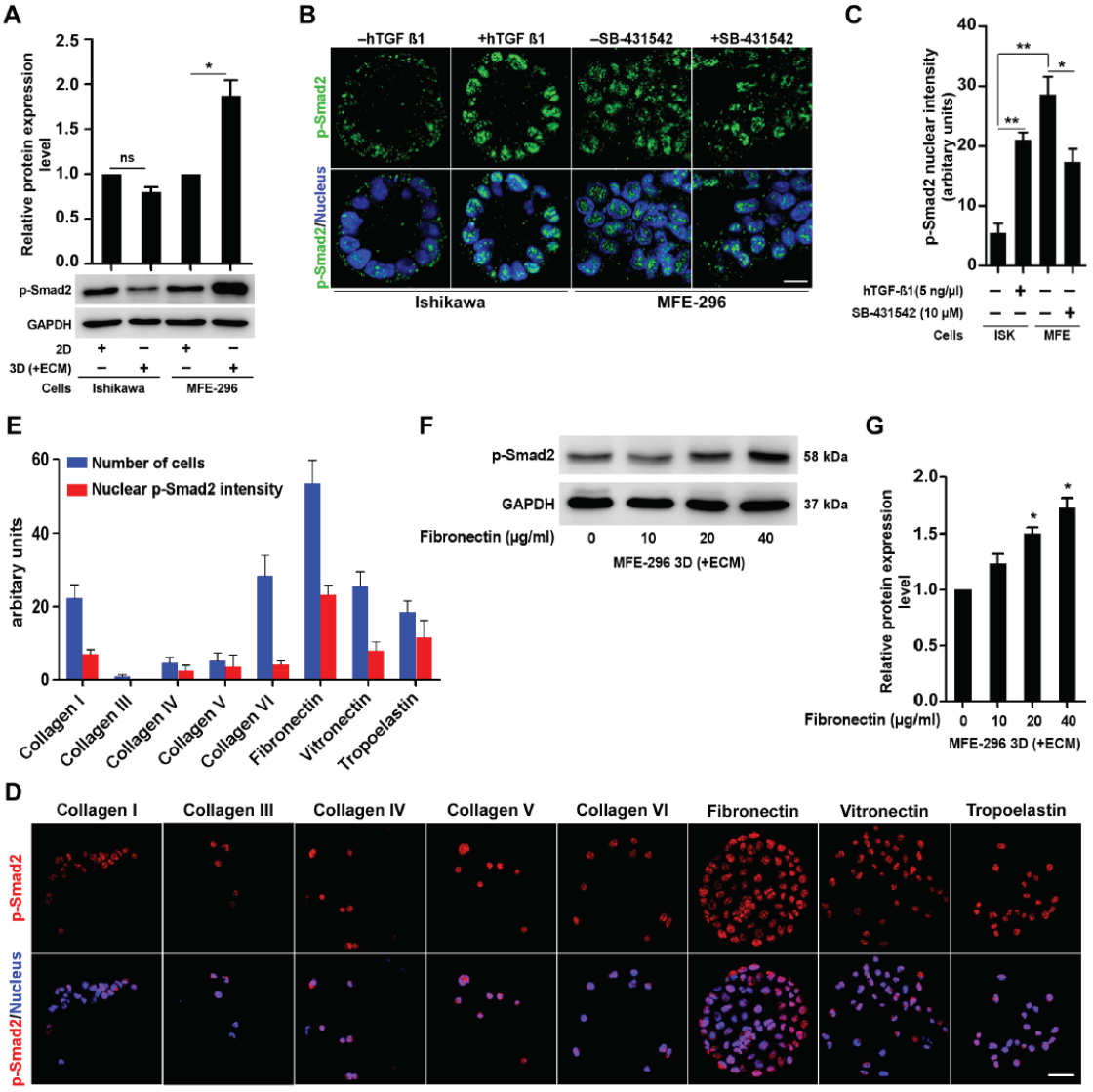

Figure 3: ECM protein, fibronectin modulates upregulation of TGF-β signalling via classical SMAD pathway. A. Immunoblot for p-Smad2 protein, in 2D and 3D culture of Ishikawa and MFE-296 cells. Error bars are mean ± SD, n = 3; $*P < 0.05$. **B.** Confocal immunofluorescence analysis of p-Smad2 protein (green) in Ishikawa and MFE-296 cells after 72 hr post hTGF-β1/SB-431542 treatment. Nucleus stained with Hoechst (blue). Scale bar, 10 µm. **C.** Quantification of nuclear p-Smad2 fluorescence signal intensity in cells treated with hTGF-β1/SB-431542. Error bars are mean ± SD, $n = 3$; $*P < 0.05$, $**P < 0.01$. **D.** MFE-296 cells were cultured on MicroMatrix ECM array slide for 48 hr, stained for p-Smad2 (red) and counterstained with Hoechst (blue). Repeated twice with each having nine biological replicates. Scale bar, 50 µm. **E.** Quantification of nuclear p-Smad2 fluorescence intensity and number of cells grown on different ECM protein components. Data are shown as mean ± SD, $n = 2$. **F.** and **G.** Western blot and quantification for p-Smad2 in MFE-296 cells with increasing concentration of human fibroblast derived fibronectin are shown. Error bars represent mean ± SD, $n = 3$; $*P < 0.05$.

by immunofluorescence staining of p-Smad2 protein (Figure 3B). At basal level, MFE-296 colonies displayed higher nuclear p-Smad2 ($P < 0.01$) fluorescence (bright green punctate) signal compared to Ishikawa colonies (Figure 3B). Compared to the basal level, treatment of hTGF-β1 and SB-431542 either increased or decreased the phosphorylated Smad protein expression in Ishikawa and MFE-296 colonies (Figure 3B and 3C). Collectively, these results suggest that TGF-β signalling has opposite activity in EC cells forming glandular and non-glandular colonies in 3D matrix. Sequestration of latent TGF-β in the ECM, as well as the dynamic interaction between multiple ECM components and latent TGF-β complexes, is crucial for activation of the latent cytokines [25, 26]. To explore the potential roles of distinct ECM proteins in regulating TGF-β signalling in EC cells, we assessed the nuclear p-Smad2 intensity of MFE-296 cells to different ECM components and relatively detected higher p-Smad2 protein expression from fibronectin-coated substratum (Figure 3D and 3E). Additionally, fibronectin relatively increased basal Smad2 phosphorylation (1.5 ± 0.1-fold) with an optimal concentration of 20 µg/ml (Figure 3F and 3G). These data suggest that fibronectin specifically induces Smad2 activation in EC cells.

TGF-β signalling regulates conversion of glandular and non-glandular epithelium

TGF-β signalling is involved in many cellular functions, including EMT [27]. EMT in epithelial cells is a cellular plasticity process involving loss of cell-cell junction molecules and acquisition of spindle morphology with increased motility [28]. Based on our observations that TGF-β signalling is highly activated in non-glandular colonies, we postulated that there might be a discrete expression of EMT markers in colonies forming glandular and non-glandular morphology. Therefore, we analysed the expression of well-known markers of EMT in 3D colonies and detected epithelial markers (E-Cadherin, Cytokeratin 8 and β-Catenin) expressed at higher levels in Ishikawa colonies whereas mesenchymal markers (N-Cadherin, Vimentin and Fibronectin) expression were more prominent in MFE-296 colonies (Figure 4A). Furthermore, we tested expression of previously reported EMT markers [29], including Snail, Slug, ZEB1 and ZO-1, by western blot analysis in Ishikawa and MFE-296 (Figure 4B). As anticipated, this analysis showed that glandular colonies tend to express epithelial markers whereas non-glandular colonies with mesenchymal features were presented with a higher expression of mesenchymal markers.

To determine if TGF-β signalling activity is responsible for some of the mesenchymal features of non-glandular colonies, we tested the effect of TGF-β signalling agonist and antagonist on endometrial cancer colonies. Treatment of Ishikawa 3D colonies with hTGF-β1 stimulated actin disorganization with loss of polarity and acquiring of non-glandular features (Figure 4C). In contrast, inhibition of TGF-β signalling by treating MFE-296 colonies with SB-431542 restored the epithelial architecture (Figure 4C). Of note, the basic difference observed between glandular and non-glandular colonies was the polarity of the individual cells. To examine cell polarity in treated (hTGF-β1 or SB-431542) and untreated colonies, we performed immunostaining for GM130 [18] and found polarized (apical-basal) Ishikawa and non-polarized MFE-296 colonies reverted their phenotype after treatment (Figure 4C). We then verified whether conversion of glandular and non-glandular morphology by disruption of cell-cell adhesions was due to the altered expression of junctional proteins. No detectable changes were observed in the expression of ZO-1 protein either by hTGF-β1 or SB-431542 (Figure 4D). However, in Ishikawa colonies, vimentin expression relatively increased to 2.7-fold with hTGF-β1 treatment whereas in MFE-296 colonies, relative E-Cadherin expression increased to 1.7-fold and Snail, Zeb1 expression decreased to 0.5-fold and 0.4-fold with SB-431542 (Figure 4D). Interestingly, the expression of Slug protein was downregulated (0.3-fold) by SB-431542 in MFE-296 colonies, which was restored (4.8-fold) by hTGF-β1 in Ishikawa colonies in a dose-dependent manner (Figure 4D).

Collectively, the results show that TGF-β pathway activity is proportionately related to the expression of EMT markers and 3D structural organization of EC cells. The glandular architecture of endometrial cancer colonies is maintained by low TGF-β signalling. Slug seems to be a key protein which expression dramatically changes in EC cells that undergo either a TGF-β induced EMT or mesenchymal-epithelial transition (MET) by the inhibitor, suggesting that TGF-β pathway regulates morphological features of endometrial glands through slug EMT marker.

Inhibition of TGF-β signalling impairs EC cell proliferation, invasion, matrix resistance and metastatic spread in non-glandular colony

The TGF-β signalling pathway is involved in a multitude of cellular processes, including cell proliferation, migration, and invasion [30]. Based on our observation that TGF-β signalling is activated in non-glandular colonies which also proliferate at a higher rate (2.6 ± 0.1 fold) than glandular one (Figure 5A), we hypothesized that inhibition of TGF-β signalling would suppress cell growth in 3D. Increasing concentration of SB-431542 significantly ($P < 0.001$) reduced proliferation of MFE-296 colonies compared to no treatment (Figure 5A). As expected, EC cells with more mesenchymal features (MFE-296) easily invade through the ECM barrier compared to cells with more epithelial characteristics (Ishikawa) (705 ± 12 MFE-

296 cells vs 87 ± 5 Ishikawa cells; Figure 5B and 5C). SB-431542 treatment strongly attenuated ($P < 0.001$) invasion of MFE-296 cells in a dose-dependent manner (Figure 5C). At 10 μM concentration, only 163 ± 6 cells were able to invade to the lower chamber (Figure 5B and 5C). Recent work in many cancer types has shown that cancer cells in 3D microenvironment are less responsive to chemotherapeutic or targeted therapies [15, 31]. We also observed that EC cells are more sensitive to chemotherapeutic drug treatments on plastic substratum compared to 3D (+ECM) culture (Figure 5D). To address whether inhibition of TGF-β signalling would increase the efficacy of chemotherapeutic drugs against EC cells, we cultured MFE-296 cells in RGF-BME for 2 days followed by treatment with Carboplatin and Paclitaxel alone or in combination with SB-431542 for 72 hr (Figure 5D). The increased matrix resistance of MFE-296 cells was reduced in dual treatment with SB-431542 in a dose dependent manner, estimated from relative cellular viability and IC50 values (Figure 5D and 5E).

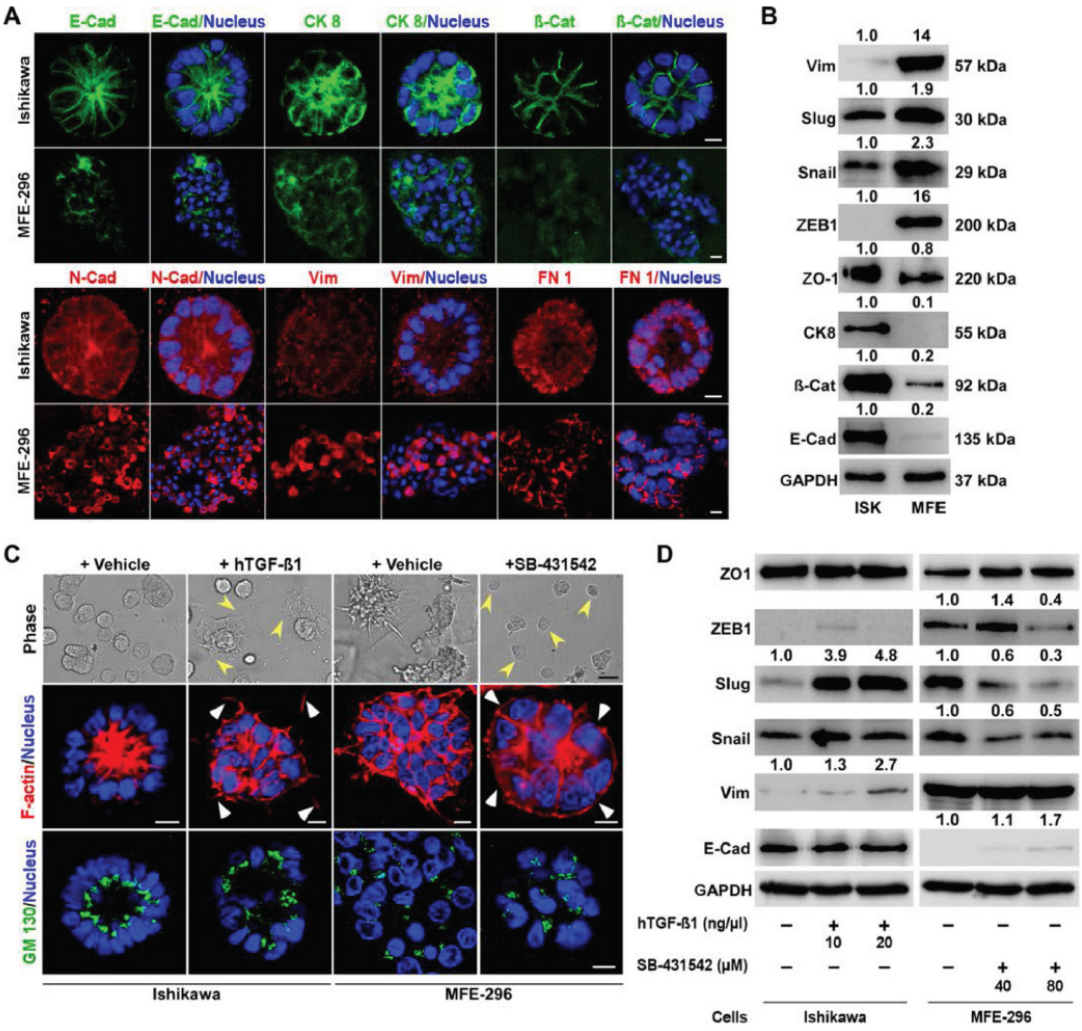

Figure 4: Differential expression of EMT markers in glandular and non-glandular endometrial cancer colonies. A. Ishikawa and MFE-296 cells were cultured in 3D matrix, fixed on day 7, stained for E-Cadherin (green), Cytokeratin 8 (green), β-Catenin (green), N-Cadherin (red), Vimentin (red), Fibronectin 1 (FN 1) (red) and imaged by confocal microscopy. **B.** Several EMT markers were validated by western blot analysis of Ishikawa and MFE-296 3D colonies. **C.** Ishikawa and MFE-296 cells were cultured in 3D, serum starved and treated with hTGF-β1 or SB-431542 for 6 days. Cells were imaged by phase contrast, fixed, stained with phalloidin (red) for actin filaments and with GM130 (green) for polarity and imaged by confocal microscopy. **D.** Western blot of different EMT markers at indicated concentrations of hTGF-β1 and SB-431542 in Ishikawa and MFE-296 3D colonies. Nucleus stained by Hoechst (blue). Confocal scale bar equal, 10 μm; phase contrast scale bar, 200 μm.

Hyper-activation of the TGF-β pathway is associated with induction of EMT and metastatic colonization of cancer cells in many organ systems [19, 32]. We have observed a higher level of TGF-β signalling activity and more mesenchymal characteristics in non-glandular colony forming EC cells compared to glandular colonies (Figure 3A and 4B), suggesting that these cells might have a higher metastatic potential. To test this, we stably transduced endometrial epithelial and stromal cells with lentiviral RFP and GFP, respectively. The RFP labelled epithelial cells were 3D cultured for 3 days to develop oncospheres and were transferred onto the layer of stromal cells (Figure 5F). Imaging was performed at regular intervals to determine the relative metastatic spread of individual colony (Figure 5F). As expected, MFE-296 cells spread at a higher rate compared to Ishikawa cells and treatment of oncospheres with SB-431542 significantly reduced the metastatic spread of MFE-296 cells in human endometrial stromal fibroblast cells, HESC (Figure 5F). In conclusion, these findings suggest EC invasion and metastasis is strongly regulated by TGF-β and inhibition of the signalling impairs tumour spread.

Inhibition of TGF-β signalling delayed and decreased metastatic potential of EC cells *in vivo*

Our *in vitro* results suggest that inhibition of TGF-β signalling during endometrial carcinogenesis may specifically reduce tumour invasion and metastasis *in vivo*. To test the effectiveness of inhibiting the TGF-β signalling pathway on *in vivo* tumour growth and metastasis, we developed EC cell-derived xenograft mouse models by intraperitoneal injection of Ishikawa^{Luc} or MFE-296^{Luc} cells in immunocompromised mice (Figure 6A). Both the cell lines were stably transduced with firefly luciferase and had equal luminescence emission (Supplementary Figure S2A and S2B). Compared to mice injected with Ishikawa^{Luc} cells, tumours in mice injected with MFE-296^{Luc} cells grew and metastasized at a higher rate (Figure

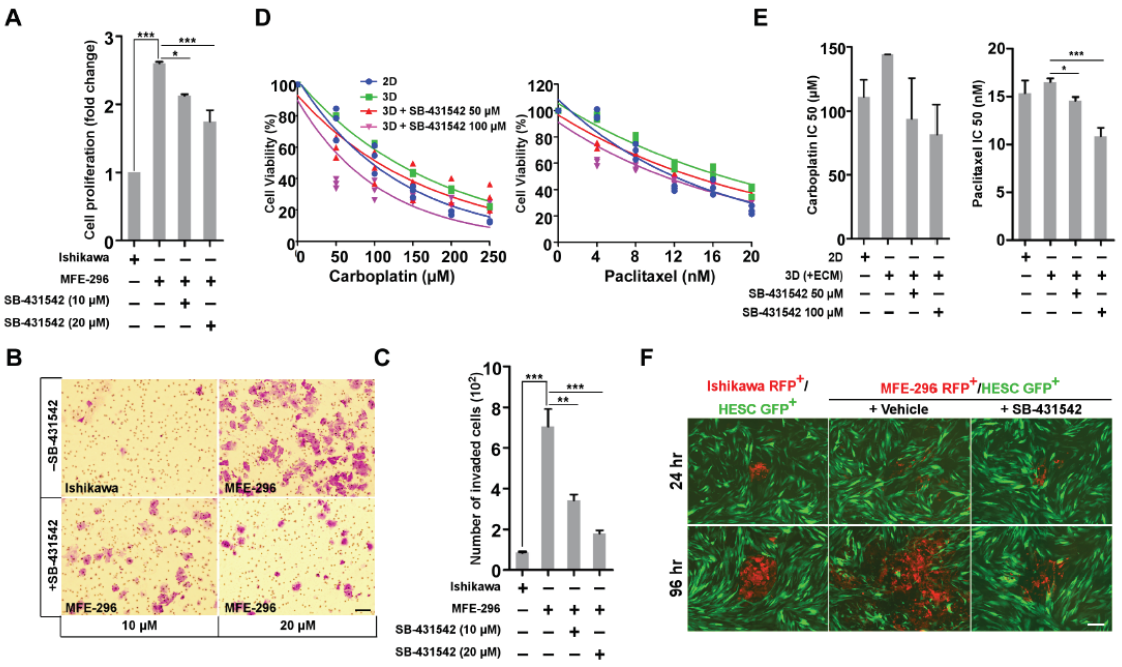

Figure 5: SB-431542 inhibits cell proliferation, invasion, chemo-resistance and metastasis *in vitro*. **A.** Ishikawa and MFE-296 cells were cultured in 3D matrix, treated with SB-431542 at indicated concentration and assayed for cell proliferation ($n = 3$). **B.** Ishikawa and MFE-296 cells (1 x10^5) were seeded onto the upper chamber of Transwell inserts and incubated for 24 hr with or without SB-431542 in the lower chamber to inhibit TGF-β signalling activity. Invasion of treated cells was determined by crystal violet staining. Cells in ten fields were imaged and counted to cover the entire filter in each group. **C.** Bar graphs represent the number of cells invaded in individual and treated groups ($n = 3$). **D.** Ishikawa and MFE-296 cells were cultured in monolayer and 3D (+ECM), treated with carboplatin (left) and paclitaxel (right) at indicated concentration with or without SB-431542 and were assayed for cell viability after 48 hr. **E.** IC50 values of carboplatin (left) and paclitaxel (right) were determined in different treatment groups from linear regression equation. **F.** Ishikawa RFP$^+$ and MFE-296 RFP$^+$ cells were grown in hanging drop 3D (+ECM) with or without SB-431542, spheroids transferred to monolayer of HESC GFP$^+$ cells and time-lapse images were taken at indicated times. Scale bar, 200 μm. Error bars represent mean ± SD; $^*P < 0.05$, $^{**}P < 0.01$, $^{***}P < 0.001$.

6A and 6B). Early metastasis was observed in mice bearing MFE-296^{Luc} tumours on day 7 (20%, 1/5 mice) and on day 14 (100%, 5/5 mice), whereas, no metastasis was observed in mice injected with Ishikawa^{Luc} cells even on day 21 (0/5 mice) (Figure 6A). Remarkably, SB-431542 treatment on mice injected with MFE-296^{Luc} cells caused marked inhibition of tumour cell metastasis up to day 14 and on day 21 late metastasis was observed (60%, 3/5 mice) (Figure 6A). Quantification of flux intensity values showed a decrease in luciferase activity and metastatic spread in mice treated with SB-431542 (Figure 6C and 6D). Furthermore, necropsy examination of the xenograft mice revealed only a solitary tumour attached to the peritoneum in the case of Ishikawa^{Luc} cells. However, metastatic spread and aggressive growth of tumours were present in mice injected with an equal number of

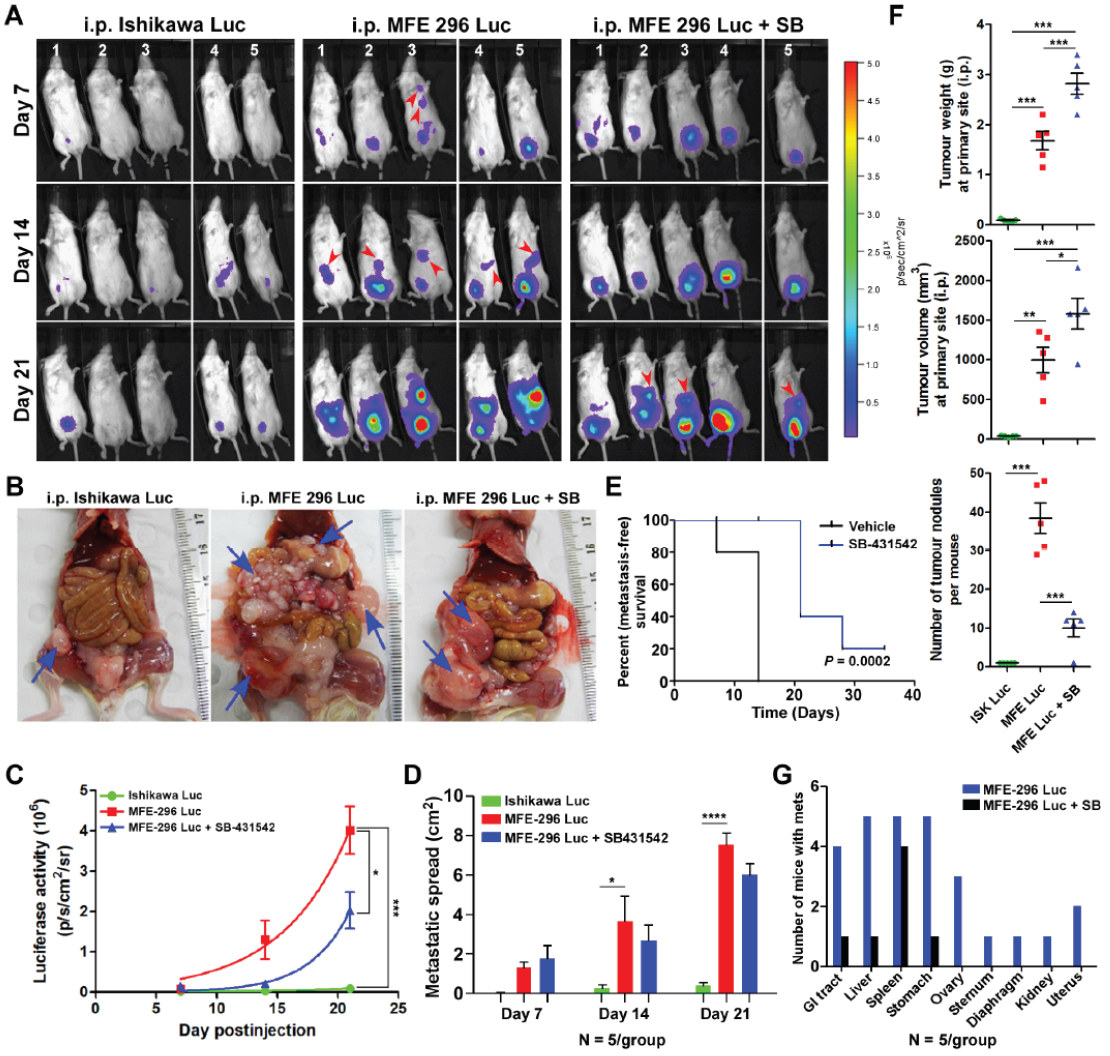

Figure 6: Inhibition of TGF-β signalling in an *in vivo* CDX model decreases metastatic spread. A. Bioluminescent images of mice injected i.p. with luciferase tagged Ishikawa and MFE-296 cells with or without SB-431542 treatment, imaged at day 7, 14 and 21. BLI imaging conducted in total 5 mice/group/time point in two repeats ($n = 3$ and $n = 2$). **B.** Necropsy examination of xenograft mice for the evaluation of tumour burden and metastasis on day 35. **C.** Average radiance in each group at the indicated time points. **D.** Metastatic spread of tumour in each group of mice at the indicated time points. **E.** Shown is a Kaplan-Meier plot with or without SB-431542 treatment. **F.** *In vivo* growth of tumours after i.p. injection of Ishikawa and MFE-296 cells with or without SB-431542. Graphs depict tumour weight, volume and number of tumour nodules measured over 35 days. **G.** Number of mice bearing secondary tumours metastasized to different organs with or without SB-431542 treatment. Error bars represent mean ± SD, $n = 5$; $^{*}P < 0.05$, $^{**}P < 0.01$, $^{***}P < 0.001$, $^{****}P < 0.0001$.

MFE-296^{Luc} cells, which was inhibited by the treatment of SB-431542 (Figure 6B). Taken together, SB-431542 significantly improves metastasis free survival *in vivo* (Figure 6E).

Measurement of total tumour weight and volume revealed that mice treated with SB-431542 had an increased mean tumour weight (2.8 ± 0.4 g) and volume (1580 ± 385mm^3) compared to the vehicle treated group mean tumour weight (1.7 ± 0.4) g and volume (997 ± 324) mm^3 at the primary site (Figure 6F). However, a significant reduction in the number of metastatic cancerous growths was observed in SB-431542 treated mice (10 ± 4) compared to control mice (38 ± 8) (Figure 6F). Gross examination of mice injected with MFE-296^{Luc} cells revealed that these cells mainly metastasized to the liver, spleen, and stomach (100%) followed by GI tract (80%), ovary (60%), uterus (20%), kidney (10%) and distant metastasized to diaphragm (10%) and sternum (10%) (Figure 6G). SB-431542 treatment successfully reduced the metastasis of tumours, with tumours limited only to the GI tract (10%), liver (10%) and stomach (10%) (Figure 6G). Haematoxylin and eosin (H&E) staining of tumour samples confirmed that SB-431542 treatment decreased the metastasis of MFE-296 cells (Supplementary Figure S3A and Supplementary Figure S3B). Immunohistochemistry (IHC) of vimentin differentiated between metastasized tumour cells (with staining) from normal adjacent cells (without staining) (Supplementary Figure S3A). Collectively, these results showed that inhibition of TGF-β signalling suppresses EC metastasis, but not the primary tumour growth. However, treatment of mice with TGF-β inhibitor and chemotherapeutic drugs (SB-431542 and either carboplatin or paclitaxel) significantly reduced metastatic

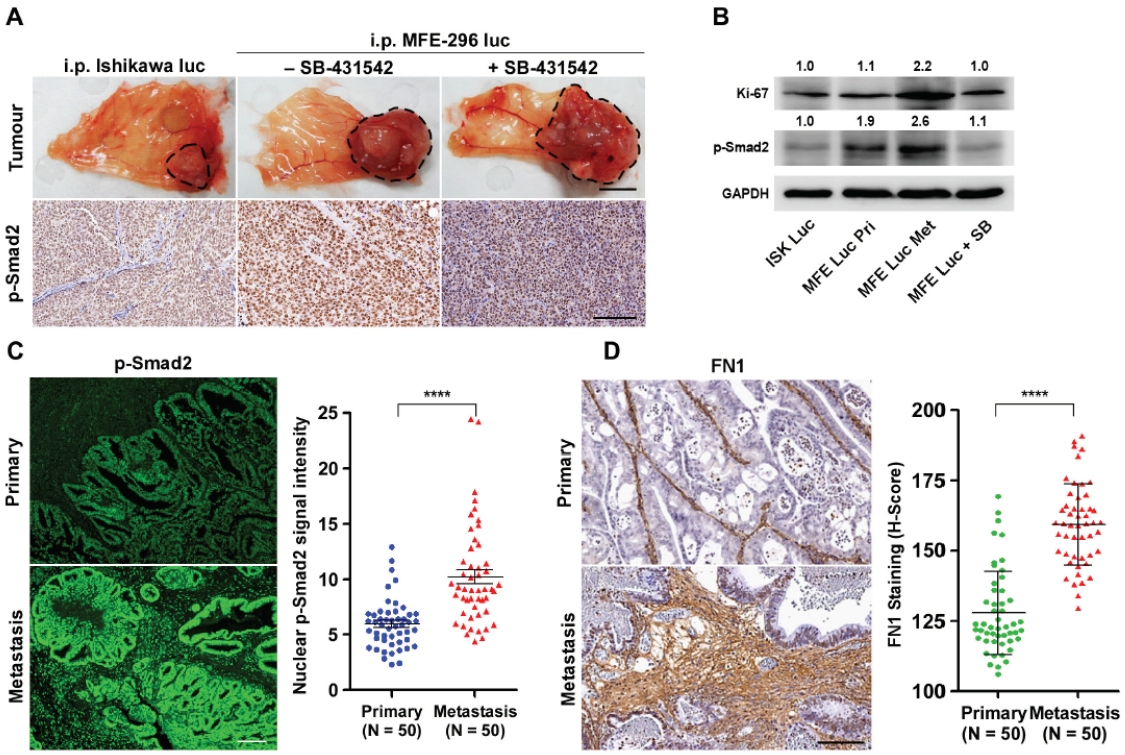

Figure 7: Up-regulation of TGF-β signalling at metastatic sites in an *in vivo* xenograft model and in fibronectin rich ECM of EC patient samples. A. Primary necropsy tumours attached to peritoneum from xenograft mice without or with SB-431542 treatment were processed for p-Smad2 IHC (brown staining). Organ image scale bar, 1 cm; IHC scale bar, 100 μm. **B.** Western blot analysis of vehicle and SB-431542 treated primary (Pri) and metastatic (Met) tumour samples. Ishikawa (ISK) and MFE-296 (MFE). **C.** Tissue sections from primary (Uterine epithelium) and metastatic sites (different body organs) of EC patients were analysed for p-Smad2 immunofluorescence (green) and representative lesions are shown. Quantification of p-Smad2 protein expression is shown, $N = 50$ (Same patient or age matched), Mann-Whitney U test, $^{****}P < 0.0001$. **D.** Immunohistochemistry staining of fibronectin (FN1) on primary and metastatic human patient tissue samples. Scale bar, 100 μm. Quantification of FN1 staining intensities was shown as H-Score, N = 50 (Same patient or age matched), Mann-Whitney U test, $^{****}P < 0.0001$.

spread as well as primary tumour growth (Supplementary Figure S2C, S2D and S2E).

Mouse EC xenografts and human EC patient samples showed similar response to TGF-β signalling during metastasis

Next, we examined whether metastatic propensity of EC cells is proportionately related with TGF-β pathway activation. We isolated primary and distant metastatic tumour samples from xenograft mice bearing tumours of Ishikawa and MFE-296 cells with or without SB-431542 treatment (Figure 7A). Gross and H&E staining analysis of tumour samples revealed that in all groups, primary tumours developed on the peritoneal wall near to the injection site (Figure 7A), which might have later metastasized to different abdominal organs. IHC of p-Smad2 protein on full-face sections taken from the edges of tumours adjacent to peritoneum lining manifested high expression of p-Smad2 protein (Figure 7A). As compared to the vehicle treated mice, SB-431542 treatment decreases p-Smad2 expression level at the primary site (Figure 7A). Protein lysates from SB-431542 treated MFE-296 tumours showed an expected decrease in Smad phosphorylation, whereas higher p-Smad2 expression was observed in MFE-296 primary tumours (1.9-fold) and metastatic tumours (2.6-fold) compared to Ishikawa tumours at the primary site (Figure 7B). A similar correlation was observed with the expression of a cell proliferation marker, Ki-67 (Figure 7B). Interestingly, Ki67 expression analysis also demonstrated that metastatic tumour cells proliferate at a higher rate (2.2-fold) compared to primary tumours (Figure 7B).

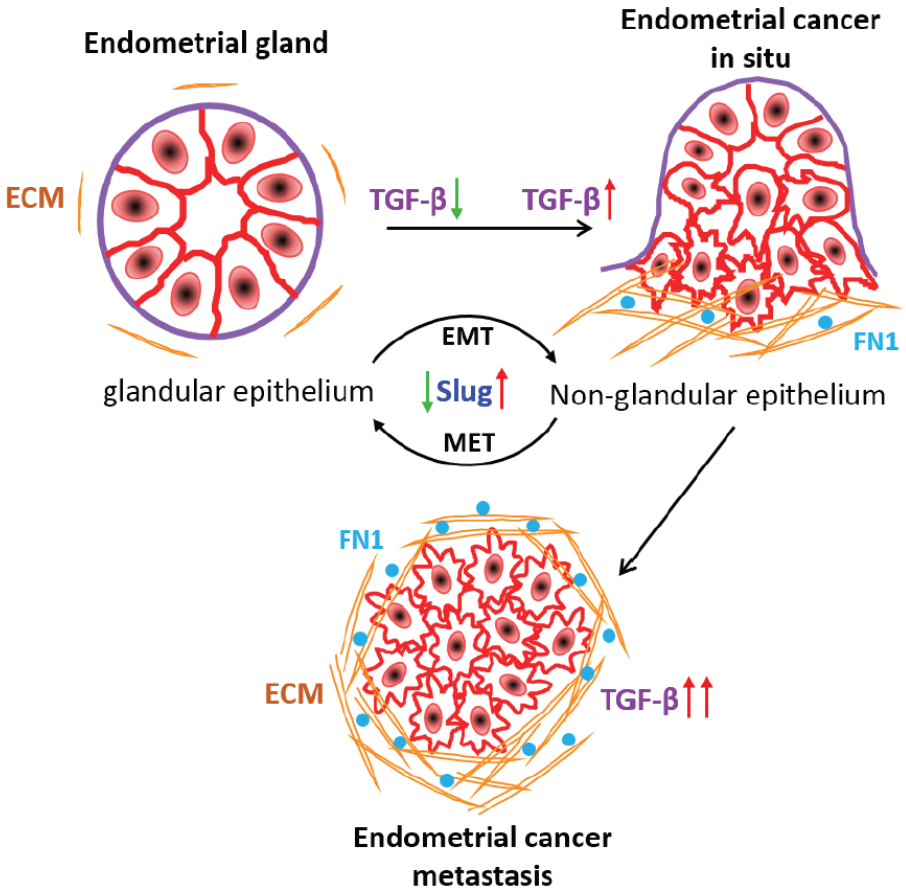

Figure 8: Working model of ECM derived TGF-β signalling during EC metastasis. Active TGF-β signalling sustains malignant transformation of EC cells and metastasis. Slug expression increases with the oncogenic transformation of acinar architecture of cells to non-glandular invasive morphology. Fibronectin in ECM deposit of in situ carcinoma relatively facilitates TGF-β signalling to promote EC metastasis.

To address whether changes in TGF-β signalling that we have observed in EC cells and xenograft models also correlate with observations in human patients, we performed p-Smad2 protein expression analysis on human EC patient tissue samples (Figure 7C). Comparison of fluorescence p-Smad2 signal intensity between primary tumour (limited to the uterus) and metastatic cancer (other organs) from 50 (same patients, $N = 33$; age matched, $N = 17$) human patients revealed significant ($P < 0.0001$) increase in p-Smad2 protein expression at the metastatic sites (Figure 7C, Supplementary Table S5). Of note, we observed more deposition of fibronectin protein in human metastatic cancer patient samples (Figure 7D) concurring *in vitro* results (Figure 3F). These data support our hypothesis that upon loss of ECM integrity, the defective ECM with high fibronectin protein activates the latent TGF-β signalling to promote EC metastasis (Figure 8).

DISCUSSION

Normal epithelial cells in the human uterus organize into an inner single layer of columnar epithelium as endometrium and into acinar structures in the stroma as endometrial glands [33]. Endometrial hyperplasia or cancer develops with the disruption of the acinar architecture of endometrial glands [34] and can be categorized as a hallmark of cancer. Epithelial cells of endometrium maintain close contact to each other through cell-cell junction proteins whereas invasive endometrial carcinoma is characterized by disorganized cells with aberrant or lack of polarization. Using a robust organotypic 3D culture model that approximates formation of human endometrial glands, we characterize normal and invasive carcinoma phenotypes. By profiling gene expression of endometrial cancer cells in the different environment, we have uncovered a major signalling pathway which is differentially expressed in glandular and non-glandular endometrial cancer colonies.

Our study began with a transcriptional dichotomy between two single cell heterogeneity in a relevant ECM context. Two-dimensionally cultured cells in contact with basement membrane matrix undergo a robust change in gene expression defined by TGF-β signalling pathway. Alteration of TGF-β pathway and downstream target genes in ECM attached cells probably occurs by post-transcriptional signalling from TGF-β family receptors. We speculate ECM proteins might bind to TGF-β ligands or receptors and exist as latent complexes or act as stimulators of the pathway [25], this requires further investigation. Moreover, we have found upregulation of TGF-β pathway in invasive endometrial cancer colonies growing on fibronectin substratum in a dose dependent manner. Given that fibronectin acts as one of the major ECM components which supports the metastatic niche [35], may explain the relative activation of TGF-β pathway on fibronectin surface to promote metastasis.

Proper dynamic regulation of the pathway is critical for establishing and stabilizing the identity of the acinar and invasive morphology of ECM attached endometrial cells. Supporting the beneficial function of TGF-β signalling inhibition in maintaining acinar organization of endometrial cancer colonies, activation of the pathway in EC cells disrupted cell polarity complex protein, GM130 and cytoskeletal organization protein, F-actin. In contrast, inhibition of the pathway in invasive colonies reversed the expression of polarity proteins. Interestingly, TGF-β pathway induced EMT proteins have contrasting levels of expression in both types of colonies. As reported earlier, EMT promotes invasiveness of cancer cells, suggesting together with our results that non-glandular colonies with mesenchymal features are more prone to metastasize. Moreover, out of several EMT proteins, we have found dynamic fold change of slug protein during activation and suppression of the TGF-β pathway in two groups of colonies respectively. Thus, slug might be a major targeted protein during the transition of differentiated to malignant endometrial cell behaviour.

Worldwide, endometrial cancer is the leading cause of cancer death in women, with most morbidity and mortality resulting from the metastatic disease [36, 37]. Additionally, the incidence of endometrial cancer continues to rise with increasing obesity rates worldwide and is likely to become one of the major obesity related cancer issues in the next 2 to 3 decades [38]. Currently, patients with metastatic endometrial cancer have a poor prognosis which might be due to chronic upregulation of TGF-β pathway. Our results on the histopathological analysis of human endometrial cancer patients show a strong correlation of active and upregulated TGF-β pathway at metastatic sites of cancer compared to primary origin of tumour in the uterus. These studies suggest that TGF-β enhances tumour progression and metastasis in endometrial cancer. In most metastatic cancers, cells first become resistant to TGF-β induced growth inhibition and later high levels of TGF-β can promote cancer progression in an autocrine and/or paracrine manner that favours invasion and metastasis [19, 39]. But how TGF-β pathway gets upregulated in malignant tumours has been enigmatic. Our data provides renewed emphasis on the ECM component of the microenvironment that regulates dynamic asynchronicity of TGF-β signalling in constituent EC cells. In the present study, we have demonstrated that SB-431542, a novel ALK5 receptor kinase inhibitor, inhibits tumour invasion and abrogated the pro-oncogenic functions of TGF-β including EMT and metastasis in both *in vitro* and *in vivo* models. Although further studies are required, our initial *in vivo* xenograft studies revealed, TGF-β inhibitor decreases the tumorigenicity of the highly aggressive MFE-296 cells in a murine EC model. Taken together, these results support the significant contribution of the TGF-β pathway in EC metastasis and suppression of the pathway might reduce the metastatic spread of cancer.

Developing a new therapeutic strategy by targeting TGF-β signalling might be promising to block TGF-β pathway in advanced stages of invasive and metastatic EC. In fact, the ECM dependent upregulation of TGF-β signalling pathway required for tumour cell growth is restricted to the specific niche of tumour population. By extension, blocking the signal from microenvironment of constituent tumour cells might be useful in suppressing tumour growth outside their normal niche.

MATERIALS AND METHODS

In vivo cell line derived xenograft (CDX) experiments

Six to eight weeks old female NOD/SCID/γ mice (Jackson lab), housed in pathogen free conventional cages on a 12 hr light-12 hr dark cycle, fed *ad libitum* were used for tumorigenicity assays. All procedures for mice experimentation were approved by the University of Newcastle Animal Care and Ethics Committee. Luciferase labelled Ishikawa and MFE-296 cells (1.5 x 10^6) in 200 µL of 1:1 sterile DPBS and Matrigel were injected intraperitoneal (i.p.) into lower abdomen region of female NOD/SCID/γ mice (5/group). Mice were injected i.p. thrice per week with SB-431542 (100 µg/kg), carboplatin (15 mg/kg) and paclitaxel (5 mg/kg) alone or in combination. The endometrial cancer cells were genetically engineered to express the firefly luciferase gene to quantitatively track *in vivo* growth and metastatic potential. Tumour development and metastatic spread were assessed weekly by monitoring luciferase signal using an IVIS bioluminescent imaging system (PerkinElmer) with a standard protocol over a period of 21 days. Animal health was monitored by daily observation and weekly assessment of weight. After 4 weeks, mice were euthanized and metastatic spread of cancer cells was assessed by counting the number of tumour nodules within the peritoneal cavity of each mouse. Recovered tumours from primary and metastasized sites were fixed in formalin, embedded in paraffin and sections stained with haematoxylin and eosin (H&E) and against antibodies to analyse tumour pathology.

Primary and metastatic patient samples

Human endometrial cancer patient samples (Primary and Metastatic) were collected at the John Hunter Hospital, Newcastle, NSW, Australia and obtained through the Hunter Cancer Tissue Biobank, University of Newcastle. The protocol was approved by the Institutional Human Research Ethics Committee of the University of Newcastle. Consent from patients was obtained as per the approved guidelines. Tumour from uterus was collected as primary and from different body parts wherever cancer has spread as the metastatic sample. In case of unavailable metastatic tissue, age matched metastatic samples were collected for this study. Detailed patient's information was listed in Supplementary Table S5.

3D glandular morphogenesis assay

Endometrial cancer cells were cultured on top of a thin layer of reduced growth factor basement membrane extract (Cultrex® RGF BME: Trevigen) purified from Engelbreth-Holm-Swarm (EHS) tumour, as previously described with minor modifications [40]. Briefly, BME was plated onto each well of a Falcon eight-well culture slide (*In Vitro* Technologies), allowed to solidify for 20 minutes at 37°C incubator, and subsequently overlaid with 400 µl of complete medium containing 1 x 10^4 trypsinized cells and 3% RGF BME. Cells were cultured for 7 days with media change every 2 or 3 days and harvested for protein and RNA isolation or imaging of 3D morphology by confocal microscopy (Olympus FluoView FV1000). Cells were also grown in three dimensions in absence of RGF BME on poly-HEMA coated (15 mg/ml in 95% EtOH and allowed to dry completely) 24-well plates for growth curve comparison.

RNA-Seq and data analysis

Total RNA was isolated from 2D monolayer and 3D grown spheroids using RNeasy Mini kit (Qiagen) following manufacturer's instructions. Library preparation was performed from total RNA using the TruSeq Stranded total RNA sample preparation kit (Illumina). Sequencing was carried out by the Australian Genome Research Facility on an Illumina HiSeq using HT version 4 chemistry with 50 bp single-end reads. A minimum of 25 million reads was achieved per sample. Raw FASTQ files were analysed using FASTQC (version 0.10.1) and adaptor contaminations were removed using Cutadapt (version 1.12). Raw reads were mapped using TopHat2 (version 2.0.13) to reference genome hg19. Mapped reads were subjected to cufflinks (version 2.2.1) for transcript assembly. Differential gene expression was determined using cuffdiff.

Cell culture and lentiviral transduction

Human endometrial cancer cell lines were cultured in MEM (HyClone) supplemented with 10% heat-inactivated fetal bovine serum (FBS, Bovogen Biologicals). Human endometrial stromal fibroblast cell line T HESCs (ATCC® #CRL-4003™) was maintained in DMEM:F12 (Sigma) without phenol red, supplemented with 10% charcoal-stripped FBS (Invitrogen). The cells

were propagated in tissue culture flasks in respective growth medium containing 2mM L-glutamine (HyClone) and antibiotics (50 units/mL penicillin, 50 mg/l streptomycin; Gibco) at 37^{0}C and 5% CO_2. STR profiling was performed for cell authentication and all the cell lines were tested mycoplasma negative.

Firefly Luciferase (GeneTarget Inc #LVP434), RFP (GeneTarget Inc #LVP428), and GFP (Qiagen #CLS-PCG) expressing stable (pooled antibiotic-resistant population) endometrial epithelial and stromal cell lines were established by transduction of lentiviral particles according to manufacturer's instructions.

In vitro Metastatic spread assay and Time-lapse imaging

RFP-expressing endometrial cancer cell spheroids were grown by culturing 100 epithelial cells (Ishikawa RFP$^+$ or MFE-296 RFP$^+$) in hanging drop fashion [41] with 3% matrigel. After 72 hr, oncospheres were transferred to 90% confluent monolayer of GFP-expressing endometrial stromal fibroblast cells (HESC GFP$^+$). Images were obtained every 24 hr using 10x objective on JuLi™ Stage Real-Time Cell History Recorder (NanoEnTek) in an incubator at 37^{0}C and humidified 5% CO_2.

3D immunofluorescence staining and microscopy

Extracellular matrix (ECM) embedded 3D colonies were fixed in 4% paraformaldehyde (PFA, Electron Microscopy Sciences, ProSciTech) for 20 minutes and processed for immunofluorescence, as previously described with minor modifications [40]. Briefly, colonies were permeabilized with 0.5% Triton X-100 in PBS for 10 minutes at 4^{0}C, blocked in immunofluorescence buffer (130 mM NaCl, 7 mM Na_2HPO_4, 3.5 mM NaH_2PO_4, 0.1% BSA, 0.2% Triton X-100, 0.05% Tween 20) containing 10% goat serum and incubated overnight at 4^{0}C with the indicated dilutions of primary antibodies. Next day, cells were washed thrice with TBS, 0.1% Tween 20, 10 minutes each and incubated with 0.5% Triton X-100 in TBS containing 5 µg/ml of Hoechst 33342 (Invitrogen) and 1:250 dilution of Alexa Fluor secondary antibodies (Jackson ImmunoResearch Laboratories) for 1 hr at room temperature. Immunofluorescence staining was visualized on a confocal LASER scanning microscope (FV1000, Olympus) using the oil-immersion 40x magnification objective and analysed with Fluoview FV10-ASW 1.7 software. 3D images were shown as mid-structure from z-stack sections.

Cellular proliferation assay

For comparison of cellular proliferation and viability, 5000 cells were seeded in 100 µL complete medium per well of 96-multiwell flat bottom plates (Corning Costar) for 2D and on basement membrane ECM-coated plates for 3D and incubated for 24 hr at 37 °C, 5 % CO2 for cells to adhere. Cells were then treated with indicated concentrations of carboplatin, paclitaxel and SB-431542 followed by further incubation of 72 hr. At the end of each incubation period, cell viability was examined by CellTiter-Glo® Luminescent cell viability assay (Promega) according to the manufacture's protocol and IC50 values were calculated.

Transwell cell invasion assay

For invasion assay, each well of Transwell assay inserts (6.5 mm diameter, 8 µm pores, Sigma #CLS3422) was coated with 0.5 mg/ml (1:30 dilution) of Matrigel (Cultrex® RGF BME: Trevigen) with ice cold sterile DPBS, and 100 µL of this slurry was pipetted into each insert of the invasion assay plate. The plate was incubated at 37^{0}C for 2 hr and then dried at room temperature (25^{0}C) overnight under sterile conditions. Ishikawa and MFE-296 cells (1 x 10^5) were serum starved for 16 hr, resuspended in MEM medium and placed in the upper chamber, whereas 10% FBS-MEM alone or containing SB-431542 with the indicated concentration was added to the lower chamber. After 24 hr incubation at 37^{0}C invaded cells were fixed in 70% alcohol and stained with crystal violet (0.5%) for 10 minutes. Matrigel and non-invading cells were mechanically wiped using cotton swabs. Cells were imaged and quantified using ImageJ software.

Western blot analysis

Cells cultured in 3D and 2D were harvested and lysed in ice-cold RIPA (radio immunoprecipitation assay) buffer (50 mM Tris-HCl pH 7.5, 150 mM NaCl, 1% NP-40, 0.5% Sodium deoxycholate, 0.1% SDS) containing protease and phosphatase inhibitors (Sigma). Lysates were purified by centrifugation at 12,000 rpm for 10 minutes at 4^{0}C and supernatant was collected. Purified lysates were boiled in 1x Laemmli sample buffer (0.04 M Tris-HCl pH 6.8, 0.2% SDS, 0.01% bromophenol blue, 10% β-mercaptoethanol and 10% glycerol) for 5 minutes at 95^{0}C. Aliquots of cell lysates containing equal protein mass were resolved by 10% SDS-PAGE gels, transferred to nitrocellulose blotting membranes (GE Healthcare Life Sciences), blocked with 5% skim milk (w/v) in TBS (20 mM Tris, 150 mM NaCl, pH 7.5), 0.1% Tween 20, for 1 hr at room temperature and probed with primary antibodies at the recommended dilutions for overnight incubation

at 4°C. Subsequently, membranes were probed with relevant secondary antibodies conjugated with horseradish peroxidase (Jackson ImmunoResearch Laboratories) for 1 hr at room temperature. After washing, western blot membranes were developed using chemiluminescent substrate for detection of HRP (Millipore) and proteins were detected by chemiluminescence (Fujifilm LAS-4000). Quantification of the mean pixel density of the protein bands was determined using NIH ImageJ plugin.

Human TGF-β signalling array

Total RNA was isolated from Ishikawa and MFE 296 cells grown as monolayer and 3D colonies, using RNeasy Mini kit (Qiagen) following manufacturer's instructions. 500 ng of total RNA was used for the cDNA synthesis using RT² First Strand Kit (Qiagen). Quantitative real-time PCR (Q-PCR) was performed using RT² SYBR Green ROX qPCR Mastermix and RT² Profiler PCR Array kit (Qiagen) on 7900 HT FAST Thermocycler (Applied Biosystems). Amplification and analysis were performed as per manufacturer's instructions. Relative quantification [comparative Ct (ΔΔCt) method] was used to compare the expression level of the test genes with the internal control (arithmetic mean of five housekeeping genes included in the array). Fold change expression of genes in 3D (+ECM) and 2D culture were plotted in log scale range.

IHC and IF

Mouse EC xenograft tumours were fixed with 4% paraformaldehyde overnight, followed by embedding and sectioning. Human EC patient-derived primary and metastatic tumour sections were deparaffinised in xylene followed by rehydration. Antigen retrieval was performed using sodium citrate buffer (10 mM Tri-sodium citrate, 0.05% Tween 20, pH 6.0). Slides were washed with TBS with 0.1% Tween 20 and incubated with 0.3% H_2O_2 to block endogenous peroxidase. Sections were blocked with 10% goat serum with 1% BSA in TBS containing 0.1% Triton X-100 for 1 hr at room temperature. After blocking, the sections were incubated with primary antibodies, followed by peroxidase-conjugated secondary antibodies (Thermo Fisher Scientific) and DAB substrate (Sigma) to detect bound antibodies. For quantification, slides were digitized at 20x absolute resolution using an Aperio AT2 scanner. Quantitative IHC analysis was performed using the Halo™ image analysis platform and the pixel intensities of DAB staining were calculated using the Area Quantification v1.0 algorithm (Indica Labs, New Mexico, USA). Immunohistochemistry intensity score (H-Score) was calculated as described previously [42]. For IF, tissue sections were incubated with primary antibodies, followed by Alexa Fluor secondary antibodies (1:250; Jackson ImmunoResearch Laboratories) to detect fluorescence signal. Images were taken at 10x magnification objective with 400 ms exposure time on a fluorescence microscope (Olympus DP72) using cellSens Standard software. Quantification of nuclear fluorescence signal was performed using the "Intensity Ratio Nuclei Cytoplasm Tool" plugin of Image J (NIH, USA).

Statistics

Statistical analyses were performed using GraphPad Prism 6.0 software. The results were presented as mean ± SD. Statistical significance was determined using a two-way analysis of variance and Bonferroni post-test unless otherwise indicated. A P value of < 0.05 was considered statistically significant.

Author contributions

S.S.S. performed most of the experiments. M.Y.Q., S.S.S. and G.G.A. performed BLI imaging of mouse xenograft experiments. J.A. and M.J.C. analysed the RNA-Seq data. S.S.S. and P.S.T. designed the study, analysed the data and wrote the paper. P.S.T. provided financial support and final approval of the manuscript. All authors approved and commented on the manuscript.

ACKNOWLEDGMENTS

Work in the Tanwar lab was in part supported by funding from the National Health and Medical Research Council, the Australian Research Council, and the Cancer Institute NSW. The Hunter Cancer Biobank is supported by the Cancer Institute NSW. S.S.S. is a recipient of the University of Newcastle Postgraduate Research Fellowship.

CONFLICTS OF INTEREST

The authors declare that they have no conflict of interest.

Editorial note

This paper has been accepted based in part on peer-review conducted by another journal and the authors' response and revisions as well as expedited peer-review in Oncotarget.

REFERENCES

1. Klemmt PA, Carver JG, Koninckx P, McVeigh EJ, Mardon HJ. Endometrial cells from women with endometriosis have increased adhesion and proliferative capacity in response to extracellular matrix components: towards a mechanistic model for endometriosis progression. Hum Reprod. 2007;

22: 3139-47. doi: 10.1093/humrep/dem262.

2. Tanwar PS, Zhang L, Roberts DJ, Teixeira JM. Stromal deletion of the APC tumor suppressor in mice triggers development of endometrial cancer. Cancer Res. 2011; 71: 1584-96. doi: 10.1158/0008-5472.CAN-10-3166.
3. Tanwar PS, Kaneko-Tarui T, Zhang L, Tanaka Y, Crum CP, Teixeira JM. Stromal liver kinase B1 [STK11] signaling loss induces oviductal adenomas and endometrial cancer by activating mammalian Target of Rapamycin Complex 1. PLoS Genet. 2012; 8: e1002906. doi: 10.1371/journal.pgen.1002906.
4. Cooke PS, Buchanan DL, Young P, Setiawan T, Brody J, Korach KS, Taylor J, Lubahn DB, Cunha GR. Stromal estrogen receptors mediate mitogenic effects of estradiol on uterine epithelium. Proc Natl Acad Sci U S A. 1997; 94: 6535-40. doi:
5. Jones A, Teschendorff AE, Li Q, Hayward JD, Kannan A, Mould T, West J, Zikan M, Cibula D, Fiegl H, Lee SH, Wik E, Hadwin R, et al. Role of DNA methylation and epigenetic silencing of HAND2 in endometrial cancer development. PLoS Med. 2013; 10: e1001551. doi: 10.1371/journal.pmed.1001551.
6. Calle EE, Kaaks R. Overweight, obesity and cancer: epidemiological evidence and proposed mechanisms. Nat Rev Cancer. 2004; 4: 579-91. doi: 10.1038/nrc1408.
7. Calle EE, Rodriguez C, Walker-Thurmond K, Thun MJ. Overweight, obesity, and mortality from cancer in a prospectively studied cohort of U.S. adults. N Engl J Med. 2003; 348: 1625-38. doi: 10.1056/NEJMoa021423.
8. Bissell MJ, Radisky D. Putting tumours in context. Nat Rev Cancer. 2001; 1: 46-54. doi: 10.1038/35094059.
9. Miles FL, Sikes RA. Insidious changes in stromal matrix fuel cancer progression. Mol Cancer Res. 2014; 12: 297-312. doi: 10.1158/1541-7786.MCR-13-0535.
10. Bissell MJ, Hines WC. Why don't we get more cancer? A proposed role of the microenvironment in restraining cancer progression. Nat Med. 2011; 17: 320-9. doi: 10.1038/nm.2328.
11. Elowitz MB, Levine AJ, Siggia ED, Swain PS. Stochastic gene expression in a single cell. Science. 2002; 297: 1183-6. doi: 10.1126/science.1070919.
12. Altschuler SJ, Wu LF. Cellular heterogeneity: do differences make a difference? Cell. 2010; 141: 559-63. doi: 10.1016/j.cell.2010.04.033.
13. Vidi PA, Bissell MJ, Lelievre SA. Three-dimensional culture of human breast epithelial cells: the how and the why. Methods Mol Biol. 2013; 945: 193-219. doi: 10.1007/978-1-62703-125-7_13.
14. Janes KA, Wang CC, Holmberg KJ, Cabral K, Brugge JS. Identifying single-cell molecular programs by stochastic profiling. Nat Methods. 2010; 7: 311-7. doi: 10.1038/nmeth.1442.
15. Muranen T, Selfors LM, Worster DT, Iwanicki MP, Song L, Morales FC, Gao S, Mills GB, Brugge JS. Inhibition of PI3K/mTOR leads to adaptive resistance in matrix-attached cancer cells. Cancer Cell. 2012; 21: 227-39. doi: 10.1016/j.ccr.2011.12.024.
16. Yamada KM, Cukierman E. Modeling tissue morphogenesis and cancer in 3D. Cell. 2007; 130: 601-10. doi: 10.1016/j.cell.2007.08.006.
17. Weigelt B, Bissell MJ. Unraveling the microenvironmental influences on the normal mammary gland and breast cancer. Semin Cancer Biol. 2008; 18: 311-21. doi: 10.1016/j.semcancer.2008.03.013.
18. Debnath J, Brugge JS. Modelling glandular epithelial cancers in three-dimensional cultures. Nat Rev Cancer. 2005; 5: 675-88. doi: 10.1038/nrc1695.
19. Massague J. TGFbeta in Cancer. Cell. 2008; 134: 215-30. doi: 10.1016/j.cell.2008.07.001.
20. Massague J. TGFbeta signalling in context. Nat Rev Mol Cell Biol. 2012; 13: 616-30. doi: 10.1038/nrm3434.
21. Ramathal C, Wang W, Hunt E, Bagchi IC, Bagchi MK. Transcription factor CCAAT enhancer-binding protein beta (C/EBPbeta) regulates the formation of a unique extracellular matrix that controls uterine stromal differentiation and embryo implantation. J Biol Chem. 2011; 286: 19860-71. doi: 10.1074/jbc.M110.191759.
22. Massague J, Seoane J, Wotton D. Smad transcription factors. Genes Dev. 2005; 19: 2783-810. doi: 10.1101/gad.1350705.
23. Inman GJ, Nicolas FJ, Callahan JF, Harling JD, Gaster LM, Reith AD, Laping NJ, Hill CS. SB-431542 is a potent and specific inhibitor of transforming growth factor-beta superfamily type I activin receptor-like kinase (ALK) receptors ALK4, ALK5, and ALK7. Mol Pharmacol. 2002; 62: 65-74. doi:
24. Laping NJ, Grygielko E, Mathur A, Butter S, Bomberger J, Tweed C, Martin W, Fornwald J, Lehr R, Harling J, Gaster L, Callahan JF, Olson BA. Inhibition of transforming growth factor (TGF)-beta1-induced extracellular matrix with a novel inhibitor of the TGF-beta type I receptor kinase activity: SB-431542. Mol Pharmacol. 2002; 62: 58-64. doi:
25. Horiguchi M, Ota M, Rifkin DB. Matrix control of transforming growth factor-beta function. J Biochem. 2012; 152: 321-9. doi: 10.1093/jb/mvs089.
26. Tian H, Mythreye K, Golzio C, Katsanis N, Blobe GC. Endoglin mediates fibronectin/alpha5beta1 integrin and TGF-beta pathway crosstalk in endothelial cells. EMBO J. 2012; 31: 3885-900. doi: 10.1038/emboj.2012.246.
27. Moustakas A, Heldin CH. Mechanisms of TGFbeta-Induced Epithelial-Mesenchymal Transition. J Clin Med. 2016; 5. doi: 10.3390/jcm5070063.
28. Nieto MA, Huang RY, Jackson RA, Thiery JP. Emt: 2016. Cell. 2016; 166: 21-45. doi: 10.1016/j.cell.2016.06.028.
29. Zeisberg M, Neilson EG. Biomarkers for epithelial-mesenchymal transitions. J Clin Invest. 2009; 119: 1429-37. doi: 10.1172/JCI36183.
30. Morikawa M, Derynck R, Miyazono K. TGF-beta and the

TGF-beta Family: Context-Dependent Roles in Cell and Tissue Physiology. Cold Spring Harb Perspect Biol. 2016; 8. doi: 10.1101/cshperspect.a021873.

31. Castells M, Thibault B, Delord JP, Couderc B. Implication of tumor microenvironment in chemoresistance: tumor-associated stromal cells protect tumor cells from cell death. Int J Mol Sci. 2012; 13: 9545-71. doi: 10.3390/ijms13089545.
32. Padua D, Massague J. Roles of TGFbeta in metastasis. Cell Res. 2009; 19: 89-102. doi: 10.1038/cr.2008.316.
33. Di Cristofano A, Ellenson LH. Endometrial carcinoma. Annu Rev Pathol. 2007; 2: 57-85. doi: 10.1146/annurev.pathol.2.010506.091905.
34. Sherman ME. Theories of endometrial carcinogenesis: a multidisciplinary approach. Mod Pathol. 2000; 13: 295-308. doi: 10.1038/modpathol.3880051.
35. Bonnans C, Chou J, Werb Z. Remodelling the extracellular matrix in development and disease. Nat Rev Mol Cell Biol. 2014; 15: 786-801. doi: 10.1038/nrm3904.
36. Amant F, Moerman P, Neven P, Timmerman D, Van Limbergen E, Vergote I. Endometrial cancer. Lancet. 2005; 366: 491-505. doi: 10.1016/S0140-6736(05)67063-8.
37. Kurra V, Krajewski KM, Jagannathan J, Giardino A, Berlin S, Ramaiya N. Typical and atypical metastatic sites of recurrent endometrial carcinoma. Cancer Imaging. 2013; 13: 113-22. doi: 10.1102/1470-7330.2013.0011.
38. Onstad MA, Schmandt RE, Lu KH. Addressing the Role of Obesity in Endometrial Cancer Risk, Prevention, and Treatment. J Clin Oncol. 2016; 34: 4225-30. doi:
39. Akhurst RJ, Hata A. Targeting the TGFbeta signalling pathway in disease. Nat Rev Drug Discov. 2012; 11: 790-811. doi: 10.1038/nrd3810.
40. Lee GY, Kenny PA, Lee EH, Bissell MJ. Three-dimensional culture models of normal and malignant breast epithelial cells. Nat Methods. 2007; 4: 359-65. doi: 10.1038/nmeth1015.
41. Foty R. A simple hanging drop cell culture protocol for generation of 3D spheroids. J Vis Exp. 2011. doi: 10.3791/2720.
42. Choudhury KR, Yagle KJ, Swanson PE, Krohn KA, Rajendran JG. A robust automated measure of average antibody staining in immunohistochemistry images. J Histochem Cytochem. 2010; 58: 95-107. doi: 10.1369/jhc.2009.953554.

Supplementary Material

www.impactjournals.com/oncotarget/ Oncotarget, Supplementary Material

Inhibition of extracellular matrix mediated TGF-β signalling suppresses endometrial cancer metastasis

Supplementary Material

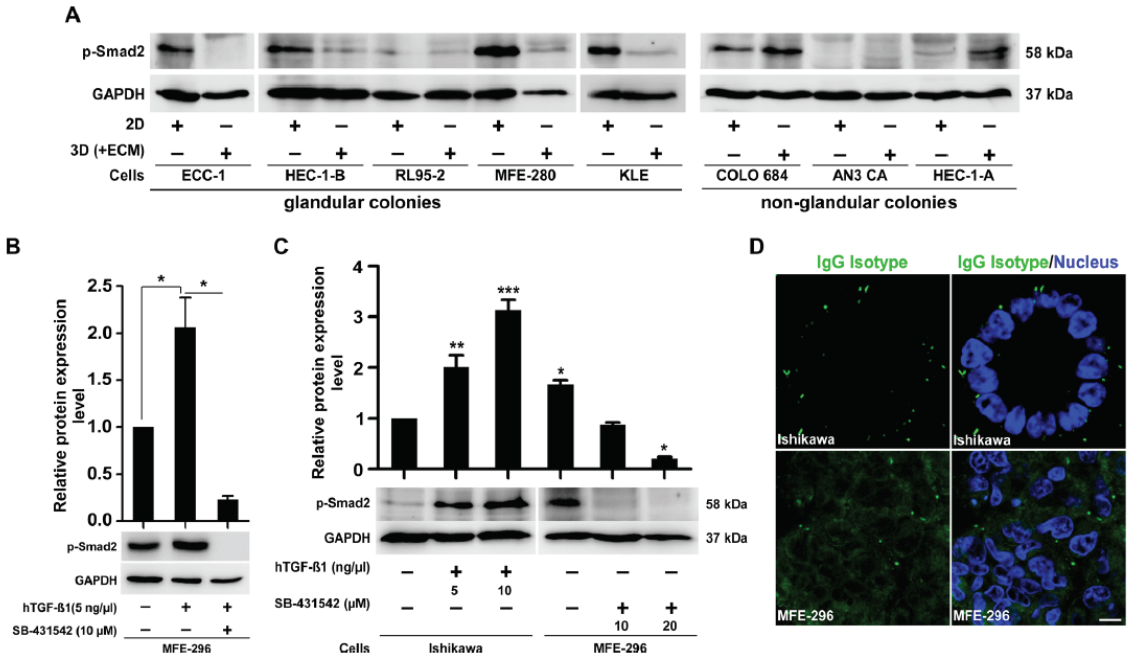

Supplementary Figure S1: Up-regulation of TGF-β signalling pathway in non-glandular endometrium colonies
(A) Western blot of p-Smad2 protein in 2D and 3D matrix culture of endometrial cancer cells forming glandular and non-glandular colonies. (B) Immunoblot for p-Smad2 protein in MFE-296 cells after 72 hr post hTGF-β1/SB-431542 treatment in 3D (n = 3). (C) Immunoblot for p-Smad2 in Ishikawa and MFE-296 cells with increasing doses of 72 hr hTGF-β1/SB-431542 treatment (n = 3). (D) Confocal immunofluorescence analysis of Ishikawa and MFE-296 cells using concentration matched Rabbit mAb IgG Isotype control (green), DNA (blue). Scale bar, 10 µm. Data are shown as mean ± SD; ns = $P > 0.05$, *$P < 0.05$, **$P < 0.01$, ***$P < 0.001$.

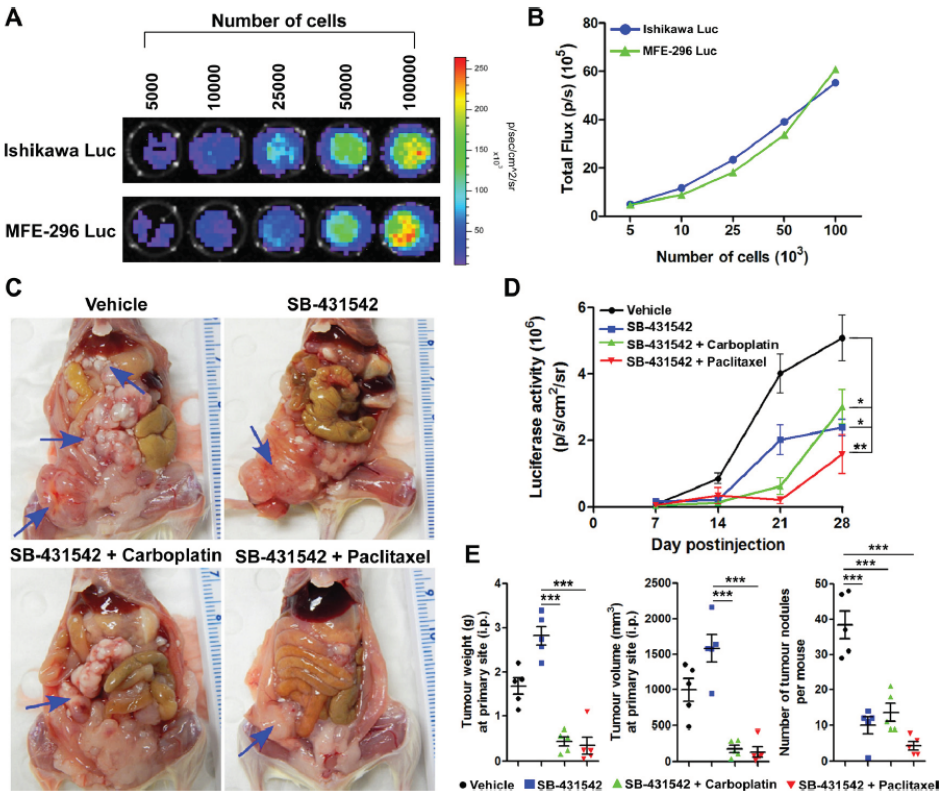

Supplementary Figure S2: In vitro luciferase activity of EC cells and inhibition of tumour growth and metastasis in vivo

(A) Bioluminescent imaging of Ishikawa^{Luc} and MFE-296^{Luc} cells after stable transduction of firefly luciferase. (B) Graph showing an estimation of total flux intensity in both the cell lines with increasing cell number. (C) Necropsy examination of xenograft mice (injected i.p. MFE-296^{Luc} cells) with dual treatment (SB-431542 and either carboplatin or paclitaxel), for evaluation of tumour burden and metastasis on day 35. (D) Average luciferase activity in each group at indicated time points. (mean ± SD, n = 5; $*P < 0.05$, $**P < 0.01$) (E) Graphs depict tumour weight, volume and number of tumour nodules measured over 35 days at indicated groups. Error bars represent mean ± SD, n = 5; $***P < 0.001$.

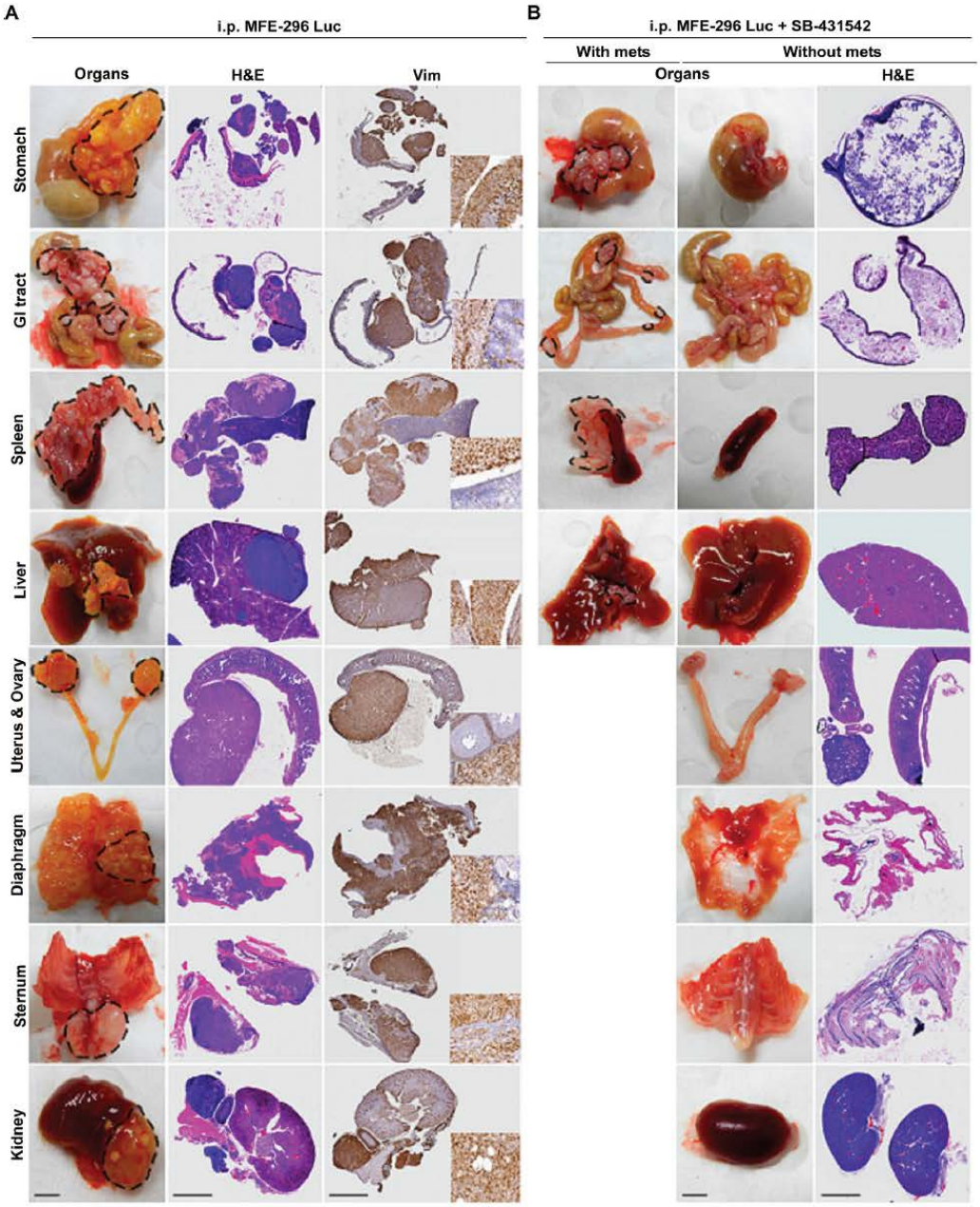

Supplementary Figure S3: NOD/SCID/γ mice bearing heterotopic xenograft of MFE-296 tumours (A and B) Necropsy tumours from different metastatic sites (as indicated with respective organ name), without (A) or with (B) SB-431542 treatment, were stained H&E, and tumours metastasized to different body organs were processed for vimentin immunohistochemistry. Organ image scale bar, 1 cm; H&E scale bar, 2 mm; IHC scale bar, 2 mm. Representative images are shown from 2 to 3 tumour sections.

For Supplementary Tables 1-5 see in supplementary Files.

Supplemental data

Supplementary Tables

***Supplementary* Table S1: TGF-β signaling pathway related genes up-regulated or down-regulated in 3D (+ECM) culture compared to 2D monolayer of Ishikawa cells (> 2.0-fold change, $p < 0.05$).**

Symbol	Gene Description	Gene Name	Fold Change	*P*-value
Up-regulated				
None				
Down-regulated				
NM_003186.3	TAGLN	Transgelin	28.25	0.00095
NM_001613.2	ACTA2	Actin, alpha 2, smooth muscle, aorta	12.71	0.0444
NM_004613.2	TGM2	Transglutaminase 2	9.13	0.01515
NM_020182.4	PMEPA1	Prostate transmembrane protein, androgen induced 1	8.98	0.004
NM_000358.2	TGFBI	Transforming growth factor, beta-induced	7.87	0.0002
NM_000212.2	ITGB3	Integrin, beta 3	6.08	0.00015
NM_002608.3	PDGFB	Platelet-derived growth factor beta polypeptide	4.45	0.00295
NM_000366.5	TPM1	Tropomyosin 1 (alpha)	3.88	0.00115
NM_001237.3	CCNA2	Cyclin A2	3.32	0.01885
NM_002467.4	MYC	V-myc avian myelocytomatosis viral oncogene homolog	2.8	0.01505
NM_003461.4	ZYX	Zyxin	2.58	0.0481
NM_005063.4	SCD	Stearoyl-CoA desaturase	2.57	0.0348
NM_017449.4	EPHB2	EPH receptor B2	2.52	0.02735
NM_004153.3	ORC1	Origin recognition complex, subunit 1	2.51	0.03825
NM_006080.2	SEMA3A	Sema domain, immunoglobulin domain (Ig), short basic domain, secreted, (semaphorin) 3A	2.37	0.0448

Supplementary **Table S2: TGF-β signaling pathway related genes up-regulated or down-regulated in 3D (+ECM) culture compared to 2D monolayer of MFE-296 cells (> 2.0-fold change, $p < 0.05$).**

Symbol	Gene Description	Gene Name	Fold Change	*P*-value
Up-regulated				
NM_139314.2	ANGPTL4	Angiopoietin like 4	23.46	5.00E-05
NM_022166.3	XYLT1	Xylosyltransferase I	14.85	0.04455
NM_003670.2	BHLHE40	Basic helix-loop-helix family, member e40	12.07	5.00E-05
NM_012258.3	HEY1	Hes-related family bHLH transcription factor with YRPW motif 1	10.59	5.00E-05
NM_005904.3	SMAD7	SMAD family member 7	9.0	5.00E-05
NM_000474.3	TWIST1	Twist family bHLH transcription factor 1	5.442	0.0342
NM_002228.3	JUN	Jun proto-oncogene	5.14	0.0016
NM_003068.4	SNAI2	Snail family zinc finger 2	4.23	0.00915
NM_003376.5	VEGFA	Vascular endothelial growth factor A	4.21	0.00015
NM_002229.2	JUNB	Jun B proto-oncogene	3.89	0.001
NM_000214.2	JAG1	Jagged 1	3.87	0.00485
NM_003088.3	FSCN1	Fascin actin-bundling protein 1	3.81	0.0013
NM_003116.1	SPAG4	Sperm associated antigen 4	3.46	0.04155
NM_006079.4	CITED2	Cbp/p300-interacting transactivator, with Glu/Asp rich carboxy-terminal domain, 2	3.18	0.0025
NM_000358.2	TGFBI	Transforming growth factor, beta-induced	2.88	0.0301
NM_022051.2	EGLN1	Egl-9 family hypoxia-inducible factor 1	2.79	0.0078
NM_019554.2	S100A4	S100 calcium binding protein A4	2.14	0.04635
Down-regulated				
NM_006080.2	SEMA3A	Sema domain, immunoglobulin domain (Ig), short basic domain, secreted, (semaphorin) 3A	2.54	0.04935
NM_006009.3	TUBA1A	Tubulin, alpha 1a	2.25	0.0332
NM_002997.4	SDC1	Syndecan 1	2.25	0.0383

Supplementary **Table S3: Validation of differentially expressed TGF-β signaling pathway genes in Ishikawa cells after 3D (+ECM) culture.**

Genes	Ishikawa 3D (+ECM) vs 2D		*P*-value
	Q-PCR Fold change	RNA-Seq Fold change	
Up-regulated genes			
EGR2	97.4	114.9	0.0374
DCN	48.3	24.2	0.009
IGF1	16.4	8.4	0.18935
COL1A2	15.7	17.0	5.00E-05
INHA	7.3	17.2	0.25415
ID2	4.7	4.2	0.0063
TGFBR3	4.2	3.6	0.00745
CDKN1A	3.0	2.4	0.0287
JUNB	2.8	3.2	0.449
BMPR1B	2.77	3.1	0.05535
ID1	2.3	2.2	0.0547
THBS1	2.1	1.9	0.13025
Down-regulated genes			
PMEPA1	13.7	9.0	0.004
PDGFB	8.1	7.9	0.00295
TGFBI	7.6	4.5	0.0002
SERPINE1	5.7	4.2	0.1357
SMAD6	4.8	3.4	0.0715
EMP1	3.3	3.4	0.0043
MYC	3.1	2.8	0.01505
FAS	2.2	2.3	0.14175
BAMBI	2.1	2.1	0.7849

Supplementary **Table S4: Validation of differentially expressed TGF-β signaling pathway genes in MFE 296 cells after 3D (+ECM) culture.**

Genes	MFE-296 3D (+ECM) vs 2D		*P*-value
	Q-PCR Fold change	RNA-Seq Fold change	
Up-regulated genes			
NOG	10.6	6.0	0.0531
SMAD6	7.9	7.7	0.0002
SMAD7	7.5	9.0	5.00E-05
ACVRL1	4.4	4.1	0.04975
GADD45B	4.1	5.6	0.0013
JUNB	3.7	3.9	0.001
KLHL24	3.3	3.3	0.00365
ID2	3.1	3.5	0.0016
SMAD3	2.9	2.5	0.05715
EGR2	2.5	3.1	0.0074
TNFSF10	2.2	1.4	0.59005
CHRD	2.0	2.1	0.2069
Down-regulated genes			
BMP4	5.3	3.1	0.0526
ACVR1	3.1	1.5	0.5371
HERPUD1	3.1	2.3	0.0302
NOV	2.7	1.3	0.74085
UBASH3B	2.1	2.6	0.0951

Supplementary **Table S5: Matched primary and metastatic human endometrial cancer samples.**

Patient ID	Primary or age matched site		Concurrent metastasis site (Age)
	Primary	Age matched (Age)	
Pt1	n/a	Endometrium (74)	Colon (77)
Pt2	Endometrium		Omentum
Pt3	n/a	Endometrium (53)	Lymph node (56)
Pt4	n/a	Endometrium (83)	Pleura (81)
Pt5	Endometrium		Pelvic side wall
Pt6	Endometrium		Paracolic gutter
Pt7	Endometrium		Thoracic
Pt8	n/a	Endometrium (72)	Vagina (74)
Pt9	n/a	Endometrium (52)	Large bowel (52)
Pt10	Endometrium		Clitoris
Pt11	n/a	Endometrium (62)	Omentum (64)
Pt12	Endometrium		Omentum
Pt13	Endometrium		Pelvic side wall
Pt14	Endometrium		Bladder/Peritoneum
Pt15	n/a	Endometrium (56)	R Ovary (56)
Pt16	Endometrium		Abdominal
Pt17	Endometrium		Sigmoid colon
Pt18	n/a	Endometrium (63)	Caecum (67)
Pt19	Endometrium		Umbilical
Pt20	n/a	Endometrium (52)	Bowel (52)
Pt21	Endometrium		R Ovary
Pt22	Endometrium		Pouch of douglas
Pt23	n/a	Endometrium (78)	Abdominal wall (81)
Pt24	Endometrium		Left parametrium
Pt25	Endometrium		Peura
Pt26	Endometrium		L fallopian tube
Pt27	Endometrium		Pelvic side wall
Pt28	n/a	Endometrium (56)	Pelvic side wall (55)
Pt29	Endometrium		Thoracic
Pt30	Endometrium		R Ovary
Pt31	Endometrium		Peritoneal wall
Pt32	n/a	Endometrium (68)	Diaphragm (68)
Pt33	n/a	Endometrium (73)	Peritoneal wall (75)
Pt34	Endometrium		Bowel
Pt35	Endometrium		R Ovary
Pt36	Endometrium		L Ovary
Pt37	Endometrium		Omentum
Pt38	n/a	Endometrium (74)	Lung (74)
Pt39	n/a	Endometrium (80)	Peritoneal wall (78)
Pt40	n/a	Endometrium (75)	Peritoneal wall (76)
Pt41	Endometrium		Bowel

Pt42	Endometrium		Perioneal surface/colon
Pt43	Endometrium		R Ovary
Pt44	Endometrium		Abdominal wall
Pt45	n/a	Endometrium (59)	Omentum (59)
Pt46	Endometrium		R Ovary
Pt47	Endometrium		L Ovary
Pt48	Endometrium		Bowel
Pt49	Endometrium		Abdominal wall
Pt50	Endometrium		R Ovary

Pt: Patient

Chapter 3

Adipose-derived VEGF-mTOR Signaling Promotes Endometrial Hyperplasia and Cancer: Implications for Obese Women

Preface

Endometrial cancer is the most common gynecological cancer. Obesity is an independent risk factor for this disease and approximately 50% of cases are associated with high body mass index (BMI). Intentional weight loss in women significantly lowers their risk of endometrial cancer. With global rise in obesity, the significant increase in endometrial cancer incidence and mortality is expected to pose a major challenge to healthcare services. At present, how adipocytes in the tumor microenvironment drive pathogenesis of endometrial hyperplasia and cancer are unclear. Understanding the molecular mechanisms involved in crosstalk between endometrial cells and adipocyte will help in developing new preventive and therapeutic measures for this disease. This chapter contains an article entitled as "**Adipose-derived VEGF-mTOR Signaling Promotes Endometrial Hyperplasia and Cancer: Implications for Obese Women"** which is published in the journal *Molecular Cancer Research.*

UON Graduate Research

Co-authorship declaration

THE UNIVERSITY OF NEWCASTLE AUSTRALIA

Statement of Authors' Contributions

This statement summarises the intellectual input by all the authors in the paper entitled **"Adipose-derived VEGF-mTOR Signaling Promotes Endometrial Hyperplasia and Cancer: Implications for Obese Women"** in the Journal ***Molecular Cancer Research***, 2017.

Authors	Statement of contribution
Subhransu S. Sahoo (First and lead author)	Designed the study Performed all the *in vitro* and *in vivo* experiments Performed statistical analysis of the data Made figures and tables for the paper Wrote and edited the manuscript
Janine M. Lombard (Co-author)	Revised the manuscript
Yvette Ius (Co-author)	Provided endometrial cancer patient samples
Rachel O'Sullivan (Co-author)	Provided endometrial cancer patient samples
Lisa G. Wood (Co-author)	Provided human adipose tissue samples Revised the manuscript
Pravin Nahar (Co-author)	Provided endometrial cancer patient samples
Kenneth Jaaback (Co-author)	Provided endometrial cancer patient samples Revised the manuscript
Pradeep S. Tanwar (Corresponding author)	Supervised and designed the study Wrote and edited the manuscript Provided financial support

Subhransu S. Sahoo

Janine M. Lombard

Yvette Ius

Rachel O'Sullivan

Lisa G. Wood

Pravin Nahar

Kenneth Jaaback

Pradeep S. Tanwar

Robert Callister - Faculty Assistant Dean Research Training

UON Graduate Research

Co-authorship declaration

THE UNIVERSITY OF NEWCASTLE AUSTRALIA

Statement of Authors' Contributions

This statement summarises the intellectual input by all the authors in the paper entitled **"Adipose-derived VEGF-mTOR Signaling Promotes Endometrial Hyperplasia and Cancer: Implications for Obese Women"** in the Journal ***Molecular Cancer Research***, 2017.

Authors	Statement of contribution
Subhransu S. Sahoo (First and lead author)	Designed the study Performed all the *in vitro* and *in vivo* experiments Performed statistical analysis of the data Made figures and tables for the paper Wrote and edited the manuscript
Janine M. Lombard (Co-author)	Revised the manuscript
Yvette Ius (Co-author)	Provided endometrial cancer patient samples
Rachel O'Sullivan (Co-author)	Provided endometrial cancer patient samples
Lisa G. Wood (Co-author)	Provided human adipose tissue samples Revised the manuscript
Pravin Nahar (Co-author)	Provided endometrial cancer patient samples
Kenneth Jaaback (Co-author)	Provided endometrial cancer patient samples Revised the manuscript
Pradeep S. Tanwar (Corresponding author)	Supervised and designed the study Wrote and edited the manuscript Provided financial support

Subhransu S. Sahoo

Janine M. Lombard

Yvette Ius

Rachel O'Sullivan

Lisa G. Wood

Pravin Nahar

Kenneth Jaaback

Pradeep S. Tanwar

Faculty Assistant Dean Research Training

UON Graduate Research

Co-authorship declaration

THE UNIVERSITY OF NEWCASTLE AUSTRALIA

Statement of Authors' Contributions

This statement summarises the intellectual input by all the authors in the paper entitled **"Adipose-derived VEGF-mTOR Signaling Promotes Endometrial Hyperplasia and Cancer: Implications for Obese Women"** in the Journal ***Molecular Cancer Research***, 2017.

Authors	Statement of contribution
Subhransu S. Sahoo (First and lead author)	Designed the study Performed all the *in vitro* and *in vivo* experiments Performed statistical analysis of the data Made figures and tables for the paper Wrote and edited the manuscript
Janine M. Lombard (Co-author)	Revised the manuscript
Yvette Ius (Co-author)	Provided endometrial cancer patient samples
Rachel O'Sullivan (Co-author)	Provided endometrial cancer patient samples
Lisa G. Wood (Co-author)	Provided human adipose tissue samples Revised the manuscript
Pravin Nahar (Co-author)	Provided endometrial cancer patient samples
Kenneth Jaaback (Co-author)	Provided endometrial cancer patient samples Revised the manuscript
Pradeep S. Tanwar (Corresponding author)	Supervised and designed the study Wrote and edited the manuscript Provided financial support

Subhransu S. Sahoo

Janine M. Lombard

Yvette Ius

Rachel O'Sullivan

Lisa G. Wood

Pravin Nahar

Kenneth Jaaback

Pradeep S. Tanwar

Faculty Assistant Dean Research Training

Publication

Oncogenes and Tumor Suppressors

Molecular Cancer Research

Adipose-Derived VEGF–mTOR Signaling Promotes Endometrial Hyperplasia and Cancer: Implications for Obese Women

Subhransu S. Sahoo[1,2], Janine M. Lombard[3], Yvette Ius[4], Rachel O'Sullivan[4], Lisa G. Wood[2], Pravin Nahar[5], Kenneth Jaaback[4], and Pradeep S. Tanwar[1,2,6,7]

Abstract

Obesity is responsible for increased morbidity and mortality in endometrial cancer. Despite the positive correlation of body mass index (BMI) or obesity in endometrial carcinogenesis, the contribution of adipose tissue to the pathogenesis of endometrial hyperplasia and cancer is unclear. This study clarifies the role of adipocytes in the pathogenesis of endometrial cancer by demonstrating that adipocyte-conditioned medium (ACM) increases proliferation, migration, and survival of endometrial cancer cells compared with preadipocyte-conditioned medium (PACM). Comparative cytokine array analysis of ACM and PACM reveal upregulation of a group of cytokines belonging to the VEGF signaling pathway in ACM. VEGF protein expression is upregulated in visceral adipose tissue (VAT) in obese patients, which is correlated with increased tumor growth in an *in vivo* xenograft model. The increased tumor size is mechanistically associated with the activation of the PI3K/AKT/mTOR pathway, a downstream target of VEGF signaling, and its suppression decreased the growth-promoting effects of VAT on endometrial cancer cells. Similar to the human model systems, pathologic changes in endometrial cells in a hyperphagic obese mouse model are associated with increased body weight and hyperactive mTOR signaling. Analysis of human tissue specimens depicts increased in tumor vasculature and VEGF-mTOR activity in obese endometrial cancer patients compared with nonobese patients. Collectively, these results provide evidence that VEGF-mTOR signaling drives endometrial cell growth leading to hyperplasia and cancer.

Implications: Adipocyte-derived VEGF–mTOR signaling may be an attractive therapeutic target against endometrial cancer in obese women. *Mol Cancer Res; 1–13. ©2017 AACR.*

Introduction

Obesity is a leading cause of several chronic diseases and has become a global health problem (1). Epidemiologic studies have shown a positive correlation between body mass index (BMI) and the incidence of various types of cancer, including breast, ovarian, colon, and endometrial (2). Of these cancer types, endometrial cancer exhibits the strongest association with obesity. Endometrial cancer is the most common gynecologic cancer and approximately 57% of cases are related to obesity in the United States (3, 4). Out of different subtypes, endometrioid endometrial cancer (Type I) is the histologic subtype that is predominantly linked to obesity with a relative risk of 1.59 (5). Despite a significant increase in the incidence of endometrial cancer in obese women during the past few decades, very limited laboratory and clinical investigations have been done to address the role of visceral adiposity (fat depots in the omentum and bowel mesentery) in endometrial cancer progression. Thus, elucidating the molecular mechanisms by which adipocytes alter the normal uterine function and physiology is important to understand the pathology of this disease.

As a primary function, adipose tissue (AT) maintains energy homeostasis of the body. Besides its role in energy storage, it is an essential endocrine organ that produces hormones and secretes growth factors and chemokines, which are collectively termed adipokines (6). Obesity is characterized by an excess of whole-body AT with an increase in the number of mature white adipocytes, which is the dominant adipocyte subtype in adult humans. In obese individuals, the hypertrophied adipocytes secrete increasing amounts of leptin, hepatocyte growth factor (HGF), angiopoietin-1 (ANGPT1), and VEGF (7). These molecules are crucial for AT communication with other cell types. Among them, VEGF is a major endothelial cell growth factor and plays a pivotal role in endothelial cell proliferation and angiogenesis. VEGF signals through transmembrane tyrosine kinase receptors, VEGFR-1 and VEGFR-2, which are expressed on the vascular epithelium (8). VEGFR-2 is the primary functional receptor that transduces angiogenic and VEGF-mediated signals whereas

[1]Gynaecology Oncology Group, University of Newcastle, Newcastle, New South Wales, Australia. [2]School of Biomedical Sciences and Pharmacy, University of Newcastle, Newcastle, New South Wales, Australia. [3]Department of Medical Oncology, Calvary Mater Newcastle, Newcastle, New South Wales, Australia. [4]Department of Gynecological Oncology, John Hunter Hospital, Newcastle, New South Wales, Australia. [5]Department of Maternity and Gynecology, John Hunter Hospital, Newcastle, New South Wales, Australia. [6]Priority Research Centre for Reproductive Science, University of Newcastle, Newcastle, New South Wales, Australia. [7]Cancer Research Program, Hunter Medical Research Institute, Newcastle, New South Wales, Australia.

Note: Supplementary data for this article are available at Molecular Cancer Research Online (http://mcr.aacrjournals.org/).

Corresponding Author: Pradeep S. Tanwar, University of Newcastle, Room 236 Life Sciences Building, Callaghan, New South Wales 2308, Australia. Phone: 612-4921-5148; Fax: 612-4921-7903; E-mail: pradeep.tanwar@newcastle.edu.au

doi: 10.1158/1541-7786.MCR-17-0466

VEGFR-1 may function as a decoy receptor (8). Upon ligand binding, VEGFR-2 undergoes autophosphorylation at tyrosine kinase domain. Phosphorylation at Tyr1175 provides a docking site for binding of adaptor proteins Shb as well as p85 subunit of the PI3 kinase (9). The p85 subunit mediates translocation of p110 to the cell membrane, where PI3K substrates are found and regulate the PI3K/AKT/mTOR pathway (10).

There is an increasing evidence that adipocytes promote the growth of different cancer cells (11–14). Adult weight gain is directly correlated with increased visceral adiposity. Currently, it is unclear how visceral fat enhances the risk of endometrial cancer. The female reproductive tract in both the mouse and the human is surrounded by visceral AT. AT and uterus are highly vascularized tissues and interconnected through blood vessels; therefore, we postulated that adipocyte-secreted growth factors might alter uterine physiology by influencing angiogenesis. Thus, the main objective of this study was to identify potential candidates that mediate the crosstalk between AT and uterine epithelial cells linking obesity and endometrial cancer. We have shown the effect of adipocyte conditioned medium (ACM) in endometrial cancer progression through *in vitro* cell proliferation, migration, and survival assays. Using paired biopsies of subcutaneous and visceral AT (SAT and VAT) from obese female patients, this study is also aimed to relate *in vitro* findings to the physiologic state. We have also used an obese mouse model, mimicking changes in high BMI patients, to examine the effect of weight gain on uterine physiology and cancer development. Our study demonstrates that the VEGF content of ACM positively correlates with ACM-induced endometrial cancer cell proliferation in both *in vitro* and *in vivo* assays. Increased body weight or BMI shows a positive correlation with VEGF and mTOR signaling in uterine epithelial cells in an obese mouse model and in human patients. Thus, collectively these results demonstrate the importance of VEGF–mTOR signaling in human endometrial cancer.

Materials and Methods

Cell lines, antibodies, and reagents

Human endometrial cancer cell line, Ishikawa (Sigma #99040201) was cultured in MEM (HyClone) supplemented with 5% heat-inactivated FBS (Bovogen Biologicals) and mouse embryonic fibroblast adipose-like cells (3T3-L1) was cultured in DMEM high glucose (HyClone) supplemented with 10% FBS. Both the cell lines were maintained in respective growth medium containing 2 mmol/L L-glutamine (HyClone) and antibiotics (50 U/mL penicillin, 50 mg/L streptomycin; Gibco) at 37°C and 5% CO_2. Cell line authentication was assessed using a short tandem repeat (STR) DNA profiling method and *Mycoplasma* contamination in cells was tested every 3 months.

Antibodies used in this study were as follows: VEGF (Santa Cruz Biotechnology #sc-7269) for western blot, VEGF (R&D Systems #MAB293R) for immunohistochemistry, VEGFR2 (CST #9698), $pVEGFR2^{Tyr1175}$ (CST #3770), CD31 (Santa Cruz Biotechnology #sc-1506), Ki-67 (Abcam #ab15580), Foxa2 (DSHB #4c7), Akt (CST #4691), pAkt (CST #4060), S6 (CST #2317), pS6 (CST #4858), ERα (Santa Cruz Biotechnology #sc-542), PR (Santa Cruz Biotechnoloby #sc-539), Stathmin (CST #D1Y5A), β-actin (DSHB #JLA20), and GAPDH (CST #5174).

Reagents used in this study were as follows: Indomethacin (Sigma #I7378), Dexamethasone (Sigma #D1756), 3-Isobutyl-1-methylxanthine (Sigma #I5879), 3,3′,5-Triiodo-L-thyronine (Sigma #T2877), Type 1 Collagenase (Sigma #C5894), Oil Red O (Sigma #O0625), Crystal violet (Sigma #C3886), Tamoxifen (Sapphire Bioscience #13258), DBL Carboplatin (Hospira #611685A00) and ANZATAX Paclitaxel (Hospira #616841AAU).

Human adipose tissue samples

The University of Newcastle Human Research Ethics Committee approved the protocol to collect human adipose tissue. Subcutaneous and visceral adipose tissue were collected in DMEM/F-12 medium from human female patients (BMI >30 kg/m^2) undergoing bariatric surgery for weight loss. Consent from patients was obtained as per approved guidelines.

Isolation of mature adipocytes from human adipose tissue

The primary adipocytes were isolated from human adipose tissue (subcutaneous and visceral) as described previously (15) with minor modifications. Briefly, adipose tissue (approximately 50–100 mg) was minced, washed with DPBS, and digested in 1 mg/mL Collagenase (Type 1) solution containing 0.5% BSA for 1 hour at 37°C with gentle shaking. The digestion mixture was passed through a 45-μm cell strainer (BD Biosciences) and centrifuged at 800 rpm for 5 minutes. The upper floating layer containing the mature adipocytes was collected, washed and cultured in DMEM/F-12. After 48 hours, the culture medium (500 μL) containing primary adipocytes was passed through a syringe filter (0.22 μm, Millipore) to collect subcutaneous and visceral adipocytes conditioned medium (SAT CM and VAT CM). Basal DMEM/F-12 medium as serum-free medium (SFM) and 20% (v/v) of SAT CM or VAT CM in DMEM/F-12 medium were used in cell proliferation experiment.

Human endometrial cancer sample analyses

Formalin-fixed paraffin-embedded (FFPE) nonobese human endometrial tissue ($n = 5$) and endometrial cancer tissue from nonobese ($n = 7$) and obese ($n = 13$) women were obtained from the Hunter Cancer Biobank with approved institutional Human Research Ethics Committee protocols. Tissue sections were cut and stained for VEGF, VEGFR2, CD31, and pS6.

Tumor xenograft experiments

The University of Newcastle Animal Care and Ethics Committee approved all procedures for mice experimentation. Six to 8-week-old, female NOD *scid* gamma mice (The Jackson Laboratory) were used for *in vivo* tumorigenicity assays. Ishikawa cells alone (1.5×10^6) or in combination with minced human subcutaneous and visceral adipose tissue (150 μL packed cell volume, PCV) were injected subcutaneously with growth factor-reduced Matrigel (50 μL) into the flanks of the mice as described previously (11). Tumor volumes were measured weekly by using digital calipers using the formula (length × $width^2$)/2. Tumor weight was determined at the end of the experiment and fixed in 10% buffered formalin, embedded in paraffin and sections stained with antibodies to analyze tumor pathology. Tumor sections also flash-frozen and stored at −80°C for protein isolation and Western blot analysis.

Tamoxifen treatments

The University of Newcastle Animal Care and Ethics Committee approved animal studies. $Alms1^{bbb/bbb}$ and $Alms1^{bbb/+}$ Blobby mice were injected intraperitoneally with vehicle (sesame oil, 100 μL) or tamoxifen (100 μL of 20 mg/mL stock concentration; 20 mg

tamoxifen dissolved in 1 mL sesame oil by shaking overnight at 37°C and stored in a light blocking vessel; $n = 4$/genotype per treatment). Treatments were repeated thrice with an interval of 48 hours between each injection. Mice were euthanized 14 days after the first injection. At the time of dissection, uterine tissues were fixed in 10% buffered formalin, embedded in paraffin, and sections stained for histologic analyses.

Differentiation of 3T3L1 fibroblasts to adipocytes

3T3L1 fibroblasts were differentiated into adipocytes as described previously (13). Undifferentiated 3T3-L1 cells (preadipocytes) were grown to approximately 95 % confluent stage (Day 3) and induced in DMEM-high glucose medium containing 10% FBS, 1 mmol/L of insulin and 30 µmol/L of T3 for 48 hours. Following induction, cells were differentiated with 125 nmol/L of indomethacin, 2 µg/mL of dexamethasone and 250 nmol/L of methylisobutylxanthine with media changes every 48 hours for an additional 7 days. On Day 12, the differentiated 3T3-L1 cells (Adipocytes) were observed with visible lipid droplets. To collect conditioned media (CM) from preadipocytes and differentiated adipocytes, cells were rinsed with DPBS and then exposed to the basal medium. After 24 hours, the media were collected and centrifuged using Amicon Ultra centrifugal filter units at 4,000 rpm for 30 minutes at 4°C. The supernatant was collected and stored at −80°C for cell proliferation, migration, and responses to chemotherapeutic drugs. Different soluble proteins, cytokines, chemokines, and growth factors in CM of preadipocyte and adipocyte cultures were identified using Mouse XL Cytokine Array Kit (R&D Systems) following the manufacturer's instructions.

Proliferation assay

Five-thousand cells were plated in triplicate in 100 µL complete medium per well of 96-multiwell flat bottom plates (Corning Costar) and incubated for 24 hours at 37°C, 5 % CO_2 for cells to adhere. Cells were then treated with indicated concentrations of carboplatin, paclitaxel, and conditioned medium from adipocytes or adipose tissue followed by further incubation for 72 hours. At the end of each incubation period, cellular proliferation, and survival were examined by CellTiter-Glo Luminescent cell viability assay (Promega) according to the manufacturer's protocol.

Clonogenic assay

Cell survival was assessed through seeding 2,000 Ishikawa cells/well in a 6-well plate and treated with 20% PACM and ACM once every 3 days. On Day 10, cells were fixed in 70% alcohol and stained with 0.5% crystal violet. A group of more than or equal to 50 cells was considered as a colony and counted using ImageJ software.

Transwell migration assay

Subconfluent Ishikawa cells were cultured overnight in serum-free medium (SFM). For migration assay, 1×10^5 cells in SFM were placed in the upper chamber of Transwell assay inserts (6.5-mm diameter, 8-µm pores, Sigma #CLS3422) whereas MEM SFM alone or containing 20% PACM and ACM was added to the lower chamber. After 24 hours incubation at 37°C, migrated cells were fixed in 70% alcohol, and stained with crystal violet (0.5%) for 10 minutes. Cells in the inner chamber were mechanically wiped using cotton swabs. Cells attached to membrane were imaged and quantified using ImageJ software.

Immunoblot analysis

The proteins of interest in human adipose tissue and mouse xenograft tumors were determined by Western blot analysis as described in our previous study (16). Briefly, adipose tissue and Ishikawa tumors were washed with PBS and homogenized in ice-cold RIPA (radioimmunoprecipitation assay) buffer containing protease and phosphatase inhibitors (Sigma). Aliquots of tissue homogenate containing equal protein mass were heated in 1X Laemmli sample buffer for 5 minutes at 95°C. The samples (30 µg protein) were subjected to SDS-PAGE (10% resolving gel), transferred to nitrocellulose blotting membrane (GE Healthcare Life Sciences) and probed with primary antibody VEGF (1/500), pS6 (1/2,000), S6 (1/2,000), pAkt (1/1,500), Akt (1/1,500), VEGFR2 (1/1,000), $pVEGFR2^{Tyr1175}$ (1/1,000) for overnight incubation at 4°C. Membranes were washed and incubated with secondary antibodies conjugated with horseradish peroxidase (Jackson ImmunoResearch Laboratories) for 1 hour at room temperature. Protein of interest was made visible by enhanced chemiluminescence using Luminescent Image Analyzer LAS-4000 (FUJIFILM) and quantified by densitometry using ImageJ (NIH, USA).

Immunohistochemistry and immunofluorescence

Blobby mice uteri and NOD *scid* gamma xenograft tumors were fixed with 10% neutral-buffered formalin overnight, followed by embedding and sectioning. Tissue sections were dewaxed in xylene and rehydrated in graded alcohols and water. Antigen retrieval using sodium citrate buffer (10 mmol/L Tri-sodium citrate, 0.05% Tween 20, pH 6.0) was performed for Ki-67 and Foxa2 staining. Endogenous peroxidase activity was blocked with 3% (v/v) hydrogen peroxide (H_2O_2) in methanol for 15 minutes. Sections were blocked with 10% goat serum with 1% BSA in TBS containing 0.1% Triton X-100 for 1 hour at room temperature, followed by incubation with primary antibodies overnight at 4°C. Next day, sections were incubated with biotin and streptavidin peroxidase-conjugated secondary antibodies (Thermo Fisher Scientific) at a concentration 1:250 (v/v) for 1 hour at room temperature. Immunoreactivity was demonstrated with 3,3'-diaminobenzidine/H_2O_2 (DAB solution), sections were lightly counterstained with hematoxylin, dehydrated, and cleared in graded alcohol and xylene and cover-slipped. For quantification, slides were digitized at 20x absolute resolution using an Aperio AT2 scanner. Quantitative IHC analysis was performed using the HaloTM image analysis platform. The pixel intensities of DAB staining were calculated using the Area Quantification v1.0 algorithm and the percentage of Ki-67–positive cells (indicated by positive DAB staining in the nucleus) were calculated using the CytoNuclear v1.4 algorithm (Indica Labs). Immunohistochemistry intensity score (H-Score) was calculated as described previously (17). Immunofluorescence staining was visualized on a confocal LASER scanning microscope (FV1000, Olympus) using the oil-immersion ×40 magnification objective and analyzed with Fluoview FV10-ASW 1.7 software. 3D images were shown as mid-structure from z-stack sections.

Statistical analysis

All experiments were repeated three to five times, with two to three biological replicates per repeat and the data were expressed

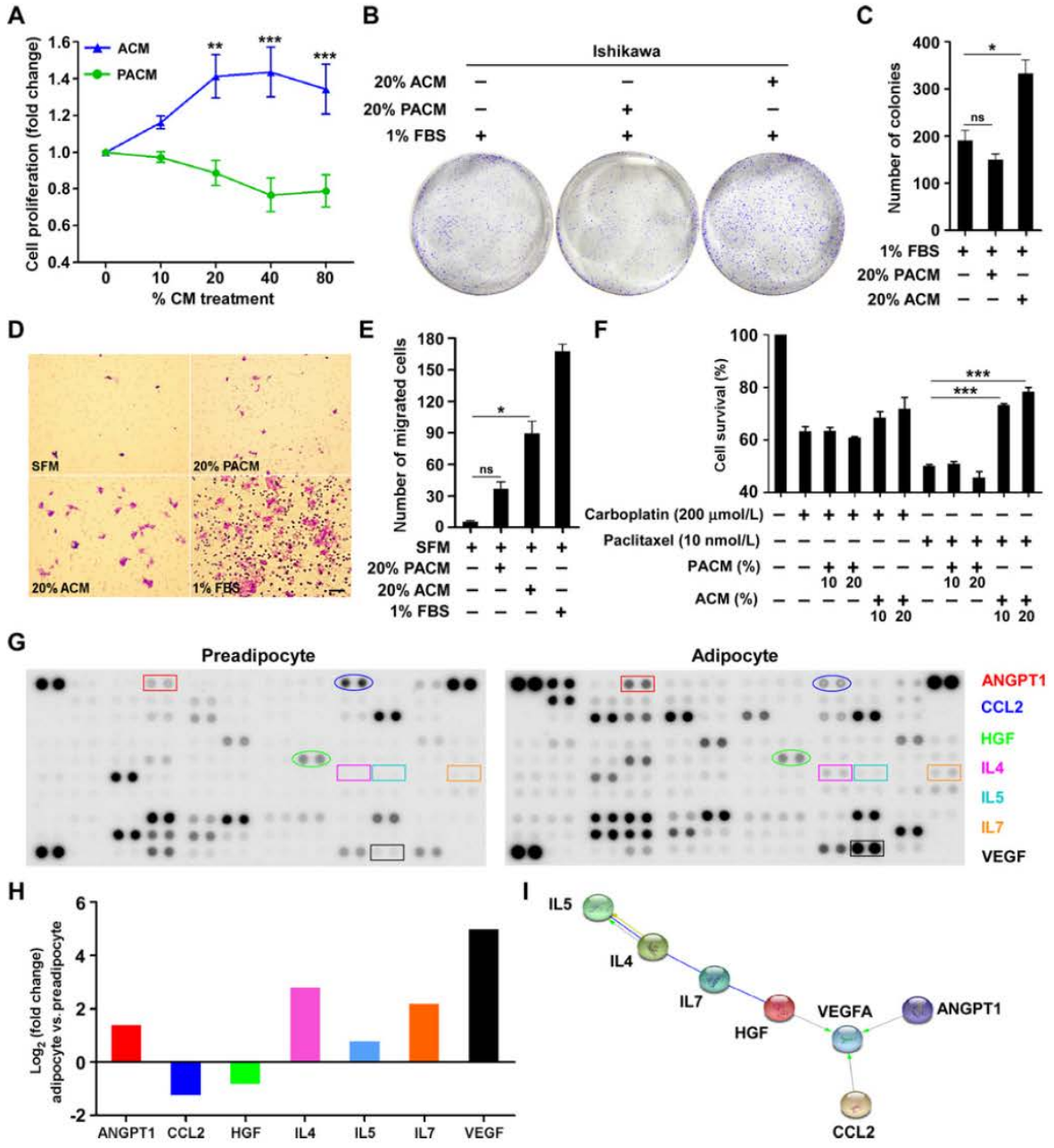

Figure 1.

Adipocyte-derived cytokines and growth factors stimulate endometrial cancer cell proliferation. **A,** Ishikawa cells were treated with increasing doses of PACM and ACM and assayed for proliferation ($n = 3$). **B,** Ishikawa cells (2×10^3) were seeded out in a 6-well plate to form colonies (a group of more than 50 cells) in presence and absence of conditioned medium and were stained with crystal violet. **C,** Bar graph represents the number of colonies formed in different treatment groups ($n = 3$). **D,** Ishikawa cells (1×10^5) were seeded onto the upper chamber of Transwell inserts and incubated for 16 hours with or without the conditioned medium in the lower chamber to enhance cell migration. Migration of treated cells was determined by crystal violet staining. Cells in 10 fields were imaged and counted to cover the entire filter in each group. SFM and 1% FBS was used as a negative and positive control for cell migration assay. **E,** Bar graphs represent the number of cells migrated in control and treated groups ($n = 3$). **F,** Ishikawa cells were treated with carboplatin and paclitaxel at the indicated concentration with or without PACM and ACM and were assayed for cell viability after 48 hours. **G,** Mouse cytokine array analysis of the conditioned medium from preadipocytes (undifferentiated 3T3-L1) and adipocytes (differentiated 3T3-L1). **H,** Summary of the fold change values of signal intensity of indicated cytokines. **I,** A depiction of protein interactome (build using STRING database with the highest confidence, 0.900) associated with ACM. SFM, Serum-Free Medium; PACM, PreAdipocyte Conditioned Medium; ACM, Adipocyte Conditioned Medium; scale bar, 200 µm; error bars represent mean ± SEM; *, $P < 0.05$; **, $P < 0.01$; ***, $P < 0.001$.

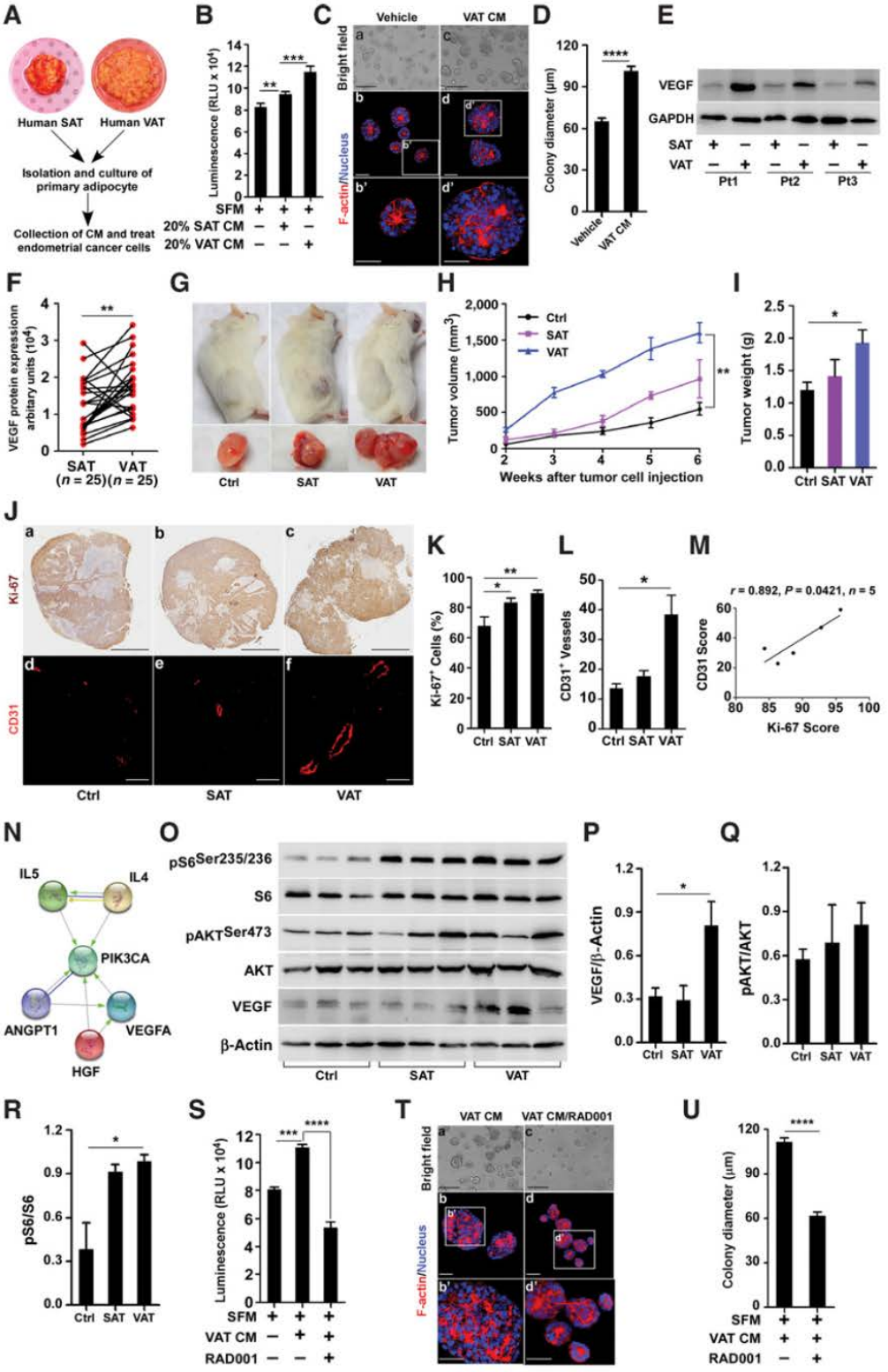
A
Human SAT
Human VAT
Isolation and culture of primary adipocyte
Collection of CM and treat endometrial cancer cells
B
Luminescence (RLU x 10⁴)
SFM
20% SAT CM
20% VAT CM
C
Vehicle
VAT CM
Bright field
F-actin/Nucleus
D
Colony diameter (μm)
Vehicle
VAT CM
E
VEGF
GAPDH
SAT
VAT
Pt1
Pt2
Pt3
F
VEGF protein expressionn arbitary units (10⁴)
SAT (n = 25)
VAT (n = 25)
G
Ctrl
SAT
VAT
H
Tumor volume (mm³)
Ctrl
SAT
VAT
Weeks after tumor cell injection
I
Tumor weight (g)
Ctrl SAT VAT
J
Ki-67
CD31
Ctrl
SAT
VAT
K
Ki-67⁺ Cells (%)
Ctrl SAT VAT
L
CD31⁺ Vessels
Ctrl SAT VAT
M
r = 0.892, P = 0.0421, n = 5
CD31 Score
Ki-67 Score
N
IL5
IL4
PIK3CA
ANGPT1
VEGFA
HGF
O
pS6Ser235/236
S6
pAKTSer473
AKT
VEGF
β-Actin
Ctrl
SAT
VAT
P
VEGF/β-Actin
Ctrl SAT VAT
Q
pAKT/AKT
Ctrl SAT VAT
R
pS6/S6
Ctrl SAT VAT
S
Luminescence (RLU x 10⁴)
SFM
VAT CM
RAD001
T
VAT CM
VAT CM/RAD001
Bright field
F-actin/Nucleus
U
Colony diameter (μm)
SFM
VAT CM
RAD001

as the mean ± SEM. Statistical analyses were performed by the Student *t* test (unpaired, two-tailed) for comparing two groups and by analysis of variance for multiple group comparisons, using GraphPad Prism 7.02 software. A *P* value of <0.05 was considered statistically significant. The Pearson correlation analysis was performed to determine the correlation between the groups.

Results

Adipocytes promote endometrial cancer cell growth

We differentiated preadipocytes (mouse embryonic fibroblast adipose-like cells, 3T3-L1) into adipocytes, which was verified by visual observation of lipid droplets and Oil Red O staining (Supplementary Fig. S1). Preadipocyte and adipocyte conditioned medium (PACM and ACM) were collected from these respective cell types. To examine the impact of adipocytes on endometrial cancer cell proliferation, Ishikawa cells (an endometrial cancer cell line, which mimics normal glandular epithelial phenotype of the human endometrium; ref. 18) were treated with PACM and ACM (Fig. 1A). Increasing concentrations of ACM significantly increased (1.4- ± 0.2-fold) Ishikawa cell proliferation as compared with PACM (Fig. 1A). We next determined the clonogenicity of Ishikawa cells as a surrogate assay for evaluating the effect of ACM on endometrial cancer cell growth. The ability of Ishikawa cells to form colonies increased approximately 2-fold in response to ACM compared with PACM at a concentration of 20% (v/v; Fig. 1B and C). In addition, ACM but not PACM significantly induced migration of Ishikawa cells under serum starvation as shown by Transwell migration assay (Fig. 1D and E).

The response to chemotherapeutic drugs differs between lean and obese patients (19). Carboplatin and paclitaxel are the first-line agents in chemotherapy treatment of endometrial cancer (20). Therefore, we tested whether adipocytes influence the sensitivity of endometrial cancer cells to these chemotherapeutic drugs. We added PACM and ACM to Ishikawa cells, which were treated with a DNA-damaging drug (carboplatin) and the microtubule-targeting agent (paclitaxel). In contrast with PACM, ACM treatment significantly increased endometrial cancer cell survival in response to both the drugs and showed higher IC_{50} value (Fig. 1F). These observations suggest that adipocytes secrete certain growth factors or cytokines, which modulate endometrial cancer cell proliferation, migration, and resistance to chemotherapeutic drugs.

To identify the growth promoting factors that are present in PACM and ACM, we performed a cytokine array (Fig. 1G–I). Among 111 cytokines tested, 18 cytokines were differentially expressed (14 upregulated and 4 downregulated) in ACM compared with PACM (>2-fold change; Supplementary Table S1). Interactome analysis of these cytokines using String database (21) revealed strong interactions between 7 cytokines with the highest confidence score (0.900) in ACM (Fig. 1I). Within the protein network, five cytokines most abundantly secreted by adipocytes were IL-5, IL-4, IL-7, ANGPT1, and VEGF (Fig. 1H). All of these seven cytokines in the interactome are predicted to activate VEGF (Fig. 1I), suggesting that VEGF is a potential factor promoting endometrial cancer cell survival and growth.

Adipocyte-derived VEGF-mTOR signaling promotes endometrial cancer growth

To validate our results from *in vitro* differentiated adipocytes in human patients, we isolated and cultured primary adipocytes from SAT and VAT of high BMI (>30 kg/m^2) female patients who underwent bariatric surgery for weight loss (Fig. 2A). The addition of human ACM at a concentration of 20% (v/v) significantly promoted endometrial cell proliferation under serum starvation conditions (Fig. 2B). Interestingly, VAT CM had a higher tendency to modulate Ishikawa cell proliferation than from SAT CM. Considering these findings, we assessed whether adipocytes influence endometrial cell growth in a three-dimensional environment (which intimately mimics *in vivo* organization of endometrial glands; Fig. 2C). As expected, Ishikawa cells of the control culture tended to form round and spherical clusters with a central lumen (Fig. 2Ca,b,b'). In comparison, Ishikawa cells cultured with VAT CM showed a trend to pleomorphism and morphologically these endometrial organoids had larger cell clusters without a defined lumen (Fig. 2Cc,d,d' and D).

Next, we examined the expression of VEGF protein in human patients and found significantly more VEGF protein in the VAT ($n = 21$ of 25) compared with SAT of the same patient (Fig. 2E and F; $n = 25$). Because VAT resides in the abdomen close to the uterus and showed higher expression of VEGF, we postulated that compared with SAT, VAT would more prominently influence endometrial cancer growth. To ascertain the influence of VAT on endometrial cancer growth, we injected Ishikawa cells alone or in

Figure 2.

Human visceral adipose tissue promotes *in vivo* tumor growth through VEGF-mTOR signaling. **A,** Primary adipocytes were isolated from obese human female adipose tissue (subcutaneous and visceral; $n = 5$) and maintained in DMEM/F-12 medium. After 48 hours culture of adipocytes in SFM, cell supernatant (conditioned medium; CM) was isolated. **B,** Ishikawa cells were treated with 20% CM (from SAT and VAT) and assayed for proliferation ($n = 5$). **C,** The organoid-forming capacity of Ishikawa cells upon *ex vivo* treatment with vehicle and VAT CM (20% v/v). Representative images of Day-12 organoids are shown. **D,** Comparison of average colony diameter of Ishikawa organoids after respective *ex vivo* treatments ($n = 5$). The diameter of at least 50 colonies was measured from individual treatment groups for the analysis. **E,** Representative western blot showing VEGF protein expression in SAT and VAT of obese human females. **F,** Quantification of VEGF protein expression in SAT and VAT (same patients, $n = 25$, Wilcoxon matched-pairs signed rank test). **G,** Representative photographs of xenografts of Ishikawa cells in flanks of NOD *scid* gamma mice ($n = 5$). Mice were euthanized and tumors harvested at 42 days after cell injection. **H** and **I,** Tumor volume ($n = 5$) and end-stage tumor weight ($n = 5$) after injection of 1.5×10^6 Ishikawa cells with or without adipocytes into the flank of the NOD *scid* gamma mice. **J,** Staining for Ki-67 (brown) and CD31 (red) in control- and SAT/VAT-induced tumors ($n = 5$). **K** and **L,** The percentage of Ki-67–positive cells ($n = 5$) and CD31-positive vessels ($n = 5$) were quantified. **M,** The correlation between Ki-67 and CD31 was analyzed and the black line indicates the correlation (Pearson correlation analysis). **N,** Protein interactome of ACM signature cytokines and growth factors with *PIK3CA* gene. **O,** Western blots of protein lysate from the xenograft tumors of Ishikawa cells alone or with SAT and VAT were performed ($n = 5$ mice/group). Representative three western blots from each group are shown. Phosphorylation is indicated by p and corresponding residues are shown. **P, Q,** and **R,** Densitometric quantification of the bands in **O** was performed, averaged and shown as a bar graph ($n = 5$). **S,** Ishikawa cells were treated with VAT CM (20%) and assayed for proliferation in presence and absence of RAD001 (100 nmol/L; $n = 5$). **T,** Representative images of Day-12 Ishikawa organoids after treatment of VAT CM (20%) and RAD001 (100 nmol/L). **U,** The bar graph shows colony diameter of Ishikawa organoids with or without RAD001 treatment ($n = 5$). Pt, Patient; Ctrl, Control; SAT, Subcutaneous Adipose Tissue; VAT, Visceral Adipose Tissue. Phase contrast scale bar, 200 μm; confocal scale bar, 50 μm; IHC scale bar, 1 mm. Data are shown as mean ± SEM; *, $P < 0.05$; **, $P < 0.01$, ***, $P < 0.001$; ****, $P < 0.0001$.

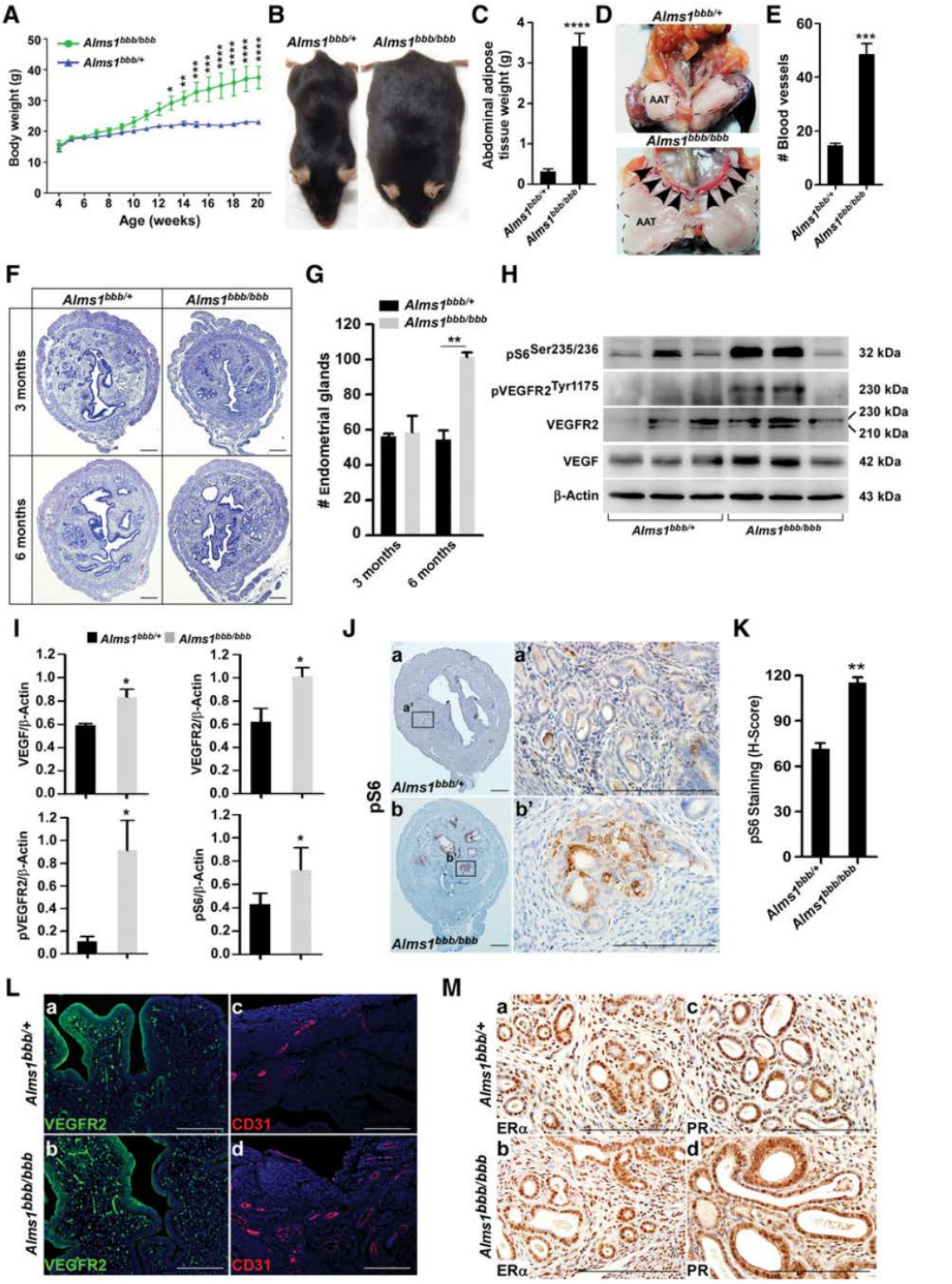
A
Alms1bbb/bbb
Alms1bbb/+
Body weight (g)
Age (weeks)
B
Alms1bbb/+
Alms1bbb/bbb
C
Abdominal adipose tissue weight (g)
D
Alms1bbb/+
AAT
Alms1bbb/bbb
AAT
E
Blood vessels
F
Alms1bbb/+
Alms1bbb/bbb
3 months
6 months
G
Alms1bbb/+
Alms1bbb/bbb
Endometrial glands
3 months
6 months
H
pS6Ser235/236
pVEGFR2Tyr1175
VEGFR2
VEGF
β-Actin
32 kDa
230 kDa
230 kDa
210 kDa
42 kDa
43 kDa
Alms1bbb/+
Alms1bbb/bbb
I
Alms1bbb/+
Alms1bbb/bbb
VEGF/β-Actin
VEGFR2/β-Actin
pVEGFR2/β-Actin
pS6/β-Actin
J
pS6
a
a'
Alms1bbb/+
b
b'
Alms1bbb/bbb
K
pS6 Staining (H-Score)
Alms1bbb/+
Alms1bbb/bbb
L
Alms1bbb/+
Alms1bbb/bbb
VEGFR2
CD31
VEGFR2
CD31
M
Alms1bbb/+
Alms1bbb/bbb
ERα
PR
ERα
PR

combination with human SAT or VAT into the flank of the female NOD *scid* gamma mice (Fig. 2G; $n = 5$). Our results indicated that subcutaneous injection of primary human VAT significantly increased tumor volume and weight by 2.9-fold and 1.6-fold, respectively (Fig. 2H and I; tumor volume: Ctrl, 548.86 ± 85.8 mm^3 vs. SAT, 963.11 ± 263.1 mm^3 vs. VAT, 1598.77 ± 138.2 mm^3 and tumor weight: Ctrl, 1.20 ± 0.1 g vs. SAT, 1.42 ± 0.3 g vs. VAT, 1.93 ± 0.2 g). Analysis of a cell proliferation marker, Ki-67, confirmed more proliferating cells in the Ishikawa-VAT tumors compared with other groups (Fig. 2 Ja-c and K).

Because VAT showed higher expression of VEGF protein and promoted tumor growth, we investigated whether VEGF-mediated angiogenesis sustains tumor growth. Immunolocalization of a well-established marker of endothelial cells, CD31, on tumors revealed a higher percentage of CD31-positive blood vessels in Ishikawa-VAT tumors than in control and SAT tumors (Fig. 2Jd-f and L). We also detected a significant positive correlation between the expression of Ki-67– and CD31-positive vessels in Ishikawa-VAT tumors (Fig. 2M; $r = 0.892$, $P = 0.0421$). These observations suggest the significant contribution of the VAT to promote endometrial cancer growth through VEGF.

High VEGF secretion stimulates the PI3K/AKT/mTOR signaling pathway, which is the most altered pathway in human endometrial cancer, accounting for almost 85% patients (22–24). PI3K/AKT/mTOR signaling is a major regulator of cellular growth and survival (25, 26). To determine whether PI3K/AKT/mTOR signaling is involved in the adipocyte-mediated growth of endometrial cancer, we analyzed the protein interactome of VEGF and other cytokines with PIK3CA (Phosphatidylinositol-4,5-bisphosphate 3-kinase, catalytic subunit alpha) protein and observed that all the secreted cytokines individually or in combination contribute to activation of PIK3CA (Fig. 2N). This suggested that PI3K/AKT/mTOR signaling operating downstream of VEGF signaling might be involved in stimulating the growth of endometrial cancer. Immunoblot analysis of Ishikawa xenograft tumors revealed higher VEGF expression in Ishikawa-VAT tumors than SAT and control tumors (Fig. 2O and P). To address the activation of mTOR signaling, we analyzed downstream targets of this pathway. Western blot analysis indicated elevated levels of AKT phosphorylation at Ser473 and S6 phosphorylation at Ser235/236 in Ishikawa-VAT tumors compared with control tumors (Fig. 2O, Q, and R). Furthermore, inhibition of mTOR signaling by RAD001 significantly reduced VAT-CM induced endometrial cancer cell proliferation (Fig. 2S) and organoid size (Fig. 2T and U). Taken together, these findings suggest that visceral adipocytes induce endometrial cancer growth through VEGF-mTOR signaling cascade.

Hyperphagic obese (Blobby) mice progressively develop endometrial hyperplasia with hyperactive VEGF-mTOR signaling

To provide evidence that incremental weight gain leads to the development of pathologic changes in the endometrium, we examined uteri from a mouse model of Alstrom syndrome (a rare human genetic disease that causes hyperphagia, which leads to severe obesity; ref. 27). Similar to humans, mice with a homozygous point mutation in the *Alms1* gene (*Alms1*: c.6507T>A) overeat and develop obesity after puberty on a standard chow diet. These mice are referred as 'Blobby' strain ($Alms1^{bbb/bbb}$; Australian Phenomics Facility). Our female homozygous Blobby ($Alms1^{bbb/bbb}$) mice gradually gained body weight relative to heterozygous ($Alms1^{bbb/+}$) littermates from 7 weeks of age and weight gain increased progressively with age (Fig. 3A). At 20 weeks of age, Blobby mice weighed on average 38 ± 2.3 g or gained nearly 2-fold body weight as compared with heterozygote littermates, 22 ± 0.6 g (Fig. 3A and B). This increased body weight was associated with an 11.4- ± 1.4-fold increase in abdominal AT mass, which localized inside the peritoneal cavity and attached to the uterus (Fig. 3C and D). Consistent with our observations in the endometrial cancer xenograft model (Fig. 2J), the Blobby mice ($Alms1^{bbb/bbb}$) also had significantly more blood vessels connecting the AT with the uterus compared with heterozygotes ($Alms1^{bbb/+}$; 48.7 ± 3.8 vs. 14.7 ± 0.9; Fig. 3D and E).

To assess the role of visceral adiposity in uterine function, female $Alms1^{bbb/bbb}$ mice were mated to wild-type male mice for 6 months. Homozygous and heterozygous Blobby mice displayed normal mating behavior. However, in all the breeding pairs ($n = 9$), $Alms1^{bbb/bbb}$ mice were completely infertile (Supplementary Table S2). In contrast, $Alms1^{bbb/+}$ mice were fertile and gave birth to normal healthy pups (Supplementary Table S2). Analysis of the ovaries and oviducts from homozygous and heterozygous Blobby mice showed no obvious defects in both organs of $Alms1^{bbb/bbb}$ and $Alms1^{bbb/+}$ (Supplementary Fig. S2; $n = 7$). Mature Graafian follicles and corpus lutea were present in ovaries of both homozygous and heterozygous Blobby mice (Supplementary Fig. S2), suggesting normal follicular development and ovulation in these mice. These data indicated that fertility defects in $Alms1^{bbb/bbb}$ mice may be due to abnormal uterine functions.

To study the effects of excessive abdominal fat deposit on the uterus, we collected uteri from homozygous and heterozygous

Figure 3.

Blobby mice ($Alms1^{bbb/bbb}$) exhibit obesity and EH through high VEGF-mTOR signaling on a regular chow diet. **A,** The graph shows the body weights of female heterozygous ($Alms1^{bbb/+}$; $n = 14$) and homozygous ($Alms1^{bbb/bbb}$; $n = 14$) Blobby mice maintained on standard chow diet from 4 to 20 weeks of age. **B,** A representative 24-week-old heterozygous ($Alms1^{bbb/+}$, left) Blobby female mice with homozygous ($Alms1^{bbb/bb}$, right) littermate. **C,** Comparison of abdominal adipose tissue weight surrounding uterus in Blobby ($Alms1^{bbb/+}$ and $Alms1^{bbb/bbb}$) mice ($n = 6$, 24-weeks-old). **D,** Grossly enlarged Blobby mice showing abdominal adipose tissue (marked in dotted line) and blood vessels (arrowhead) connecting adipose tissue to the uterus. **E,** Quantification of the number of blood vessels attached to the uterus in Blobby mice ($n = 6$). **F,** H&E-stained uterine section showing endometrial glands in 3 and 6 months Blobby mice. **G,** Bar graph represents the number of endometrial glands at indicated time points in Blobby mice ($n = 5$). **H,** Western blots of protein lysate from $Alms1^{bbb/+}$ and $Alms1^{bbb/bbb}$ mice uteri were analyzed for VEGF, VEGFR2, pVEGFR2^{Tyr1175}, and pS6 ($n = 5$ mice/group). Representative three western blots from each group are shown. Phosphorylation is indicated by p and corresponding residues are shown. **I,** Densitometric quantification of the bands in **H** was performed, averaged and shown as a bar graph ($n = 5$). **J,** Immunohistochemical analysis of pS6 in uteri of $Alms1^{bbb/+}$ and $Alms1^{bbb/bbb}$ mice. **K,** Quantification of pS6 staining intensities is shown as H-Score ($n = 5$). **L,** VEGFR2 expression (green) and CD31-positive endothelial cells (red) are shown by immunofluorescence in $Alms1^{bbb/+}$ and $Alms1^{bbb/bbb}$ mice. **M,** Expression of ERα and PR is shown by immunohistochemistry in $Alms1^{bbb/+}$ and $Alms1^{bbb/bbb}$ mice. AAT, Abdominal Adipose Tissue; scale bar, 200 μm. The results represent the mean ± SEM; *, $P < 0.05$; **, $P < 0.01$; ***, $P < 0.001$; ****, $P < 0.0001$.

Blobby mice. At 3 months of age when the body weight of homozygous and heterozygous Blobby mice was not significantly different, no obvious histologic differences were present in the uterine sections of *Alms1*$^{bbb/bbb}$ and *Alms1*$^{bbb/+}$ mice (Fig. 3F). However, at 6 months of age when homozygous Blobby mice were significantly overweight compared with controls, histologic and immunohistochemical (Foxa2: a glandular marker) analysis showed a significant increase in the number of endometrial glands in the stroma, which is indicative of endometrial hyperplasia (EH; ref. 28; Fig. 3F and G; Supplementary Fig. S3; endometrial glands: *Alms1*$^{bbb/bbb}$, 101.33 ± 2.6 vs. *Alms1*$^{bbb/+}$, 54.67 ± 4.1).

To further understand the link between abdominal adiposity and EH in obese Blobby mice (*Alms1*$^{bbb/bbb}$), we assessed the activation of VEGF and mTOR signaling cascades. Consistent with Ishikawa-VAT tumor xenograft findings, western blot analysis revealed an activation of the VEGF/mTOR pathway in *Alms1*$^{bbb/bbb}$ uteri (Fig. 3H and I). VEGF signals through its major receptor VEGFR2 and activates mTOR pathway by phosphorylating VEGFR2 at Tyr1175 (9, 10). In contrast with *Alms1*$^{bbb/+}$, western blot of *Alms1*$^{bbb/bbb}$ uterine tissues showed an activation of both VEGF and VEGFR2 (Fig. 3H and I). Furthermore, phosphorylation of VEGFR2 at Tyr1175 was elevated in *Alms1*$^{bbb/bbb}$ mice confirming activation of VEGF signaling (Fig. 3H and I). To determine whether active VEGF signaling leads to upregulation of mTOR signaling, we analyzed expression of pS6, a downstream target of mTOR pathway. Both immunoblot and immunohistochemical analysis revealed a significant increase in pS6 expression in *Alms1*$^{bbb/bbb}$ mice compared with *Alms1*$^{bbb+}$ mice (Fig. 3H–K). The histologic analysis also identified an increase in pS6 expression in the glandular epithelium of the obese Blobby mice (*Alms1*$^{bbb/bbb}$) uteri compared with nonobese littermates (*Alms1*$^{bbb+}$; Fig. 3J and K). VEGF is crucial for maintenance of the vascular system and high VEGF content leads to increased angiogenesis (29). Therefore, we tracked the outcome of high VEGF content in *Alms1*$^{bbb/bbb}$ mice by immunofluorescence analysis of VEGFR2 and CD31. Compared with *Alms1*$^{bbb+}$ mice, the uterine section of *Alms1*$^{bbb/bbb}$ mice showed high VEGFR2 expression as well as more vasculature as evidenced by an increase in CD31 positive blood vessels (Fig. 3L). These results further support high VEGF content and activation of VEGF signaling in *Alms1*$^{bbb/bbb}$ mice.

Ovarian hormones are a major regulator of uterine function and diseases (30). To determine whether steroid hormones (estrogen and progesterone) have any effect on the hyperplastic uterus of *Alms1*$^{bbb/bbb}$ mice, we examined the expression of estrogen and progesterone receptor (ERα and PR) and found no difference in the expression pattern of these two hormone receptors between obese and nonobese Blobby mice (Fig. 3M). In summary, these results demonstrate that progressive weight gain with increased abdominal fat deposition leads to the pathogenesis of EH in blobby mice, a precursor state of endometrial cancer.

Tamoxifen treatment of obese Blobby mice results in the development of endometrial carcinoma *in situ*

Unopposed estrogenic stimulation for a long duration leads to EH and possibly cancer (31). We postulated that external supplementation of estrogen or its mimetic would fuel the growth of precancer lesions present in the uterus of obese Blobby mice. Tamoxifen treatment in mice and humans leads to EH and/or endometrial cancer (32). Six-month-old homozygous and heterozygous Blobby mice were injected intraperitoneally with vehicle and tamoxifen and uterine tissues were examined 14 days (n = 4/genotype/treatment) after treatment. Obese Blobby mice treated with tamoxifen showed a significant increase in uterine weight (*Alms1*$^{bbb/bbb}$, 0.223 ± 0.02 g vs. *Alms1*$^{bbb/+}$, 0.124 ± 0.02 g) compared with nonobese littermates under the same treatment conditions (Fig. 4A and B). Histologic analysis of the uterine sections revealed endometrial carcinoma *in situ* in obese Blobby mice compared with simple hyperplasia in nonobese control mice (Fig. 4C). Analysis of Ki-67 staining showed more proliferating cells in uteri of *Alms1*$^{bbb/bbb}$ mice compared with *Alms1*$^{bbb/+}$ mice (Fig. 4Da-b and E). Examination of stathmin, a well-established marker of endometrial cancer (33), revealed increased stathmin expression in obese Blobby mice relative to nonobese control mice (n = 4/genotype; Fig. 4Dc-d and F). These results show that tamoxifen administration is sufficient to cause the development of endometrial carcinoma *in situ* in *Alms1*$^{bbb/bbb}$ mice (n = 4 of 4). Furthermore, the complex EH with carcinoma *in situ* in *Alms1*$^{bbb/bbb}$ mice is induced by the additive effect of abdominal adipocyte-derived VEGF-mTOR signaling which is absent in *Alms1*$^{bbb/+}$ mice.

Human endometrial cancer samples from high BMI patients show increased vasculature and upregulation of VEGF-mTOR signaling

To determine whether changes similar to the endometrial cancer xenograft model and homozygous Blobby mice also occur in human patients, we collected and examined primary endometrial cancer tissues from nonobese controls (BMI <30 kg/m^2; n = 5), nonobese endometrial cancer patients (BMI <30 kg/m^2; n = 7), and obese endometrial cancer patients (BMI >30 kg/m^2; n = 13; Supplementary Table S3). Slides of endometrial cancer samples were stained for VEGF, VEGFR2 (a marker of active VEGF signaling), CD31 (a marker of endothelial cells), and pS6 (a marker of active mTOR signaling; Fig. 5A). The uterine sections from the control groups showed normal histology with well-differentiated glands and stroma (Fig. 5A). In the 20 endometrial cancer patients, VEGF expression correlated with BMI and the results showed that VEGF expression directly correlates with BMI (Fig. 5A–C). Furthermore, immunofluorescence analysis of VEGFR2 and CD31 staining demonstrated high VEGFR2 expression and more number of CD31-positive blood vessels in obese compared with nonobese patients (Fig. 5A and D; CD31$^+$ vessels: HEndoCa/HBMI, 123.2 ± 8.4 vs. HEndoCa/NBMI, 34.3 ± 4.9). We also observed a significant positive correlation between BMI of endometrial cancer patients and CD31-positive blood vessels in tumor section (Fig. 5E; r = 0.916, P < 0.0001). Immunohistochemical staining also showed an increased in the protein levels of pS6 in obese endometrial cancer patients (n = 9/13) compared with nonobese endometrial cancer patients (Fig. 5A and F). In addition, we also detected a significant positive correlation between the expression of VEGF and pS6 (Fig. 5G; r = 0.668, P = 0.0013) and CD31 and pS6 (Fig. 5H; r = 0.693, P = 0.0007). Taken together, these results indicate that visceral adiposity leads to upregulated VEGF signaling, which results in more tumor vasculature and high mTOR activity promoting endometrial cancer in obese women (Fig. 5I).

Discussion

Endometrial cancer is the most common gynecologic malignancy with one of the leading cause of cancer-related mortality in

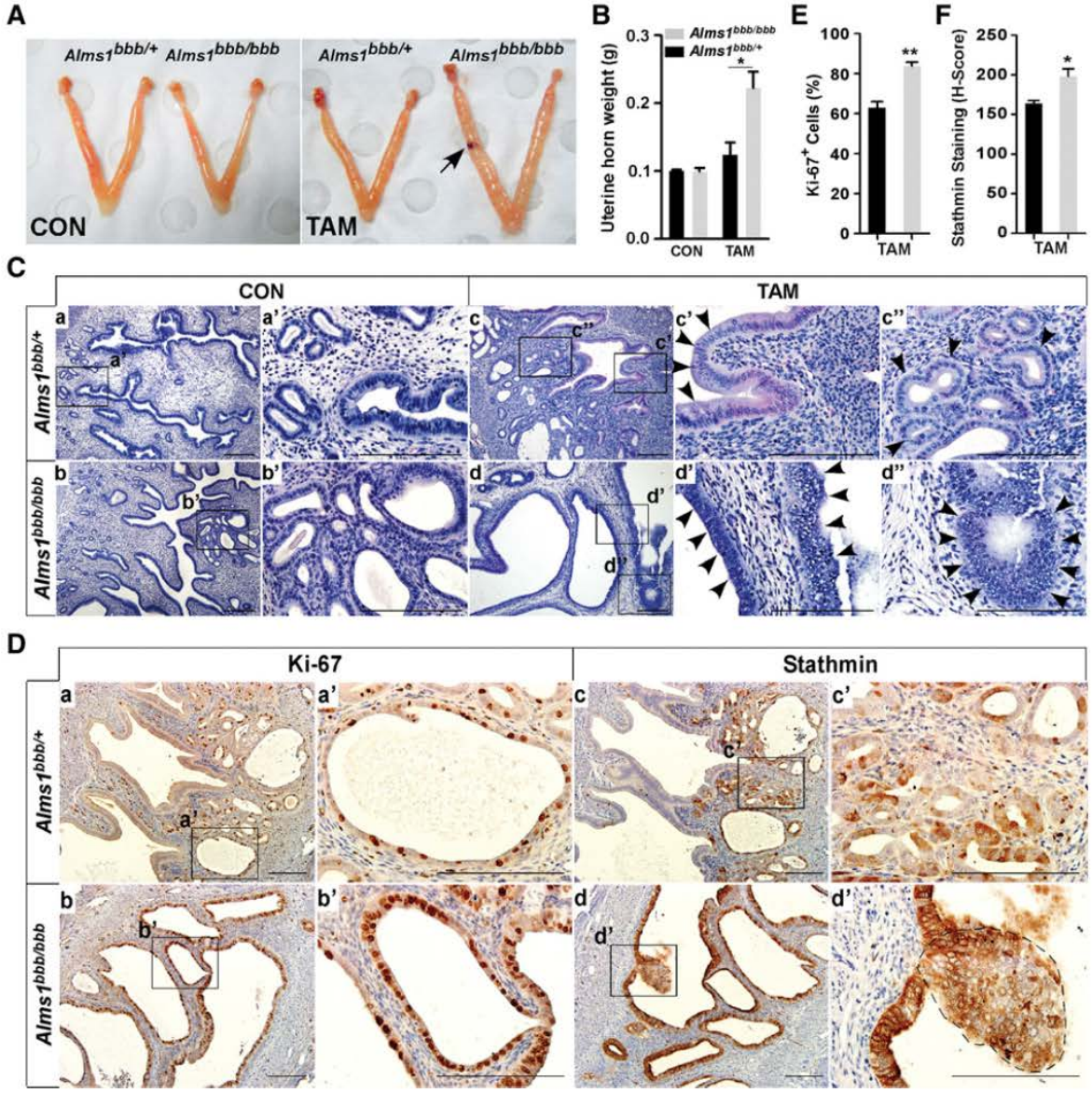

Figure 4.
Tamoxifen-driven endometrial carcinoma *in situ* in *Alms1*$^{bbb/bbb}$ mice. **A,** Gross anatomy of the *Alms1*$^{bbb/+}$ and *Alms1*$^{bbb/bbb}$ mice uteri treated with or without tamoxifen for 14 days. The black arrow indicates uteri with blood filled cyst. **B,** Quantitative weights of uteri in *Alms1*$^{bbb/+}$and *Alms1*$^{bbb/bbb}$ mice after tamoxifen treatment ($n = 4$). **C,** H&E-stained section showing normal and simple hyperplastic uterus in the *Alms1*$^{bbb/+}$and *Alms1*$^{bbb/bbb}$ mice (left). Formation of simple EH and endometrial carcinoma *in situ* in *Alms1*$^{bbb/+}$and *Alms1*$^{bbb/bbb}$ mice after tamoxifen treatment (right). Examination of tamoxifen-treated uterine sections show single layer of columnar epithelium (arrowhead in c'), irregularly shaped and sized glands (arrowhead in c'') in *Alms1*$^{bbb/+}$mice whereas multilayered epithelium with shedding (arrowhead in d') and complex crowded glands with nuclear atypia (arrowhead in d'') in *Alms1*$^{bbb/bbb}$ mice. **D,** Ki-67 and stathmin protein expression were assessed by immunohistochemistry in tamoxifen-treated *Alms1*$^{bbb/+}$and *Alms1*$^{bbb/bbb}$ mice. The dotted line in d' represents carcinoma *in situ* lesions. **E** and **F**, The percentage of Ki-67–positive cells ($n = 4$) and stathmin staining intensity ($n = 4$) were quantified. CON, Control; TAM, tamoxifen; scale bar, 200 μm. The results are shown as mean ± SEM; *, $P < 0.05$; **, $P < 0.01$.

women. Up to 80% of endometrial cancer patients have genetic aberrations in the members of the PI3K-mTOR (phosphoinositide 3-kinase-mammalian target of rapamycin) pathway (34). Obesity is a well-established risk factor for developing endometrial cancer (35). Epidemiologic studies suggest that obese endometrial cancer patients have decreased life expectancy compared with their nonobese counterparts (36). Although 10%–20% of endometrial cancer are serous and clear cell carcinomas with a

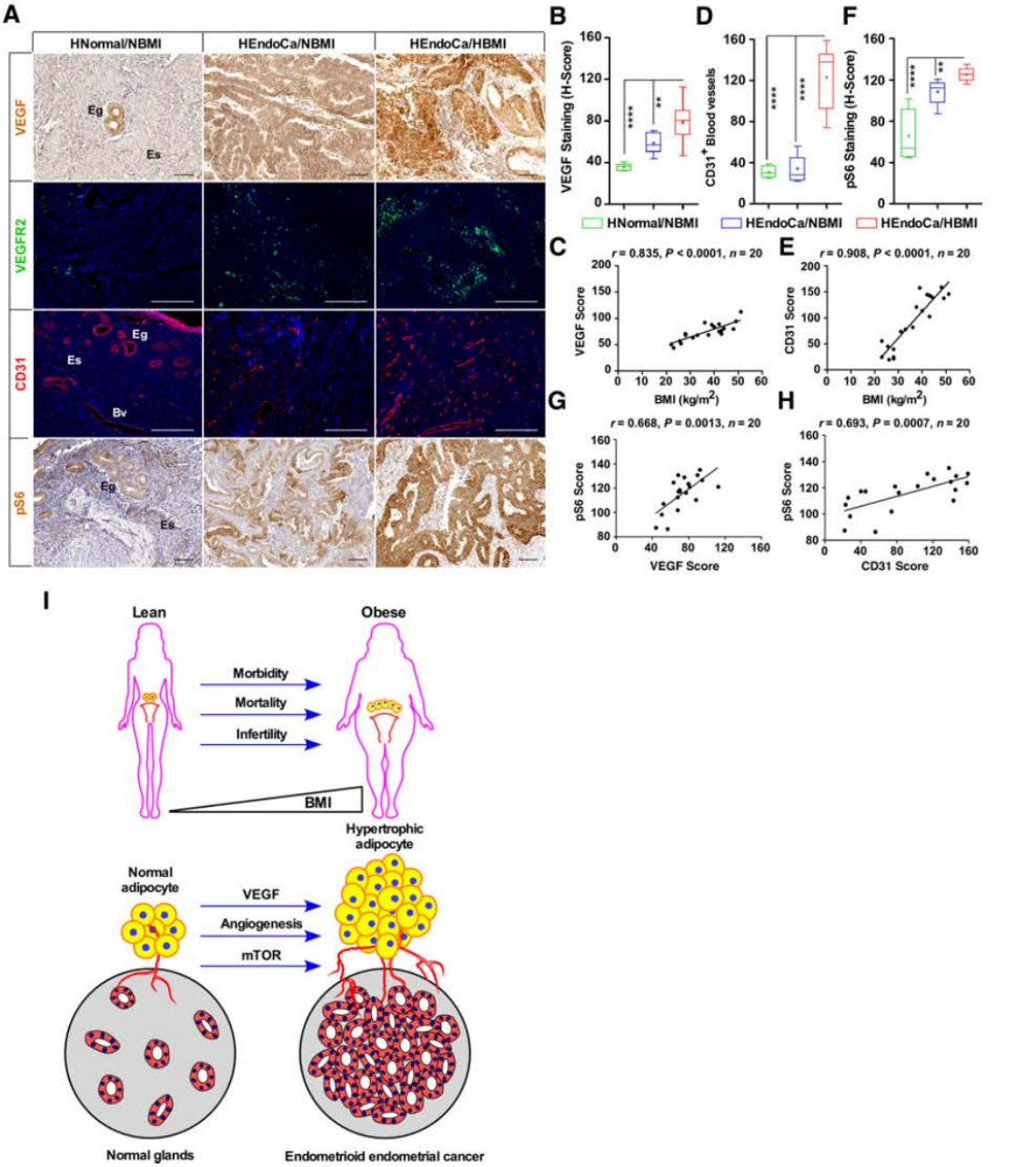

Figure 5.

High BMI women with endometrial cancer show a positive correlation between VEGF and mTOR signaling. **A,** Immunohistochemical analysis of VEGF and pS6 expression in nonobese ($n = 7$) and obese ($n = 13$) human endometrial cancer tissues compared with the endometrium of nonobese controls ($n = 5$). VEGFR2 expressing cells (green) and CD31-positive endothelial cells (red) are shown by immunofluorescence in normal and endometrial cancer tissues. **B,** Quantification of VEGF staining intensities is shown as H-score. **C,** Correlation analysis of VEGF and BMI in endometrioid endometrial cancer tissues from 20 patients. **D,** Whisker plot shows the number of CD31-positive endothelial cells in different tissue sections. **E,** Correlation analysis of CD31 and BMI in endometrial cancer patients. **F,** Quantification of pS6 staining intensities is shown as H-Score. **G** and **H,** Correlation analysis of pS6, VEGF, and CD31 in endometrial cancer patients. VEGF, pS6 expression levels were determined by immunohistochemistry staining and scored as described in Materials and Methods. **I,** A schematic of endometrial cancer cell–adipocyte interaction on a BMI scale. VEGF acts as a key mediator of endometrial cancer cell–adipocyte interaction through blood vessels. High BMI or visceral adiposity increases angiogenesis in the adipose tissue and uterus, which potentially elevates mTOR signaling in the endometrial glands and induces endometrial hyperplasia and/or cancer. Eg, endometrial gland; Es, endometrial stroma; Bv, blood vessel; HNormal, normal human endometrium; HEndoCa, human endometrial cancer; NBMI, nonobese body mass index; HBMI, high body mass index; scale bar, 50 μm. ± SEM; **, $P < 0.01$; ****, $P < 0.0001$.

more aggressive clinical course (Type II), the majority of high BMI women express endometrioid histology (Type I; ref. 37).

Epidemiologic studies have provided strong evidence for the role of obesity in various cancers including endometrial cancer (2, 4, 36, 38, 39). However, the precise role of adiposity at the molecular level has not yet been addressed. Our study for the first time demonstrates a plausible mechanism between obesity and development of endometrial cancer. We show that CM of *in vitro* differentiated adipocytes induces proliferation of endometrial cancer cells in association with the adipokine content of CM. Searching for an active component of CM being responsible for endometrial cancer cell proliferation and resistance to chemotherapeutic drugs, we found VEGF in CM to be significantly correlated with proliferation. Various adipokines such as IL-5, IL-4, IL-7, CCL2, HGF, and ANGPT1 cumulatively activate VEGF; suggesting that in addition to VEGF, these factors might also be involved in the synergistic effects of CM. Our results also show that VEGF expression in obese patients is higher in the VAT as compared with SAT. Visceral adipocytes mainly reside in the abdomen and in close proximity to the uterus in both mouse and human. VEGF within AT stimulates angiogenesis, which is crucial for increasing blood capillaries to expand AT. It has also been suggested that AT hypoxia and inflammation can induce VEGF expression in expanded AT (40). Thus, high VEGF expression is beneficial to induce hypertrophic and hyperplastic growth of AT. Conversely, reported studies have demonstrated that increased levels of VEGF are associated with poor outcomes in endometrioid endometrial cancer patients (41).

In the present study, we have developed and characterized a subcutaneous xenograft model for endometrial cancer using a cell line derived from patients with endometrioid adenocarcinoma. We also combined the endometrial cancer cell line with SAT and VAT from human obese patients. In addition to an increase in size and volume of the endometrial cancer cell-VAT tumor, the human VAT-derived xenografts maintained a high expression of VEGF and downstream targets of the PI3K pathway such as pAkt and pS6. We also observed more tumor vasculature in VAT xenografts, suggesting a potential role of VEGF in activating the mTOR pathway. In a recent study, it has been shown that dual inhibition of the mTOR and VEGF pathway enhanced antitumor effects in metastatic pancreatic neuroendocrine tumors (PNET; ref. 42). Our study also demonstrated that the mTOR inhibitor, RAD001, significantly decreased VAT CM induced endometrial cancer cell proliferation. On the basis of these observations, combined mTOR and VEGF pathway–targeted therapy might be promising to reduce the incidence of endometrial cancer in obese women.

In an obese mouse model, our study also shows an increasing number of endometrial glands (a typical feature of EH) in the uterus as compared with healthy lean mice. This illustrates evidence of a direct link between weight gain with uterine physiology and function. With increasing body weight or AT deposits, pS6 expression in the glands also increases, indicating high mTOR activity. Examination of endometrial cancer tissue sections from human patients also support high pS6 expression or upregulated mTOR signaling in obese endometrial cancer patients. In fact, type I endometrioid carcinoma is induced by EH due to excess estrogen exposure during the proliferative phase of the menstrual cycle (31). In this context, tamoxifen-treated obese mice show carcinoma *in situ* compared with simple EH in lean mice, which explains an additive effect of adipocytes on the hyperplastic state of the uterus. Our fertility experiment also demonstrates that obese mice are completely infertile. Thus, adipocytes predispose to the hyperplastic and infertile uterus.

In summary, the main and novel finding of the present study is that high expression of the angiogenic marker, VEGF, in visceral adipocytes directly promotes vasculature in the uterus and mTOR activity in the endometrial glands. Bariatric surgery and long-term anti-mTOR and anti-VEGF therapy might suppress the VEGF–mTOR pathway in the uterine glands to maintain normal uterine function. However, interrupting the signal or crosstalk between adipocytes and uterine epithelial cells will be crucial to maintain healthy uterine function in obese women. Thus, evaluation of combination mTOR and VEGF pathway inhibitors is warranted.

Disclosure of Potential Conflicts of Interest

J. Lombard is a consultant/advisory board member for AstraZeneca. No potential conflicts of interest were disclosed by the other authors.

Authors' Contributions

Conception and design: S.S. Sahoo, J.M. Lombard, P.S. Tanwar
Development of methodology: S.S. Sahoo, P.S. Tanwar
Acquisition of data (provided animals, acquired and managed patients, provided facilities, etc.): Y. Ius, R. O'Sullivan, L.G. Wood, K. Jaaback, P.S. Tanwar
Analysis and interpretation of data (e.g., statistical analysis, biostatistics, computational analysis): S.S. Sahoo, L.G. Wood, P.S. Tanwar
Writing, review, and/or revision of the manuscript: S.S. Sahoo, J.M. Lombard, L.G. Wood, K. Jaaback, P.S. Tanwar
Administrative, technical, or material support (i.e., reporting or organizing data, constructing databases): P.S. Tanwar
Study supervision: P.S. Tanwar
Other (helped with the collection of specimen as clinician): P. Nahar

Acknowledgments

This work was supported by grants from National Health and Medical Research Council APP1081461, the Australian Research Council FT130101289, the Cancer Institute NSW 2014/CDF121 (P.S. Tanwar). S.S. Sahoo is a recipient of the University of Newcastle Postgraduate Research Fellowship.

The authors thank Professor Xu Dong Zhang (University of Newcastle, Australia) for the 3T3-L1 cell line and Dr. Ksenia Katyk for helping with primary endometrial cancer collection.

The costs of publication of this article were defrayed in part by the payment of page charges. This article must therefore be hereby marked *advertisement* in accordance with 18 U.S.C. Section 1734 solely to indicate this fact.

Received August 24, 2017; revised October 12, 2017; accepted November 1, 2017; published OnlineFirst November 13, 2017.

References

1. Finucane MM, Stevens GA, Cowan MJ, Danaei G, Lin JK, Paciorek CJ, et al. National, regional, and global trends in body-mass index since 1980: systematic analysis of health examination surveys and epidemiological studies with 960 country-years and 9.1 million participants. Lancet 2011; 377:557–67.
2. Calle EE, Kaaks R. Overweight, obesity and cancer: epidemiological evidence and proposed mechanisms. Nat Rev Cancer 2004;4: 579–91.
3. Siegel R, Ma J, Zou Z, Jemal A. Cancer statistics, 2014. CA Cancer J Clin 2014;64:9–29.

4. Renehan AG, Tyson M, Egger M, Heller RF, Zwahlen M. Body-mass index and incidence of cancer: a systematic review and meta-analysis of prospective observational studies. Lancet 2008;371:569–78.
5. Onstad MA, Schmandt RE, Lu KH. Addressing the role of obesity in endometrial cancer risk, prevention, and treatment. J Clin Oncol 2016;34: 4225–30.
6. Waki H, Tontonoz P. Endocrine functions of adipose tissue. Annu Rev Pathol 2007;2:31–56.
7. Ouchi N, Parker JL, Lugus JJ, Walsh K. Adipokines in inflammation and metabolic disease. Nat Rev Immunol 2011;11:85–97.
8. Ferrara N, Gerber HP, LeCouter J. The biology of VEGF and its receptors. Nat Med 2003;9:669–76.
9. Holmqvist K, Cross MJ, Rolny C, Hagerkvist R, Rahimi N, Matsumoto T, et al. The adaptor protein shb binds to tyrosine 1175 in vascular endothelial growth factor (VEGF) receptor-2 and regulates VEGF-dependent cellular migration. J Biol Chem 2004;279:22267–75.
10. Ito Y, Hart JR, Ueno L, Vogt PK. Oncogenic activity of the regulatory subunit p85beta of phosphatidylinositol 3-kinase (PI3K). Proc Natl Acad Sci U S A 2014;111:16826–9.
11. Nieman KM, Kenny HA, Penicka CV, Ladanyi A, Buell-Gutbrod R, Zillhardt MR, et al. Adipocytes promote ovarian cancer metastasis and provide energy for rapid tumor growth. Nat Med 2011;17: 1498–503.
12. Dirat B, Bochet L, Dabek M, Daviaud D, Dauvillier S, Majed B, et al. Cancer-associated adipocytes exhibit an activated phenotype and contribute to breast cancer invasion. Cancer Res 2011;71:2455–65.
13. Kushiro K, Chu RA, Verma A, Nunez NP. Adipocytes promote B16BL6 melanoma cell invasion and the epithelial-to-mesenchymal transition. Cancer Microenviron 2012;5:73–82.
14. Tokuda Y, Satoh Y, Fujiyama C, Toda S, Sugihara H, Masaki Z. Prostate cancer cell growth is modulated by adipocyte-cancer cell interaction. BJU Int 2003;91:716–20.
15. Carswell KA, Lee MJ, Fried SK. Culture of isolated human adipocytes and isolated adipose tissue. Methods Mol Biol 2012;806:203–14.
16. Sahoo SS, Quah MY, Nielsen S, Atkins J, Au GG, Cairns MJ, et al. Inhibition of extracellular matrix mediated TGF-beta signalling suppresses endometrial cancer metastasis. Oncotarget 2017;8:71400-17.
17. Choudhury KR, Yagle KJ, Swanson PE, Krohn KA, Rajendran JG. A robust automated measure of average antibody staining in immunohistochemistry images. J Histochem Cytochem 2010;58:95–107.
18. Hannan NJ, Paiva P, Dimitriadis E, Salamonsen LA. Models for study of human embryo implantation: choice of cell lines? Biol Reprod 2010; 82:235–45.
19. Renehan AG, Harvie M, Cutress RI, Leitzmann M, Pischon T, Howell S, et al. How to manage the obese patient with cancer. J Clin Oncol 2016; 34:4284–94.
20. Moxley KM, McMeekin DS. Endometrial carcinoma: a review of chemotherapy, drug resistance, and the search for new agents. Oncologist 2010;15:1026–33.
21. von Mering C, Huynen M, Jaeggi D, Schmidt S, Bork P, Snel B. STRING: a database of predicted functional associations between proteins. Nucleic Acids Res 2003;31:258–61.
22. Bradford LS, Rauh-Hain A, Clark RM, Groeneweg JW, Zhang L, Borger D, et al. Assessing the efficacy of targeting the phosphatidylinositol 3-kinase/AKT/mTOR signaling pathway in endometrial cancer. Gynecol Oncol 2014;133:346–52.
23. Slomovitz BM, Coleman RL. The PI3K/AKT/mTOR pathway as a therapeutic target in endometrial cancer. Clin Cancer Res 2012;18:5856–64.
24. Cancer Genome Atlas Research Network, Kandoth C, Schultz N, Cherniack AD, Akbani R, Liu Y, et al. Integrated genomic characterization of endometrial carcinoma. Nature 2013;497:67–73.
25. Bajwa P, Sahoo SS, Tanwar PS. Age-related mTOR in gynaecological cancers. Aging (Albany NY) 2017;9:301–2.
26. Saxton RA, Sabatini DM. mTOR Signaling in Growth, Metabolism, and Disease. Cell 2017;169:361–71.
27. Girard D, Petrovsky N. Alstrom syndrome: insights into the pathogenesis of metabolic disorders. Nat Rev Endocrinol 2011;7:77–88.
28. Sanderson PA, Critchley HO, Williams AR, Arends MJ, Saunders PT. New concepts for an old problem: the diagnosis of endometrial hyperplasia. Hum Reprod Update 2017;23:232–54.
29. Coultas L, Chawengsaksophak K, Rossant J. Endothelial cells and VEGF in vascular development. Nature 2005;438:937–45.
30. Tanwar PS, Zhang L, Roberts DJ, Teixeira JM. Stromal deletion of the APC tumor suppressor in mice triggers development of endometrial cancer. Cancer Res 2011;71:1584–96.
31. Emons G, Fleckenstein G, Hinney B, Huschmand A, Heyl W. Hormonal interactions in endometrial cancer. Endocr Relat Cancer 2000;7:227–42.
32. Hu R, Hilakivi-Clarke L, Clarke R. Molecular mechanisms of tamoxifen-associated endometrial cancer (Review). Oncol Lett 2015;9:1495–501.
33. Reyes HD, Miecznikowski J, Gonzalez-Bosquet J, Devor EJ, Zhang Y, Thiel KW, et al. High stathmin expression is a marker for poor clinical outcome in endometrial cancer: An NRG oncology group/gynecologic oncology group study. Gynecol Oncol 2017;146:247–253.
34. Bajwa P, Nielsen S, Lombard JM, Rassam L, Nahar P, Rueda BR, et al. Overactive mTOR signaling leads to endometrial hyperplasia in aged women and mice. Oncotarget 2017;8:7265–75.
35. Schmandt RE, Iglesias DA, Co NN, Lu KH. Understanding obesity and endometrial cancer risk: opportunities for prevention. Am J Obstet Gynecol 2011;205:518–25.
36. Arem H, Irwin ML. Obesity and endometrial cancer survival: a systematic review. Int J Obes 2013;37:634–9.
37. Amant F, Moerman P, Neven P, Timmerman D, Van Limbergen E, Vergote I. Endometrial cancer. Lancet 2005;366:491–505.
38. Calle EE, Rodriguez C, Walker-Thurmond K, Thun MJ. Overweight, obesity, and mortality from cancer in a prospectively studied cohort of U.S. adults. N Engl J Med 2003;348:1625–38.
39. Fader AN, Arriba LN, Frasure HE, von Gruenigen VE. Endometrial cancer and obesity: epidemiology, biomarkers, prevention and survivorship. Gynecol Oncol 2009;114:121–7.
40. Sun K, Wernstedt Asterholm I, Kusminski CM, Bueno AC, Wang ZV, Pollard JW, et al. Dichotomous effects of VEGF-A on adipose tissue dysfunction. Proc Natl Acad Sci U S A 2012;109:5874–9.
41. Kamat AA, Merritt WM, Coffey D, Lin YG, Patel PR, Broaddus R, et al. Clinical and biological significance of vascular endothelial growth factor in endometrial cancer. Clin Cancer Res 2007;13:7487–95.
42. Bergsland EK.Combined mammalian target of rapamycin and vascular endothelial growth factor pathway inhibition in pancreatic neuroendocrine tumors: more than the sum of its parts? J Clin Oncol 2015;33:1523–6.

Supplemental Data

Supplementary Figures

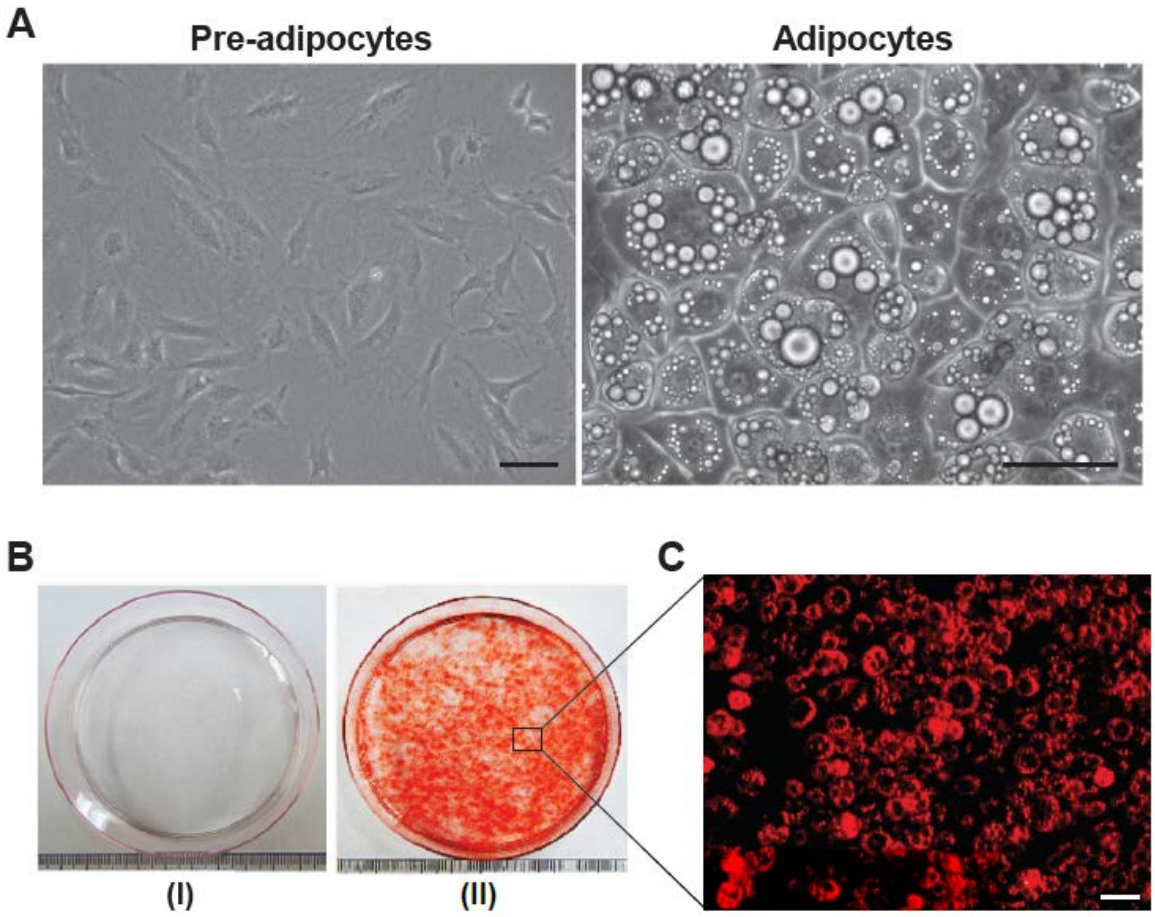

Figure S1. In vitro adipogenesis and Oil Red O staining.

Phase-contrast microscopy images of the 3T3-L1 mouse embryonic fibroblast adipose-like cells. Undifferentiated 3T3-L1 cells (Pre-adipocytes) were grown to ~95 % confluent stage (Day 3) and induced in DMEM-high glucose medium containing 1 mM of insulin and 30 µM of T3 for 48 hours. Following induction, cells were differentiated with 125 nM of indomethacin, 2 µg/ml of dexamethasone and 250 nM of methylisobutylxanthine with media changes every 48 hours for an additional 7 days. On Day 12, the differentiated 3T3-L1 cells (Adipocytes) were observed with visible lipid droplets. (B) Comparison of Oil Red O staining of (I) undifferentiated and (II) differentiated 3T3-L1 cells. (C) Magnified stereoscopic image of Oil Red O-stained differentiated 3T3-L1 cells. Adipogenesis was demonstrated by the accumulation of neutral lipid vacuoles that stain with Oil Red O. Scale bar equal, 100 µm.

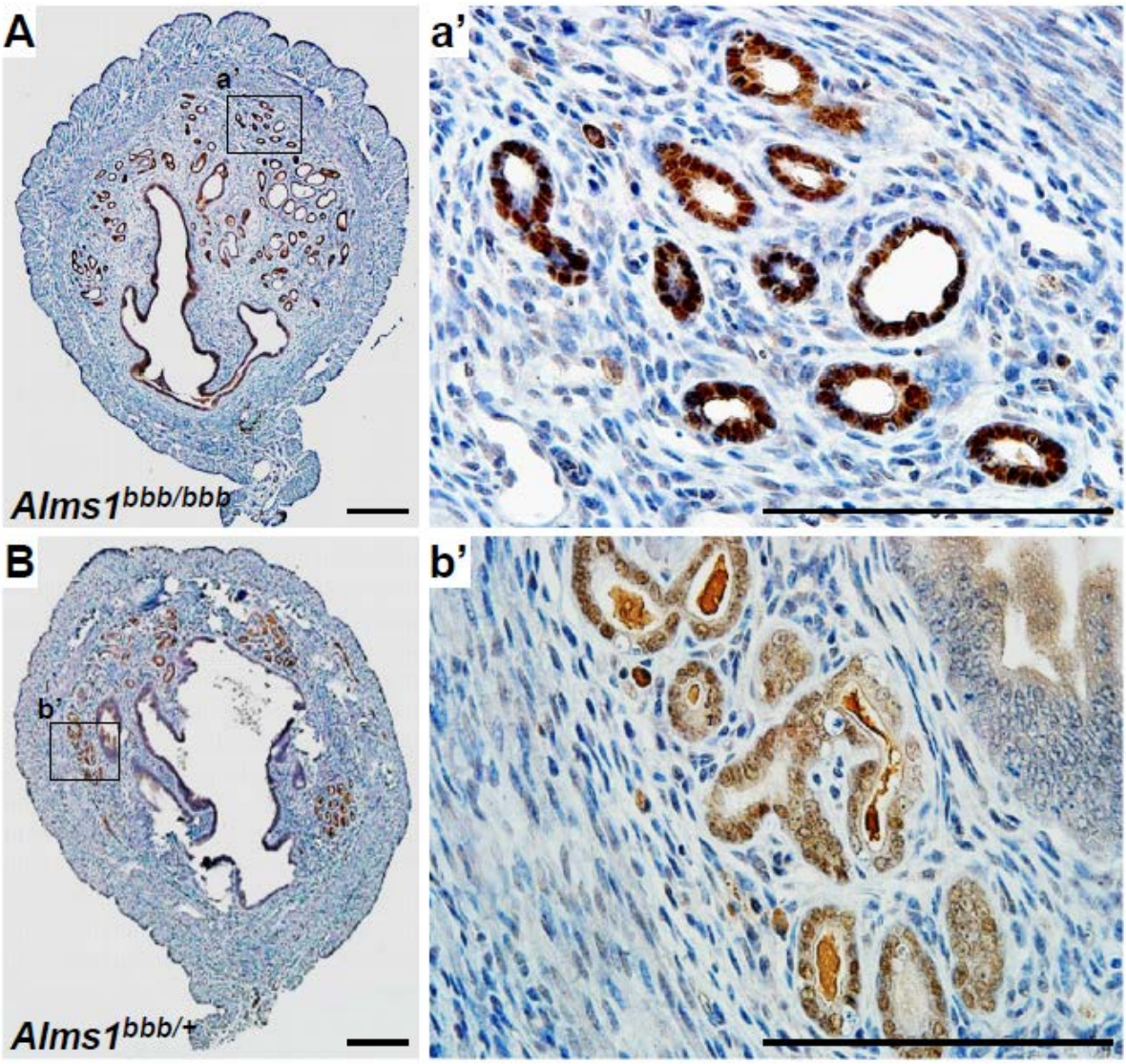

Figure S2. Characterisation of endometrial glands by FOXA2 staining.

Photomicrograph of the cross-section of Blobby (A) homozygous mutant (*Alms1*$^{bbb/bbb}$) and (B) heterozygous mutant (*Alms1*$^{bbb/+}$) mouse uterus (6 months old) showing glands in the stroma, stained immunohistochemically for FOXA2 (brown). Respective magnified images (a' and b') are shown. Scale bar equal, 200 µm.

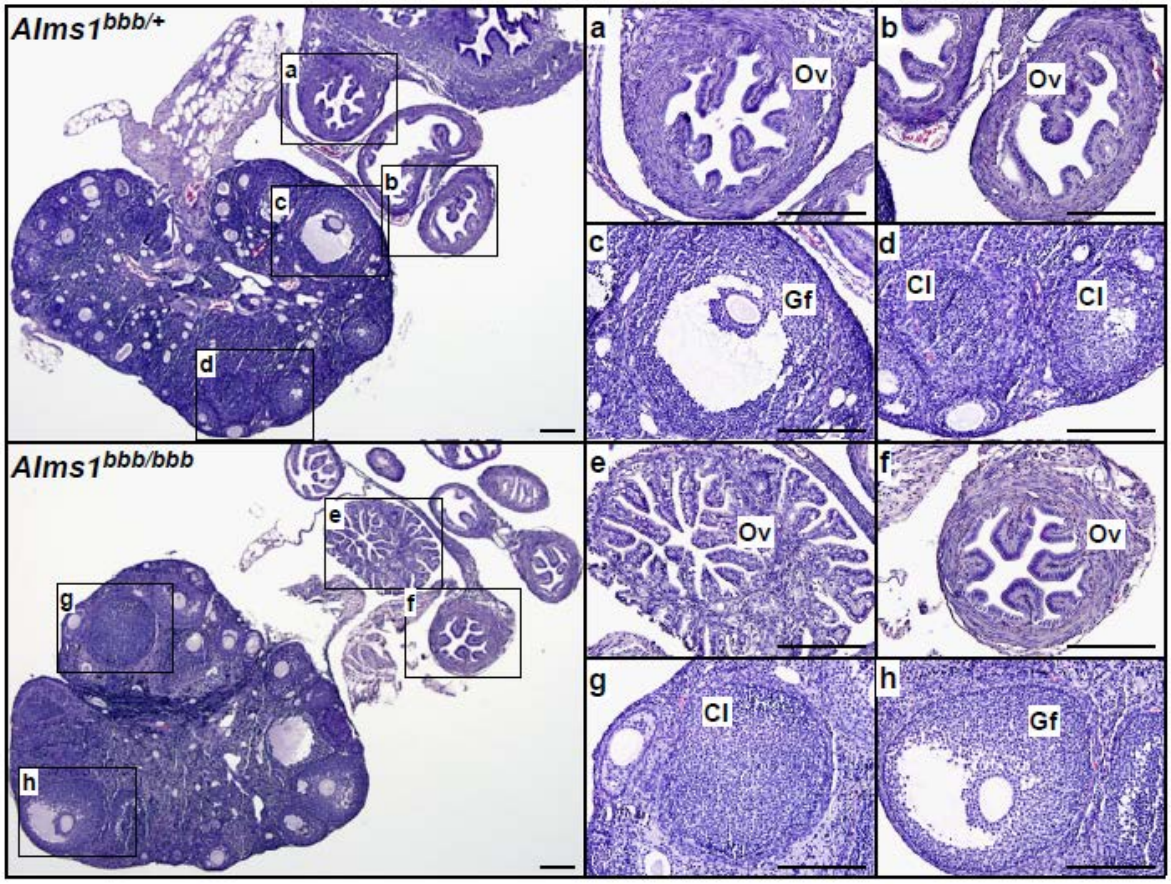

Figure S3. Histologic analysis of Blobby ovary and oviduct.

Representative histological sections of lean (*Alms1*$^{bbb/+}$) and obese (*Alms1*$^{bbb/bbb}$) Blobby ovary and oviduct show normal morphology and physiology with different sized follicles. Higher magnification images of the oviduct (a, b, e, f), the graafian follicle (c, h) and the corpus luteum (d, g) are shown. Ov, Oviduct; Gf, Graafian follicle; Cl, Corpus luteum. Scale bar equal, 200 µm.

Supplementary Tables

Table S1. Profiling of differentially expressed proteins in pre-adipocyte and adipocyte supernate

Cytokine/Chemokine/Growth factors/Soluble proteins	Mean spot pixel density		Fold change
	Pre-adipocyte CM	Adipocyte CM	
Up-regulated			
Resistin	15427	1043697	67.7
Chemerin	29819	964773.5	32.4
VEGF	69304.5	2177157	31.4
Complement Factor D	16251.5	507405	31.2
Adiponectin/Arcp30	41613	1263109	30.4
Lipocalin-2/NGAL	38264.5	937070.5	24.5
CCL6/C10	50819	896408	17.6
IL-4	15612	107292	6.9
Coagulation Factor III/Tissue Factor	251942.5	1351617	5.4
IL-7	24563	111513	4.5
Chitinase 3-like 1	124732.5	513208	4.1
Endostatin	114027	413182	3.6
Gas 6	154058	530636.5	3.4
Angiopoietin-1	187988	497715.5	2.6
VCAM-1/CD106	299436	603526	2
Osteopontin (OPN)	524198	1044466	2
Periostin/OSF-2	499019.5	903898	1.8
Cystatin C	324492	579775	1.8
IL-5	15716	25951	1.7
MMP-2	934450.5	1407607	1.5
Down-regulated			
WISP-1/CCN4	335067	115184	2.9
CCL2/JE/MCP-1	610017	257672	2.4
IGFBP-6	1017099	457033	2.2
Serpin E1/PAI-1	543554.5	251175	2.2
HGF	613972	346689	1.8

Table S2: Fertility defect of *Alms1*$^{bbb/bbb}$ mice

Genotype	Number of mice tested	Number of litters	Number of pups	Mean of pups/litter	Mean of litter/mouse
Alms1$^{bbb/+}$	9	43	287	6.67 ± 0.29	4.78 ± 0.15
Alms1$^{bbb/bbb}$	9	0	0	0	0

Table S3: Human endometrial tissue samples from healthy women and from women with endometrioid endometrial cancer

Patient ID	BMI	Tumour site	Diagnosis
Pt1	22	Uterus	Normal Tissue
Pt2	20	Uterus (body)	Normal Tissue
Pt3	25	Endometrium	Normal Tissue
Pt4	23	Endometrium	Normal Tissue
Pt5	26	Uterus	Normal Tissue
Pt6	25	Uterus	Carcinoma
Pt7	20	Uterus (body)	Carcinoma
Pt8	25	Endometrium	Carcinoma
Pt9	23	Endometrium	Carcinoma
Pt10	28	Endometrium	Carcinoma
Pt11	28	Endometrium	Carcinoma
Pt12	25.5	Endometrium	Carcinoma
Pt13	33	Uterus	Adenocarcinoma
Pt14	44	Uterus	Carcinoma
Pt15	43	uterus	carcinoma
Pt16	51.1	Uterus	Carcinoma
Pt17	37.5	Uterus	Carcinoma
Pt18	49	Uterus	Carcinoma
Pt19	36	Uterus	Carcinoma
Pt20	31	Uterus	Leiomyosarcoma
Pt21	39	Endometrium	Carcinoma
Pt22	43	Endometrium	Carcinoma
Pt23	42	Endometrium	Carcinoma
Pt24	48	Endometrium	Carcinoma
Pt25	40	Endometrium	Adenocarcinoma

Pt: Patient

Chapter 4

Human Placental-like Alkaline Phosphatase (ALPPL2) as a Prognostic Biomarker in Endometrial Cancer

Preface

Endometrial cancer is the most frequently diagnosed gynecological cancer and the occurrence is very high in post-menopausal women. Although there has been an improvement in the treatment of this disease, the 5-year survival rate for these patients shows poor outcome due to the diagnosis of the disease at an advanced stage. Obesity is an independent risk factor for this disease and lack of public awareness increases the occurrence of this disease in women with high body mass index (BMI). Therefore, early diagnosis of the disease is necessary to suppress the spread of cancer and improve patient outcomes. Due to insufficient power of clinicopathological features of endometrial cancer, early detection of the disease is currently unavailable. In this study, we investigated differential expression of soluble and secreted proteins in healthy and cancer patients and found placental-like alkaline phosphatase (ALPPL2) as a potential secreted protein in endometrial cancer patients, which can be used for prognosis of the disease.

UON Graduate Research

Co-authorship declaration

THE UNIVERSITY OF NEWCASTLE AUSTRALIA

Statement of Authors' Contributions

This statement summarises the intellectual input by all the authors in the paper entitled **"Human placental-like alkaline phosphatase (ALPPL2) as a prognostic biomarker in endometrial cancer"**. This research article is submitted to the Journal ***Proceedings of the National Academy of Sciences of the United States of America***.

Authors	Statement of contribution
Subhransu S. Sahoo (First and lead author)	Designed the study Performed all the *in vitro* and *in vivo* experiments Performed statistical analysis of the data Made figures and tables for the paper Wrote and edited the manuscript
Preety Bajwa (Co-author)	Helped with animal experiment
Yi-An Ko (Co-author)	Helped with collection of endometrial cancer patient samples
Pravin Nahar (Co-author)	Provided endometrial cancer patient samples
Pradeep S. Tanwar (Corresponding author)	Supervised and designed the study Edited the manuscript Provided financial support

Subhransu S. Sahoo

Preety Bajwa

Yi-An Ko

Pravin Nahar

Pradeep S. Tanwar

Robert Callister - Faculty Assistant Dean Research Training

UON Graduate Research

Co-authorship declaration

THE UNIVERSITY OF NEWCASTLE AUSTRALIA

Statement of Authors' Contributions

This statement summarises the intellectual input by all the authors in the paper entitled **"Human placental-like alkaline phosphatase (ALPPL2) as a prognostic biomarker in endometrial cancer"**.
This research article is submitted to the Journal ***Proceedings of the National Academy of Sciences of the United States of America***.

Authors	Statement of contribution
Subhransu S. Sahoo (First and lead author)	Designed the study Performed all the *in vitro* and *in vivo* experiments Performed statistical analysis of the data Made figures and tables for the paper Wrote and edited the manuscript
Preety Bajwa (Co-author)	Helped with animal experiment
Yi-An Ko (Co-author)	Helped with collection of endometrial cancer patient samples
Pravin Nahar (Co-author)	Provided endometrial cancer patient samples
Pradeep S. Tanwar (Corresponding author)	Supervised and designed the study Edited the manuscript Provided financial support

Subhransu S. Sahoo

Preety Bajwa

Yi-An Ko

Pravin Nahar

Pradeep S. Tanwar

Faculty Assistant Dean Research Training

Publication

This manuscript has submitted to the journal ***Proceedings of the National Academy of Sciences of the United States of America***.

Human placental-like alkaline phosphatase (ALPPL2) as a prognostic biomarker in endometrial cancer

Subhransu S. Sahoo[1,2], Preety Bajwa[1,2], Yi-An Ko[1,2], Pravin Nahar[3], Pradeep S. Tanwar[1,2*]

[1]Gynaecology Oncology Group, University of Newcastle, Newcastle, New South Wales, Australia; [2]School of Biomedical Sciences and Pharmacy, University of Newcastle, Newcastle, New South Wales, Australia; [3]Department of Maternity and Gynecology, John Hunter Hospital, Newcastle, New South Wales, Australia

Short title: Endometrial cancer biomarker

*Address correspondence to:
Dr. Pradeep S. Tanwar
Australian Research Council Future Fellow
Cancer Institute NSW Career Development Fellow
Group Leader, Gynecology Oncology Group
LS236, University Drive
University of Newcastle
Callaghan NSW 2308 Australia
Email: pradeep.tanwar@newcastle.edu.au
Phone: +61-2-49215148

Disclosure statement: The authors have nothing to disclose

Chapter 4: Human Placental-like Alkaline Phosphatase (ALPPL2) as a Prognostic Biomarker in Endometrial Cancer

Abstract

Endometrial cancer is the most frequently diagnosed gynecological cancer. Lack of early diagnosis is one of the main causes of endometrial cancer mortality. To identify novel biomarkers that can facilitate early diagnosis we performed transcriptome analysis and identified ALPPL2 (Alkaline Phosphatase, Placental-Like 2) as one of the most abundantly secreted protein by endometrial cancer organoids. Given that extensive exposure to estrogen (E2) is generally acknowledged as a risk factor for endometrial cancer, we investigated the expression of ALPPL2 in presence of E2. The E2 induced increase in organoid growth *in vitro* and endometrial hyperplasia *in vivo* was associated with an increased ALPPL2 expression. qRT-PCR and western blot analysis also confirmed an agonist action of E2 on ALPPL2 expression in endometrial cancer organoids and mouse uteri. Immunohistochemically, we also showed significant upregulation of ALPPL2 in a cohort of 97 endometrial cancer patients. Furthermore, ROC analysis on 100 patients' plasma samples demonstrated that ALPPL2 (AUC = 0.71) is a better prognostic biomarker than CA-125 (AUC = 0.55), particularly in patients with low-grade endometrioid tumors (sensitivity 0.477 vs 0.154 for CA-125). Collectively, ectopic expression and chronic secretion of the oncofetal protein, ALPPL2, by endometrial cancer cells supports its potential use in the serum-based diagnosis of endometrial cancer.

Keywords

Endometrial cancer, ALPPL2, Prognostic biomarker, Steroid signaling

Introduction

Uterine (endometrial) cancer is the fifth most common gynecological cancer worldwide, with over 60,000 new cases diagnosed and nearly 10,000 deaths every year (Morice et al., 2016; Siegel et al., 2017). In terms of clinical and pathological features, type I (endometrioid carcinoma) is associated with hyperestrogenism and endometrial hyperplasia (80-90%) whereas type II (non-endometrioid carcinoma) is an estrogen-independent malignancy with high-risk histological subtypes (serous, clear cell or high-grade endometrioid) (Morice et al., 2016). The overall 5-year survival of endometrial cancer patients without metastasis ranges from 74% to 91% (Morice et al., 2016). However, in case of women at stage IV of endometrial cancer, the long-term survival rate drops to 20% (Creasman et al., 2006). Obesity is an independent risk factor for this disease and approximately 50% of cases are associated with high body mass index (BMI, >30 kg/m^2) (Renehan et al., 2008).

Standard treatment for the vast majority of endometrial cancer patients requires surgery either hysterectomy or bilateral salpingo-oophorectomy. However, identification of these patients before surgery remains challenging. Therefore, there is an urgent need for a highly standardized biomarker that would improve risk assessment. Identification of a prognostic and pre-operative biomarker can facilitate early detection and diagnosis of the disease in clinics.

A perfect tumor marker will be one that is produced at much higher levels by tumor cells and secreted in measurable amounts into body fluids. Thus, profiling of cancer cell secretome is crucial to identify such markers. In contrast to conventional two-dimensional culture, the culture of organoids are beneficial as they are self-organizing, stable and resemble the tissue of origin. The endometrial organoids imitate *in vivo* uterine glands, respond to steroid signaling and secrete components of 'uterine milk' (Turco et al., 2017). To identify a candidate gene, which can be used as a biomarker, we analyzed the transcriptome of endometrial cancer organoids and identified ALPPL2 (Alkaline Phosphatase, Placental-Like 2) as the most significant and enormously secreted protein in endometrial cancer organoids.

ALPPL2 is a membrane bound glycosylated enzyme and at elevated level secreted to extracellular space. In humans, a gene family composed of four loci; three tissue-specific ALP (TSALP) genes on chromosome 2q34-q37 and a single tissue-nonspecific ALP (TNALP) gene on chromosome 1p36.1-

p34 encodes alkaline phosphatase (ALP, E.C.3.1.3.1) (Millan and Fishman, 1995). Thus, there are four distinct but related ALP: intestinal (ALPI), placental (ALPP), germ cell or placental-like (ALPPL2) as TSALP and the TNALP is expressed in liver/bone/kidney (ALPL) (Millan and Fishman, 1995). In a healthy individual, ALP is only expressed in placenta and synthesized by syncytiotrophoblast during pregnancy. As pregnancy proceeds, the serum ALPP concentration increases and directly correlates with the growth of the placenta (Okamoto et al., 1990). ALP dephosphorylates proteins and alkaloids and provides an alkaline environment, suggesting a unique role of ALP in feto-maternal metabolism and placental differentiation (Okamoto et al., 1990). ALP expression is also increased during liver cholestasis, bone mineralization and intestinal absorption (Millan and Fishman, 1995). In addition, ectopic overexpression of placental-like ALP in testicular cancer patients has shown a potential use for serum-based diagnosis of seminomas (Lange et al., 1982; Neumann et al., 2011). Nevertheless, the function of ALPPL2 has never been studied in the context of uterine cancer.

In this study, we have demonstrated that *ALPPL2* is upregulated in endometrial cancer organoids at mRNA and protein level. We have also demonstrated that steroid signaling drives the expression of ALPPL2. Moreover, due to ectopic expression of ALPPL2 in endometrial cancer patients, this oncofetal protein can be an attractive target for the serum-based diagnosis of endometrial cancer.

Results

ALPPL2 as a candidate secretory protein in human endometrial cancer organoids

To identify a potential tumor biomarker for diagnosis of endometrial cancer patients, our strategy was to characterize the secretome of endometrial cancer cells. To characterize the secretome of human endometrial cancer cells, we cultured Ishikawa cells in three-dimension (3D) on an extracellular matrix substratum to form organoids. Endometrial cancer organoids formed in 3D was typically initiated from a single cell to organize into a relevant multicellular polarized (shown by GM130 on the apical side) and glandular (shown by actin filaments arrangement) architecture (Fig 1A). In a 3D environment by acquiring a native glandular pattern, endometrial cancer cells turn into secretory in nature and synthesized more number of secretory proteins compared to other proteins (nuclear, cytoplasmic and membranous) (Fig 1B). Our transcriptome analysis of Ishikawa organoids identified 111 secreted protein-coding genes (90 upregulated, 21 downregulated) compared to the monolayer of Ishikawa cells (>2-fold change, $P < 0.05$) (Fig 1B). Further cumulative analysis of all the highly significant (GFOLD > 2; $P < 0.05$; eFDR, 1) transcripts revealed ALPPL2 as the most abundantly secreted protein-coding gene (~80-fold) in Ishikawa organoids (Fig 1C, Table S1). *ALPPL2* expression was also validated at translational level using immunoblot and showed distinct expression in Ishikawa organoids, in concordant with the RNA-seq data (Fig 1D). These results suggest that endometrial cancer cells secrete ALPPL2 abundantly in their native state.

Endometrial cancer organoid growth and ALPPL2 expression show similar trend towards estrogen and progesterone

Reported studies in human patients suggest that steroid hormones, estrogen (E2) and progesterone (P4) act reciprocally in the development of endometrial cancer (Hecht and Mutter, 2006; Takahashi-Shiga et al., 2009). Our preliminary results demonstrated that size and proliferation of Ishikawa organoids were increased upon E2 administration and the mitogenic action of E2 was counterbalanced by P4 (Fig 2A-2C). As endometrial cancer cells secrete ALPPL2, we questioned whether E2 mediated endometrial cancer cell proliferation also stimulates ALPPL2 expression. We performed quantitative real-time PCR analysis of *ALPPL2* on Ishikawa organoids grown in E2 alone or P4 alone or E2 and P4. *ALPPL2* mRNA expression was significantly upregulated in E2 treated organoids whereas P4 inhibited this effect (Fig 2D). Overexpression of ALPPL2 was also confirmed by western blot analysis on total cell lysate of Ishikawa cells and

organoids treated with E2 and/or P4 (Fig 2E and 2F). The results concluded that E2 promotes Ishikawa organoid proliferation with elevated ALPPL2 expression.

Steroid hormones regulate ALPPL2 expression in mouse and human uterus

To validate response of ALPPL2 to steroid hormones *in vivo*, wild-type C57BL/6 mice were ovariectomized and treated with vehicle, E2 or E2 and P4 for 3 months (*n* = 3 per treatment). Effect of steroid hormones on mice uteri was confirmed by histological analysis, which showed increased endometrial hyperplasia in E2 treated group compared to E2 and P4 treated uteri (Fig 3A). Immunohistochemical analysis showed an increase in ALPPL2 expression in E2 treated mice whereas in E2 and P4 treated mice, P4 attenuated the effect of E2 (Fig 3A and 3B). The expression of ALPPL2 in E2 and/or P4 treated mice uterus was also ascertained at mRNA and protein level (Fig 3C-3E). ALPPL2 protein expression was also checked during proliferative (E2 response) and secretory phase (P4 response) of the menstrual cycle. In consistent with our previous *in vitro* and *in vivo* findings, human secretory endometrium displayed modest ALPPL2 expression compared to the proliferative endometrium (Fig 3F-3G). Taken together, these results demonstrate that *ALPPL2* is an E2 responsive gene and hyperestrogenic state of the uterus can be detected by ALPPL2 expression level.

ALPPL2 predicts survival in patients with endometrial adenocarcinoma

The positive correlation between sex-steroid hormones and endometrial cancer has been described within the framework of the 'unopposed estrogen hypothesis', which implicates that women with high endogenous estrogen level are at increased risk of developing endometrial cancer. In our present study, we found ALPPL2 expression positively correlates with an increase in E2 concentration. To evaluate the relevance of these findings in a clinical cohort, publicly available RNA-seq gene expression data from the TCGA's (The Cancer Genome Atlas) uterine corpus endometrial carcinoma subset was analyzed. TCGA data analysis revealed amplification of ALPPL2 is strongly associated with poor outcome in endometrial cancer patients (Cancer Genome Atlas Research et al., 2013). Kaplan-Meier analysis of 548 samples with median cut and log-rank test showed a significant difference in overall (Cox hazard ratio of 0.2183, 95% CI: 0.0458-1.041, *P* = 0.0139) and disease-free (Cox hazard ratio of 0.8976, 95% CI: 0.2062-3.908, *P* = 0.5067) survival time, linking ALPPL2 with poor prognosis (Fig 4A and 4B). Those patients with high ALPPL2 expression were found to have decreased overall survival (36% deceased) compared to patients

with low ALPPL2 expression (16% deceased). Moreover, TCGA dataset analysis demonstrated that ALPPL2 is a better predictor of patient survival than CA-125 (MUC16 expression: high, 8.6% deceased vs. low, 17.9% deceased; Fig S1). These data suggest ALPPL2 up-regulation is an indicator of poor prognosis in endometrial cancer patients.

Prognostic significance of ALPPL2: Comparison of endometrial adenocarcinomas versus normal tissue

To test the prognostic value of ALPPL2 protein levels in endometrial cancer patients, immunohistochemistry was performed on a formalin-fixed, paraffin-embedded (FFPE) tissue microarray consisting of 61 low-grade and 30 high-grade endometrial adenocarcinomas (Table 1). The average ALPPL2 protein staining intensity was higher in adenocarcinoma cases compared to the normal endometrium (Fig 4C and 4D; ALPPL2 H-Score: normal, 159 ± 5.83 vs. adenocarcinoma, 180.1 ± 4.37; P = 0.0174). In addition, analysis of different grades of adenocarcinomas also demonstrated a significant increase in ALPPL2 protein expression compared to normal (Fig 4D). The corresponding area under the receiver operating curve (ROC) of normal versus adenocarcinoma patients was 0.82 (95% CI 0.69-0.93, P = 0.0197) (Fig 4E). Furthermore, we compared ALPPL2 expression level between endometrial cancer tissue and corresponding normal adjacent tissue from the same patient. All the normal adjacent and endometrial cancer tissue sections were histologically analyzed before proceeding to protein isolation (Fig 4F and Fig S2). In consistent with tissue microarray data, western blot analysis ascertained significant upregulation of ALPPL2 in endometrial cancer tissue than normal adjacent endometrium (Fig 4G and 4H). Collectively, these data show that significant upregulation of ALPPL2 protein during endometrial cancer can be utilized for patient prognosis.

ALPPL2 as a clinically useful serum tumor marker for endometrial carcinomas

ALPPL2 expression was analyzed and compared with CA-125 levels in the plasma of 100 endometrial cancers of various histological types (low- and high-grade) and 60 normal women. Median ALPPL2 levels were significantly higher in grade I endometrial cancer patients (control, 1.172 ng/mL vs. case, 1.486 ng/mL; $P < 0.0001$) whereas patients with advanced stage disease (grade III/IV) displayed higher CA-125 values (control, 18.21 U/mL vs. case, 28.15 U/mL; P = 0.0002; Fig 5A and 5B). However, overall plasma ALPPL2 level in the patients with endometrial cancer (median, 1.4 ng/mL; range, 0.54-11.12 ng/mL) was significantly higher than normal women (median, 1.1 ng/mL; range, 0.35-2.99 ng/mL; P = 0.0101) as compared with CA-125 level (case:

median, 19.48 U/mL; range, 2.59-169.20 U/mL vs. control: 18.21 U/mL; range, 4.84-132.20 U/mL; *P* = 0.2832). We also compared ALPPL2 values with CA-125 values for individual case and control samples (Fig 5C). With a threshold of 1.5 ng/mL, ALPPL2 was positive in 40 of 100 cases (40%) whereas only 24 of 100 (24%) cases were detected by CA-125 cutoff values (35 U/mL, Fig 5D). Overall, in a cohort of 160 women, 52 individuals (33%) had higher ALPPL2 threshold values whereas only 33 individuals (12%) had elevated CA-125 values (Fig 5E). Furthermore, to determine the prognostic significance of ALPPL2, we generated ROC curves to discriminate cancer cases from the controls. The superiority of ALPPL2 over CA-125 was strengthened when the analysis was limited to grade I endometrioid endometrial cancer patients (ALPPL2 AUC, 0.71 vs. CA-125 AUC, 0.55; Fig 5F). Compared with grade I case, CA-125 displayed better prognosis for grade III/IV patients (CA-125 AUC, 0.73 vs. ALPPL2 AUC, 0.55; Fig 5G). However, for all patients, the sensitivity of ALPPL2 (0.40) was higher than CA-125 (0.24, Fig 5H). Thus, it appears that ALPPL2 titers independently can recognize early stage endometrial cancer patients than CA-125.

Materials and Methods

Cell line and culture condition

The human endometrial adenocarcinoma cell line Ishikawa (Sigma #99040201) was cultured in MEM (HyClone) medium supplemented with 5% heat-inactivated FBS (Bovogen Biologicals), 2 mmol/L L-glutamine (HyClone), and antibiotics (50 U/mL penicillin, 50 mg/L streptomycin; Gibco) in a humidified atmosphere at 37°C containing 5% CO_2. Cell line authentication was done by short tandem repeat (STR) DNA profiling method and mycoplasma contamination in cells was routinely conducted using MycoAlert™ Plus Mycoplasma detection kit (Lonza).

Clinical samples

***Human endometrial cancer patient samples*:** Human endometrial cancer and adjacent normal tissue samples were collected from patients undergoing tumor resection or surgical debulking at John Hunter Hospital using a protocol approved by the University of Newcastle Human Research Ethics Committee. Fresh tissue samples were transported to the laboratory, washed with phosphate buffered saline (PBS) and fixed in 10% buffered formalin for paraffin embedding and sectioning. Corresponding normal adjacent and tumor sections were also flash frozen and stored in liquid nitrogen for protein isolation and western blot analysis.

***Human plasma samples*:** The University of Newcastle Human Research Ethics Committee approved the protocol to collect human plasma sample. Blood plasma samples from normal and endometrial adenocarcinoma patients were collected from Victorian Cancer Biobank, Australia.

***Tissue microarray*:** Endometrial cancer tissue microarray (EMC1021, US Biomax) including 97 cases of carcinoma (Grade 1, 2, and 3) and 5 normal sections were immunohistochemically analyzed for ALPPL2 protein expression. Quantification of ALPPL2 staining intensities was performed using the Halo™ image analysis platform; H-scores were calculated and used to establish the receiver-operating characteristic (ROC) curve between normal and adenocarcinoma cases.

***TCGA data*:** The association between ALPPL2 or MUC16 expression and patient survival was validated using a uterine cancer data set from TCGA (Cancer Genome Atlas Research et al., 2013). The TCGA microarray gene expression data was used to calculate the ALPPL2 or MUC16 mRNA expression z-scores for 548 tumor samples. A z-score of ±2 was used as a cutoff for to classify the samples into high and low ALPPL2 or MUC16 expression groups. The overall and disease-free Kaplan-Meier survival analysis for these two groups of patients were performed using the cBioPortal for Cancer Genomics (Cerami et al., 2012).

Animals and Hormone Treatments

The University of Newcastle Animal Care and Ethics Committee approved all procedures for mice experimentation. To study the effect of steroid hormones, 8- to 12-weeks-old female C57BL/6 mice were ovariectomized and allowed to rest for seven days. One week post-ovariectomy, mice were subcutaneously implanted with hormone pellets of 17-β-oestradiol (0.72 mg per pellet, 90 days release, *n* = 3) or 17-β-oestradiol and progesterone (0.72 mg and 100 mg per pellet respectively, 90 days release, *n* = 3, Innovative Research of America). Mice with subcutaneous incision but no pellet were used as controls (Sham, *n* = 3). After 3 months, uterine tissues were collected, processed for formalin-fixed paraffin-embedding (FFPE) and snap frozen for protein or RNA isolation.

RNA-Seq and data analysis

Total RNA was isolated from 2D monolayer and 3D grown Ishikawa organoids using RNeasy Mini kit (Qiagen) following manufacturer's instructions. Library preparation, sequencing, and analysis of read counts were performed as described previously (Sahoo et al., 2017b). Transcripts with generalized log2 fold change (GFOLD) value greater than 2 were considered statistically significant (Feng et al., 2012).

3D organoid formation assay and Immunofluorescence staining

5,000 Ishikawa cells/well were seeded in triplicate in 100 µL medium onto 96-well tissue culture plates coated with a thin layer of reduced growth factor basement membrane extract (Cultrex® RGF BME: Trevigen) and were allowed to form organoids. After 24 hours, the organoids were subjected to desired hormonal treatments: 10 nmol/L estrogen (β-Estradiol, Sigma #E8875) and 100 nmol/L progesterone (Medroxyprogesterone 17-acetate, Sigma #M1629). The culture medium containing desired hormone concentration was changed on every 48 hours. On day 7, colony size was measured and images were photographed using JuLI™ Stage Real-Time Cell History Recorder (NanoEnTek) in an incubator at 37^0C humidified with 5% CO_2. 72 hours post-treatment, cells were incubated with CellTiter-Glo® 3D Reagent (Promega) for 30 minutes at room temperature and luminescence signal was recorded using the FLUOstar OPTIMA (BMG Labtech). Ishikawa 3D organoids were fixed in 4% paraformaldehyde (Electron Microscopy Sciences, ProSciTech) for 20 minutes and processed for immunofluorescence, as described previously (Sahoo et al., 2017b).

Immunoblotting

Human endometrial cancer samples, mouse uterine tissue, and Ishikawa cells were lysed in ice-cold RIPA (radioimmunoprecipitation assay) buffer (50 mmol/L Tris-HCl pH 7.5, 150 mmol/L NaCl, 1% NP-40, 0.5% Sodium deoxycholate, 0.1% SDS) containing protease and phosphatase inhibitors (Sigma). The lysates were centrifuged at 12,000 rpm for 10 minutes at 4^0C and supernatant was collected. Aliquots of purified lysates containing equal protein mass were boiled in 1x Laemmli sample buffer (0.04 mol/L Tris-HCl pH 6.8, 0.2% SDS, 0.01% bromophenol blue, 10% β-mercaptoethanol and 10% glycerol) for 5 minutes at 95^0C and resolved by 10% SDS-PAGE gels. The protein bands were electrophoretically transferred to nitrocellulose blotting membranes (GE Healthcare Life Sciences), blocked in TBS-T (0.1% Tween 20 in TBS) containing 5% skim milk (w/v) for 1 hour at room temperature and probed with primary antibody ALPPL2 (1:500 dilution, Santa Cruz Biotechnology #sc-134255) for overnight incubation at 4^0C. The membrane was washed and incubated with secondary horseradish peroxidase-conjugated anti-mouse antibody (Jackson ImmunoResearch Laboratories) for 1 hour at room temperature. The membrane was washed again in TBS-T, developed using a chemiluminescent substrate (Millipore) for detection of HRP and the protein bands were detected by chemiluminescence (Fujifilm LAS-4000). GAPDH was used as a loading control. Densitometric quantification was performed using ImageJ software (NIH, USA).

Histology, immunohistochemistry (IHC) and digital quantification

For histological analyses, human endometrial cancer tissue and mouse uteri were fixed in 10% neutral buffered formalin solution overnight at 4°C and transferred to 70% ethanol until further processing. Formalin-fixed tissues were processed, embedded in paraffin wax and sectioned at 5 µm thickness. Haematoxylin and eosin staining and immunohistochemistry were performed using standard protocols as described before (Sahoo et al., 2017a). Tissue sections were incubated with primary antibody ALPPL2 (1:50 dilution, Santa Cruz Biotechnology #sc-134255) for overnight at 4°C, followed by peroxidase-conjugated secondary antibodies (Thermo Fisher Scientific) and DAB substrate (Sigma) to detect bound antibodies. Tissues were counterstained with hematoxylin to visualize cellular morphology. Images were captured using an Aperio AT2 slide scanner (Leica Biosystems, Victoria, Australia) with same gain and exposure time. Quantitative IHC analysis was performed using the Halo™ image analysis platform and the pixel intensities of DAB staining were calculated using the Area Quantification v1.0 algorithm (Indica Labs, New Mexico, USA). Immunohistochemistry intensity score (H-Score) was calculated from pixel intensity values (the

sum of 3 x % of pixels with strong staining + 2 x % of pixels with moderate staining + 1 x % pixels with weak staining).

RNA extraction, synthesis of first strand cDNA and qRT-PCR

Total RNA was isolated from estrogen or progesterone treated mouse uterus and Ishikawa cells using RNeasy Mini kit (Qiagen) following manufacturer's instructions. 250 ng of total RNA was used for the synthesis of cDNA using RT² First Strand Kit (Qiagen). The cDNA was amplified using sequence-specific *Alppl2* primers. Quantitative real-time PCR (Q-PCR) was performed using RT² SYBR Green ROX qPCR Mastermix (Qiagen) on a 7900 HT FAST Thermocycler (Applied Biosystems) through a pre-incubation step, and 40 amplification cycles (including denaturation, annealing and extension segments). Relative quantification [comparative Ct ($2^{-\Delta\Delta Ct}$) method] was used to compare the expression level of the target gene with the housekeeping gene (*Gapdh*) in different treatment groups. Primer sequences were: human *ALPPL2* (F: 5' TGTTACCGAGAGCGAGAGC 3', R: 5' GTGGGTCTCTCCGTCCAG 3'), mouse *Alppl2* (F: 5' ACACATGGCTCTGTCCAAGA 3', R: 5' TCGTGTTGCACTGGTTGAAG 3'), human *GAPDH* (F: 5' GCCACATCGCTCAGACACCAT 3', R: 5' GAAGGGGTCATTGATGGCAA 3') and mouse *Gapdh* (F: 5' TGGCAAAGTGGAGATTGTTGCC 3', R: 5' AAGATGGTGATGGGCTTCCCG 3').

ELISA

Plasma ALPPL2 and CA-125 level in normal and endometrial adenocarcinoma patients were analyzed using human ALPPL2 (CUSABIO Life science #CSB-EL001633HU) and CA-125 (Abcam #ab195213) ELISA kit following the manufacturer's instructions. Briefly, the assay plate was incubated with standards and samples. Following incubation, the plate was incubated with biotin and HRP-avidin labeled antibody for 1 hour. After washing, the plate was developed with a colorimetric reagent and read at 450 nm wavelength.

Statistical analysis

Statistical analysis was performed with GraphPad Prism 7.02 software. All *in vitro* experiments were repeated thrice with three biological replicates per repeat and the data were expressed as the mean ± SEM. Statistical analyses were performed by the Student's *t*-test (unpaired, two-tailed). ALPPL2 and CA-125 protein levels were compared across groups using the Mann-Whitney test. The Chi-square or Fisher's exact test was used for categorical data. Differences between overall and disease-free survival were estimated using Kaplan-Meier analysis and log-rank test.

The prognostic power of ALPPL2 and CA-125 biomarker was compared using the area under the receiver-operating characteristic curve (AUC); AUC = 0 means extremely unlikely to happen in clinical practice, values close to 0.5 indicates the discrimination of performance close to chance while AUC = 1 means the diagnostic test is perfect in the differentiation between the disease and normal. A *P* value < 0.05 was considered statistically significant.

Discussion

Although there has been an improvement in the treatment of endometrial cancer, the 5-year survival rate for these patients shows poor outcome due to the diagnosis of the disease at an advanced stage. In fact, uterine cancer death rates continued to increase from 2010 to 2014 by about 2% per year (Siegel et al., 2017). Endometrial cancer is most common in women aged between 55 and 65 with a median age of 62 (Pfeiffer et al., 2013). Early menarche and late menopause or long duration of estrogen exposure lead to a prolonged growth of endometrium followed by endometrial hyperplasia and/or cancer. In addition, most of the patients diagnosed with endometrial cancer are obese (Sahoo et al., 2017a). The hypertrophied adipocytes in obese women are a predominant source of the enzyme aromatase, which synthesizes excess *in situ* estrogen and promotes endometrial adenocarcinomas (Zhao et al., 2016). Therefore, an elevated level of estrogen is strongly associated with patient susceptibility towards endometrial cancer.

Due to insufficient power of clinicopathological features of endometrial cancer, early detection of the disease is currently unavailable. High levels of oncoprotein, Stathmin has recently been shown to be associated with aggressive endometrial cancer and poor prognosis (Reyes et al., 2017; Wik et al., 2013). In contrast, the prognostic impact and possible clinical use of Stathmin have not been studied for early stage endometrial cancer and is limited to patients with advanced stages of endometrial cancer. However, the majority of endometrial cancer patients (~90%) have endometrioid histology, which is significantly associated with a hyperestrogenic state. Thus, identification of estrogen-responsive biomarkers may be beneficial in earlier detection of elevated estrogen level and endometrial cancer diagnosis.

In our study, we found a significant positive correlation between estrogen level and ALPPL2 expression both *in vitro* and *in vivo*. In addition, ALPPL2 was also overexpressed in human endometrial cancer patient tissue and plasma samples. These findings represent an ectopic synthesis of ALPPL2 by endometrial tumor cells. Due to ectopic expression ALPPL2, it is a very useful biomarker in several cancers. Both placental (ALPP) and placental-like (ALPPL2) alkaline phosphatases have been found to be overexpressed in germ cells and some non-germ cells malignancy. Reported studies have already shown overexpression of ALPPL-2 in testicular and pancreatic cancers (Dua et al., 2013; Jeppsson et al., 1984; Paiva et al., 1983). Alkaline phosphatases are glycosylated membrane proteins that can dimerize and are secretory in nature (Millan and Fishman, 1995). The secretory nature of ALPPL2 is also demonstrated by our

transcriptome analysis of endometrial cancer organoids (Fig 1C and 1D). In addition, analysis of TCGA dataset suggests amplification of ALPPL2 is associated with a poor survival rate in endometrial cancer patients. These findings highlight the clinical relevance of ALPPL2 as a biomarker.

Currently, there is no universally approved biomarker for endometrial cancer. Although CA-125 is used for pre-operative serum detection, its sensitivity and specificity are low and its main utility appears to predict extra-uterine disease (Nicklin et al., 2012). ALPPL2 may be of value for detection and risk stratification of low grade or early stage endometrial cancer. The strength of this biomarker includes the fact that ALPPL2 expression predicts estrogen levels and elevated estrogen levels is a major risk factor for endometrioid endometrial cancer. In addition, ALPPL2 is an independent prognostic marker and superior to CA-125.

Taken together, our study ascertained that ALPPL2 expression is significantly associated with tumor cell proliferation and can be used as a prognostic marker in endometrial carcinomas. The present data also suggest a potential role of steroid hormones in regulating ALPPL2 expression. Therefore, measurement of this isoenzyme can be clinically useful in monitoring progression or regression of endometrial tumor cells. Moreover, due to the fact that estrogen promotes ALPPL2 expression, this oncofetal protein can also be used as a prognostic marker for other estrogen-induced cancers such as breast and ovarian cancer.

Author contributions

S.S.S. performed most of the experiments, analyzed the data and wrote the paper. P.B. helped in animal experiments. P.B., Y.K., and P.N. helped with the collection of endometrial cancer patient biopsy samples. P.S.T. supervised the study, provided financial support and final approval of the manuscript.

Acknowledgments

Work in the Tanwar lab is in part supported by funding from the National Health and Medical Research Council, the Australian Research Council, and the Cancer Institute NSW. The Hunter Cancer Biobank is supported by the Cancer Institute NSW. S.S.S. and P.B. are recipients of the University of Newcastle Postgraduate Research Fellowship.

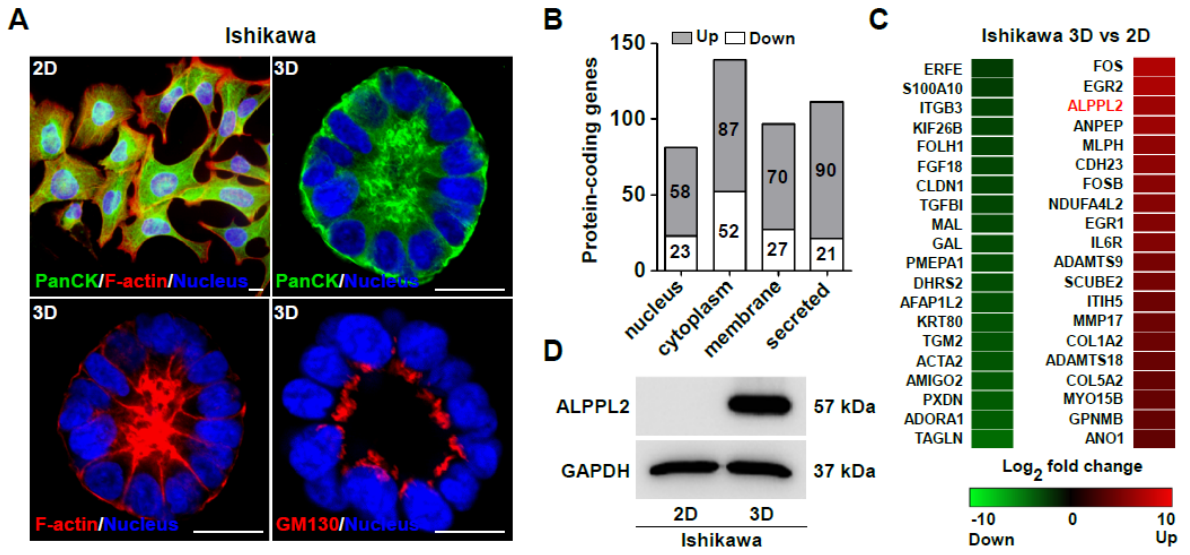

Figure 1. The secretome of human endometrial cancer cells.

(A) Ishikawa monolayers and organoids were stained with pan-cytokeratin (green), actin (red), GM130 (red), and Hoechst (blue). One representative confocal section of Ishikawa organoid is shown. (B) The stacked column chart shows the number of nuclear, cytoplasmic, membranous and secreted protein-coding genes upregulated (grey) or downregulated (white) (> 2-fold change, $P < 0.05$) in Ishikawa organoids compared to two-dimensionally cultured cells. (C) The heat map shows differential gene expression profile of Ishikawa organoids (generalized log2 fold change; GFOLD > 2, $P < 0.05$). Red represents an up-regulation and green a down-regulation in gene expression. (D) Immunoblot for ALPPL2 protein in 2D and 3D culture of Ishikawa cells.

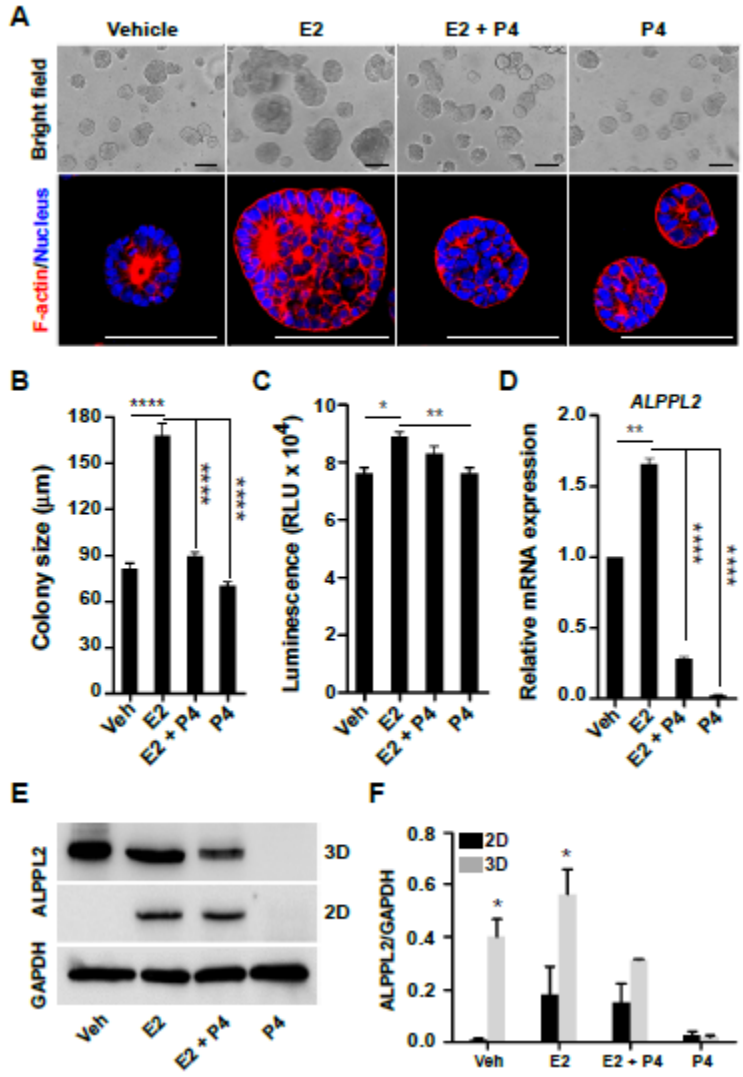

Figure 2. Estrogen and progesterone regulate endometrial cancer organoid growth and ALPPL2 expression.

(A) Ishikawa cells were grown in 3D and treated with estrogen (E2, 10 nmol/L) and progesterone (P4, 100 nmol/L). Representative bright field and confocal images of day-7 organoids from each treatment group are shown. (B) The bar graph shows average colony size from different treatment groups (n = 3). The diameter of 50 colonies from each treatment group was analyzed. (C) Ishikawa cells were treated with E2 and P4 and assayed for proliferation (n = 3). (D) Quantitative real-time PCR analysis of *ALPPL2* mRNA expression levels on cDNA from Ishikawa organoids dosed with E2 and/or P4 (n = 3). (E) Immunoblot analysis of ALPPL2 protein from Ishikawa cells in 2D and 3D environment under different treatment condition (n = 3). (F) Densitometric quantification of the western blots in panel E. Scale bar, 100 µm. The results represents the mean ± SEM; *, $P < 0.05$; **, $P < 0.01$; ****, $P < 0.0001$.

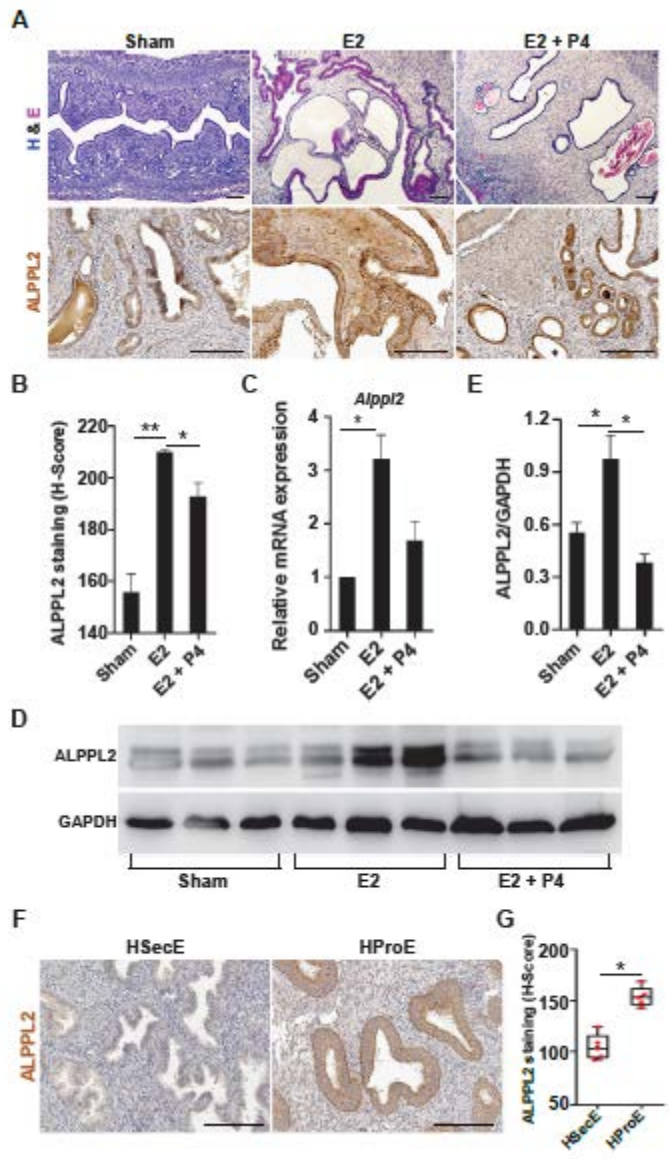

Figure 3. Estrogen promotes and progesterone suppresses ALPPL2 expression in mouse and human uterus.

(A) Histology and ALPPL2 protein expression were assessed by H&E (top row) and immunohistochemistry (bottom row) in E2 and P4 treated mice. (B) The graph shows quantification of ALPPL2 staining intensity (n = 3). (C) *Alppl2* mRNA expression levels on cDNA from E2 and P4 treated mouse uterus (n = 3). (D) Western blot of protein lysate from E2 and P4 treated mice uteri was analyzed for ALPPL2 (n = 3 mice/group). (E) Densitometric quantification of ALPPL2 western blot bands is shown as a bar graph (n = 3). (F) ALPPL2 immunohistochemical staining of normal human proliferative and secretory endometrium. (G) ALPPL2 staining intensity was quantified by H-score and shown as a bar graph (n = 5). HSecE, human secretory endometrium; HProE, human proliferative endometrium. Scale bar, 100 µm. The results represents the mean ± SEM; *, $P < 0.05$; **, $P < 0.01$.

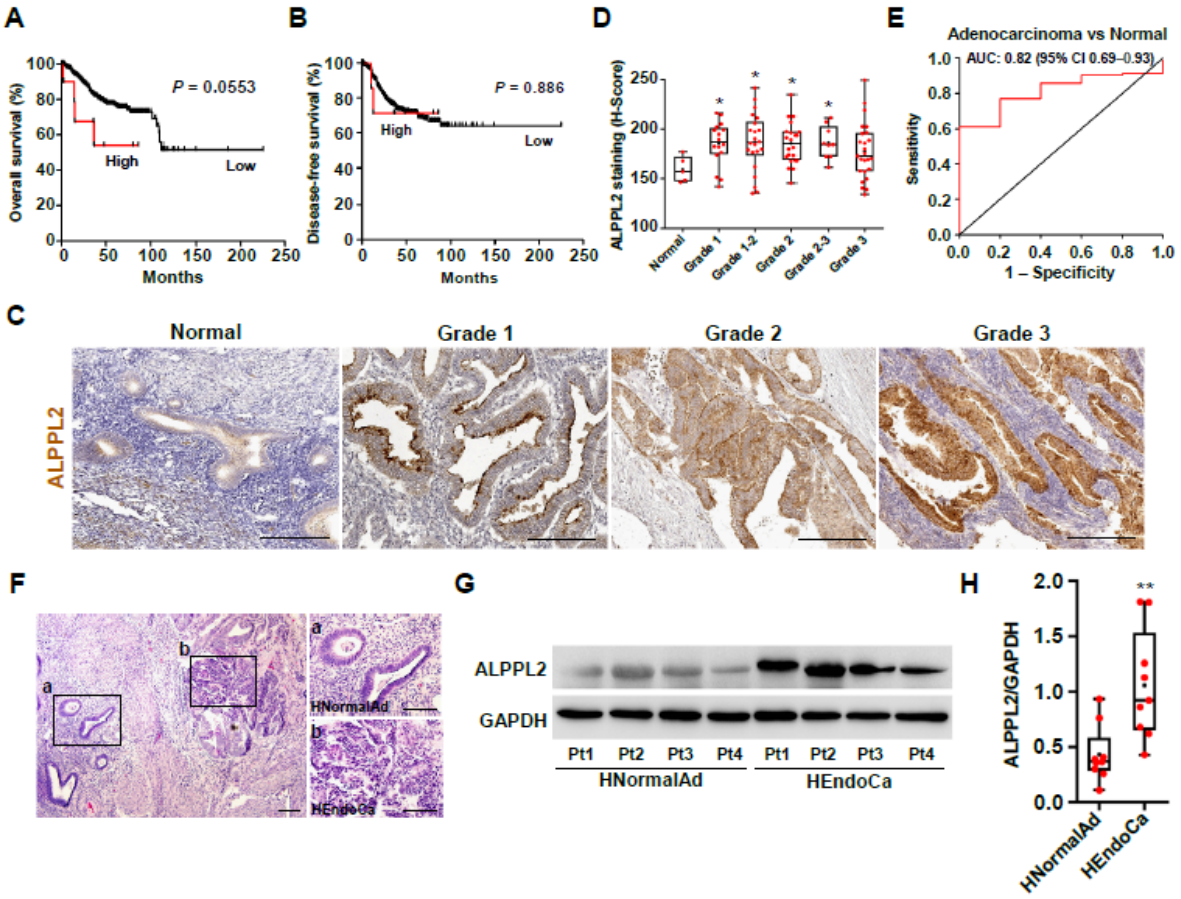

Figure 4. Identification of *ALPPL2* as a prognostic gene in endometrial carcinomas.

(A) Overall and (B) Disease-free Kaplan-Meier analysis of ALPPL2 expression in patients with endometrial cancer (TCGA Project). The analysis was done by median cut with the *P* value of the log-rank test. Black lines, samples with low ALPPL2; red lines, samples with high ALPPL2. (C) Immunohistochemical expression of ALPPL2 in grade 1, 2 and 3 human endometrial adenocarcinomas. ALPPL2 expression was observed in the plasma membrane in grade 1 and grade 2 tumors and exclusively in the extracellular space of grade 3 carcinomas. (D) Quantification of ALPPL2 staining intensities is shown as H-Score in normal (*n* = 5), grade 1 (*n* = 16), grade 1-2 (*n* = 22), grade 2 (*n* = 20), grade 2-3 (*n* = 9) and grade 3 (*n* = 25) endometrial cancer patients. Whisker box plot represents medians with minimum and maximum values. *P* value was determined by Mann-Whitney U tests as compared to normal cases. (E) Shown is a ROC curve for ALPPL2 expression levels in endometrioid adenocarcinomas versus normal cases. (F) The H&E stained human uterine section shows endometrial carcinoma with normal adjacent endometrium. (G) Western blot of protein lysate from cancerous and normal adjacent uterine tissue was analyzed for ALPPL2 expression (*n* = 9 patients per group). Representative western blot of normal and cancerous tissue from four patients is shown. (H) Densitometric quantification of the bands in F was performed, averaged and shown as a whisker box plot (*n* = 9). Pt, patient; AUC, area under the ROC curve; CI, confidence interval; HNormalAd, normal adjacent human endometrium; HEndoCa, human endometrial cancer. Scale bar, 100 µm. The results represent the mean ± SEM; *, $P < 0.05$; **, $P < 0.01$.

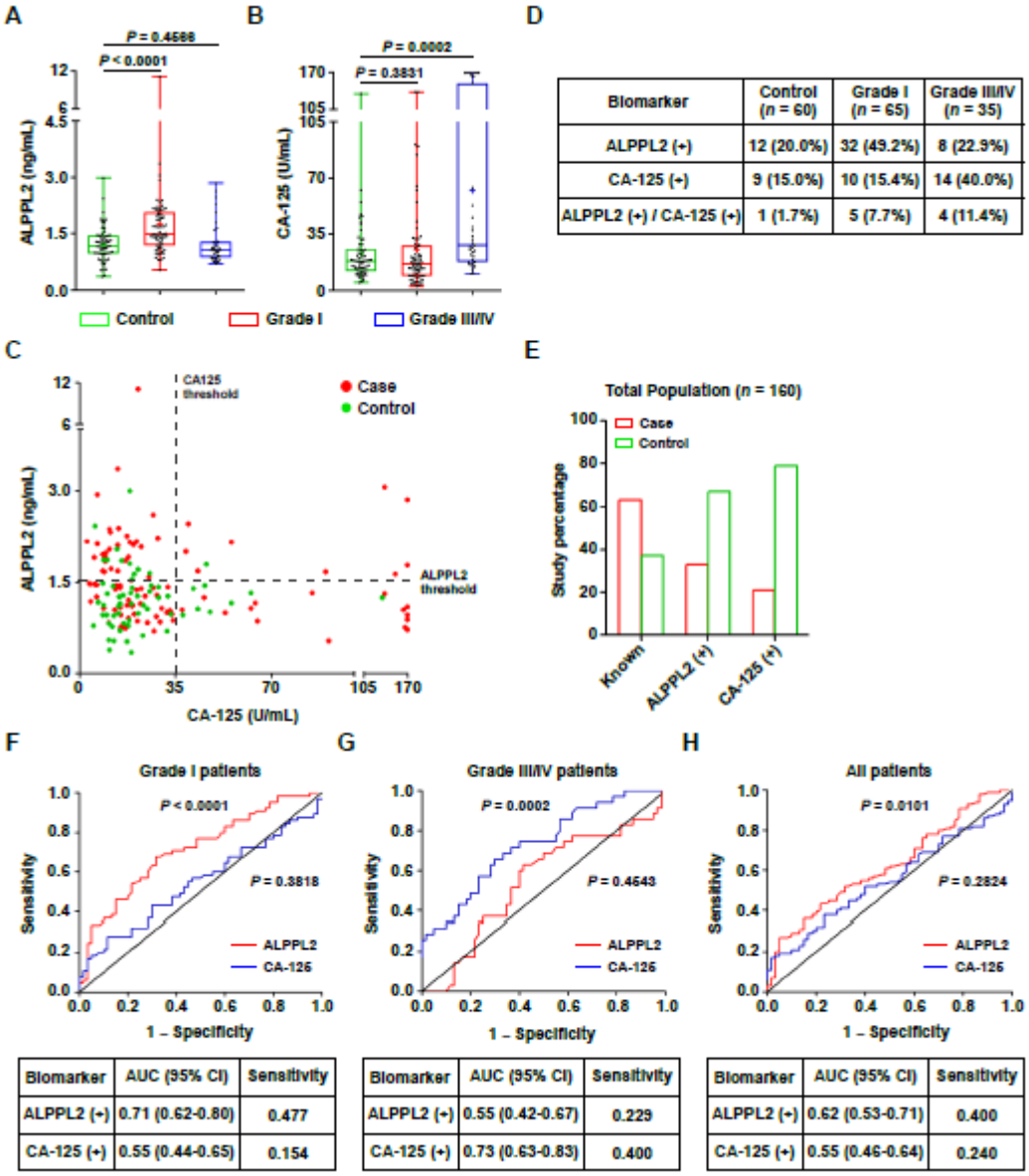

Biomarker	Control (n = 60)	Grade I (n = 65)	Grade III/IV (n = 35)
ALPPL2 (+)	12 (20.0%)	32 (49.2%)	8 (22.9%)
CA-125 (+)	9 (15.0%)	10 (15.4%)	14 (40.0%)
ALPPL2 (+) / CA-125 (+)	1 (1.7%)	5 (7.7%)	4 (11.4%)

Biomarker	AUC (95% CI)	Sensitivity
ALPPL2 (+)	0.71 (0.62-0.80)	0.477
CA-125 (+)	0.55 (0.44-0.65)	0.154

Biomarker	AUC (95% CI)	Sensitivity
ALPPL2 (+)	0.55 (0.42-0.67)	0.229
CA-125 (+)	0.73 (0.63-0.83)	0.400

Biomarker	AUC (95% CI)	Sensitivity
ALPPL2 (+)	0.62 (0.53-0.71)	0.400
CA-125 (+)	0.55 (0.46-0.64)	0.240

Figure 5. Comparison of CA-125 and ALPPL2 values in plasma samples of endometrial carcinomas. Whisker box plots show (A) ALPPL2 and (B) CA-125 values in plasma of endometrial cancer patients and normal women. Each box represents maximum, upper quartile, median, lower quartile, and minimum values. (C) Comparison of the discriminatory power of ALPPL2 versus CA-125 for endometrial cancer cases. The vertical line represents the CA-125 threshold (35 U/mL) above which women would be sent to a gynecologist. The horizontal line represents the ALPPL2 threshold, which was selected by taking 75th percentile of all control samples and a range between median and 75th percentile was considered as borderline. (D) The table displays ALPPL2- and CA-125-positive numbers in case, and control cohorts. (E) The bar graph shows the percentage of total known cases and control samples identified by CA-125 and ALPPL2 biomarker screening. ROC curve analysis of ALPPL2 and CA-125 in grade I (F), grade III/IV (G) and all (H) endometrial cancer case and control groups. AUC, area under the ROC curve; CI, confidence interval.

Table 1. Association of clinicopathologic variables with ALPPL2 expression in patients with endometrial cancer

Clinical parameters in cancers	ALPPL2 expression		*P* value
	Low	High	
Histology			0.3829
Adenocarcinoma, *n* = 91	45 (49.5%)	46 (50.5%)	
Adenosquamous carcinoma, *n* = 4	2 (50.0%)	2 (50.0%)	
Undifferentiated carcinoma, *n* = 2	0	2	
Histopahtological grade			0.0632
Low (1 or 2), *n* = 61	26 (42.6%)	35 (57.4%)	
High (3), *n* = 30	19 (63.3%)	11 (36.7%)	
Age (Years)			0.0110
<50, *n* = 34	10 (29.4%)	24 (70.6%)	
≥50, *n* = 63	36 (57.1%)	27 (42.9%)	

Supplemental Data

Supplementary Figures

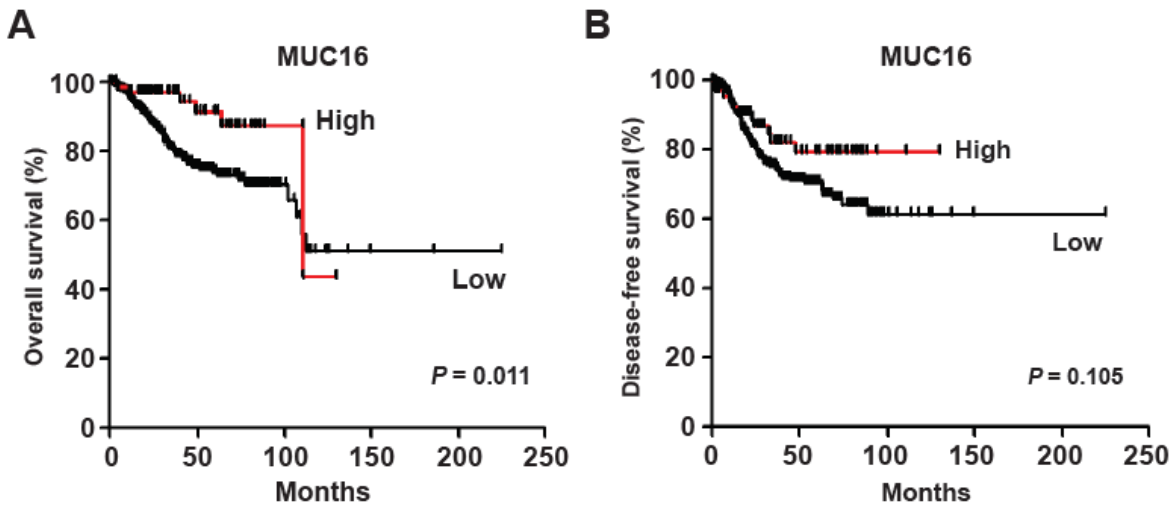

Figure S1. Impact of MUC16 amplification on endometrial cancer patient survival.
Kaplan-Meier plots show endometrial cancer patient survival over time (A) and after diagnosis (B) with low and high amplification of MUC16. The analysis was done by median cut with the *P* value of the log-rank test from the TCGA database. Black lines, samples with low MUC16; red lines, samples with high MUC16.

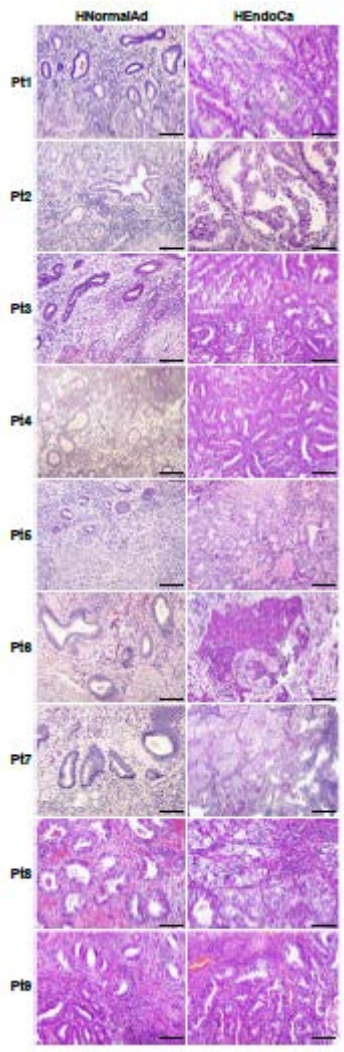

Figure S2. Histological analysis of human endometrial cancer and normal adjacent endometrium. Fresh endometrial cancer tissue samples and corresponding normal adjacent endometrium were stained with hematoxylin and eosin to validate normal and tumor sections. The panel shows histology of carcinoma and normal tissue sections from 9 different patients. Pt, Patient; HNormalAd, normal adjacent human endometrium; HEndoCa, human endometrial cancer. Scale bar, 100 μm.

Supplementary Tables

Table S1. The list of differentially expressed genes in Ishikawa organoids ($p < 0.05$)

Gene Id	Symbol	GFOLD	eFDR	log2FC	RPKM	
					Ishikawa 2D	Ishikawa 3D
ENSG00000149591	TAGLN	-3.98	1	-4.34	31.58	1.72
ENSG00000163485	ADORA1	-3.38	1	-3.74	19.81	1.63
ENSG00000130508	PXDN	-3.29	1	-3.68	6.17	0.53
ENSG00000139211	AMIGO2	-3.2	1	-3.57	19.2	1.78
ENSG00000167767	KRT80	-2.97	1	-3.32	16.09	1.77
ENSG00000169129	AFAP1L2	-2.95	1	-3.22	19.55	2.33
ENSG00000100867	DHRS2	-2.85	1	-3.13	12.7	1.6
ENSG00000172005	MAL	-2.79	1	-2.89	412.08	61.42
ENSG00000107796	ACTA2	-2.72	1	-3.43	5.67	0.57
ENSG00000163347	CLDN1	-2.67	1	-2.83	72.25	11.26
ENSG00000156427	FGF18	-2.63	1	-2.82	86.53	13.53
ENSG00000120708	TGFBI	-2.59	1	-2.87	10.62	1.6
ENSG00000198959	TGM2	-2.5	1	-3.33	1.43	0.15
ENSG00000124225	PMEPA1	-2.44	1	-3.08	3.05	0.39
ENSG00000162849	KIF26B	-2.36	1	-2.75	2.79	0.46
ENSG00000197747	S100A10	-2.35	1	-2.51	139.38	27.03
ENSG00000259207	ITGB3	-2.33	1	-2.69	10.41	1.78
ENSG00000086205	FOLH1	-2.33	1	-2.76	8.47	1.38
ENSG00000178752	ERFE	-2.31	1	-2.49	49.7	9.82
ENSG00000069482	GAL	-2.27	1	-2.99	9.58	1.3
ENSG00000266714	MYO15B	3.32	1	3.81	0.28	4.35
ENSG00000204262	COL5A2	3.34	1	3.81	0.54	8.43
ENSG00000136235	GPNMB	3.36	1	3.76	0.9	13.62
ENSG00000131620	ANO1	3.39	1	3.62	2.67	36.64
ENSG00000140873	ADAMTS18	3.48	1	3.91	0.68	11.5
ENSG00000198598	MMP17	3.64	1	4.13	0.87	17.03
ENSG00000123243	ITIH5	3.85	1	4.17	0.56	11.15
ENSG00000175356	SCUBE2	3.87	1	4.53	0.25	6.48
ENSG00000164692	COL1A2	3.94	1	4.11	2.8	53.48
ENSG00000163638	ADAMTS9	4.02	1	4.55	0.27	7.12
ENSG00000107736	CDH23	4.04	1	5.55	0.02	1.04
ENSG00000160712	IL6R	4.25	1	4.96	0.22	7.97
ENSG00000125740	FOSB	4.46	1	5.25	0.2	8.93
ENSG00000122877	EGR2	4.66	1	6.53	0.04	4.99
ENSG00000185633	NDUFA4L2	4.7	1	5.17	1.27	51.47
ENSG00000120738	EGR1	4.85	1	5.08	5.13	193.1
ENSG00000115648	MLPH	5.01	1	5.6	0.29	16.12
ENSG00000166825	ANPEP	5.64	1	6.12	0.72	56.24
ENSG00000163286	ALPPL2	5.79	1	6.17	2.26	181.94
ENSG00000170345	FOS	6.37	1	6.95	0.68	95.76

Discussion and Conclusion

Uterine (endometrial) cancer death rates are continued to increase every year with an estimation of 2% per year from 2010 to 2014 (Siegel et al., 2017). The increasing rate of endometrial cancer imposes a significant burden on the healthcare system as well as to women at their reproductive stages of life. Standard treatment for the vast majority of these patients requires surgery either hysterectomy or bilateral salpingo-oophorectomy. Chemotherapy and radiotherapy have also been implicated in many cases. However, all these current treatment options show poor patient outcomes. This might be due to the diagnosis of the disease at a late stage where cancer has already spread beyond the uterus and use of traditional chemo or radiotherapy to kill cancer cells. The work done in this thesis brings new approaches for endometrial cancer treatment as well as its early diagnosis to improve patient outcomes.

Key Outcomes

1. Organotypic 3D culture depicts metastatic propensity of endometrial cancer cells

As compared to established 3D culture models to study cellular phenotypic changes and drug resistance mechanism (Debnath and Brugge, 2005; Muranen et al., 2012; Yamada and Cukierman, 2007), in our 3D organoids we addressed the molecular alterations of a cell by changing its microenvironment. Despite grade and stage of the disease, endometrial cancer cells form two distinct architectures in 3D, glandular and non-glandular. Consecutively from 2D to 3D culture in absence and presence of ECM, we also found significant alteration in gene expression pattern. TGF-β signaling was found to be upregulated in non-glandular colonies but not in glandular one. The upregulation of TGF-β pathway in non-glandular colonies drives metastasis. Thus, a non-glandular architecture of endometrial cancer cells in 3D predicts its metastatic ability.

2. TGF-β signaling regulates conversion of glandular and non-glandular epithelium of uterus through slug protein

The dichotomous role of TGF-β signaling as pro-tumorigenic or tumor-suppressive is well known in many human cancers (Massague, 2008). Upregulation of TGF-β pathway mostly drives cancer progression through EMT. With our findings, that TGF-β pathway is upregulated in non-glandular colonies, we further analyzed the expression of well-known EMT markers in both types of colonies. With the treatment of TGF-β agonist, the glandular colonies turned into non-glandular one whereas treatment of TGF-β antagonist turned non-glandular colonies to glandular one. This process is facilitated by slug EMT protein, whose expression was increased during the conversion of glandular colonies to non-glandular one and decreased from non-glandular to glandular

conversion. Therefore, slug might be a major targeted protein for malignant properties of endometrial cancer cells.

3. Fibronectin, a key ECM protein stimulates TGF-β signaling and drive endometrial cancer metastasis

In the normal state, TGF-β regulates tissue homeostasis whereas, during tumor initiation and progression, the same pathway acts as a tumor promoter (Massague, 2012). High levels of TGF-β in the TME promotes cancer progression in an autocrine and/or paracrine manner that favors invasion and metastasis (Akhurst and Hata, 2012). Nevertheless, how TGF-β pathway gets upregulated in malignant cancers has been enigmatic. Our data provide renewed emphasis on the ECM component of TME, which regulates TGF-β pathway in endometrial cancer colonies. Furthermore, using an array of ECM proteins, we found fibronectin significantly activates TGF-β signaling in non-glandular endometrial cancer colonies.

4. Targeting endometrial cancer microenvironment for chemoprevention

The standard treatment strategy for many cancers including endometrial cancers is to kill cancer cells by using different chemotherapeutic drugs or radiotherapy. In case of endometrial cancer, many approaches also target PI3K/Akt/mTOR signaling pathway, which is a well-known upregulated pathway in endometrial tumor cells. However, if we can inhibit the supporting TME during cancer progression, it can significantly reduce cancer spread. With our findings (details in Chapter 2) that ECM upregulates TGF-β pathway which helps in endometrial cancer metastasis, we sought to inhibit TGF-β pathway. In a metastatic endometrial cancer CDX mouse model, our results clearly demonstrated that use of small molecule TGF-β inhibitor significantly suppresses cancer metastasis with no side effects. This is a novel finding in our study as well as a different way of approach to target endometrial cancer.

5. Visceral adipose tissue secrete VEGF, which stimulates angiogenesis in the uterus

Out of several risk factors for endometrial cancers, obesity or hypertrophied adipocytes significantly increase endometrial cancer risk. However, until now the molecular mechanism underlying this association is unclear. For the first time, our results (details in Chapter 3) describes visceral adipocytes secrete surplus amount of vascular endothelial growth factor (VEGF) as compared to subcutaneous adipocytes. The secreted VEGF in a paracrine manner acts on the uterus and stimulates angiogenesis. In an obese mouse model as well as in high BMI endometrial

cancer patients, our results have ascertained increasing number of blood vessels in the uterus of obese mice and women.

6. VEGF-mTOR signaling links obesity and endometrial cancer

Over past few decades, epidemiological and clinical data suggest that obesity is an independent risk factor for endometrial cancer (Arem and Irwin, 2013; Onstad et al., 2016). In our study, we deciphered this enigma, which associates endometrial cancer in obese women. Initially, we found visceral adipocytes in obese patients secrete more VEGF and stimulate angiogenesis in the uterus. Further, we investigated histology of uterus in obese and non-obese mice littermates and observed an increased number of endometrial glands in obese mice, which predisposes to cancer. In a subsequent experiment, we found the increased number of endometrial glands was associated with an increased pS6 expression (a downstream target of mTOR signaling) in endometrial glands (details in Chapter 3). Collectively, our results showed increased secretion of VEGF from visceral adipocytes act on the uterus to stimulate mTOR pathway and endometrial cancer.

7. ALPPL2, an oncofetal protein as a prognostic biomarker in endometrial cancer

In addition to treatment of endometrial cancer, our study also aims to emphasize early diagnosis of the disease. Currently used biomarkers such as stathmin and CA-125 only detects high-grade endometrial cancers (Nicklin et al., 2012; Reyes et al., 2017). In our transcriptome analysis study, we found a novel secreted protein ALPPL2, which is highly expressed on the membrane of endometrial cancer organoids as well as secreted to extracellular space. We also ascertained its high expression in a cohort of endometrial cancer patient samples by a series of *in vitro* and *in vivo* experiments. Most importantly compared to CA-125, ALPPL2 is a better prognostic biomarker with a good sensitivity for serum-based diagnosis approach. This finding is completely new in the endometrial cancer research field and we believe ALPPL2 will prognosticate this disease at an early stage.

8. Estrogen promotes and progesterone suppresses ALPPL2 expression in endometrial cancer cells

A growing body of evidence suggests that steroid hormones, estrogen promotes and progesterone suppresses endometrial cancer development (Hecht and Mutter, 2006; Takahashi-Shiga et al., 2009). Our investigations showed upregulation of ALPPL2 protein in human endometrial cancer patient samples. Interestingly, we also found ALPPL2 expression is regulated

by estrogen and progesterone level. The significance and impact of this finding are that ALPPL2 expression level can be used as an assessment of estrogen level in the serum.

Addendum (A1)

Age-related mTOR in Gynaecological Cancers

Preface

Both endometrial and ovarian cancers are age-related disease and are most common in women aged between 55 and 65 with a median age of 62. Early menarche and/or late menopause lead to a prolonged growth of ovarian surface epithelium (OSE) and inner epithelial lining of the uterus (endometrium) which results in hyperplasia and/or cancer. Majority of these patients have genetic aberrations in the members of the PI3K-mTOR (phosphoinositide 3-kinase-mammalian target of rapamycin) pathway. In this chapter, we have summarised our previous research findings where we found pharmacological as well as genetic suppression of mTOR pathway significantly reduces precancerous lesions in endometrium and OSE of aged women promoting healthy aging. This chapter comprises an editorial entitled as **"Age-related mTOR in gynaecological cancers"** which is published in the journal *Aging*.

THE UNIVERSITY OF NEWCASTLE AUSTRALIA

Statement of Authors' Contributions

This statement summarises the intellectual input by all the authors in the Editorial entitled **"Age-related mTOR in gynaecological cancers"** in the Journal ***Aging***, 2017.

Authors	Statement of contribution
Preety Bajwa (First author)	Wrote and edited the manuscript
Subhransu S. Sahoo **(Co-first author)**	Wrote and edited the manuscript Made figure for the manuscript
Pradeep S. Tanwar (Corresponding author)	Edited the manuscript

Preety Bajwa

Subhransu S. Sahoo

Pradeep S. Tanwar

Robert Callister - Faculty Assistant Dean Research Training

Publication

www.aging-us.com AGING 2017, Vol. 9, No. 2

Editorial

Age-related mTOR in gynaecological cancers

Preety Bajwa, Subhransu S. Sahoo, Pradeep S. Tanwar

Aging is an uninvited sequel of organismal growth and the ultimacy of which is death. At the molecular level, organismal aging is a conversion from cellular quiescence to senescence state. Age is a major risk factor for many diseases including diabetes, obesity, neurodegenerative disorders, and cancer. Other consequences of aging are not defined by diseases, but rather considered 'stages of life', because they normally occur in everyone, such as menopause in females. However, deregulated female reproductive cycles (early menarche and/or late menopause) lead to hormonal imbalance and cancer at later stages of life. Endometrial and ovarian cancers are the most frequently diagnosed cancers in aged women and account for significant mortality. The incidence of both these cancer increases with advancing age, peaking around 60 to 70 years of age [1, 2]. Up to 80% of such patients are found to have genetic aberrations in the members of the PI3K-mTOR (phosphoinositide 3-kinase-mammalian target of rapamycin) pathway [3, 4]. mTOR signaling is important in regulating the cell cycle of the majority of proliferating cells, where homeostasis is maintained by either cell division or quiescence [5]. In contrast, hyperactive mTOR signaling causes cellular hypertrophy, which alters homeostasis, leading to cellular senescence, cancer and age-related diseases [5].

Recently, we demonstrated that with advancing age, female mice and humans develop endometrial and ovarian surface epithelial (OSE) cell hyperplasia, papillary growth and inclusion cysts [4, 6]. Histopathological examination of these abnormal growths revealed expression of bonafide markers of human ovarian cancer precursor lesions, Pax8 and Stathmin 1, and concurrent elevated expression of pS6 protein (a downstream target of the mTOR pathway) compared to young mice and humans [6]. Genetic deletion or overexpression of *PTEN* (a negative regulator of mTOR signaling) significantly altered the age-associated changes in female mice and human reproductive tract organs [4]. Furthermore, pharmacological suppression of the mTOR pathway using rapamycin treatment significantly reduced both endometrial and OSE hyperplasia in aged mice [4, 6]. Taken together, these observations established that the age-associated pathological changes in the female reproductive tract organs are driven by aberrant mTOR signaling.

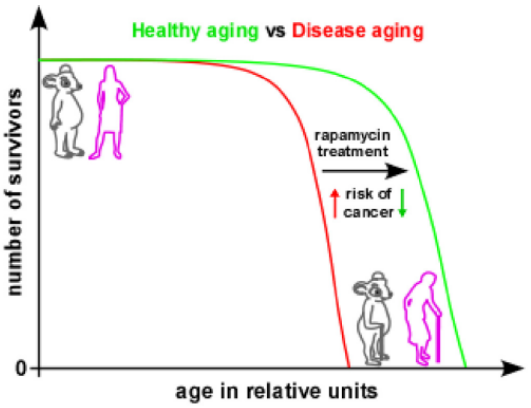

Figure 1. Hypothetical model of mTOR-driven cancer in aged women. A potential therapeutic opportunity for the treatment of gynaecologic cancers is outlined. In post-menopausal aged women, rapamycin treatment can suppress hyperactive mTOR signalling in ovarian and uterine epithelium, potentially promoting healthy aging.

Cancer is an age-related disease and any lifestyle changes or interventions that slow aging also delay cancer [7]. Many independent studies have already demonstrated the effectiveness of an anti-aging drug, rapamycin, in many species. In model organisms, rapamycin prolongs lifespan and delays cancer, even when calorie restriction does not. The TOR signaling is a major evolutionarily conserved player in longevity regulation as pharmacological modulation of this pathway extends lifespan in flies, worms, yeast and mice. Under these circumstances, our study provides evidence that rapamycin treatment inhibits mTOR-driven precancerous lesions in the female reproductive tract organs and may also extend lifespan or promote healthy aging in post-menopausal women. Our study highlights that even rapamycin treatment in genetically heterogeneous, 9 months-old mice (equivalent to ~50 years age of human) significantly suppresses mTOR activity and gynaecologic cancer lesions. Thus, if

rapamycin can rescue aging phenotypes in cancer-prone transgenic mice, it is predictable that rapamycin intervention in post-menopausal women should delay age-related cancers and promote a healthy life. Nevertheless, many questions remain to be answered. In aged mice and women, why is overactive mTOR specific to a few cell types of the reproductive tract organs? Is there any link between unopposed estrogen signaling and the mTOR pathway that leads to hyperplastic epithelium of the uterus and ovary? Moreover, how can we use this knowledge to treat cancer? Our studies, therefore, open up an avenue to explore the mTOR pathway as a target for prevention and/or treatment of gynaecological cancers.

REFERENCES

1. Damle RP, et al. J Clin Diagn Res. 2013; 7:2774-76. doi: 10.7860/JCDR/2013/6291.3755
2. Lambrou NC and Bristow RE. 2003; 17:1075-81; discussion 1081, 1085-6, 1091.
3. Tanwar PS, et al. Carcinogenesis. 2014; 35:546-53. doi: 10.1093/carcin/bgt357
4. Bajwa P, et al. Oncotarget. 2017; 8:7265-75. doi: 10.18632/oncotarget.13919
5. Serrano M. Cell Cycle. 2012; 11:2231-32. doi: 10.4161/cc.21065
6. Bajwa P, et al. Oncotarget. 2016; 7:19214-27. doi: 10.18632/oncotarget.8468
7. Blagosklonny MV. Cancer Biol Ther. 2012; 13:1349-54. doi: 10.4161/cbt.22859

Pradeep Tanwar: Gynaecology Oncology Group, School of Biomedical Sciences and Pharmacy, University of Newcastle, Callaghan, New South Wales, Australia

Correspondence: *Pradeep Tanwar*
Email: *pradeep.tanwar@newcastle.edu.au*
Keywords: *aging, mTOR, cancer*

Received: February 20, 2017
Published: February 28, 2017

Addendum (A2)

Age Related Increase in mTOR Activity Contributes to the Pathological Changes in Ovarian Surface Epithelium

Preface

Ovarian cancer is a lethal gynaecological cancer and most frequently diagnosed in aged women. Up to 80% of such patients harbor genetic mutations in the PI3K-mTOR (phosphoinositide 3-kinase-mammalian target of rapamycin) pathway. Currently, the molecular mechanisms of overactive mTOR and aging towards pathogenesis of ovarian cancer is unclear. In this chapter, we have demonstrated suppression of mTOR signaling, which is a major regulator of age-associated phenotypes, significantly decreases ovarian surface epithelium (OSE) hyperplasia in aged mice. This outcome can be used as a novel therapeutic intervention of aged women with ovarian cancer. This chapter contains a research article entitled as **"Age related increase in mTOR activity contributes to the pathological changes in ovarian surface epithelium"** which is published in the journal *Oncotarget*.

UON Graduate Research

Co-authorship declaration

Statement of Authors' Contributions

This statement summarises the intellectual input by all the authors in the paper entitled **"Age related increase in mTOR activity contributes to the pathological changes in ovarian surface epithelium"** in the Journal ***Oncotarget***, 2017.

Authors	Statement of contribution
Preety Bajwa (First author)	Performed all the *in vitro* and *in vivo* experiments Performed statistical analysis of the data Made figures and tables for the paper Wrote and edited the manuscript
Prathima B. Nagendra (Co-author)	Helped with IHC experiment
Sarah Nielson (Co-author)	Provided ovarian cancer patient tissue sections
Subhransu S. Sahoo (Co-author)	Performed protein array Helped with western blot and cell culture experiments Revised the manuscript
Amanda Bielanowicz (Co-author)	Helped with IHC experiment
Janine M. Lombard (Co-author)	Provided ovarian cancer patient samples
J. Erby Wilkinson (Co-author)	Revised and edited the manuscript
Richard A. Miller (Co-author)	Provided rapamycin treated mice Revised the manuscript
Pradeep S. Tanwar (Corresponding author)	Supervised and designed the study Wrote the manuscript Provided financial support

Preety Bajwa

Prathima B. Nagendra

Sarah Nielson

Subhransu S. Sahoo

Amanda Bielanowicz

Janine M. Lombard

J. Erby Wilkinson

Richard A. Miller

Pradeep S. Tanwar

Robert Callister - Faculty Assistant Dean Research Training

UON Graduate Research

Co-authorship declaration

THE UNIVERSITY OF NEWCASTLE AUSTRALIA

Statement of Authors' Contributions

This statement summarises the intellectual input by all the authors in the paper entitled **"Age related increase in mTOR activity contributes to the pathological changes in ovarian surface epithelium"** in the Journal ***Oncotarget***, 2017.

Authors	Statement of contribution
Preety Bajwa (First author)	Designed the study Performed all the *in vitro* and *in vivo* experiments Performed statistical analysis of the data Made figures and tables for the paper Wrote and edited the manuscript
Prathima B. Nagendra (Co-author)	Helped with IHC experiment
Sarah Nielson (Co-author)	Provided ovarian cancer patient tissue sections
Subhransu S. Sahoo (Co-author)	Helped with western blot and cell culture experiments Revised the manuscript
Amanda Bielanowicz (Co-author)	Helped with IHC experiment
Janine M. Lombard (Co-author)	Provided ovarian cancer patient samples
J. Erby Wilkinson (Co-author)	Revised and edited the manuscript
Richard A. Miller (Co-author)	Provided rapamycin treated mice Revised the manuscript
Pradeep S. Tanwar (Corresponding author)	Supervised and designed the study Wrote the manuscript Provided financial support

Preety Bajwa

Prathima B. Nagendra

Sarah Nielson

Subhransu S. Sahoo

Amanda Bielanowicz

Janine M. Lombard

J. Erby Wilkinson

Richard A. Miller

Pradeep S. Tanwar

Faculty Assistant Dean Research Training

Publication

www.impactjournals.com/oncotarget/ Oncotarget, Vol. 7, No. 15

Age related increase in mTOR activity contributes to the pathological changes in ovarian surface epithelium

Preety Bajwa[1], Prathima B. Nagendra[1], Sarah Nielsen[2], Subhransu S. Sahoo[1], Amanda Bielanowicz[1], Janine M. Lombard[3,4], J. Erby Wilkinson[5], Richard A. Miller[6] and Pradeep S. Tanwar[1]

[1] Gynaecology Oncology Group, School of Biomedical Sciences and Pharmacy, New South Wales, Australia

[2] Hunter Cancer Biobank, New South Wales, Australia

[3] School of Medicine and Public Health, University of Newcastle, Callaghan, New South Wales, Australia

[4] Division of Gynaecology Oncology, Department of Medical Oncology, Calvary Mater Newcastle, Waratah, New South Wales, Australia

[5] Unit for Laboratory Animal Medicine, University of Michigan School of Medicine, Ann Arbor, MI, USA

[6] Department of Pathology and Geriatrics Center, University of Michigan, Ann Arbor, MI, USA

Correspondence to: *Pradeep S. Tanwar,* ***email:*** *pradeep.tanwar@newcastle.edu.au*

Keywords: ovarian aging, rapamycin, mTOR, ovary, OSE, Gerotarget

Received: *February 04, 2016* ***Accepted:*** *March 23, 2016* ***Published:*** *March 29, 2016*

ABSTRACT

Ovarian cancer is a disease of older women. However, the molecular mechanisms of ovarian aging and their contribution to the pathogenesis of ovarian cancer are currently unclear. mTOR signalling is a major regulator of aging as suppression of this pathway extends lifespan in model organisms. Overactive mTOR signalling is present in up to 80% of ovarian cancer samples and is associated with poor prognosis. This study examined the role of mTOR signalling in age-associated changes in ovarian surface epithelium (OSE). Histological examination of ovaries from both aged mice and women revealed OSE cell hyperplasia, papillary growth and inclusion cysts. These pathological lesions expressed bonafide markers of ovarian cancer precursor lesions, Pax8 and Stathmin 1, and were presented with elevated mTOR signalling. To understand whether overactive mTOR signalling is responsible for the development of these pathological changes, we analysed ovaries of the *Pten* trangenic mice and found significant reduction in OSE lesions compared to controls. Furthermore, pharmacological suppression of mTOR signalling significantly decreased OSE hyperplasia in aged mice. Treatment with mTOR inhibitors reduced human ovarian cancer cell viability, proliferation and colony forming ability. Collectively, we have established the role of mTOR signalling in age-related OSE pathologies and initiation of ovarian cancer.

INTRODUCTION

Age is a major risk factor for the development of epithelial ovarian cancer (OvCa). Every year approximately 238,700 new cases are diagnosed and 151,900 deaths are attributed to OvCa, worldwide [1]. The majority of OvCa patients are 50 years of age or older and postmenopausal [2]. Although the impact of aging in germ cell biology and fertility is well known [3], very little information is available regarding the contribution of ovarian aging to the pathogenesis of OvCa.

In mammalian ovary, germ cells are surrounded by the somatic cells to form a basic functional unit known as follicles. During every oestrous cycle, some of the early stage follicles, known as the primordial follicles, are recruited to grow and ultimately these developed follicles either undergo atresia or ovulation to release a mature egg for fertilization [4]. However, with age, mammalian ovaries progressively run out of follicles due to various reasons and females undergo menopause, a stage in which women do not regularly experience monthly oestrous cycles. In 1971, Fathalla proposed

that repetitive rupture and repair of the ovarian surface epithelium (OSE) during the process of ovulation creates opportunities for accumulation of genetic aberrations leading to the abnormal growth of these cells [5]. This hypothesis explained high prevalence of OvCa in modern women and domestic egg-laying hens compared to other mammals [6]. Epidemiological association studies also provided support for Fathalla's hypothesis, whereby physiological conditions that suppress ovulation, such as pregnancy and breast-feeding, protected against OvCa [6-8]. Whereas, nulliparous women with a higher number of ovulatory cycles due to the absence of pregnancy and lactation, for example nuns, are more prone to developing OvCa compared to the general population [9].

In mouse models, increase in the frequency of ovulations either by hormonal treatments or by controlled exposure to the male mice leads to abnormal OSE cell proliferation and formation of inclusion cysts [10, 11]. However, these studies were conducted in relatively young mice with a limited follow up and therefore the pathogenic potential of these cysts is unknown. Interestingly, a higher number of inclusion cysts are observed in the contralateral ovaries of unilateral OvCa patients and in the ovaries of patients with hereditary predisposition to OvCa compared to general population [12, 13]. Assessment of genetic aberrations in ovaries of patients with OvCa, borderline tumours and non-neoplastic disease showed chromosomal alterations in OSE and inclusion cysts [14]. Moreover, a higher proportion of aneusomic cells were present in the inclusion cysts from OvCa and borderline tumour patients than controls [14], suggesting that these OSE-derived cysts have the potential to progress to OvCa. These findings are well supported by observations in genetically modified mouse models where, in addition to the Fallopian tube epithelium, genetic alterations in OSE causes development of OvCa that are phenotypically similar to human OvCa [15-17].

Incessant ovulation hypothesis and related work from many other laboratories have provided possible explanation for the development of ovarian epithelial inclusion cysts and their probable involvement in pathogenesis of OvCa but there are still many outstanding questions which need to be addressed for better understanding of this disease. Firstly, mice with germ cell deficiency also exhibit OSE hyperplasia and inclusion cysts, and develop ovarian epithelial tumours with advancing age [18]. Secondly, ovaries of women with anovulatory polycystic ovary syndrome also have inclusion cysts even though these women rarely or never ovulate [8]. Thirdly, inclusion cysts are more prevalent in aged human ovaries (> 60 years of age), even when there is no ovulation [19]. Collectively, these findings suggest that age associated changes in ovary/OSE contribute to the formation of inclusion cysts and consequently, OvCa.

The mammalian target of rapamycin (mTOR) pathway is involved in various cellular processes and inhibition of mTOR signalling has been shown to extend life span in several different species, including yeast, flies, worms, and mice, in part by suppressing age related pathologies and cancer [20-25]. Widespread genetic alterations in the mTOR pathway members are common in OvCa patients and comparable aberrations lead to the development of histopathologically similar tumours in mouse models [16]. On the basis of these studies, we hypothesised that age related increase in mTOR activity contributes to the development of OSE hyperplasia and inclusion cysts. In this study, we have shown hyperactivation of mTOR signalling in OSE lesions of the aged human and mouse ovaries, and inhibition of this signalling pathway suppressed development of these pathologies in mouse ovaries.

RESULTS

OSE hyperplasia in aged human and mouse ovaries

To understand how aging affects OSE cells, we examined human ovaries collected from pre- and post-menopausal women. Analysis of the premenopausal ovaries showed the presence of follicles in different stages of their development and a single layer of epithelial cells, known as OSE, covering the outer surface of these ovaries (Figure 1A-1C; $N = 3$). As expected, there were no follicles in the postmenopausal ovaries (Figure 1D-1I; $N = 9$). However, epithelial inclusion cysts (Figure 1E and 1H), OSE papillary and stratified growth (Figure 1F and 1I), and deep surface invaginations were clearly present in the postmenopausal ovaries (Figure 1D-1I), which were absent in the premenopausal ovaries (Figure 1A-1C). To evaluate if these epithelial lesions represent the precancerous state of ovarian cancer, we performed immunohistochemical localization of Pax8 and Stathmin 1, well-established markers of ovarian cancer precursor lesions and malignant disease [26, 27]. Expression of these two markers was absent in normal OSE cells of the premenopausal ovaries (Figure 1J and 1N). However, these markers were expressed by the epithelial inclusion cysts and abnormal OSE growths present in the postmenopausal ovaries (Figure 1K, 1L, 1M and 1O), suggesting that OSE in aged ovaries undergo metaplastic changes to acquire some of the features of ovarian cancer precursor lesions. Fallopian tube sections were used as positive controls as both the markers are known to be expressed in this tissue (Figure 1P and 1Q). Postmenopausal ovarian tissue slides that were exposed to IgG showed no staining and were used as negative controls (Supp. Figure 1).

To confirm whether similar changes occur in mouse ovaries, we aged 50 C57BL/6 mice for 22 months and tissues were collected at regular intervals. Histological

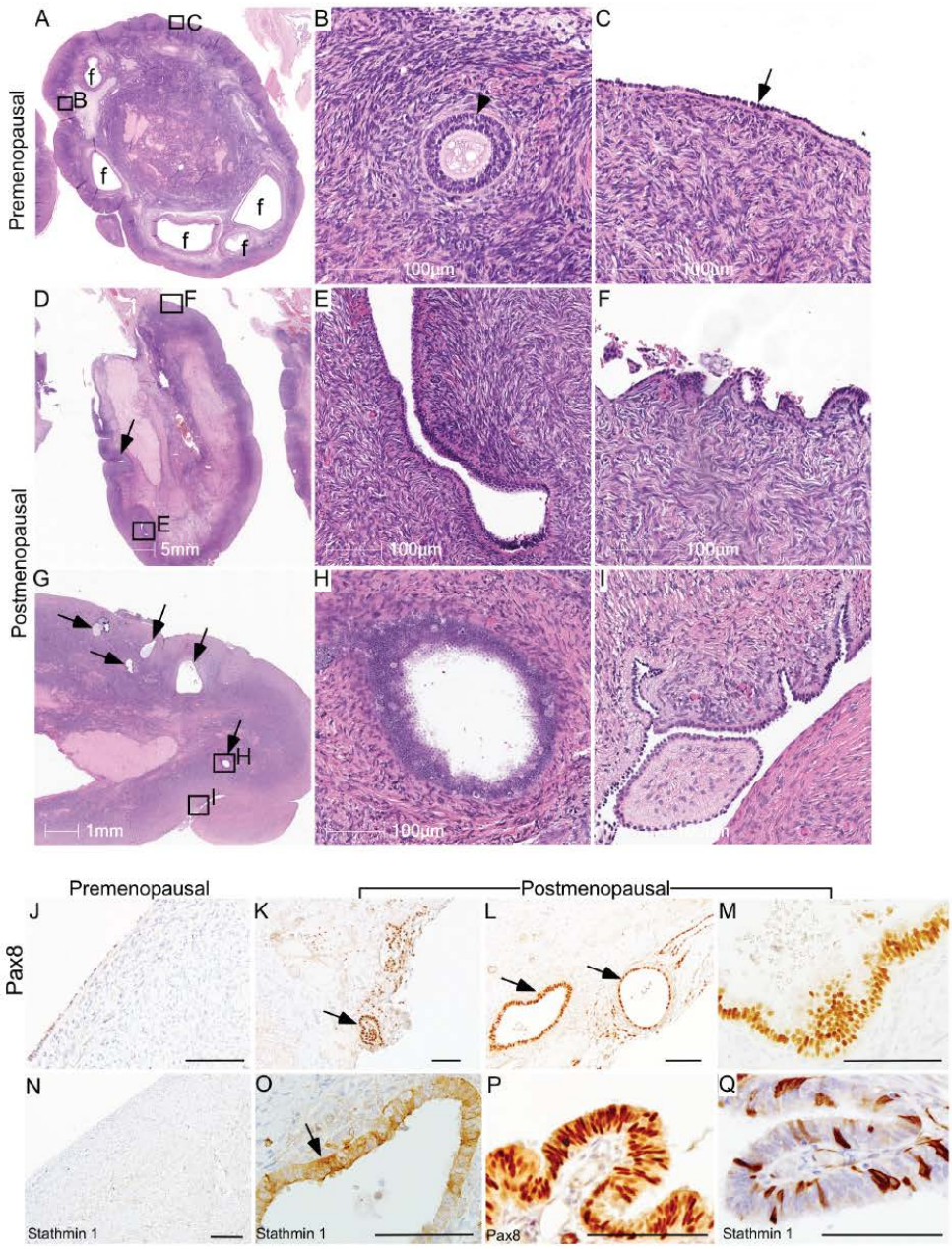

Figure 1: Ovarian surface epithelium hyperplasia and epithelial inclusion cysts in postmenopausal human ovaries. A.-C. Representative histological sections of premenopausal human ovaries showing normal morphology with different sized follicles (marked with f) and a single layer of ovarian surface epithelium (arrow in panel C). A representative picture of a preantral follicle (arrowhead) is presented in Panel B. **B.** and **C.** are higher magnification images of boxed areas in panel A. **D.-I.** Examination of postmenopausal ovaries showing absence of follicles and displaying OSE cell hyperplasia with deep surface invaginations (arrow in panel D), abnormal papillary growth **F.**, inclusion cysts (E, arrows in panel G and a high magnification image in panel H), epithelial outgrowths and shedding **I.**. Boxed areas in **D.** and **G.** are presented at a higher magnification in **E.**, **F.**, **H.** and **I. K.-M.** PAX8 immunolocalization in abnormal epithelial lesions (arrows in panel **K.** and **L.**) of postmenopausal human ovaries. **O.** Inclusion cysts in a postmenopausal ovary were also positive for Stathmin 1 (arrow). OSE of control premenopausal ovaries stained negative for both PAX8 **J.** and Stathmin 1 **N.**. **P.** and **Q.** Fallopian tube epithelial cells were used as a positive control for both the markers. Bars: 100 µm, if not specified in a panel.

examination of young mouse ovaries (Age: 8 weeks; $N = 10$) showed follicles, corpora lutea, and a single layer of flattened-to-cuboidal OSE cells (Figure 2A-2C). Similar to the post-menopausal human ovaries, aged mouse ovaries exhibited features such as OSE hyperplasia (Figure 2E and 2F), papillary growth (Figure 2G), deep surface invaginations (Figure 2H), inclusion cysts (Figure 2I and 2J) and shedding (Figure 2K). Staining with cytokeratin 8 (CK8), a well-known marker of epithelial cells [16], validated the epithelial origin of these pathological lesions (Figure 2M).

Ovarian inclusion cysts have been proposed to derive from the deep invaginations of OSE cells or entrapment of the fallopian tube epithelial cells during the process of repetitive ovulatory wound and repair [19]. To ascertain the possible cell of origin of epithelial inclusion cysts, we performed extensive serial sectioning of the aged mouse ovaries and found that these cysts are connected to the OSE cells (Figure 2I and 2J), suggesting that epithelial inclusion cysts in the aged ovaries are coming from the invaginations of the hyperplastic OSE cells. Using a well-established method of scoring OSE hyperplasia (Supp. Figure 2), as described in [10], we demonstrated that aged mouse ovaries (Age: 16 months; $N = 30$) have a significantly higher hyperplasia score compared to young ovaries (Figure 2L). To evaluate if abnormal OSE growths in aged mouse ovaries are similar to the epithelial lesions observed in postmenopausal human ovaries, we analysed expression of Pax8 and Stathmin 1 and found expression of both of these markers in abnormal epithelial growths of aged mouse ovaries (Figure 2N). In summary, these results suggest that OSE hyperplasia and inclusion cysts development occurs during ovarian aging, and these abnormal growths express markers of ovarian cancer precursor lesions.

Hyperactive mTOR signalling in OSE of aged human and mouse ovaries

We [16] and others [28, 29] have shown that overactivation of mTOR signalling occurs in approximately 80% of human ovarian carcinomas. In mouse ovary, constitutive activation of PI3K/mTOR signalling results in the development of similar tumours confirming the role of this pathway in pathogenesis of ovarian cancer. As OvCa is a disease of aged women [6], we hypothesised that mTOR activation contributes to the development of pathological changes in the OSE of aged ovaries. To test this hypothesis, we analysed the expression of phosphorylated form of S6 ribosomal protein (pS6), a known marker of active mTOR signalling [16], in both young and aged ovaries (Figure 3). In young mouse ovaries, pS6 is highly expressed in the somatic cells of the ovary but absent in OSE (Figure 3A and 3B). However, both OSE and somatic cells of the aged mouse ovaries showed expression of pS6 protein (Figure 3C and 3D). A similar expression pattern was observed in human ovaries where pS6 was localised in OSE and somatic cells of the postmenopausal ovaries but only present in the somatic cells of the premenopausal ovaries (Figure 3E-3H and Supp. Figure 3). In conclusion, our expression analysis revealed that overactivation of mTOR signalling occurs in OSE during ovarian aging.

Genetic suppression of mTOR signalling inhibits OSE hyperplasia in aged ovaries

A previous study has shown that overexpression of *Pten*, a negative regulator of PI3K/mTOR signalling, significantly extends lifespan of mice, partially by decreasing incidences of cancer in aged mice [30]. For this study, we collected ovaries from aged *Pten* transgenic ($Pten^{tg}$) and wild type (WT) control mice ($N = 5$/each; age: 26-27 months). Examination of WT mouse ovaries revealed OSE shedding, inclusion cysts and invasive papillary growths (Figure 4A-4G). Next, we serially sectioned the ovaries and the Fallopian tubes of the WT mice and showed that the papillary growths within the WT ovaries are connected with OSE and are distinct from the fallopian tube epithelial cells (Figure 4E-4G), suggesting that these abnormal epithelial growths are extensions of invasive OSE cells. Analysis of aged $Pten^{tg}$ ovaries depicted a single layer of OSE cells around the whole ovarian surface with no evidence of invasive growth (Figure 4H and 4I), which was similar to young mouse ovaries (Figure 2A-2C). The ovaries of the $Pten^{tg}$ mice had a significantly lower OSE hyperplasia score compared to the WT controls (Figure 4J). Immunolocalization of CK8, Pax8 and Stathmin 1 confirmed phenotypic changes in the OSE of $Pten^{tg}$ and control ovaries (Figure 4K-4P and Supp. Figure 4). As expected, compared to controls, lower expression of pS6 protein was observed in the $Pten^{tg}$ ovaries (Supp. Figure 4). The mammalian ovaries progressively lose their follicles through ovulation or apoptosis and eventually run out of these germ cell units leading to menopause [4]. The majority of the follicles are lost by one year of age in mice and by 50 years of age in humans [3]. Consistently, no follicles were observed in the ovaries of aged $Pten^{tg}$ and control mice (Figure 4A and 4H). These results establish that suppression of mTOR signalling by overexpression of *Pten* is sufficient to inhibit pathological changes in aged OSE cells.

Pharmacological inhibition of mTOR signalling suppresses age-associated changes in OSE

Several independent studies have established that treatment with rapamycin, an inhibitor of mTOR kinase, extends lifespan by delaying the onset of age related pathological disorders including cancer [21-23, 25, 31,

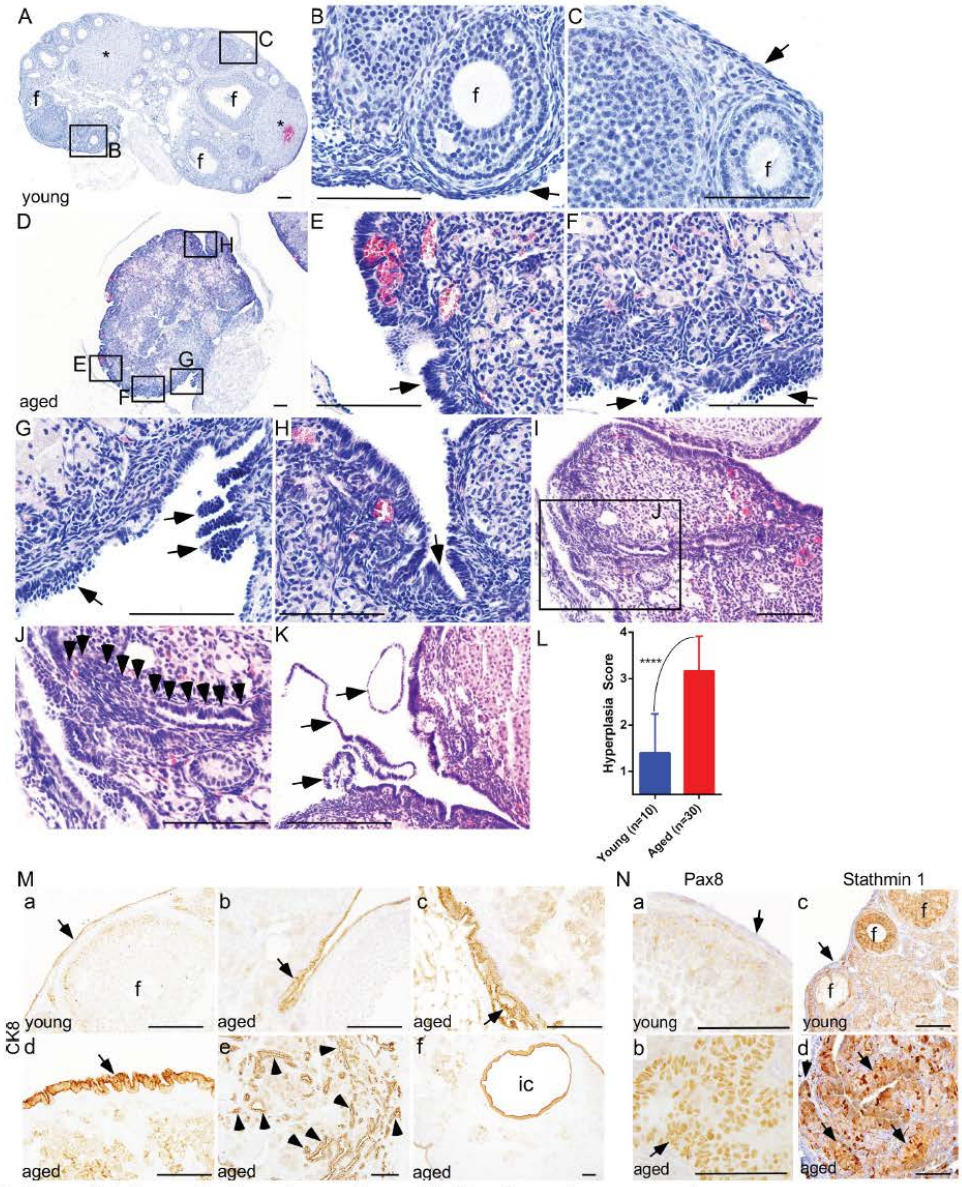

Figure 2: Deregulated growth of ovarian surface epithelium in aged mouse ovaries. A.-C. Histological analysis of a young mouse ovary (8 wk) showing follicles (B; marked with f), corpora lutea (asterisks in panel A), and a single flattened layer of ovarian surface epithelial cells (C; arrow). **D.** An abnormal looking hyperplastic ovary of aged mice. Higher magnification images of boxed areas in panel D revealed irregular morphology and ovarian surface epithelial cell hyperplasia (arrows in **E.** and **F.**), epithelial multilayering and abnormal papillary growth (arrows in **G.**), and epithelial invaginations into stroma **H. I.** and **J.** OSE cells in an aged ovary infiltrating (arrowheads in panel J) into the stroma forming inclusion cysts and glandular structures. Panel J is a higher magnification picture of boxed area in panel I. Extensive epithelial shedding and outgrowths (arrows in panel **K.**) in aged ovaries. **L.** Significant increase in ovarian surface epithelial hyperplasia score of ovaries of the aged mice compared to young controls. **M.** Epithelial origin of abnormal lesions confirmed by CK8 staining. (**M.**, a) Normal CK8-postive OSE cells (arrow) were seen in young mouse ovary. (**M.**, b-f) CK8 expression was observed in abnormal invasive and hyperplastic growths (arrow in panel b-d, arrowheads in panel e) of OSE in aged mice. (**M.**, f) CK8-positive inclusion cyst (ic) present in an aged ovary. (**N.**, b and d) PAX8 and Stathmin 1 expression in invasive and hyperplastic epithelial growths (arrow) of aged mice ovaries. (**N.**, a and c) Ovarian surface epithelium (arrow) of young mouse ovary was negative for PAX8 and Stathmin 1 staining. (**N.**, c) Stathmin 1 was expressed by the somatic cells of follicles (marked with f) in young ovaries. Bars: 100 μm.

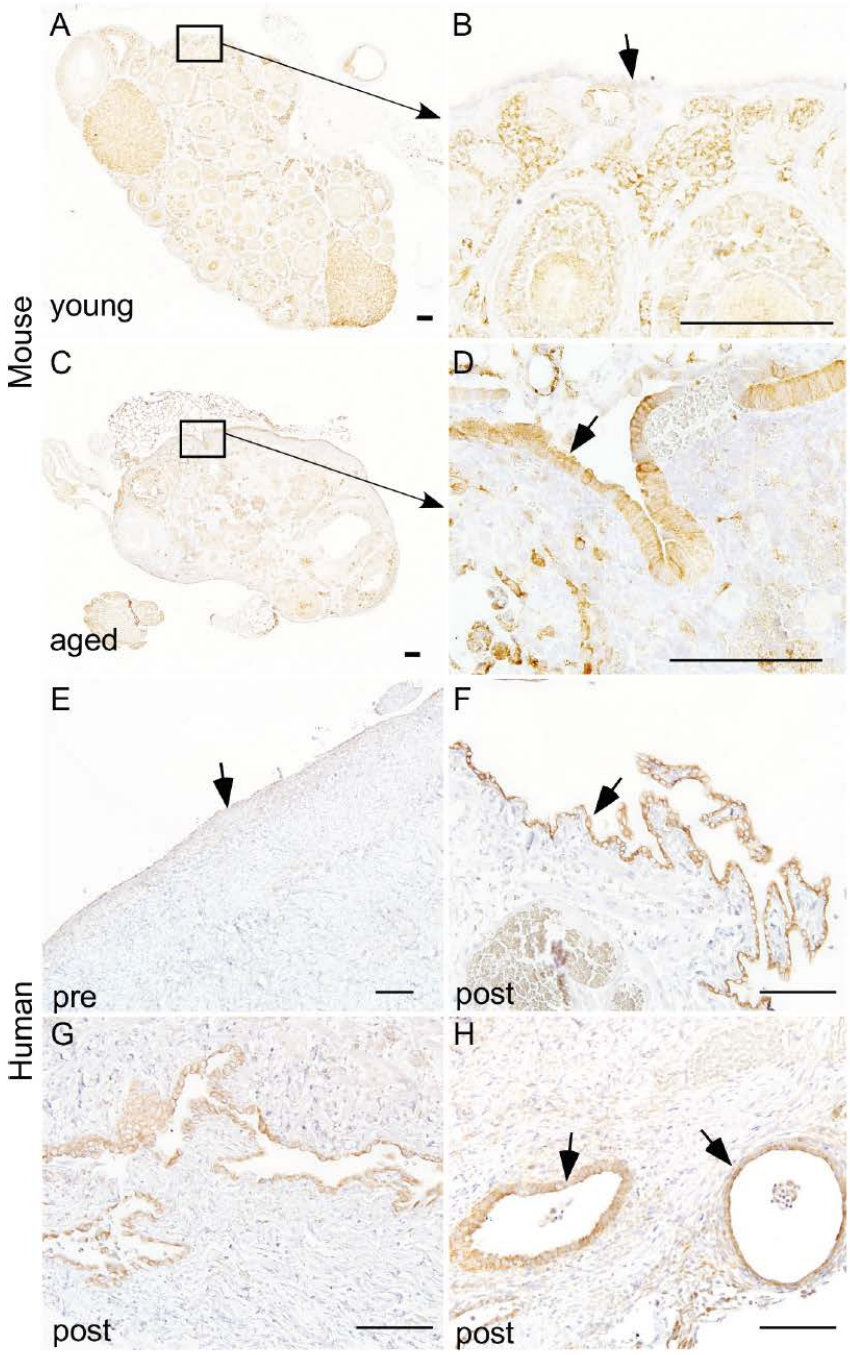

Figure 3: Hyperactive mTOR signalling in ovarian surface epithelium of aged human and mouse ovaries. Increased expression of pS6, a marker for mTOR activation, was observed in hyperplastic ovarian surface epithelium (arrow in panel **D.**) of aged mouse ovaries **C.-D.** and papillary growths of ovarian surface epithelium of postmenopausal human ovaries (arrow in panel **F.**). Increased expression of pS6 was also observed in invasive epithelial growths **G.** and inclusion cysts (arrows in panel H) of postmenopausal human ovaries. Ovarian surface epithelium of young mouse **A.-B.** and human ovary **E.** showed negative staining for pS6. Panel **B.** and **D.** represent higher magnification images of boxed areas in panel **A.** and **C.** Bars: 100 μm.

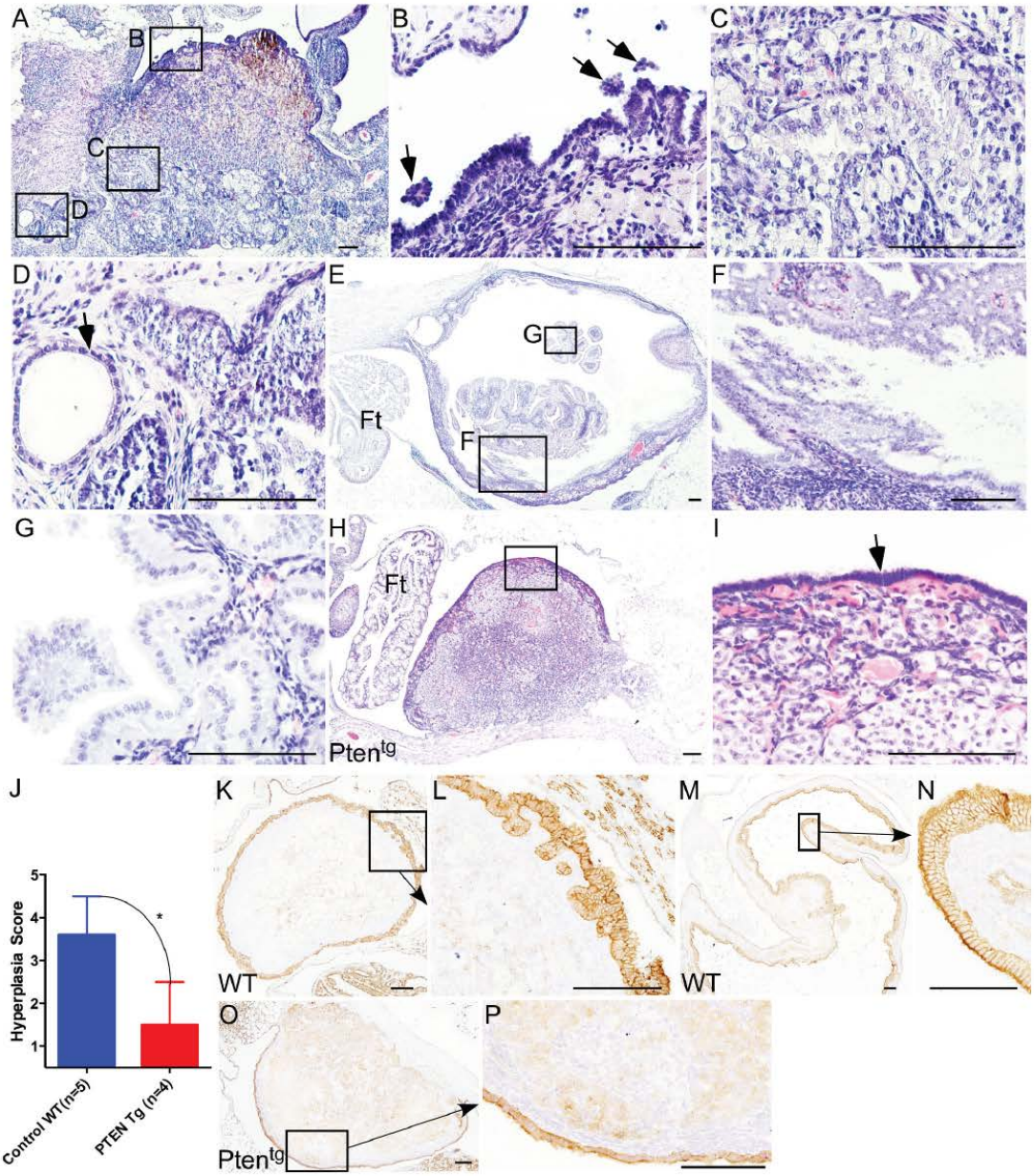

Figure 4: Overexpression of Pten inhibits ovarian surface epithelial hyperplasia in aged ovaries. A.-G. Haematoxylin and eosin-stained sections of aged control mice ovaries. Boxed areas in panel A are shown at a higher magnification in panel **B.-D.** Ovarian surface epithelial cell hyperplasia and shedding (B; arrows), invasive epithelial growths **C.**, and inclusion cysts (D; arrow) in age matched control ovaries. **E.-G.** Papillary growths inside aged ovaries that are distinct from the fallopian tube epithelium. Panel **F.** and **G.** are high magnification images of boxed areas in panel E. **H.** Ovaries of the Pten^{tg} mice showed relatively normal morphology and are covered by single layer of ovarian surface epithelial cells, presented at a higher magnification and marked with an arrow in panel **I. J.** Significant decrease in hyperplasia score of the Pten^{tg} mice ovaries compared to age-matched controls. **K.-N.** Ovarian surface epithelium hyperplasia and invasive epithelial growths were confirmed by CK8 staining in wild type aged control mouse ovaries. CK8-positive papillary growths and deep surface invaginations are shown in panel L and N, respectively. **O.-P.** Normal looking CK8-positive OSE cells in Pten^{tg} mice ovaries. Ft: Fallopian tube. Bars: 100 μm.

32]. To test if the inhibition of mTOR signalling using an mTOR inhibitor will suppress the pathological changes in aged ovaries, we collected ovaries from genetically heterogeneous mice that had been treated with rapamycin from 9 months of age at three different doses (4.7, 14, or 42 parts per million in food) for 13 months. Consistent with previous results (Figure 2), histological examination of ovaries from 22-month-old untreated mice revealed OSE hyperplasia and papillary growth (Figure 5A; $N = 8$). Rapamycin treatment significantly suppressed these pathological changes in OSE cells in a dose dependent manner (Figure 5B-5D and 5F). The highest dose of rapamycin (42ppm) was most effective in inhibiting epithelial hyperplasia and OSE of the ovaries belonging to this treatment group were similar to young ovaries (Figure 5D and 5E). Overall, these results showed that chronic suppression of mTOR signalling inhibits age related incidences of OSE hyperplasia, and therapeutic targeting of this pathway might be an effective strategy for the prevention and/or treatment of OvCa.

mTOR inhibitors suppress the growth of human OvCa cells

OvCa is a disease that mainly occurs in postmenopausal women [6]. Our analysis of aged human and mouse ovaries found epithelial lesions with hyperactive mTOR signalling that share histopathological features of the OvCa precursor lesions and malignant disease (Figure 1-3). To test whether pharmacological suppression of mTOR signalling using two FDA-approved drugs (Everolimus and BEZ235) will suppress the growth of OvCa, we treated OvCa cell lines (COV318 and COV362) with the different doses of these two mTOR inhibitors (Figure 6). COV318 and COV362 cells were selected based upon their genetic similarity to human OvCa [33]. Treatment with Everolimus or BEZ235 decreased cell viability of these OvCa cell lines in a dose dependent manner (Figure 6A). Assessment of cell proliferation using 5-bromo-2′-deoxyuridine (BrdU) incorporation and colony forming assays revealed significant decrease in OvCa cell proliferation upon exposure with mTOR inhibitors (Figure 6B and 6C). To confirm the efficacy of these inhibitors in suppressing

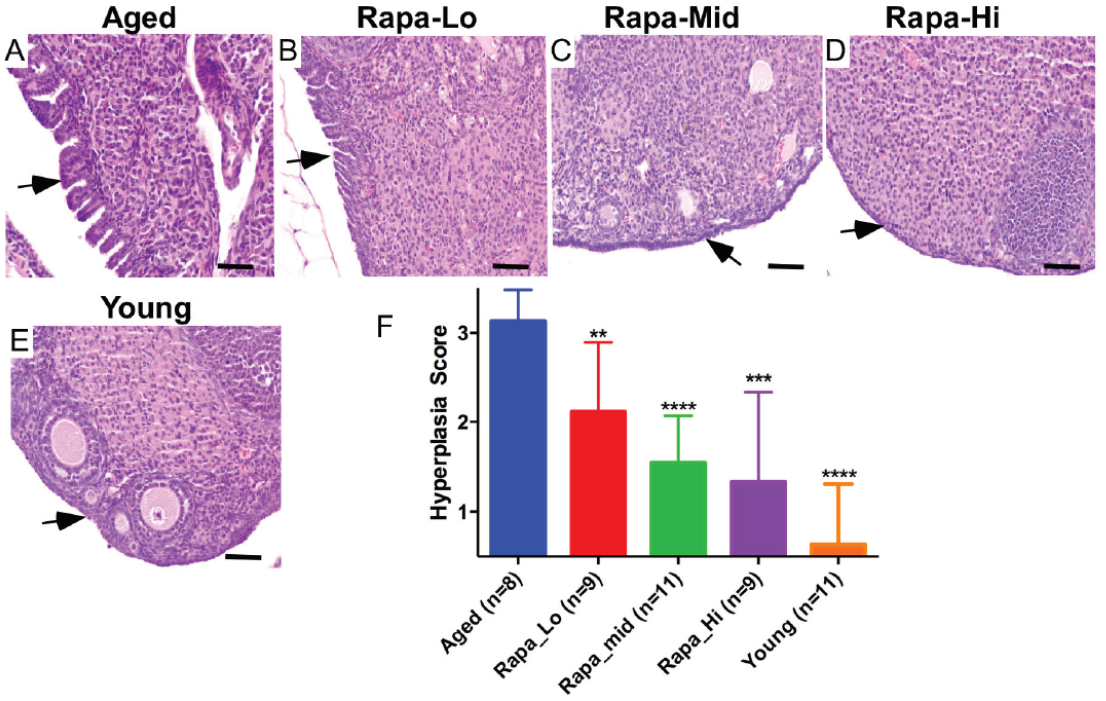

Figure 5: Chronic rapamycin treatment suppresses age-associated pathological changes in ovarian surface epithelium. **A.** Aged control mice showing abnormal papillary epithelial growth (arrow). **B.-D.** Treatment with rapamycin decreased hyperplastic growth (arrows) of ovarian surface epithelium in a dose-dependent manner. Histology of ovaries of the aged mice treated with low dose **B.**, medium dose **C.** and high dose **D.** of rapamycin. In panel **E.** is a representative section of the ovary from young control mice with normal ovarian surface epithelial cell lining. **F.** Hyperplasia score confirmed significant decrease in abnormal epithelial growth of the aged ovaries treated with increasing doses of rapamycin. Bars: 100 μm.

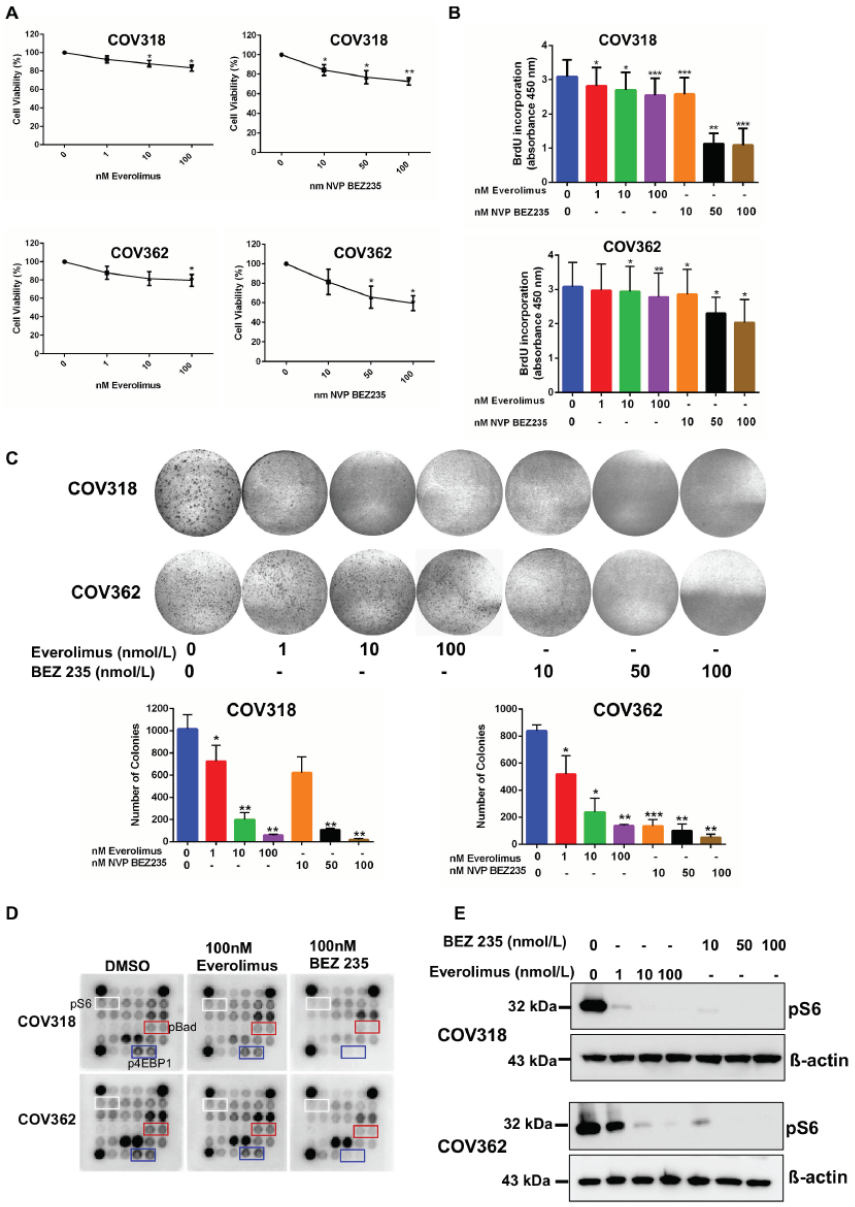

Figure 6: mTOR inhibitors suppress the growth of ovarian cancer cells. A. COV318 and COV362 cells were treated with increasing doses of mTOR inhibitors, Everolimus and NVP BEZ235. Forty-eight hours later, cell viability was assessed using cell viability assay kit from Promega. The data shown are mean ±SEM of three individual experiments. $*P < 0.05$, $**P < 0.01$, Student's *t*-test. **B.** Cells treated with mTOR inhibitors were subjected to BrdU incorporation assay. The data represents mean ±SEM of three individual experiments. $*P < 0.05$, $**P < 0.01$, $***P < 0.001$, Student's *t*-test. **C.** COV318 and COV362 cells treated with increasing dose of mTOR inhibitors were subjected to clonogenic assays. The data shown are representative of three individual experiments. Pictures were taken at the same magnification. $*P < 0.05$, $**P < 0.01$, $***P < 0.001$, Student's *t*-test. **D.** COV318 and COV362 cells were treated with DMSO control or 100 nmol/L of Everolimus or BEZ235. Forty-eight hours later, whole cell lysates were subjected to AKT/mTOR signalling antibody protein array. **E.** Whole cell lysates from COV318 and COV362 cells treated with increasing doses of Everolimus and BEZ235 were subjected to western blot analysis for pS6. The data shown are representative of three individual western blot analyses. β-actin was used as a loading control.

mTOR activity, we performed AKT/mTOR protein array and showed that the treatment with Everolimus or NVP BEZ235 (100nmol/L) leads to the reduction in expression of the active form of the key downstream target proteins (pS6, p4E binding protein 1 and pBad) of this pathway (Figure 6D). To validate our AKT/mTOR array data, we performed western blot analysis for pS6 on protein extracts collected from COV318 and COV362 cells treated with increasing doses of Everolimus or BEZ235. Both inhibitors decreased the levels of pS6 protein (Figure 6E). Collectively, these findings showed that suppression of mTOR signalling decreases viability and proliferation of OvCa cells.

DISCUSSION

PI3K/mTOR signalling is a key regulator of the major cellular processes such as cell proliferation and cell growth, and deregulation of this signalling pathway contributes to the pathogenesis of various diseases such as cancer, diabetes, obesity, hereditary diseases, and neurodegenerative disorders [34]. Studies in several different model systems have provided evidence that mTOR signalling is one of the main regulators of ageing process and genetic or pharmacological modulation of this signalling pathway affects lifespan [20, 32, 35]. Genetic deletion of the *mTor* or overexpression of the *tuberous sclerosis 1/2* (Tsc1/2) gene significantly increases mean life span in both worms and flies [20]. Similarly, pharmacological suppression of mTOR signalling using rapamycin or loss of the *mTor* or *S6K1* gene extends mouse lifespan [22, 25, 31, 36, 37]. These findings coupled with observations that the constitutive activation of mTOR signalling decreases [38] mean lifespan established that counteracting age related increase in mTOR signalling is one of the keys to controlling ageing. However, some recent studies have shown an opposite trend, where mTOR activity is decreased when determined in whole tissue samples of the aged mice compared young controls [39, 40]. For example, western blot analysis of pS6 protein in liver, muscle and fat tissue samples collected from young and aged C57BL/6J mice showed decrease in mTOR activity with aging [39]. Our examination of mTOR activity by measuring pS6 protein expression showed higher level of mTOR activity in young ovaries compared to aged ovaries, consistent with the idea that mTOR signalling plays an important role in germ and follicular development and young ovaries are filled with these structures, which are nearly absent in aged ovaries (Figures 2 and 3). However, OSE of the aged human and mouse ovaries showed strong expression of pS6 protein that was almost absent in the OSE of young ovaries (Figure 3). Our data is supported by the observations in fasting aged mice where the level of hepatic pS6 protein increases with age [41]. These findings suggest that changes in the level of mTOR activity with aging are distinct in each cell type and that assessment of mTOR signalling in a particular cell type might provide much more useful information compared to the whole tissue-based approaches.

OvCa is a very heterogeneous disease. There are three major types of OvCa: epithelial carcinomas, germ cell tumours, and stromal tumours [8]. The epithelial carcinomas represent the most malignant and common form of OvCa. Approximately 80% of the epithelial OvCa patients presented with overactivation of the mTOR pathway [16]. Constitutive activation of mTOR signalling by the deletion of the *Lkb1*/*Tsc1*/*Tsc2* gene in both OSE and stromal cells causes OSE hyperplasia and epithelial OvCa but no stromal tumours [16]. Similarly, overactivation of this signalling pathway in germ cells leads to premature germ cell loss and ovarian insufficiency [42]. However, no germ cell tumours were observed in these mice [42]. These findings imply that each cell type in an organ shows differential response to hyperactive mTOR signalling and high mTOR activity in a particular cell type rather than the whole organ is responsible for age related pathologies.

During each ovarian cycle, few primordial follicles are activated to grow, and these follicles under the influence of gonadotropins go on to develop to a preovulatory stage where they are ready to release mature eggs for fertilization. The process of primordial follicle recruitment is quite important for female fertility as any aberrations in this process lead to infertility [42]. Intra-follicular mTOR signalling is a key regulator of primordial follicle recruitment and growth. Sustained activation of mTOR in germ cells by genetic ablation of the *Pten*/*Tsc1*/*Tsc2* causes untimely recruitment of primordial follicles leading to premature ovarian failure and infertility [43]. This raises a possibility that the suppression of mTOR signalling might inhibit primordial follicle activation and consequently, delay menopause. However, examination of ovaries from the $Pten^{tg}$ and rapamycin treated mice revealed no differences in follicle/stromal cells compared to control groups (Figures 4 and 5). This suggests that there are other compensatory mechanisms involved in the activation of primordial follicles.

Crosstalk between gonads and the hypothalamus-pituitary axis is an important determinant of mammalian fertility. Both hypothalamus and pituitary gland secrete hormones that affect ovarian function. In turn, ovarian hormones operate in feedback loop to regulate secretions from the hypothalamus-pituitary axis [4]. During aging, ovaries are almost devoid of follicles and endocrine feedback loop of the ovary is no longer operational leading to excessive secretion of gonadotropins, follicle-stimulating hormone (FSH) and luteinising hormone (LH). As gonadotropin receptors are present on OSE cells, these hormones are proposed to stimulate the growth of

OSE and aid in development of inclusion cysts [8, 44]. In cell culture, both FSH and LH stimulate the growth of OSE cells by up regulating PI3K/mTOR signalling, and suppression of this signalling pathway inhibits gonadotropin-induced proliferation of OSE cells [44, 45]. This indicates that gonadotropins act through PI3K/mTOR signalling in regulating OSE growth, and similar mechanisms might be operational *in vivo* in aged ovaries.

Aging is a major risk factor for many solid cancers [46]. Lifestyle changes and pharmaceutical-based approaches that extend lifespan by counteracting the age-related pathological changes are also known to retard tumor development [21-23, 46-48]. We have previously shown that treatment with rapamycin extends mouse lifespan even when started as late as 20 months of age [31], suggesting that it may provide benefits related to mTOR action in growth or transformation of many different kinds of tumors, not just ovarian tumors. In summary, our examination of aged human and mouse ovaries showed hyperactivation of mTOR signalling in OSE pathological lesions. Suppression of mTOR signalling inhibited the development of these lesions in the Pten^{tg} and rapamycin treated mice. Treatment of human OvCa cells with mTOR inhibitors significantly decreased the growth and viability of these cells suggesting that targeting the mTOR pathway might be an effective therapeutic strategy for preventing OvCa.

MATERIALS AND METHODS

Mouse genetics and husbandry

Mice used in the present study were housed under standard animal housing conditions. All procedures for mice experimentation were approved by the Animal Care and Ethics Committee at the University of Newcastle. Generation and characterization of *Pten*^{tg} mice is described in [30]. Rapamycin treatment in genetically heterogeneous mice is described by us in detail [32]. 50 C57BL/6 were aged for 22 months and tissues were collected at regular intervals.

Human ovarian tissue samples

Human ovarian tissue samples from 12 patients were obtained from the Hunter Cancer Tissue Biobank using a protocol approved by the Institutional Human Research Ethics Committee at the University of Newcastle.

Cell lines, reagents and culture conditions

The human ovarian cancer cells COV318 and COV362 (Sigma, MO, USA) were grown at 37°C in Dulbecco's Modified Eagle Medium supplemented with 10% fetal bovine serum (FBS), L-glutamine, and pencillin/streptomycin in a humidified atmosphere containing 5% CO_2. Everolimus (RAD001) and NVP-BEZ235 were obtained from Selleckchem (Provided by Sapphire Biosciences, NSW, Australia). Short tandem repeat profiling and mycoplasma testing (MycoAlert™ Plus Mycoplasma detection kit, Lonza, MD, USA) were conducted at regular intervals for the quality control of cell culture conditions and validation of these cell lines.

Histology and Immunohistochemistry (IHC)

For histological analyses, ovaries were fixed in 10% formalin solution (Sigma, MO, USA) overnight at 4°C and then transferred to 70% ethanol until processing. The fixed tissues were dehydrated in a graded ethanol series, cleared in xylene, and embedded in paraffin wax. Embedded tissue samples were sectioned at 6 µm and mounted on slides. Haematoxylin and eosin (H&E) staining and IHC were performed using standard protocols [16]. Briefly, for IHC, antigen retrieval was performed in 1mM EDTA buffer (0.05% Tween-20, pH 8) followed by the endogenous peroxidase block using 3% (v/v) hydrogen peroxide in absolute methanol. Tissue sections were then blocked in blocking solution (5% Goat Serum in TBS, 0.1% Triton X-100) for 1 hr at room temperature. Following this, tissue sections were incubated overnight at 4°C with normal IgG or following primary antibodies: Stathmin 1 (1:2000), Phospho-S6 Ribosomal protein Ser235/236 (1:400; Cell Signalling Technologies, MA, USA), Pax8 (1:500, Proteintech, IL, USA) and CK8 (Developmental Studies Hybridoma Bank, IA, USA). Biotinylated secondary antibodies (Jackson ImmunoResearch Labs, PA, USA or Thermo Fischer Scientific, Australia) were used followed by incubation with horseradish peroxidase-conjugated streptavidin (Thermo Fischer Scientific). Sections were then exposed to Diaminobenzidine (DAB, Sigma) to develop colour. Sections were counterstained with hematoxylin. Images were photographed using Olympus DP72 microscope and the Aperio Scanscope slide scanner. The gain and exposure time were set constant across tissue samples.

Hyperplasia scoring of mouse ovaries

For scoring OSE hyperplasia, histological sections of a mouse ovary were divided into four anatomical locations: hilus, perpendicular to the hilus, opposite from the hilus and centre of the ovary (as shown in Supp. Figure 2). Based upon the presence of morphological lesions or hyperplasia, a +1 score was assigned to each location. An overall score > 2 was considered as positive for hyperplasia.

Cell proliferation assay

Cell proliferation assays were performed using BrDU cell proliferation assay kit (Cell Signaling Technology) as per the manufacturer's instructions. Briefly, 2500 cells/well were seeded onto 96-well plates and allowed to grow for 24 h followed by drug treatments. BrdU (10µmol/L) was added and cells were incubated for another 24 h before assay was carried out. Absorbance was read at 450 nm using SpectraMax microplate reader (Molecular Devices, CA, USA).

Cell viability

Cell viability was quantitated using a Cell viability assay kit (Promega, NSW, Australia). Briefly, Cells were seeded at 5,000 cells per well onto 96-well culture plates and allowed to grow for 24 h followed by desired drug treatments. Post 48 hour treatment, cells were incubated with CellTiter-Blue® reagent for 1 hour at 37°C. The fluorescent signal was recorded using the FLUOstar OPTIMA (BMG Labtech, VIC, Australia).

Clonogenic assays

Cells were seeded at 2500 cells/ well onto 6-well culture plates and allowed to grow for 24 h followed by drug treatments. Cells were then allowed to grow for another 8 days before fixation with 70% ethanol and staining with 0.5% crystal violet. The images were captured with a Bio-rad VersaDoc™ image system (Bio-Rad, Gladsville, NSW). Colonies were counted using the National Institute of Health image J software.

Western blot analyses and Akt signalling antibody array

Protein extracts from COV318 and COV362 treated with different concentrations of Everolimus or BEZ235 were prepared in ice-cold radioimmunoprecipitation assay buffer (RIPA) supplemented with protease and phosphatase inhibitors. Equal amounts of protein were loaded and separated by 10% SDS-PAGE gel and thereafter transferred to nitrocellulose membrane. Afterwards, the membrane was blocked in 5% milk (w/v) in Tris-buffered saline/Tween 20 for 1 hr at room temperature and then incubated overnight at 4°C with rabbit mAb Phospho-S6 Ribosomal protein (1:2000 in 2.5% w/v BSA, 1xTBS, 0.1% Tween-20; Cell Signalling Technologies). This was followed by incubation with secondary horseradish peroxidase-conjugated anti-rabbit antibody (Jackson ImmunoResearch, West Grove, PA) for 1hr at RT. βactin was used as a loading control. Akt/mTOR signalling antibody array was performed as per manufacturer's instructions (Cell Signalling Technologies).

Statistical analysis

Statistical analyses were performed using GraphPad Prism 6.0 (Graphpad Software, San Diego, CA). Values are expressed as mean± SEM. The Student *t* test was used to calculate differences between the groups (N≥3/ group), and p values ≤ 0.05 were considered statistically significant.

ACKNOWLEDGMENTS

We thank: Prof Manuel Serrano (Spanish National Cancer Research Centre) for *Pten* transgenic mice and members of the gynaecology oncology group for critical reading of this manuscript. This work in part was supported by funding from the National Health and Medical Research Council, the Australian Research Council, and the Cancer Institute NSW (P.S.T). Work in the Miller lab was supported by NIH grant AG022303 and the Glenn Foundation for Medical Research. The Hunter Cancer Biobank is supported by the Cancer Institute NSW. P.B., P.B.N., and S.S.S. are recipients of the University of Newcastle Postgraduate Research Fellowship.

CONFLICTS OF INTEREST

The authors declare no conflict of interest.

REFERENCES

1. Torre LA, Bray F, Siegel RL, Ferlay J, Lortet-Tieulent J and Jemal A. Global cancer statistics, 2012. CA Cancer J Clin. 2015; 65:87-108.
2. DeSantis CE, Lin CC, Mariotto AB, Siegel RL, Stein KD, Kramer JL, Alteri R, Robbins AS and Jemal A. Cancer treatment and survivorship statistics, 2014. CA Cancer J Clin. 2014; 64:252-271.
3. Broekmans FJ, Soules MR and Fauser BC. Ovarian aging: mechanisms and clinical consequences. Endocr Rev. 2009; 30:465-493.
4. Edson MA, Nagaraja AK and Matzuk MM. The mammalian ovary from genesis to revelation. Endocr Rev. 2009; 30:624-712.
5. Fathalla MF. Incessant ovulation—a factor in ovarian neoplasia? Lancet. 1971; 2:163.
6. Smith ER and Xu XX. Ovarian ageing, follicle depletion, and cancer: a hypothesis for the aetiology of epithelial ovarian cancer involving follicle depletion. Lancet Oncol. 2008; 9:1108-1111.
7. Kotsopoulos J, Lubinski J, Gronwald J, Cybulski C, Demsky R, Neuhausen SL, Kim-Sing C, Tung N, Friedman

S, Senter L, Weitzel J, Karlan B, Moller P, Sun P, Narod SA and Hereditary Breast Cancer Clinical Study G. Factors influencing ovulation and the risk of ovarian cancer in BRCA1 and BRCA2 mutation carriers. Int J Cancer. 2015; 137:1136-1146.

8. Auersperg N, Wong AS, Choi KC, Kang SK and Leung PC. Ovarian surface epithelium: biology, endocrinology, and pathology. Endocr Rev. 2001; 22:255-288.
9. Britt K and Short R. The plight of nuns: hazards of nulliparity. Lancet. 2012; 379:2322-2323.
10. Burdette JE, Oliver RM, Ulyanov V, Kilen SM, Mayo KE and Woodruff TK. Ovarian epithelial inclusion cysts in chronically superovulated CD1 and Smad2 dominant-negative mice. Endocrinology. 2007; 148:3595-3604.
11. Tan OL, Hurst PR and Fleming JS. Location of inclusion cysts in mouse ovaries in relation to age, pregnancy, and total ovulation number: implications for ovarian cancer? J Pathol. 2005; 205:483-490.
12. Mittal KR, Zeleniuch-Jacquotte A, Cooper JL and Demopoulos RI. Contralateral ovary in unilateral ovarian carcinoma: a search for preneoplastic lesions. Int J Gynecol Pathol. 1993; 12:59-63.
13. Werness BA, Afify AM, Bielat KL, Eltabbakh GH, Piver MS and Paterson JM. Altered surface and cyst epithelium of ovaries removed prophylactically from women with a family history of ovarian cancer. Hum Pathol. 1999; 30:151-157.
14. Korner M, Burckhardt E and Mazzucchelli L. Different proportions of aneusomic cells in ovarian inclusion cysts associated with serous borderline tumours and serous high-grade carcinomas support different pathogenetic pathways. J Pathol. 2005; 207:20-26.
15. Kim J, Coffey DM, Ma L and Matzuk MM. The ovary is an alternative site of origin for high-grade serous ovarian cancer in mice. Endocrinology. 2015; 156:1975-1981.
16. Tanwar PS, Mohapatra G, Chiang S, Engler DA, Zhang L, Kaneko-Tarui T, Ohguchi Y, Birrer MJ and Teixeira JM. Loss of LKB1 and PTEN tumor suppressor genes in the ovarian surface epithelium induces papillary serous ovarian cancer. Carcinogenesis. 2014; 35:546-553.
17. Kim J, Coffey DM, Creighton CJ, Yu Z, Hawkins SM and Matzuk MM. High-grade serous ovarian cancer arises from fallopian tube in a mouse model. Proc Natl Acad Sci U S A. 2012; 109:3921-3926.
18. Yang WL, Cai KQ, Smedberg JL, Smith ER, Klein-Szanto A, Hamilton TC and Xu XX. A reduction of cyclooxygenase 2 gene dosage counters the ovarian morphological aging and tumor phenotype in Wv mice. Am J Pathol. 2007; 170:1325-1336.
19. Banet N and Kurman RJ. Two types of ovarian cortical inclusion cysts: proposed origin and possible role in ovarian serous carcinogenesis. Int J Gynecol Pathol. 2015; 34:3-8.
20. Lamming DW, Ye L, Sabatini DM and Baur JA. Rapalogs and mTOR inhibitors as anti-aging therapeutics. J Clin Invest. 2013; 123:980-989.
21. Popovich IG, Anisimov VN, Zabezhinski MA, Semenchenko AV, Tyndyk ML, Yurova MN and Blagosklonny MV. Lifespan extension and cancer prevention in HER-2/neu transgenic mice treated with low intermittent doses of rapamycin. Cancer Biol Ther. 2014; 15:586-592.
22. Anisimov VN, Zabezhinski MA, Popovich IG, Piskunova TS, Semenchenko AV, Tyndyk ML, Yurova MN, Antoch MP and Blagosklonny MV. Rapamycin extends maximal lifespan in cancer-prone mice. Am J Pathol. 2010; 176:2092-2097.
23. Komarova EA, Antoch MP, Novototskaya LR, Chernova OB, Paszkiewicz G, Leontieva OV, Blagosklonny MV and Gudkov AV. Rapamycin extends lifespan and delays tumorigenesis in heterozygous p53+/- mice. Aging (Albany NY). 2012; 4:709-714. doi: 10.18632/aging.100498.
24. Comas M, Toshkov I, Kuropatwinski KK, Chernova OB, Polinsky A, Blagosklonny MV, Gudkov AV and Antoch MP. New nanoformulation of rapamycin Rapatar extends lifespan in homozygous p53-/- mice by delaying carcinogenesis. Aging (Albany NY). 2012; 4:715-722. doi: 10.18632/aging.100496.
25. Anisimov VN, Zabezhinski MA, Popovich IG, Piskunova TS, Semenchenko AV, Tyndyk ML, Yurova MN, Rosenfeld SV and Blagosklonny MV. Rapamycin increases lifespan and inhibits spontaneous tumorigenesis in inbred female mice. Cell Cycle. 2011; 10:4230-4236.
26. Laury AR, Hornick JL, Perets R, Krane JF, Corson J, Drapkin R and Hirsch MS. PAX8 reliably distinguishes ovarian serous tumors from malignant mesothelioma. Am J Surg Pathol. 2010; 34:627-635.
27. Novak M, Lester J, Karst AM, Parkash V, Hirsch MS, Crum CP, Karlan BY and Drapkin R. Stathmin 1 and p16(INK4A) are sensitive adjunct biomarkers for serous tubal intraepithelial carcinoma. Gynecol Oncol. 2015; 139:104-111.
28. Altomare DA, Wang HQ, Skele KL, De Rienzo A, Klein-Szanto AJ, Godwin AK and Testa JR. AKT and mTOR phosphorylation is frequently detected in ovarian cancer and can be targeted to disrupt ovarian tumor cell growth. Oncogene. 2004; 23:5853-5857.
29. Kinross KM, Montgomery KG, Kleinschmidt M, Waring P, Ivetac I, Tikoo A, Saad M, Hare L, Roh V, Mantamadiotis T, Sheppard KE, Ryland GL, Campbell IG, Gorringe KL, Christensen JG, Cullinane C, et al. An activating Pik3ca mutation coupled with Pten loss is sufficient to initiate ovarian tumorigenesis in mice. J Clin Invest. 2012; 122:553-557.
30. Ortega-Molina A, Efeyan A, Lopez-Guadamillas E, Munoz-Martin M, Gomez-Lopez G, Canamero M, Mulero F, Pastor J, Martinez S, Romanos E, Mar Gonzalez-Barroso M, Rial E, Valverde AM, Bischoff JR and Serrano M. Pten positively regulates brown adipose function, energy expenditure, and longevity. Cell Metab. 2012; 15:382-394.

31. Harrison DE, Strong R, Sharp ZD, Nelson JF, Astle CM, Flurkey K, Nadon NL, Wilkinson JE, Frenkel K, Carter CS, Pahor M, Javors MA, Fernandez E and Miller RA. Rapamycin fed late in life extends lifespan in genetically heterogeneous mice. Nature. 2009; 460:392-395.
32. Wilkinson JE, Burmeister L, Brooks SV, Chan CC, Friedline S, Harrison DE, Hejtmancik JF, Nadon N, Strong R, Wood LK, Woodward MA and Miller RA. Rapamycin slows aging in mice. Aging Cell. 2012; 11:675-682.
33. Domcke S, Sinha R, Levine DA, Sander C and Schultz N. Evaluating cell lines as tumour models by comparison of genomic profiles. Nat Commun. 2013; 4:2126.
34. Laplante M and Sabatini DM. mTOR signaling in growth control and disease. Cell. 2012; 149:274-293.
35. Lamming DW, Mihaylova MM, Katajisto P, Baar EL, Yilmaz OH, Hutchins A, Gultekin Y, Gaither R and Sabatini DM. Depletion of Rictor, an essential protein component of mTORC2, decreases male lifespan. Aging Cell. 2014; 13:911-917.
36. Wu JJ, Liu J, Chen EB, Wang JJ, Cao L, Narayan N, Fergusson MM, Rovira, II, Allen M, Springer DA, Lago CU, Zhang S, DuBois W, Ward T, deCabo R, Gavrilova O, et al. Increased mammalian lifespan and a segmental and tissue-specific slowing of aging after genetic reduction of mTOR expression. Cell Rep. 2013; 4:913-920.
37. Selman C, Tullet JM, Wieser D, Irvine E, Lingard SJ, Choudhury AI, Claret M, Al-Qassab H, Carmignac D, Ramadani F, Woods A, Robinson IC, Schuster E, Batterham RL, Kozma SC, Thomas G, et al. Ribosomal protein S6 kinase 1 signaling regulates mammalian life span. Science. 2009; 326:140-144.
38. Kapahi P, Zid BM, Harper T, Koslover D, Sapin V and Benzer S. Regulation of lifespan in Drosophila by modulation of genes in the TOR signaling pathway. Curr Biol. 2004; 14:885-890.
39. Baar EL, Carbajal KA, Ong IM and Lamming DW. Sex- and tissue-specific changes in mTOR signaling with age in C57BL/6J mice. Aging Cell. 2015.
40. Houtkooper RH, Argmann C, Houten SM, Canto C, Jeninga EH, Andreux PA, Thomas C, Doenlen R, Schoonjans K and Auwerx J. The metabolic footprint of aging in mice. Sci Rep. 2011; 1:134.
41. Leontieva OV, Paszkiewicz GM and Blagosklonny MV. Fasting levels of hepatic p-S6 are increased in old mice. Cell Cycle. 2014; 13:2656-2659.
42. Adhikari D, Flohr G, Gorre N, Shen Y, Yang H, Lundin E, Lan Z, Gambello MJ and Liu K. Disruption of Tsc2 in oocytes leads to overactivation of the entire pool of primordial follicles. Mol Hum Reprod. 2009; 15:765-770.
43. Adhikari D and Liu K. mTOR signaling in the control of activation of primordial follicles. Cell Cycle. 2010; 9:1673-1674.
44. Gharwan H, Bunch KP and Annunziata CM. The role of reproductive hormones in epithelial ovarian carcinogenesis. Endocr Relat Cancer. 2015; 22:R339-363.
45. Hilliard TS, Modi DA and Burdette JE. Gonadotropins activate oncogenic pathways to enhance proliferation in normal mouse ovarian surface epithelium. Int J Mol Sci. 2013; 14:4762-4782.
46. Riera CE and Dillin A. Can aging be 'drugged'? Nat Med. 2015; 21:1400-1405.
47. Blagosklonny MV. Rapalogs in cancer prevention: anti-aging or anticancer? Cancer Biol Ther. 2012; 13:1349-1354.
48. Blagosklonny MV. Rapamycin extends life- and health span because it slows aging. Aging (Albany NY). 2013; 5:592-598. doi: 10.18632/aging.100591.

Supplementary Material

Age related increase in mTOR activity contributes to the pathological changes in ovarian surface epithelium

Supplementary Material

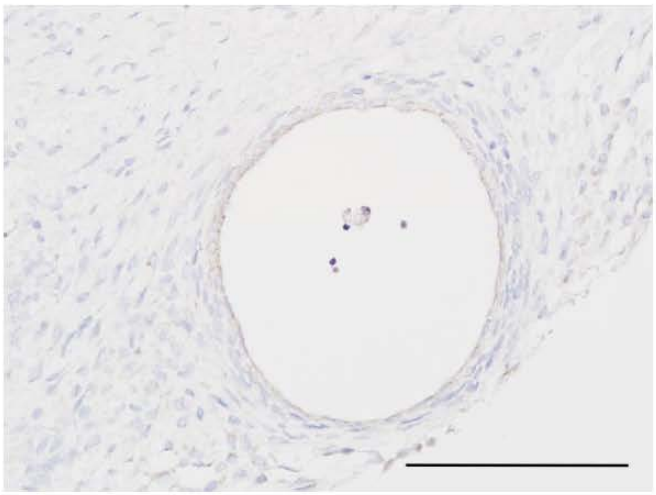

Supp. Fig. 1. No staining was observed in postmenopausal ovarian tissue sections that were exposed to normal IgG. Bars: 100 µm.

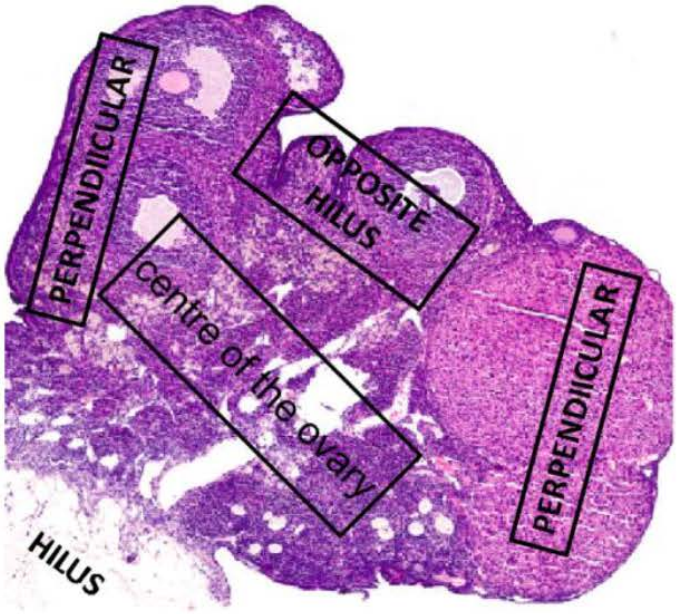

Supp. Fig. 2. Mouse ovaries were divided into four anatomical locations, namely, hilus, perpendicular to the hilus, opposite from the hilus and centre of the ovary, for the assessment of ovarian surface epithelial hyperplasia.

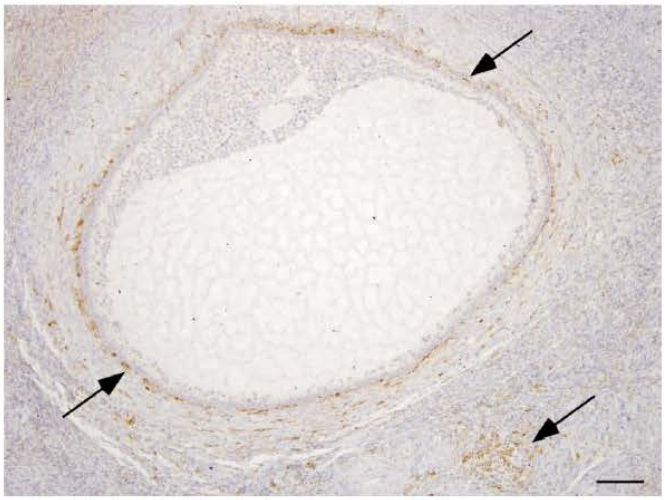

Supp. Fig. 3. A representative section from premenopausal human ovary showing pS6 immunostaining in stromal cells (arrows). Bars: 100 µm.

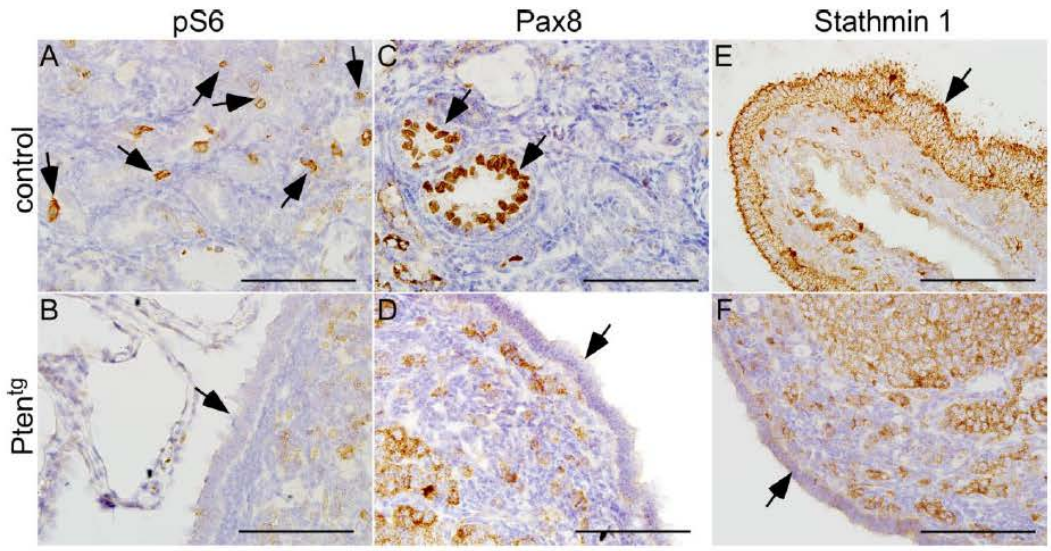

Supp. Fig. 4. Analysis of pS6, Pax8 and Stathmin 1 expression in Pten^{tg} and control mice ovaries. Arrows in panel A, C and E mark specific staining for these three markers in aged control mice ovaries. OSE (arrow in panel B, D and F) of the Pten^{tg} mice showed no expression of these markers. Bars: 100 µm.

Appendices

Additional Publications

1. Manuscript related to the study entitled as **"Age-related changes in stromal-epithelial communication leads to endometrial hyperplasia and cancer"** is part of this thesis and is now under preparation for publication.

2. The study entitled **"Targeting EphA2 pathway inhibits mTOR resistance in endometrial cancer"** is a supplementary paper to this thesis. Manuscript of this study is now under preparation for publication purpose.

3. The paper entitled **"Organotypic co-culture model mimics the architecture and functional responses of human endometrium"** is another supplementary paper to this thesis and is now under preparation for publication.

Conferences

Oral Presentations

1. **Sahoo SS**, Tanwar PS "Mechanical control of human endometrium: Role of ECM-mediated TGF-β signaling in uterine epithelium" **Society of Reproductive Biology/Endocrine Society of Australia Annual Scientific Meeting**, Gold Coast, QLD, Australia 2016, 21 Aug 2016 - 24 Aug 2016. SRB/ESA. 24 Aug 2016

2. **Sahoo SS**, Tanwar PS "Influence of microenvironment in endometrial cancer progression" **Hunter Cancer Research Alliance Annual Symposium**. Newcastle, NSW, Australia, 11 Nov 2016. HCRA/Asia-Pacific Journal of Clinical Oncology. 11 Nov 2016, DOI: 10.1111/ajco.12618

Poster Presentations

1. **Sahoo SS**, Tanwar PS "Inhibition of extracellular matrix mediated TGF-β signaling suppresses endometrial cancer metastasis" **Sydney Cancer Conference**, Sydney, 22 Sep 2016 – 23 Sep 2016

2. **Sahoo SS**, Tanwar PS "Extracellular matrix mediated TGF-β signaling supports endometrial cancer metastasis" **Lorne Cancer Conference**, Lorne, Vic, Australia, 12 Feb 2016 – 14 Feb 2016

Others

1. Syed S, Goad J, **Sahoo SS**, Cardona J, Tanwar PS "Influence of bad neighbourhood: Stromal contribution to endometrial cancer development" Hunter Cancer Research Alliance Annual Symposium, Newcastle, NSW, Australia, 27 Nov 2015. HCRA/Asia-Pacific Journal of Clinical Oncology. 27 Nov 2015

2. Syed S, Goad J, **Sahoo SS**, Cardona J, Kumar J, Tanwar PS "Endometrial hyperplasia and cancer: Side effects of miscommunication" Society of Reproductive Biology/Endocrine Society of Australia Annual Scientific Meeting, Adelaide, SA, Australia, 21 Aug 2015 - 24 Aug 2015. SRB/ESA. 74. 2015

3. Sercombe L, **Sahoo SS**, Tanwar PS "mTORC1 hyperactivation induces the ovarian phenotype of PCOS" Society of Reproductive Biology/Endocrine Society of Australia Annual Scientific Meeting, Adelaide, SA, Australia, 21 Aug 2015 - 24 Aug 2015. SRB/ESA. 131. 2015

4. Kumar M, **Sahoo SS**, Tanwar PS "mTOR: a novel target for testicular cancer" Hunter Cancer Research Alliance Annual Symposium 2014, Newcastle, NSW, 18 Nov 2014 - 18 Nov 2014. Asia-Pacific Journal of Clinical Oncology. Wiley-Blackwell. 10: 2-3 (2 pages). 01 Dec 2014

List of Awards

2014

International Tuition Fees Scholarship

The University of Newcastle

UNRS Central 50:50 Scholarship

The University of Newcastle

2016

Travel Grant

Society for Reproductive Biology

Travel Grant

Sydney Cancer Conference

2017

Beautiful Science Award

The University of Newcastle

Highlight of the Issue

The Journal Molecular Cancer Research has selected the paper “Adipose-derived VEGF-mTOR Signaling Promotes Endometrial Hyperplasia and Cancer: Implications for Obese Women” (mentioned in Chapter 3) for the highlight of the issue.

News

1. The study entitled as "Inhibition of extracellular matrix mediated TGF-β signalling suppresses endometrial cancer metastasis" (details in Chapter 2) is highlighted in a few news channel.

Hunter Medical Research Institute's news

https://hmri.org.au/news-article/protein-pinpointed-uterus-cancer-spread

SBS World News Australia

http://www.sbs.com.au/news/article/2017/05/25/breakthrough-uterine-cancer-research

news.com.au — Australia's #1 news site

http://www.news.com.au/national/breaking-news/breakthrough-in-uterine-cancer-research/news-story/f94f6b2585e5219154976ed3c1c36d5d

2. The paper entitled as "Adipose-derived VEGF-mTOR signaling promotes endometrial hyperplasia and cancer: Implications for obese women" (details in Chapter 3) is also featured in many media reports **(altogether 106 citations)**.

The University of Newcastle's news

https://www.newcastle.edu.au/newsroom/featured-news/fat-cells-a-key-suspect-for-endometrial-cancer-in-obese-women

Hunter Medical Research Institute's news

https://hmri.org.au/news-article/fat-cells-suspect-endometrial-cancer

Newcastle Herald – News site of the year

http://www.theherald.com.au/story/5082320/research-links-fat-cells-and-cancer/

Health Canal

https://www.healthcanal.com/cancers/242208-fat-cells-key-suspect-endometrial-cancer-obese-women.html

SBS World News Australia

https://www.sbs.com.au/news/article/2017/11/27/fat-cells-drive-endometrial-cancer-growth

Bibliography

1. Akhurst, R.J., and Hata, A. (2012). Targeting the TGFbeta signalling pathway in disease. Nat Rev Drug Discov *11*, 790-811.
2. Arem, H., and Irwin, M.L. (2013). Obesity and endometrial cancer survival: a systematic review. Int J Obes (Lond) *37*, 634-639.
3. Bajwa, P., Nielsen, S., Lombard, J.M., Rassam, L., Nahar, P., Rueda, B.R., Wilkinson, J.E., Miller, R.A., and Tanwar, P.S. (2017). Overactive mTOR signaling leads to endometrial hyperplasia in aged women and mice. Oncotarget *8*, 7265-7275.
4. Baxter, R.C. (2014). IGF binding proteins in cancer: mechanistic and clinical insights. Nat Rev Cancer *14*, 329-341.
5. Bhowmick, N.A., and Moses, H.L. (2005). Tumor-stroma interactions. Curr Opin Genet Dev *15*, 97-101.
6. Bissell, M.J., and Hines, W.C. (2011). Why don't we get more cancer? A proposed role of the microenvironment in restraining cancer progression. Nat Med *17*, 320-329.
7. Bissell, M.J., and Radisky, D. (2001). Putting tumours in context. Nat Rev Cancer *1*, 46-54.
8. Boilly, B., Faulkner, S., Jobling, P., and Hondermarck, H. (2017). Nerve Dependence: From Regeneration to Cancer. Cancer Cell *31*, 342-354.
9. Bonnans, C., Chou, J., and Werb, Z. (2014). Remodelling the extracellular matrix in development and disease. Nat Rev Mol Cell Biol *15*, 786-801.
10. Calle, E.E., and Kaaks, R. (2004). Overweight, obesity and cancer: epidemiological evidence and proposed mechanisms. Nat Rev Cancer *4*, 579-591.
11. Calle, E.E., Rodriguez, C., Walker-Thurmond, K., and Thun, M.J. (2003). Overweight, obesity, and mortality from cancer in a prospectively studied cohort of U.S. adults. N Engl J Med *348*, 1625-1638.
12. Cancer Genome Atlas Research, N., Kandoth, C., Schultz, N., Cherniack, A.D., Akbani, R., Liu, Y., Shen, H., Robertson, A.G., Pashtan, I., Shen, R.*, et al.* (2013). Integrated genomic characterization of endometrial carcinoma. Nature *497*, 67-73.
13. Carino, C., Olawaiye, A.B., Cherfils, S., Serikawa, T., Lynch, M.P., Rueda, B.R., and Gonzalez, R.R. (2008). Leptin regulation of proangiogenic molecules in benign and cancerous endometrial cells. Int J Cancer *123*, 2782-2790.
14. Carlson, M.J., Thiel, K.W., Yang, S., and Leslie, K.K. (2012). Catch it before it kills: progesterone, obesity, and the prevention of endometrial cancer. Discov Med *14*, 215-222.
15. Cerami, E., Gao, J., Dogrusoz, U., Gross, B.E., Sumer, S.O., Aksoy, B.A., Jacobsen, A., Byrne, C.J., Heuer, M.L., Larsson, E.*, et al.* (2012). The cBio cancer genomics portal: an open platform for exploring multidimensional cancer genomics data. Cancer Discov *2*, 401-404.
16. Che, Q., Liu, B.Y., Liao, Y., Zhang, H.J., Yang, T.T., He, Y.Y., Xia, Y.H., Lu, W., He, X.Y., Chen, Z.*, et al.* (2014). Activation of a positive feedback loop involving IL-6 and aromatase promotes

intratumoral 17beta-estradiol biosynthesis in endometrial carcinoma microenvironment. Int J Cancer *135*, 282-294.

17. Choi, D.S., Kim, H.J., Yoon, J.H., Yoo, S.C., Jo, H., Lee, S.Y., Min, C.K., and Ryu, H.S. (2009). Endometrial cancer invasion depends on cancer-derived tumor necrosis factor-alpha and stromal derived hepatocyte growth factor. Int J Cancer *124*, 2528-2538.
18. Chung, D., Gao, F., Jegga, A.G., and Das, S.K. (2015). Estrogen mediated epithelial proliferation in the uterus is directed by stromal Fgf10 and Bmp8a. Mol Cell Endocrinol *400*, 48-60.
19. Creasman, W.T., Odicino, F., Maisonneuve, P., Quinn, M.A., Beller, U., Benedet, J.L., Heintz, A.P., Ngan, H.Y., and Pecorelli, S. (2006). Carcinoma of the corpus uteri. FIGO 26th Annual Report on the Results of Treatment in Gynecological Cancer. Int J Gynaecol Obstet *95 Suppl 1*, S105-143.
20. Cristancho, A.G., and Lazar, M.A. (2011). Forming functional fat: a growing understanding of adipocyte differentiation. Nat Rev Mol Cell Biol *12*, 722-734.
21. Daley-Brown, D., Oprea-Ilies, G.M., Lee, R., Pattillo, R., and Gonzalez-Perez, R.R. (2015). Molecular cues on obesity signals, tumor markers and endometrial cancer. Horm Mol Biol Clin Investig *21*, 89-106.
22. Debnath, J., and Brugge, J.S. (2005). Modelling glandular epithelial cancers in three-dimensional cultures. Nat Rev Cancer *5*, 675-688.
23. Decruze, S.B., and Green, J.A. (2007). Hormone therapy in advanced and recurrent endometrial cancer: a systematic review. Int J Gynecol Cancer *17*, 964-978.
24. Dirat, B., Bochet, L., Escourrou, G., Valet, P., and Muller, C. (2010). Unraveling the obesity and breast cancer links: a role for cancer-associated adipocytes? Endocr Dev *19*, 45-52.
25. Dua, P., Kang, H.S., Hong, S.M., Tsao, M.S., Kim, S., and Lee, D.K. (2013). Alkaline phosphatase ALPPL-2 is a novel pancreatic carcinoma-associated protein. Cancer Res *73*, 1934-1945.
26. Dun, E.C., Hanley, K., Wieser, F., Bohman, S., Yu, J., and Taylor, R.N. (2013). Infiltration of tumor-associated macrophages is increased in the epithelial and stromal compartments of endometrial carcinomas. Int J Gynecol Pathol *32*, 576-584.
27. Espinosa, I., Catasus, L., E, D.A., Mozos, A., Pedrola, N., Bertolo, C., Ferrer, I., Zannoni, G.F., West, R.B., van de Rijn, M*., et al.* (2014). Stromal signatures in endometrioid endometrial carcinomas. Mod Pathol *27*, 631-639.
28. Espinosa, I., Jose Carnicer, M., Catasus, L., Canet, B., D'Angelo, E., Zannoni, G.F., and Prat, J. (2010). Myometrial invasion and lymph node metastasis in endometrioid carcinomas: tumor-associated macrophages, microvessel density, and HIF1A have a crucial role. Am J Surg Pathol *34*, 1708-1714.

29. Fader, A.N., Arriba, L.N., Frasure, H.E., and von Gruenigen, V.E. (2009). Endometrial cancer and obesity: epidemiology, biomarkers, prevention and survivorship. Gynecol Oncol *114*, 121-127.
30. Fang, H., and Declerck, Y.A. (2013). Targeting the tumor microenvironment: from understanding pathways to effective clinical trials. Cancer Res *73*, 4965-4977.
31. Felix, A.S., Weissfeld, J., Edwards, R., and Linkov, F. (2010). Future directions in the field of endometrial cancer research: the need to investigate the tumor microenvironment. Eur J Gynaecol Oncol *31*, 139-144.
32. Feng, J., Meyer, C.A., Wang, Q., Liu, J.S., Shirley Liu, X., and Zhang, Y. (2012). GFOLD: a generalized fold change for ranking differentially expressed genes from RNA-seq data. Bioinformatics *28*, 2782-2788.
33. Friedenreich, C.M., Langley, A.R., Speidel, T.P., Lau, D.C., Courneya, K.S., Csizmadi, I., Magliocco, A.M., Yasui, Y., and Cook, L.S. (2013). Case-control study of inflammatory markers and the risk of endometrial cancer. Eur J Cancer Prev *22*, 374-379.
34. Gelmini, S., Mangoni, M., Castiglione, F., Beltrami, C., Pieralli, A., Andersson, K.L., Fambrini, M., Taddei, G.L., Serio, M., and Orlando, C. (2009). The CXCR4/CXCL12 axis in endometrial cancer. Clin Exp Metastasis *26*, 261-268.
35. Gordon, L.K., Kiyohara, M., Fu, M., Braun, J., Dhawan, P., Chan, A., Goodglick, L., and Wadehra, M. (2013). EMP2 regulates angiogenesis in endometrial cancer cells through induction of VEGF. Oncogene *32*, 5369-5376.
36. Guo, S., Liu, M., Wang, G., Torroella-Kouri, M., and Gonzalez-Perez, R.R. (2012). Oncogenic role and therapeutic target of leptin signaling in breast cancer and cancer stem cells. Biochim Biophys Acta *1825*, 207-222.
37. Hanahan, D., and Coussens, L.M. (2012). Accessories to the crime: functions of cells recruited to the tumor microenvironment. Cancer Cell *21*, 309-322.
38. Hanahan, D., and Weinberg, R.A. (2011). Hallmarks of cancer: the next generation. Cell *144*, 646-674.
39. He, Y.Y., Cai, B., Yang, Y.X., Liu, X.L., and Wan, X.P. (2009). Estrogenic G protein-coupled receptor 30 signaling is involved in regulation of endometrial carcinoma by promoting proliferation, invasion potential, and interleukin-6 secretion via the MEK/ERK mitogen-activated protein kinase pathway. Cancer Sci *100*, 1051-1061.
40. Hecht, J.L., and Mutter, G.L. (2006). Molecular and pathologic aspects of endometrial carcinogenesis. J Clin Oncol *24*, 4783-4791.
41. Hlavna, M., Kohut, L., Lipkova, J., Bienertova-Vasku, J., Dostalova, Z., Chovanec, J., and Vasku, A. (2011). Relationship of resistin levels with endometrial cancer risk. Neoplasma *58*, 124-128.

42. Janzen, D.M., Rosales, M.A., Paik, D.Y., Lee, D.S., Smith, D.A., Witte, O.N., Iruela-Arispe, M.L., and Memarzadeh, S. (2013). Progesterone receptor signaling in the microenvironment of endometrial cancer influences its response to hormonal therapy. Cancer Res *73*, 4697-4710.
43. Jeppsson, A., Wahren, B., Brehmer-Andersson, E., Silfversward, C., Stigbrand, T., and Millan, J.L. (1984). Eutopic expression of placental-like alkaline phosphatase in testicular tumors. Int J Cancer *34*, 757-761.
44. Jobling, P., Pundavela, J., Oliveira, S.M., Roselli, S., Walker, M.M., and Hondermarck, H. (2015). Nerve-Cancer Cell Cross-talk: A Novel Promoter of Tumor Progression. Cancer Res *75*, 1777-1781.
45. Jones, A., Teschendorff, A.E., Li, Q., Hayward, J.D., Kannan, A., Mould, T., West, J., Zikan, M., Cibula, D., Fiegl, H.*, et al.* (2013). Role of DNA methylation and epigenetic silencing of HAND2 in endometrial cancer development. PLoS Med *10*, e1001551.
46. Kalluri, R. (2016). The biology and function of fibroblasts in cancer. Nat Rev Cancer *16*, 582-598.
47. Kalluri, R., and Zeisberg, M. (2006). Fibroblasts in cancer. Nat Rev Cancer *6*, 392-401.
48. Kamat, A.A., Merritt, W.M., Coffey, D., Lin, Y.G., Patel, P.R., Broaddus, R., Nugent, E., Han, L.Y., Landen, C.N., Jr., Spannuth, W.A.*, et al.* (2007). Clinical and biological significance of vascular endothelial growth factor in endometrial cancer. Clin Cancer Res *13*, 7487-7495.
49. Kelly, M.G., Francisco, A.M., Cimic, A., Wofford, A., Fitzgerald, N.C., Yu, J., and Taylor, R.N. (2015). Type 2 Endometrial Cancer is Associated With a High Density of Tumor-Associated Macrophages in the Stromal Compartment. Reprod Sci *22*, 948-953.
50. Kodama, J., Hasengaowa, Seki, N., Kusumoto, T., and Hiramatsu, Y. (2007). Expression of the CXCR4 and CCR7 chemokine receptors in human endometrial cancer. Eur J Gynaecol Oncol *28*, 370-375.
51. Kokka, F., Brockbank, E., Oram, D., Gallagher, C., and Bryant, A. (2010). Hormonal therapy in advanced or recurrent endometrial cancer. Cochrane Database Syst Rev, CD007926.
52. Kubler, K., Ayub, T.H., Weber, S.K., Zivanovic, O., Abramian, A., Keyver-Paik, M.D., Mallmann, M.R., Kaiser, C., Serce, N.B., Kuhn, W.*, et al.* (2014). Prognostic significance of tumor-associated macrophages in endometrial adenocarcinoma. Gynecol Oncol *135*, 176-183.
53. Lange, P.H., Millan, J.L., Stigbrand, T., Vessella, R.L., Ruoslahti, E., and Fishman, W.H. (1982). Placental alkaline phosphatase as a tumor marker for seminoma. Cancer Res *42*, 3244-3247.
54. Lax, S.F., Kendall, B., Tashiro, H., Slebos, R.J., and Hedrick, L. (2000). The frequency of p53, K-ras mutations, and microsatellite instability differs in uterine endometrioid and serous carcinoma: evidence of distinct molecular genetic pathways. Cancer *88*, 814-824.
55. Li, M., Xin, X., Wu, T., Hua, T., and Wang, H. (2015a). HGF and c-Met in pathogenesis of endometrial carcinoma. Front Biosci (Landmark Ed) *20*, 635-643.

56. Li, M., Xin, X., Wu, T., Hua, T., Wang, H., and Wang, H. (2015b). Stromal cells of endometrial carcinoma promotes proliferation of epithelial cells through the HGF/c-Met/Akt signaling pathway. Tumour Biol *36*, 6239-6248.
57. Longoria, T.C., and Eskander, R.N. (2016). Erratum to: Immunotherapy in endometrial cancer - an evolving therapeutic paradigm. Gynecol Oncol Res Pract *3*, 2.
58. Lu, P., Weaver, V.M., and Werb, Z. (2012). The extracellular matrix: a dynamic niche in cancer progression. J Cell Biol *196*, 395-406.
59. Lumeng, C.N., Bodzin, J.L., and Saltiel, A.R. (2007). Obesity induces a phenotypic switch in adipose tissue macrophage polarization. J Clin Invest *117*, 175-184.
60. Massague, J. (2008). TGFbeta in Cancer. Cell *134*, 215-230.
61. Massague, J. (2012). TGFbeta signalling in context. Nat Rev Mol Cell Biol *13*, 616-630.
62. Miles, F.L., and Sikes, R.A. (2014). Insidious changes in stromal matrix fuel cancer progression. Mol Cancer Res *12*, 297-312.
63. Millan, J.L., and Fishman, W.H. (1995). Biology of human alkaline phosphatases with special reference to cancer. Crit Rev Clin Lab Sci *32*, 1-39.
64. Morice, P., Leary, A., Creutzberg, C., Abu-Rustum, N., and Darai, E. (2016). Endometrial cancer. Lancet *387*, 1094-1108.
65. Mu, N., Zhu, Y., Wang, Y., Zhang, H., and Xue, F. (2012). Insulin resistance: a significant risk factor of endometrial cancer. Gynecol Oncol *125*, 751-757.
66. Mueller, M.M., and Fusenig, N.E. (2004). Friends or foes - bipolar effects of the tumour stroma in cancer. Nat Rev Cancer *4*, 839-849.
67. Muranen, T., Selfors, L.M., Worster, D.T., Iwanicki, M.P., Song, L., Morales, F.C., Gao, S., Mills, G.B., and Brugge, J.S. (2012). Inhibition of PI3K/mTOR leads to adaptive resistance in matrix-attached cancer cells. Cancer Cell *21*, 227-239.
68. Neumann, A., Keller, T., Jocham, D., and Doehn, C. (2011). [Human placental alkaline phosphatase (hPLAP) is the most frequently elevated serum marker in testicular cancer]. Aktuelle Urol *42*, 311-315.
69. Nicklin, J., Janda, M., Gebski, V., Jobling, T., Land, R., Manolitsas, T., McCartney, A., Nascimento, M., Perrin, L., Baker, J.F.*, et al.* (2012). The utility of serum CA-125 in predicting extra-uterine disease in apparent early-stage endometrial cancer. Int J Cancer *131*, 885-890.
70. Nieman, K.M., Romero, I.L., Van Houten, B., and Lengyel, E. (2013). Adipose tissue and adipocytes support tumorigenesis and metastasis. Biochim Biophys Acta *1831*, 1533-1541.
71. Noy, R., and Pollard, J.W. (2014). Tumor-associated macrophages: from mechanisms to therapy. Immunity *41*, 49-61.

72. Okamoto, T., Seo, H., Mano, H., Furuhashi, M., Goto, S., Tomoda, Y., and Matsui, N. (1990). Expression of human placenta alkaline phosphatase in placenta during pregnancy. Placenta *11*, 319-327.
73. Onstad, M.A., Schmandt, R.E., and Lu, K.H. (2016). Addressing the Role of Obesity in Endometrial Cancer Risk, Prevention, and Treatment. J Clin Oncol *34*, 4225-4230.
74. Ouchi, N., Parker, J.L., Lugus, J.J., and Walsh, K. (2011). Adipokines in inflammation and metabolic disease. Nat Rev Immunol *11*, 85-97.
75. Paget, S. (1989). The distribution of secondary growths in cancer of the breast. 1889. Cancer Metastasis Rev *8*, 98-101.
76. Paiva, J., Damjanov, I., Lange, P.H., and Harris, H. (1983). Immunohistochemical localization of placental-like alkaline phosphatase in testis and germ-cell tumors using monoclonal antibodies. Am J Pathol *111*, 156-165.
77. Paunescu, V., Bojin, F.M., Tatu, C.A., Gavriliuc, O.I., Rosca, A., Gruia, A.T., Tanasie, G., Bunu, C., Crisnic, D., Gherghiceanu, M.*, et al.* (2011). Tumour-associated fibroblasts and mesenchymal stem cells: more similarities than differences. J Cell Mol Med *15*, 635-646.
78. Pena, C.G., Nakada, Y., Saatcioglu, H.D., Aloisio, G.M., Cuevas, I., Zhang, S., Miller, D.S., Lea, J.S., Wong, K.K., DeBerardinis, R.J.*, et al.* (2015). LKB1 loss promotes endometrial cancer progression via CCL2-dependent macrophage recruitment. J Clin Invest *125*, 4063-4076.
79. Pfeiffer, R.M., Park, Y., Kreimer, A.R., Lacey, J.V., Jr., Pee, D., Greenlee, R.T., Buys, S.S., Hollenbeck, A., Rosner, B., Gail, M.H.*, et al.* (2013). Risk prediction for breast, endometrial, and ovarian cancer in white women aged 50 y or older: derivation and validation from population-based cohort studies. PLoS Med *10*, e1001492.
80. Quail, D.F., and Joyce, J.A. (2013). Microenvironmental regulation of tumor progression and metastasis. Nat Med *19*, 1423-1437.
81. Ramos, P., and Bentires-Alj, M. (2015). Mechanism-based cancer therapy: resistance to therapy, therapy for resistance. Oncogene *34*, 3617-3626.
82. Reeves, G.K., Pirie, K., Beral, V., Green, J., Spencer, E., Bull, D., and Million Women Study, C. (2007). Cancer incidence and mortality in relation to body mass index in the Million Women Study: cohort study. BMJ *335*, 1134.
83. Renehan, A.G., Tyson, M., Egger, M., Heller, R.F., and Zwahlen, M. (2008). Body-mass index and incidence of cancer: a systematic review and meta-analysis of prospective observational studies. Lancet *371*, 569-578.
84. Reyes, H.D., Miecznikowski, J., Gonzalez-Bosquet, J., Devor, E.J., Zhang, Y., Thiel, K.W., Samuelson, M.I., McDonald, M., Stephan, J.M., Hanjani, P.*, et al.* (2017). High stathmin expression is a marker for poor clinical outcome in endometrial cancer: An NRG oncology group/gynecologic oncology group study. Gynecol Oncol *146*, 247-253.

85. Rudd, M.L., Price, J.C., Fogoros, S., Godwin, A.K., Sgroi, D.C., Merino, M.J., and Bell, D.W. (2011). A unique spectrum of somatic PIK3CA (p110alpha) mutations within primary endometrial carcinomas. Clin Cancer Res *17*, 1331-1340.
86. Sahoo, S.S., Lombard, J., Ius, Y., O'Sullivan, R., Wood, L.G., Nahar, P., Jaaback, K.S., and Tanwar, P. (2017a). Adipose-derived VEGF-mTOR Signaling Promotes Endometrial Hyperplasia and Cancer: Implications for Obese Women. Mol Cancer Res.
87. Sahoo, S.S., Quah, M.Y., Nielsen, S., Atkins, J., Au, G.G., Cairns, M.J., Nahar, P., Lombard, J.M., and Tanwar, P.S. (2017b). Inhibition of extracellular matrix mediated TGF-beta signalling suppresses endometrial cancer metastasis. Oncotarget *8*, 71400-71417.
88. Saloniemi, T., Jarvensivu, P., Koskimies, P., Jokela, H., Lamminen, T., Ghaem-Maghami, S., Dina, R., Damdimopoulou, P., Makela, S., Perheentupa, A.*, et al.* (2010). Novel hydroxysteroid (17beta) dehydrogenase 1 inhibitors reverse estrogen-induced endometrial hyperplasia in transgenic mice. Am J Pathol *176*, 1443-1451.
89. Schmandt, R.E., Iglesias, D.A., Co, N.N., and Lu, K.H. (2011). Understanding obesity and endometrial cancer risk: opportunities for prevention. Am J Obstet Gynecol *205*, 518-525.
90. Siegel, R.L., Miller, K.D., and Jemal, A. (2016). Cancer statistics, 2016. CA Cancer J Clin *66*, 7-30.
91. Siegel, R.L., Miller, K.D., and Jemal, A. (2017). Cancer Statistics, 2017. CA Cancer J Clin *67*, 7-30.
92. Simo, R., Saez-Lopez, C., Lecube, A., Hernandez, C., Fort, J.M., and Selva, D.M. (2014). Adiponectin upregulates SHBG production: molecular mechanisms and potential implications. Endocrinology *155*, 2820-2830.
93. Steffan, J.J., Coleman, D.T., and Cardelli, J.A. (2011). The HGF-met signaling axis: emerging themes and targets of inhibition. Curr Protein Pept Sci *12*, 12-22.
94. Subramaniam, K.S., Omar, I.S., Kwong, S.C., Mohamed, Z., Woo, Y.L., Mat Adenan, N.A., and Chung, I. (2016). Cancer-associated fibroblasts promote endometrial cancer growth via activation of interleukin-6/STAT-3/c-Myc pathway. Am J Cancer Res *6*, 200-213.
95. Subramaniam, K.S., Tham, S.T., Mohamed, Z., Woo, Y.L., Mat Adenan, N.A., and Chung, I. (2013). Cancer-associated fibroblasts promote proliferation of endometrial cancer cells. PLoS One *8*, e68923.
96. Sun, X., Cheng, G., Hao, M., Zheng, J., Zhou, X., Zhang, J., Taichman, R.S., Pienta, K.J., and Wang, J. (2010). CXCL12 / CXCR4 / CXCR7 chemokine axis and cancer progression. Cancer Metastasis Rev *29*, 709-722.
97. Takahashi-Shiga, N., Utsunomiya, H., Miki, Y., Nagase, S., Kobayashi, R., Matsumoto, M., Niikura, H., Ito, K., and Yaegashi, N. (2009). Local biosynthesis of estrogen in human

endometrial carcinoma through tumor-stromal cell interactions. Clin Cancer Res *15*, 6028-6034.

98. Tanwar, P.S., Kaneko-Tarui, T., Zhang, L., Tanaka, Y., Crum, C.P., and Teixeira, J.M. (2012). Stromal liver kinase B1 [STK11] signaling loss induces oviductal adenomas and endometrial cancer by activating mammalian Target of Rapamycin Complex 1. PLoS Genet *8*, e1002906.
99. Tanwar, P.S., Zhang, L., Roberts, D.J., and Teixeira, J.M. (2011). Stromal deletion of the APC tumor suppressor in mice triggers development of endometrial cancer. Cancer Res *71*, 1584-1596.
100. Turco, M.Y., Gardner, L., Hughes, J., Cindrova-Davies, T., Gomez, M.J., Farrell, L., Hollinshead, M., Marsh, S.G.E., Brosens, J.J., Critchley, H.O.*, et al.* (2017). Long-term, hormone-responsive organoid cultures of human endometrium in a chemically defined medium. Nat Cell Biol *19*, 568-577.
101. Ungefroren, H., Sebens, S., Seidl, D., Lehnert, H., and Hass, R. (2011). Interaction of tumor cells with the microenvironment. Cell Commun Signal *9*, 18.
102. Vanderstraeten, A., Luyten, C., Verbist, G., Tuyaerts, S., and Amant, F. (2014). Mapping the immunosuppressive environment in uterine tumors: implications for immunotherapy. Cancer Immunol Immunother *63*, 545-557.
103. Vanderstraeten, A., Tuyaerts, S., and Amant, F. (2015). The immune system in the normal endometrium and implications for endometrial cancer development. J Reprod Immunol *109*, 7-16.
104. Wik, E., Birkeland, E., Trovik, J., Werner, H.M., Hoivik, E.A., Mjos, S., Krakstad, C., Kusonmano, K., Mauland, K., Stefansson, I.M.*, et al.* (2013). High phospho-Stathmin(Serine38) expression identifies aggressive endometrial cancer and suggests an association with PI3K inhibition. Clin Cancer Res *19*, 2331-2341.
105. Wincewicz, A., Koda, M., Sulkowska, M., Kanczuga-Koda, L., and Sulkowski, S. (2008). Comparison of STAT3 with HIF-1alpha, Ob and ObR expressions in human endometrioid adenocarcinomas. Tissue Cell *40*, 405-410.
106. Yamada, K.M., and Cukierman, E. (2007). Modeling tissue morphogenesis and cancer in 3D. Cell *130*, 601-610.
107. Zhao, H., Zhou, L., Shangguan, A.J., and Bulun, S.E. (2016). Aromatase expression and regulation in breast and endometrial cancer. J Mol Endocrinol *57*, R19-33.